

Master's thesis

Feasibility study on fiber reinforced polymer cylindrical truss bridges for heavy traffic

Mathis Chlosta

July 2012

Cover: Woven carbon fiber sheet typically used by the automotive industry. These sheets form the basis of high quality, high fiber content carbon fiber reinforced epoxy composites that serve as structural material in frame- or body-parts of state-of-the-art automobiles. [WEB: www.thetruthaboutcars.com]

MASTER'S THESIS

“FEASIBILITY STUDY ON FIBER REINFORCED POLYMER CYLINDRICAL TRUSS BRIDGES FOR HEAVY TRAFFIC”

“HAALBAARHEIDSSTUDIE NAAR CILINDRISCHE VAKWERKBRUGGEN VAN VEZELVERSTERKT
KUNSTSTOF VOOR ZWAAR VERKEER”

MATHIS CHLOSTA

JULY 2012

© Copyright 2012 Mathis Chlosta, Delft University of Technology, Delft, the Netherlands

All rights reserved. No part of this document may be reproduced for commercial purposes without written consent from the author. Permission is granted to reproduce for personal and educational use only with the use of proper citation. Commercial copying, hiring, lending and selling is prohibited without written consent from the author.

For inquiries regarding this thesis please contact the author via email: mchlosta@gmail.com

PREFACE

The document that you are facing provides a thorough overview of the MSc graduation design study, in which a feasible 'design for a fiber reinforced polymer cylindrical truss traffic bridge' is developed and optimized. Furthermore a fire safety and –protection strategy is developed for the application of fiber reinforced polymers in the civil engineering industry in general and in bridge engineering in specific.

This thesis was written in support of candidature for the Master of Science title in Civil Engineering at Delft University of Technology. The research was carried out in cooperation with Delft University of Technology, Faculty of Civil Engineering & Geosciences, Department Design & Construction and the Dutch infrastructure authority Rijkswaterstaat, Dienst Infrastructuur, Kennisveld Materialen.

Prior to this document an extensive literature study was written on the use of fiber reinforced polymers for civil engineering applications in general and for bridge engineering in specific. The research study presented here very much relies on this document and is therefore often referred to. Due to its nature and size the literature study was not added as an annex to this research but should be seen and used as a separate document that acts as a foundation of this research.

This document is split in three parts: First 'Part A, Material Properties & Fire Safety', secondly 'Part B, Design Study & Parameter Study', and third 'Part C, Final Design & Finite element analysis'. First, a fiber reinforced polymer composite with abundant fire safety properties is chosen as structural material for the bridge. Secondly, several shapes for the cylindrical truss are derived, analyzed and optimized. Third, the optimized cylindrical truss shape is used and adapted for the final design which is then analyzed for all design loads and compared to a similar steel structure.

My gratitude goes to my graduation committee for providing me with all the information, help and support I needed. I want to especially express my appreciation to the 'CUR Bouw en Infra' and their 'VC94-CUR96+ committee' for providing me an insight on their view on FRP materials, as well as Dr. ir. A. de Boer and the 'International Association for Bridge and Structural Engineering' for giving me the opportunity to participate in the 'IABSE-WC8 FRP Composite Structures Symposium'. Next to that I would also like to thank Mr. Jan Peeters of 'Fibercore Europe B.V.' for providing me with detailed information and support on short notice as well as Mr. Christian Scholze of 'Fiberline Composites'.

My graduation committee consisted of the following members:

Prof.ir. F.S.K. Bijlaard

Head of the graduation committee, Professor at Delft University of Technology, Faculty of Civil Engineering & Geosciences, Department of Design and Construction, Section Steel & Composite Structures

Dr.ir. M.H. Kolstein

Associate Professor at Delft University of Technology, Faculty of Civil Engineering & Geosciences, Department of Design and Construction, Section Steel & Composite Structures

Dr.ir. M.A.N. Hendriks

Assistant Professor at Delft University of Technology, Faculty of Civil Engineering & Geosciences, Department of Design and Construction, Section Structural Mechanics

Dr.ir. A. de Boer

Senior Advisor/Specialist at Rijkswaterstaat, Dienst Infrastructuur, Directie Techniek en Infrastructuur,

The Hague, July 2012

Mathis Chlosta

ABSTRACT

Considering the recent increase in the use of fiber reinforced polymers in the civil engineering industry in general and in the bridge engineering industry in particular, as well as the recently more and more applied cylindrical truss bridge type, this research focuses on the question whether it is possible to combine fiber reinforced polymers as stand-alone structural material and this bridge type to construct a bridge suitable for heavy traffic as well as bicycle and pedestrian traffic.

This research combines an extensive literature study on the use of fiber reinforced polymers for bridge engineering with a theoretical feasibility- and design-study on fiber reinforced polymer cylindrical truss bridges for heavy traffic. During the design study the spatial needs of all bridge users were defined to obtain an initial shape of the bridge. This shape was then optimized in several steps using finite-element-modeling and -analysis, yielding a final shape of the bridge. The behavior of this structure under design loads was then extensively investigated, again using finite element analysis, showing that the bridge could very well meet the self-derived deflection limit for fiber reinforced polymers at relatively low stress levels.

Since fiber reinforced materials are a very diverse field of material, with hundreds of different compositions being available, the first result of this study was the choice of a suitable composite for further analysis. For this bridge design very high fiber content (>60%) carbon/epoxy composite was used. The main reason for this choice was the high modulus and -strength of the carbon fibers and the high durability and strength of the epoxy resin.

A major reason of the slow implementation of fiber reinforced polymers in the bridge engineering industry are the worries concerning the lack of fire safety of the material. The literature study of this research showed however that it is possible to construct a heavy traffic full-FRP truss bridge, while complying with the known fire safety standards. The virgin FRP material can be adapted by several fire-protection measures; it turned out that a combination of intumescent gel-coating and low volume phosphorous filler systems works best in increasing the fire resistance and thereby providing a fire resistance class of R30 for hydrocarbon fire curve loading.

The initial shape of the bridge was optimized in three stages: first several different truss topologies, which were derived with a parametric geometric model, were analyzed and compared using finite element analysis software, yielding the square truss with one diagonal as most efficient topology. In the next steps several grid sizes of this truss as well as several cross section dimensions were compared, again using finite element analysis software. An optimum was found between minimum material usage and minimum deflection, which reduced the material usage of the main load bearing elliptical truss by about 40% compared to the initial variant.

The optimized structure was then fitted with the inner bridge deck supporting trusses as well as the cantilever trusses. The elliptical truss bridge performed very well considering the maximum deflections and stresses under Eurocode design loads and load combinations that were derived in finite element modeling software. When comparing the full-FRP bridge design with similar, existing steel structures, the maximum deformations and -stresses were considerably lower for the full-FRP bridge while only weighing about 60% of the steel structure.

This research showed that the 'new' cylindrical truss bridge type is not only an aesthetically appealing structure but also performs structurally very well when combined with fiber reinforced polymer as structural material. It turned out that fiber reinforced polymers can be used as stand-alone structural material for medium span heavy traffic bridges. Next to that, this research clarified that there is no legitimate structural reason for the fact that fiber reinforced polymers are used relatively scarcely in the civil engineering- and bridge engineering industry compared to traditional building materials such as steel and concrete.

Since this research is one of the first researches of its kind, using FRP as stand-alone structural material for a relatively new and complex bridge type, more research is needed in the field of high order connections for fiber reinforced polymer circular hollow sections. Next to that the possibility of the use of differently sized and shaped cross sections for the truss members should be investigated.

Keywords: Fiber reinforced polymers, plastics, FRP, civil engineering, bridge engineering, structural engineering, structural design, bridge design, stiffness driven design, cylindrical truss, elliptical truss, tubular truss, spatial truss, truss topology optimization, grid size optimization, space efficiency, heavy traffic road bridge, truss topology, mechanical properties of FRP materials, fire safety, fire resistance, steel viaduct comparison, FEA, FEM, finite element modeling, finite element analysis, CFRP, carbon, epoxy

TABLE OF CONTENTS

1. INTRODUCTION	1
1.1 CHOICE OF SHAPE.....	2
1.2 RESEARCH OBJECTIVE.....	3
1.3 RESEARCH QUESTIONS.....	4
PART A: MATERIAL PROPERTIES & FIRE SAFETY	
2. MECHANICAL PROPERTIES OF UNIDIRECTIONALLY REINFORCED COMPOSITES	7
2.1 CALCULATION METHODS.....	7
2.1.1 Longitudinal modulus of elasticity.....	7
2.1.2 Transverse modulus of elasticity.....	7
2.1.3 Longitudinal Shear Modulus.....	8
2.1.4 Transverse Shear modulus.....	8
2.1.5 Longitudinal-Transverse Poisson Ratio.....	8
2.1.6 Bulk modulus.....	8
2.1.7 Tensile Strength.....	8
2.1.8 Compressive Strength.....	9
2.1.9 Coefficient Of Linear Thermal Expansion.....	9
2.2 MECHANICAL PROPERTIES OF REINFORCEMENT FIBERS AND MATRIX MATERIALS.....	9
2.2.1 Reinforcement Fibers.....	10
2.2.2 Matrix Materials.....	10
2.3 MECHANICAL PROPERTIES OF SEVERAL UNIDIRECTIONALLY REINFORCED COMPOSITES.....	10
2.4 REMARK ON THE CALCULATION OF MULTIDIRECTIONALLY REINFORCED LAMINATES.....	12
3. CHOICE ON THE TYPE OF FIBER REINFORCED POLYMER COMPOSITE	13
3.1 REINFORCEMENT FIBER.....	13
3.2 MATRIX MATERIAL.....	14
3.3 UNIDIRECTIONALLY REINFORCED COMPOSITE.....	14
3.4 DESIGN VALUES OF MECHANICAL PROPERTIES OF THE UNIDIRECTIONALLY REINFORCED COMPOSITE.....	15
3.5 PRODUCTION METHODS.....	16
3.5.1 Truss member production.....	17
3.5.2 Connection production.....	17
4. FIRE SAFETY FOR FIBER REINFORCED POLYMER COMPOSITES IN BRIDGE ENGINEERING	19
4.1 SPECIFIC TRAFFIC BRIDGE FIRE SAFETY.....	19
4.1.1 Methods of protecting traffic bridges.....	20
4.2 FIBER REINFORCED POLYMER SPECIFIC FIRE PROPERTIES.....	21
4.2.1 Behavior of fiber reinforced polymer composites in FIRE.....	21
4.2.1.1 Char Formation.....	22
4.2.1.2 Delamination damage.....	23
4.2.2 Fire Properties of Selected Fiber reinforced polymer composites.....	23
4.2.2.1 Polyester.....	23
4.2.2.2 Epoxy.....	23
4.2.2.3 Phenolic.....	24
4.2.2.4 Glass Fiber.....	24
4.2.2.5 Carbon Fiber.....	24
4.2.2.6 Aramid Fiber.....	24
4.2.2.7 Assembled Fiber reinforced polymer Composites.....	24
4.2.2.8 Conclusion on the fire properties of virgin assembled composites.....	30
4.3 POSSIBLE FIRE PROTECTION MEASURES.....	30
4.3.1 Flame retardant fillers.....	30
4.3.2 Flame retardant polymers.....	32
4.3.3 Fire protective surface coatings.....	32
4.4 DESIGN FIRE.....	34
4.4.1 Performance criterion to be used.....	34
4.4.2 Fire curve to be used.....	35
4.4.3 Maximum fire load and fire scenario.....	35
4.5 CHOICE ON FIRE SAFETY MEASURES.....	36
4.5.1 Measures concerning the bridge.....	36
4.5.2 Measures concerning the material.....	37
4.5.3 Validation of Fire Protection Measures.....	38

PART B: DESIGN STUDY & PARAMETER STUDY

5. GEOMETRIC REQUIREMENTS OF THE BRIDGE	43
5.1 SPATIAL DEMANDS OF THE BRIDGE USERS	44
5.1.1 Road category and Design Speed	44
5.1.2 Heavy traffic requirements	44
5.1.3 Pedestrian requirements	47
5.1.4 Bicyclist requirements	48
5.2 GENERATION OF BRIDGE DECK LAYOUT VARIANTS	48
5.2.1 Layout variant 1	49
5.2.2 Layout variant 2	50
5.2.3 Layout variant 3	52
5.2.4 Layout variant 4	54
5.2.5 Layout variant 5	55
5.2.6 Layout variant 6	56
5.2.7 Comparison of the variants	57
5.2.8 Cantilever variant	59
5.3 REQUIREMENTS FOR THE DESIGN SPAN OF THE BRIDGE	60
5.4 GENERATION OF CYLINDRICAL TRUSS TOPOLOGY VARIANTS	62
5.4.1 Choosing suitable software	62
5.4.2 Parametric model of the cylindrical truss	62
5.4.2.1 Basic cylindrical shape	62
5.4.2.2 Generation of the horizontal and vertical members	63
5.4.2.3 Generation of the diagonal members	66
5.4.2.4 Generation of other grid types	67
6. LOAD & DEFLECTION REQUIREMENTS OF THE HEAVY TRAFFIC BRIDGE	73
6.1 ENVIRONMENTAL- & DEAD LOADS	73
6.1.1 Snow load	73
6.1.2 Wind load	73
6.1.3 Self-weight	77
6.1.4 Thermal load	77
6.2 VERTICAL HEAVY TRAFFIC LOADS	78
6.2.1 Load model 1 (LM1).....	79
6.2.2 Load model 2 (LM2).....	80
6.2.3 Load model 4 (LM4).....	81
6.3 BICYCLE AND PEDESTRIAN LOADS	82
6.4 HORIZONTAL TRAFFIC FORCES	82
6.4.1 Braking and acceleration	83
6.4.2 Collision	83
6.4.3 Centrifugal forces	83
6.4.4 Vehicular impact	83
6.5 COMBINATION OF TRAFFIC LOADS	84
6.6 COMBINATION OF TRAFFIC LOADS WITH OTHER LOADS	85
6.7 FATIGUE & VIBRATION LOADS	86
6.7.1 Vibration behavior	88
6.8 LIGHT RAIL LOADS	89
6.9 DEFLECTION LIMITS	90
7. CYLINDRICAL TRUSS PARAMETER STUDY	91
7.1 COMPARISON OF TRUSS TOPOLOGIES	91
7.1.1 Adapting the Grasshopper models	91
7.1.2 Transforming the Grasshopper models to FEA models	94
7.1.2.1 Material & cross-section	95
7.1.2.2 Support conditions	95
7.1.2.3 Loads & load cases	97
7.1.3 Comparing the truss topologies	97
7.1.3.1 General results	100
7.1.3.2 Choice of sub variant based on deflection	102
7.1.3.3 Choice of Main variant based on deflection	103
7.1.3.4 Choice of main variant based on other parameters	105
7.1.3.5 Final choice on truss topology	105

7.2 LOAD CASES FOR FURTHER ANALYSIS	106
7.3 INFLUENCE OF BRIDGE DECK SUBSTRUCTURE ON OVERALL BRIDGE STIFFNESS	106
7.3.1 Addition of inner bridge deck substructure to the main load bearing structure	107
7.3.2 Comparative Finite element analysis for the determination of the stiffness influence of the bridge deck substructure	108
7.4 DETERMINATION OF MOST EFFICIENT GRID SIZE	109
7.4.1 Finite element Analysis for the grid size determination	110
7.4.1.1 Material usage of the grid size variants	111
7.4.1.2 Maximum deflection of the grid size variants	112
7.4.1.3 Maximum compressive and tensile stresses of the grid size variants	113
7.4.1.4 Choice on the most efficient grid size variant	115
7.5 DETERMINATION OF MOST EFFICIENT CROSS SECTION DIMENSIONS	117
7.5.1 Choice On the most efficient cross section cimensions	122
7.6 FINAL CYLINDRICAL TRUSS GEOMETRY	123
7.6.1 Truss topology	123
7.6.2 Design span	124
7.6.3 Dimensions and shape of the main load bearing structure	124
7.6.4 Grid size of the cylindrical truss	125
7.6.5 Cross section dimensions of the truss elements	126

PART C: FINAL DESIGN & FINITE ELEMENT ANALYSIS

8. FINAL DESIGN	129
8.1 ADDITION OF INNER BRIDGE DECK SUBSTRUCTURE	129
8.2 ADDITION OF CANTILEVER BRIDGE DECK SUBSTRUCTURE	131
8.3 DRAWINGS OF THE FINAL DESIGN	133
8.4 LOADS & LOAD CASES	138
8.5 SUPPORT CONDITIONS	139
8.6 MATERIAL & CROSS SECTION	140
9. FINITE ELEMENT ANALYSIS ON THE FINAL DESIGN OF THE BRIDGE	141
9.1 DEFORMATION RESULTS FOR SEVERAL DESIGN LOADS	141
9.1.1 Heavy traffic load LM1	141
9.1.2 Bicycle & pedestrian load	142
9.1.3 Crowd loading LM4	143
9.1.4 Wind load in lateral direction	144
9.1.5 Thermal load	146
9.1.6 Vehicular impact load on the superstructure	146
9.2 FINITE ELEMENT ANALYSIS RESULTS FOR THE NORMATIVE LOAD COMBINATION CASE	147
9.2.1 Finite element analysis results for the overall normative load combination case LCC1	148
9.2.2 Finite element analysis results For the x- and y-deformation normative load combination cases LCC5 and LCC6	150
9.3 FATIGUE ANALYSIS	151
9.4 VIBRATION BEHAVIOR AND MODAL ANALYSIS	154
10. CONNECTIONS	157
10.1 CONNECTION PROPERTIES	157
10.2 STRESS DISTRIBUTION IN A PLANAR CONNECTION	158
10.3 STRESS DISTRIBUTION IN A MULTIPLANAR CONNECTION	159
10.4 MAKEABILITY OF FRP CHS CONNECTIONS	161
11. DESIGN OF OTHER BRIDGE ELEMENTS	163
11.1 BRIDGE DECK	163
11.1.1 Choice of bridge deck system	163
11.1.2 Demands for the bridge deck of the Full-FRP bridge design	165
11.1.3 Fiberline FBD600 ASSET bridge deck	165
11.1.4 Calculation of minimum supporting girder grid size for the Fiberline FBD600 Asset bridge deck	167
11.1.5 Fibercore Infracore bridge deck system	168
11.1.6 Wearing surface	169
11.2 BRIDGE SUBSTRUCTURE	170
11.2.1 Weight of the bridge	170
11.2.2 Reaction forces in the supports due to all load combination cases	170
11.3 DURABILITY & SUSTAINABILITY	173
11.4 COST ESTIMATION FOR THE FULL-FRP BRIDGE DESIGN	173
12. COMPARISON OF THE FULL-FRP BRIDGE TO AN EXISTING STEEL STRUCTURE	175
12.1 COMPARISON OF STRUCTURAL BEHAVIOR	179

12.2 COMPARISON OF GEOMETRIC PROPERTIES AND MATERIAL USAGE.....	181
12.3 MODAL ANALYSIS.....	182
12.4 CONCLUSION ON THE COMPARISON OF FULL-FRP AND STEEL CYLINDRICAL TRUSS BRIDGES	185
13. CONCLUSION & RECOMMENDATIONS	187
13.1 CONCLUSION.....	187
13.1.1 <i>Part A – Material properties & fire safety</i>	187
13.1.2 <i>Part B – Design study & Parameter study</i>	188
13.1.3 <i>Part C – Final Design & Finite Element analysis</i>	189
13.2 RECOMMENDATIONS	190
13.2.1 <i>Shape</i>	190
13.2.2 <i>Material</i>	191
13.2.3 <i>Connections</i>	191
13.2.4 <i>Fire Safety</i>	192
13.2.5 <i>Codification</i>	192

1. INTRODUCTION

Until now a normal traffic bridge would typically be constructed in concrete or steel. Some, mostly small-span bridges are made of timber. During the last decades a promising new material has slowly entered the civil engineering market: fiber reinforced polymer (FRP). This material's origin lies in the aerospace- and aviation industry, where it has been in use for many years already; mainly due to its very good strength-to-weight ratio. FRP deserves further investigation on application in the bridge industry.

During the last decade several smaller FRP pedestrian and cycling bridges have been constructed in the Netherlands, the rest of Western Europe and the USA. But there exist only very few FRP bridges which are suited for the heaviest traffic load classes. One bridge to call out is the 'Infracore' full-FRP Bridge installed in Oosterwolde in the Netherlands on the 8th of July 2010. This bridge has a span of 12m.

So why a cylindrical truss bridge, and foremost, what exactly is a cylindrical truss bridge? The idea of cylindrical truss bridges is that the space above and next to the driving lanes is used for structural strength. One could say that it is essentially a tunnel tube placed as a bridge. The main advantage of this kind of structures is the high possible span due to the large available construction height. Combined with the low weight of FRP this could lead to extremely efficient bridge structures.

One of the biggest problems in using FRP is to achieve abundant fire resistance within the structure. Therefore a theoretical investigation has to be made on how this fire resistance can be improved in such a way that the needed fire safety can be guaranteed when applying FRP in bridge construction. This investigation will lead to design choices on how the base material can be passively protected and how the active fire suppression on the bridge will take shape.

The theoretical research on the fire properties of bridges and fiber reinforced polymers and the choice of the fire safety measures that are to be taken is one part of this preliminary research. Furthermore choices will be made on the exact material composition of the base FRP-material, primarily based on the mechanical properties of unidirectional reinforced- and multi-layered-laminate composites. These are derived using the most appropriate calculation models found in the literature study.

The next important section of this research is focused on the general shape of the main load bearing cylindrical truss. Therefore several variants of different bridge deck layouts are generated that all accommodate the bridge users according to Dutch legislation. These bridge deck layouts lead to the general dimension of the bridge cross section. Also, by investigating the needs of a typical highway that is to be spanned by the bridge, the design span of the bridge is derived.

Furthermore several dynamic parametric geometric model of the main cylindrical truss will be made, this way several truss topology variants are derived that can all be dynamically adapted for different spans and overall dimensions by adjusting these design parameters. Later on, these parametric model will be the basis for the finite element analysis that will be used to make a choice on the mechanically most efficient truss topology and further optimize this layout. To be able to quickly proceed with FEA programming after this preliminary research the codes and demands for the design loads of a heavy traffic bridge will be summarized from the literature study and exactly quantified in this preliminary research. That way they can be quickly inserted the finite element models.

Besides the complex main load bearing structure the bridge also features somewhat simpler elements such as the bridge deck, the bridge deck supporting structure, the bridge pillars and the foundation. These bridge parts are not the main design objective of this research, but they nonetheless have to be given attention. The last part of this preliminary research gives some thoughts on the bridge deck and its substructure. The other elements will be dealt with in a later stage.

1.1 CHOICE OF SHAPE

Nowadays a typical highway bridge will be made of pre-stressed concrete girders in most of the cases. The most probable reason for this is likely to be the low cost and high efficiency of this structural system for spans of roughly 20-50m. Other spans call for different concepts, such as cable stayed bridges for long spans and truss bridges for medium spans. For longer spans steel is used very often, and steel truss bridges were introduced mid-19th century. In that time and the years after, industrial steel fabrication was still in early stage of development. Back then truss bridges typically had a rectangular cross section. Many examples can still be found through Europe, thousands of railway bridges of this type still exist. Earlier examples of steel truss bridges are the covered bridges, mainly found in North America, where the bridge was protected by a wooden cover and roof.



Fig. 1: Selection of modern truss bridges: (clockwise from top left): Webb Bridge, Melbourne, Australia; Peace Bridge, Calgary, Canada; Greenside Place Link Bridge, Edinburgh, Scotland; Light Rail Viaduct, The Hague, The Netherlands

Since then truss as structural system of heavy traffic bridge have somewhat fallen into oblivion, and more large-size cross section box girder bridges are built nowadays. However in the last 10-20 years interesting developments have been going on in the field of pedestrian bridges. Usually, due to the lower load conditions, developments of new structural shapes are much faster in pedestrian bridges than in heavy traffic bridges. More and more examples of modern truss pedestrian bridges can be found all over the world. The above picture shows a few recent examples of modern truss bridges.

Except for the last example, which is a railway bridge, all bridges are pedestrian bridges. The structural system is their common denominator; they all feature a cylindrical truss which wraps around the bridge deck. This shape is a new concept in the field of bridge engineering. It combines the high load bearing capacities of trusses with the slenderness of tube girders by transforming the traditional 2D truss bridge concept into a 3D cylindrical truss where the occurring forces are more evenly distributed between the members.

Next to the mechanical advantages of a cylindrical truss, it is also very slender and appealing, modern, innovative and futuristic, thus making it a perfect example of the cooperation of architect and engineer. Since this striking shape fits very well in modern architecture, and forms a real challenge for the engineer, it makes up a very interesting shape to study and analyze. Cylindrical trusses are very new in the bridge engineering industry and even newer in the heavy traffic bridge industry, which makes them an even more interesting object to study. Very little research has been done on tubular trusses as load bearing system for heavy traffic bridges.

The given examples are all made of steel; by nature steel has a very high modulus of elasticity, thus making it very deformation resistant, even with smaller cross-sections. To achieve the same stiffness as steel elements, which is the product of modulus and the element's second moment of area, fiber reinforced plastic elements need a higher second moment of area, and thus larger element dimension. This is caused by the inherently lower modulus of elasticity which fiber reinforced polymers generally exhibit. The bridge examples can be seen as large diameter tubes, which make them a perfect shape for the application of fiber reinforced plastic as building material.

Also, Rijkswaterstaat expressed one of their future visions of so-called "traffic tubes". In this vision future highways will be placed inside large tubes or cylinders made of light weight structural materials such as fiber reinforced plastics. These tubes are both used as load bearing system and as containment for noise and emissions, enabling highways through urban, densely populated areas without any disturbance. Tubular trusses could very well be a suitable solution to the traffic tube vision. The voids between the structural members can be filled up, or the whole tube can be covered by impermeable, sound insulating layers.

1.2 RESEARCH OBJECTIVE

"Analysis on the structural feasibility of a cylindrical truss bridge design with a superstructure made up completely of fiber reinforced polymers. This bridge has to withstand heavy traffic loads and remain structurally safe under fire and heat loads. The structural design of the cylindrical truss and its members will be the primary research objective."

The main objective of this research is to analyze whether it is possible to make a feasible design of a fiber reinforced polymer tube type traffic bridge using the finite element method. In this design the fire safety will receive extra attention since it is one of the most unfavorable aspects of the application of FRP in the civil engineering industry.

To make a logical, modern and efficient design a range of examples of existing cylindrical truss type bridges and FRP bridges has been analyzed in the literature study. The design of the FRP structure will be based on the material-specific properties of FRP. The design will also incorporate constructability of the bridge superstructure. The aim of the design is to keep the number of in-situ connections as low as possible. It is expected that a high percentage of the structure is prefabricated.

The structural behavior of the fiber reinforced tube type bridge will be compared to a corresponding design in steel. The aim is to show that FRP can compete with (more) traditional steel structures. The consequences of the application of FRP for the foundation and the roadway will be shown.

The occurring deformations and stresses under design loading will be analyzed for the FRP and steel bridges and possible flaws will be resolved or redesigned. The FRP structure will be optimized in terms of material usage and maximum occurring deformations and stresses.

Vibrations, fatigue and long term problems such as durability and sustainability issues will be addressed, though they will not be the main point of interest during this research. The same holds for the costs of the designed structure.

1.3 RESEARCH QUESTIONS

The preceding chapter covers the research objective; from this objective the main research question can be directly derived:

“How can fiber reinforced polymer be used as stand-alone structural material to design a cylindrical truss bridge with a circular- or elliptical cross-section, which is able to withstand heavy traffic loads, while complying with known fire safety standards?”

Below a list of sub-questions can be found, which further describe the goals of this thesis. Some of the questions were already answered in the literature study of this research; however the majority can only be answered in design stage of this research:

1. What are the structural characteristics of fiber reinforced polymers? What makes them (more) suitable for bridge construction (than other materials)?
2. What are the specific mechanical properties of fiber reinforced polymers? How can they be derived, described and calculated? Which FRP composition is most suitable for this design in terms of mechanical properties?
3. What are the required structural demands for road-traffic bridges? What are the design loads that are described by EU- and national law? How can they be quantified for the bridge that is to be designed?
4. How can a heavy traffic bridge made of fiber reinforced polymer composite be designed such that abundant fire safety is guaranteed? What active and passive measures are needed to achieve this fire safety level?
5. What are the values of the main design parameters such as span, width, height, radius or radii, etc. of the cylindrical load bearing structure? What are the needed dimensions of the cylindrical truss for different bridge deck layouts?
6. Which truss topologies are possible for the main load bearing cylinder? What is their influence on the mechanical behavior of the cylindrical truss and which of these truss layouts is structurally most efficient?
7. How can the design be optimized, concerning maximum deflections and stresses, material use, and the number of the connections?
8. How do the connections of the cylindrical truss members behave? How complex can they be, while still being easy to fabricate. What are their mechanical properties?
9. How can the bridge be designed to meet the durability- and sustainability-needs and a design-life of 100 years?
10. How does the designed full-FRP bridge behave in comparison to a comparable steel structure? What are the advantages of the use of FRP instead of steel for a cylindrical truss bridge?

Part A

Material Properties & Fire Safety

2. MECHANICAL PROPERTIES OF UNIDIRECTIONALLY REINFORCED COMPOSITES

In order to be able to calculate the stiffness values for different types of unidirectional reinforced fiber reinforced polymer composites an Excel-sheet was programmed in which several formulae were used to calculate the different stiffness values in a quick and efficient way. In this chapter the stiffness values of different unidirectional reinforced polymer composites are calculated.

2.1 CALCULATION METHODS

Since a lot of different approaches do exist for the stiffness estimation of FRP composites, the preceding literature study performed by the author was used for an appropriate choice. It showed that the following formulae are most accurate [LS, ch. 2.6.2; LS, ch. 2.6.3] and are thus used for further stiffness calculations of unidirectional reinforced fiber reinforced polymer composites.

2.1.1 LONGITUDINAL MODULUS OF ELASTICITY

The law of mixtures approach yields values for the longitudinal modulus of elasticity E_L that are at least equally accurate as more sophisticated models such as for example the Halpin-Tsai approach [LS, 2.6.2.4]. As advised in [LS, ch. 2.6.3] a so-called misalignment factor κ is incorporated in the calculation, which takes account of the misalignment of the fibers, which are never perfectly parallel in practice. In the literature study this calculation was given by the following equation [LS, eq. 2.7, p76]:

$$E_L \cong V_m E_m + V_f E_f \quad (2.1)$$

$$E_{L(\kappa)} \cong \kappa (V_m E_m + V_f E_f) \quad (2.2)$$

$$0,9 < \kappa < 1,0$$

2.1.2 TRANSVERSE MODULUS OF ELASTICITY

The transverse modulus of elasticity E_T is best approached by the lower boundary of the Hashin-Shtrikman model [LS, eq. 2.18, p78]. The following formula uses expression for other stiffness values with a minus- or plus-superscript, these values denote the upper- or lower boundaries of other stiffness values, calculated with the Hashin-Shtrikman-model as well. They will be described in the following chapters.

$$E_T \cong \left[\frac{1}{4G_{TT}^{(-)}} + \frac{1}{4k^{(-)}} + \frac{(v_{LT}^{(+)})^2}{4E_L^{(-)}} \right]^{-1} \quad (2.3)$$

2.1.3 LONGITUDINAL SHEAR MODULUS

The longitudinal shear modulus G_{LT} can be calculated in the most accurate way by the lower boundary of the Hashin-Shtrikman model [LS, eq. 2.16, p77].

$$G_{LT} \cong G_m + \frac{V_f}{\frac{1}{G_f - G_m} + \frac{V_m}{2G_m}} \quad (2.4)$$

2.1.4 TRANSVERSE SHEAR MODULUS

Just as the two preceding stiffness values, the transverse shear modulus G_{TT} is also best approached by the lower boundary of the Hashin-Shtrikman model [LS, eq. 2.17, p78].

$$G_{TT} \cong G_m + \frac{V_f}{\frac{1}{G_f - G_m} + \frac{V_m(k_m + 2G_m)}{2G_m(k_m + G_m)}} \quad (2.5)$$

2.1.5 LONGITUDINAL-TRANSVERSE POISSON RATIO

The literature study showed that the longitudinal-transverse Poisson ratio v_{LT} is best approached by the normal law-of-mixtures approach. The following equation [LS, eq. 2.9, p76] describes this model:

$$v_{LT} = v_f V_f + v_m V_m \quad (2.6)$$

2.1.6 BULK MODULUS

Since the Hashin-Shtrikman model for the transverse modulus of elasticity uses the lower boundary of the bulk modulus k for its calculation, it is necessary to incorporate these equations [LS, eq. 2.13, p77] too. The literature study also showed that this approximation is most accurate:

$$k \cong k_m + \frac{V_f}{\frac{1}{k_f - k_m} + \frac{V_m}{k_m + G_m}} \quad (2.7)$$

2.1.7 TENSILE STRENGTH

The tensile strength value of FRP-composites is calculated using the simple law of mixtures, similar to that used for the longitudinal modulus of elasticity, described in [ch. 2.1.1]. This approach is valid for UD-reinforced composites with high fiber contents, see also [B28, ch. 4.2.2]. Since in this research only fiber

contents of 60% and higher are used, this approach is certainly valid. The formula below can be used for the longitudinal tensile strength only:

$$S_{tensile} = V_m S_{m-tensile} + V_f S_{f-tensile} \quad (2.8)$$

2.1.8 COMPRESSIVE STRENGTH

The compressive strength of FRP-composites is primarily affected by the buckling of fibers, however the methods of calculation are very complex and do not always yield satisfying results. Even when test data is available the results are often not unambiguous. See also [LS, ch. 2.6.5.2, p84] and [B01, p162]. In this research it is therefore chosen to use the values of [B01, p24, table 1.4] if possible. This table gives some experimentally derived values for a large number of mechanical properties for epoxy-composite with a variety of reinforcement materials.

2.1.9 COEFFICIENT OF LINEAR THERMAL EXPANSION

Since this coefficient is not of major importance for the structural design of the bridge, and information on it for several FRP composites is readily available, it was decided to use the values derived in [B01, p24, table 1.4]. This coefficient is used for the calculation of the thermal loads [ch. 6.1.4] only.

2.2 MECHANICAL PROPERTIES OF REINFORCEMENT FIBERS AND MATRIX MATERIALS

In the preceding formulae it became clear that a lot of basic mechanical properties are needed from the two main composites ingredients, the fiber material and the matrix material. Since these values are not too readily available, the information derived in the literature study [LS, ch. 2.6.1] had to be replenished with some extra information that was found in [B28, ch. 4, table 4.2, table 4.3]. Also, the bulk modulus is a quantity that can be calculated by standard mechanical relations for isotropic materials; The following equation is used for both the reinforcement as well as the matrix material. Originally, this formula is only applicable for isotropic materials, but since the final FRP material is modeled as quasi-isotropic it can also be used for the reinforcement fibers in this research:

$$k = \frac{2G(1 + \nu)}{3(1 - 2\nu)} \quad (2.9)$$

The following tables resulted. Please note that this table is still in preliminary state. It is not yet complete and may undergo changes, due to extra information of any kind.

2.2.1 REINFORCEMENT FIBERS

Property	Symbol	Unit	Carbon M35J	S-Glass	E-Glass	Aramid Kevlar49
Density	ρ_f	kg/m ³	1.770	2.490	2.490	1.470
Long. Modulus of elasticity	E_f	N/mm ²	343.000	85.000	75000	150000
Poisson's ratio	ν_f	-	0,2	0,2	0,2	0,35
Tensile strength	s_f	N/mm ²	2740,00	4140,00	2760,00	2760,00
Compressive strength	s_c	N/mm ²	2042,00	3450,00	2400,00	500,00
Shear Strength	s_s	N/mm ²	624,00	1050,00	690,00	400,00
Rupture strain	e_f	%	-	-	-	-
Long. Lin.Therm. Exp.Coeff.	α_{fl}	10 ⁻⁶ /K	1,00	5,00	5,00	-
Trnsv. Lin.Therm. Exp.Coeff.	α_{ft}	10 ⁻⁶ /K	10,10	5,00	5,00	-
Shear Modulus	G_{LT-f}	N/mm ²	14.211	36.000	30.000	2.900
Bulk Modulus	K_m^*	N/mm ²	18.948	48.000	40.000	8.700

Table 1: Extended mechanical properties of selected fiber materials

2.2.2 MATRIX MATERIALS

Property	Symbol	Unit	Polyester	Polyimide	Phenolic	Epoxy 0	Nylon
Curing temperature	T_c	°C	-	-	-	-	-
Density	ρ_m	kg/m ³	1.200,00	1.220,00	1.200,00	1.300,00	1.140,00
Modulus of elasticity	E_m	10 ³ N/mm ²	3.000,00	3.450,00	11.000,00	3.450,00	3.450,00
Poisson's ratio	ν_m	-	0,35	0,35	0,35	0,35	0,35
Tensile strength	s_{tm}	N/mm ²	60,00	120,00	60,00	90,00	81,40
Compressive strength	s_{cm}	N/mm ²	140,00	210,00	200,00	130,00	60,70
Shear strength			50,00	90,00	80,00	60,00	66,20
Rupture strain	e_m	%	-	-	-	-	-
Lin. Therm. Exp. Coeff.	α_m	10 ⁻⁶ /K	80,00	36,00	80,00	64,30	46,00
Shear Modulus	G_{LT-m}	N/mm ²	1.100,00	1.280,00	4.070,00	1.280,00	1.280,00
Bulk Modulus	K_m^*	N/mm ²	3.300	3.840	12.210	3.840	3.840

Table 2: Extended mechanical properties of selected matrix materials

2.3 MECHANICAL PROPERTIES OF SEVERAL UNIDIRECTIONALLY REINFORCED COMPOSITES

The following table gives some examples of typical UD reinforced composites that might be used as structural material for the bridge. The readily available Carbon Toray M35J, S-Glass and Aramid Kevlar 49 fibers are considered as reinforcement material. Standard Toray Epoxy-, Phenolic- and Polyester-resins are considered as matrix material.

Furthermore only two common high strength fiber/matrix ratios are considered in this table: 60% fibers and 70% fibers. A conservative fiber misalignment reduction factor of $\kappa = 0,9$ is covered by E_L (K). Degradation of mechanical properties due to additives and fire-retardant fillers are not considered.

The mechanical properties of the assembled were calculated using the property tables of the source materials [ch. 2.2.1] [ch. 2.2.2] and the calculation methods described in the chapters before [ch. 2.1].

		60% Carbon M35J	70% Carbon M35J	60% Carbon M35J	70% Carbon M35J	60% Carbon M35J	70% Carbon M35J
		40% Epoxy 0	30% Epoxy 0	40% Phenolic	30% Phenolic	40% Polyester	30% Polyester
ρ	kg/m ³	1.582	1.629	1.542	1.599	1.542	1.599
E_L	N/mm ²	207.180	241.135	210.200	243.400	207.000	241.000
$E_L(K)$	N/mm ²	186.462	217.022	189.180	219.060	186.300	216.900
E_T	N/mm ²	8.860	10.170	17.675	18.896	7.961	9.720
ν_{LT}	-	0,260	0,245	0,260	0,245	0,260	0,245
G_L	N/mm ²	10.298	12.692	6.900	7.575	3.157	3.944
G_T	N/mm ²	9.465	11.677	6.745	7.420	2.880	3.598
k^*	N/mm ²	7.165	8.190	12.024	13.168	6.493	7.539
$S_{L-tensile}$	N/mm ²	1.680	1.945	1.668	1.936	1.668	1.936
$S_{L-compr.}$	N/mm ²	1.277	1.468	1.305	1.489	1.281	1.471
α_{fl}	10 ⁻⁶ /K	1,50	1,75	-	-	-	-
α_{fT}	10 ⁻⁶ /K	25,00	29,2	-	-	-	-

		60% S-Glass	70% S-Glass	60% S-Glass	70% S-Glass	60% S-Glass	70% S-Glass
		40% Epoxy 0	30% Epoxy 0	40% Phenolic	30% Phenolic	40% Polyester	30% Polyester
ρ	kg/m ³	2.014	2.133	1.974	2.103	1.974	2.103
E_L	N/mm ²	52.380	60.535	55.400	62.800	52.200	60.400
$E_L(K)$	N/mm ²	49.761	57.508	52.630	59.660	49.590	57.380
E_T	N/mm ²	11.123	14.619	28.210	34.336	9.721	12.860
ν_{LT}	-	0,260	0,245	0,260	0,245	0,260	0,245
G_L	N/mm ²	4.522	6.075	11.527	14.338	3.951	5.342
G_T	N/mm ²	3.957	5.273	10.539	13.115	3.444	4.616
k^*	N/mm ²	9.794	12.457	23.636	27.307	8.597	11.030
$S_{L-tensile}$	N/mm ²	1536	1777	1524	1768	1524	1768
$S_{L-compr.}$	N/mm ²	500	583,3333333	-	-	-	-
α_{fl}	10 ⁻⁶ /K	7,00	-	-	-	-	-
α_{fT}	10 ⁻⁶ /K	20,00	-	-	-	-	-

		60% Aramid Kevlar 49	70% Aramid Kevlar 49	60% Aramid Kevlar 49	70% Aramid Kevlar 49	60% Aramid Kevlar 49	70% Aramid Kevlar 49
		40% Epoxy 0	30% Epoxy 0	40% Phenolic	30% Phenolic	40% Polyester	30% Polyester
ρ	kg/m ³	1.402	1.419	1.362	1.389	1.362	1.389
E_L	N/mm ²	91.380	106.035	94.400	108.300	91.200	105.900
$E_L(K)$	N/mm ²	86.811	100.733	89.680	102.885	86.640	100.605
E_T	N/mm ²	5.981	6.514	9.806	9.502	5.526	6.116
ν_{LT}	-	0,350	0,350	0,350	0,350	0,350	0,350
G_L	N/mm ²	2.056	2.233	3.325	3.214	1.914	2.112
G_T	N/mm ²	2.018	2.197	3.314	3.204	1.866	2.064
k^*	N/mm ²	5.954	6.488	9.905	9.583	5.473	6.063
$S_{L-tensile}$	N/mm ²	1692	1959	1680	1950	1680	1950
$S_{L-compr.}$	N/mm ²	270	315	-	-	-	-
α_{fl}	10 ⁻⁶ /K	-2,00	-	-	-	-	-
α_{fT}	10 ⁻⁶ /K	60,00	-	-	-	-	-

Table 3: Extended mechanical properties of several unidirectional reinforced composites, calculated using the calculation methods described before

In the chapter on the choice of the most applicable unidirectional reinforced composite [ch. 3] the values that were derived and represented in this table will be compared and analyzed, leading to a choice of which matrix- and fiber-materials will be eventually used as main structural

2.4 REMARK ON THE CALCULATION OF MULTIDIRECTIONALLY REINFORCED LAMINATES

Since the objective of this research is the design of a spatial truss structure which exclusively uses linear, prismatic elements it is chosen not to go into detail about multidirectional reinforced laminate FRP materials. Due the nature of truss structures, its elements almost exclusively have to endure axial stresses and can therefore be unidirectional reinforced and produced by pultrusion only; see [ch. 3.5] [ch. 3.5.1] for more backgrounds on this choice. The general method of calculation of multidirectional reinforced laminate composites was already described in the literature study [LS, ch. 2.6.6, p85-92]

The main focus of this research lies on the general layout of the main load bearing structure and not on the detailed local analysis of the connections, which are the only elements of the main load bearing structure in which multidirectional stresses occur and multidirectional reinforcement is needed. However to give some guidance on the shape and type of connections, [ch. 3.5.2] and [ch. 10] provide some more information.

3. CHOICE ON THE TYPE OF FIBER REINFORCED POLYMER COMPOSITE

In this chapter a choice on the type of fiber reinforced polymer composite will be made based on the mechanical properties that were derived in [ch. 2]. In this chapter the number of possible materials was limited to six: Three common matrix materials and three common fiber materials. These were chosen based on their availability, price and commonness. A very exotic combination of high strength fiber or whisker reinforcement with a metal or ceramic matrix could very well yield much better mechanical properties [LS, ch. 2.5.1.5, p42] [LS, ch. 2.5.2, p43], but is not applicable and affordable in large civil applications.

The matrix materials that were chosen to be compared are unsaturated polyester, phenolic and epoxy. These materials are not exotic and exist in thousands of special formulations. For this comparison standard formulations were used, again to be able to use them in large bulk quantities while still being reasonably competitive in terms of costs. For the same reason three widely available 'standard' fiber materials were chosen: S-Glass, Carbon T300 and Aramid Kevlar-49. These three materials have been used in many applications and are available in many types of densities, tow sizes etc. The T300 carbon for example has been in production for over 30 years by the Japanese company 'Toray' and features a standard modulus and standard strength.

Another important prerequisite that was used for the choice process is the limitation of the fiber-matrix-volume-ratio to 60/40 and 70/30. Although a lot of other ratio would be possible, it was chosen to only use these two ratios. First of all, in high strength applications only fiber-volume ratios in excess of about 55% are used. Using state-of-the-art production processes such as continuous filament winding and pultrusion fiber volume ratios of about 30%-50%-70% are very common [LS, table 19, p71], thus using only the highest fiber contents is perfectly reasonable considering their production technique and high mechanical load.

This chapter features two main choices: First the choice of the best matrix- and reinforcement based on the mechanical properties of unidirectional reinforced FRP composite [ch. 2.3], which is for example the case for most FRP elements produced by pultrusion. Secondly, a decision on the most suitable production methods for both the truss elements as well as the connections will be made. Note that the multidirectional FRP material that should be used for the connections will not be covered in such depth as the unidirectional FRP material used for the truss elements. The reason for this lies in the main focus of research on the overall structural design of the main load bearing structure and not on the local detail design of the connections. The exact method of calculation for multidirectional reinforced FRP laminates however can be found in the literature study [LS, ch. 2.6.6, p85-92].

3.1 REINFORCEMENT FIBER

The choice for the reinforcement material is primarily based on the modulus of elasticity and the strength of the material: Medium modulus carbon fibers already feature a longitudinal modulus more than 2x times larger than that of S-Glass and about 1,5x times bigger than that of Aramid Kevlar-49 [ch. 2.2.1]. It is therefore chosen to use carbon fiber as reinforcement material for the FRP composite.

Next to their high strength and stiffness, carbon fibers are also very versatile, because of their extremely high strength- and stiffness- to weight ratio. They are also chemically inert, electrically conductive, thermic

stabile, infusibile, biocompatibile. Although now a the standard modulus carbon fiber of the type of 'Toray' M35J has been chosen, its elasticity values can still reach values of three times that of steel. Carbon fiber stiffness or modulus of elasticity can range from that of glass to three times that of steel. The most widely used types have a modulus of 200.000-400.000 N/mm². [LS, ch. 2.5.1.2, p34] Carbon fiber M35J has a longitudinal modulus of elasticity of 343.000 N/mm² and a tensile strength of 2740N/mm² [ch. 2.2.1, table 1]

3.2 MATRIX MATERIAL

The choice for the matrix material somewhat differs from the choice on reinforcement material. Besides from having to be stiff, matrix materials also have to ductile and not behave brittle. Phenolic for example is a very stiff matrix material, but also behaves very brittle. [ch. 2.2.2, table 2]. Next to that the durability performance is also very important for the choice on the best possible matrix material, it is therefore chosen to use Toray epoxy as matrix material for the FRP composite.

Epoxyes are characterized by very high strength in compression, tension and flexure while their stiffness is also good. Next to that they exhibit a very low shrinkage, very good adhesion values, very good electrical properties and chemical resistance and low moisture absorption. Also, they offer excellent resistance to corrosion, high strength-to-weight ratio, and dimensional stability.

Epoxyes are the most widely used thermosets in high performance reinforced plastics. Due to the very good properties of epoxy resins, they are often used with high performance reinforcements, such as carbon fiber or high fiber contents of glass fiber. Because of their high corrosion resistance, they are also used as surface-coating layer for other materials or plastics. The epoxyes chemical resistance, toughness, flexibility and adhesion is unmatched by most other plastics. With suitable additives they can exhibit excellent resistance to heat, going up to 290°C. [B16, p136-137] [LS, ch. 2.5.2.5, p48]

3.3 UNIDIRECTIONALLY REINFORCED COMPOSITE

Here the properties of 70/30 and 60/40 carbon/epoxy fiber reinforced polymer composite will be given, these values were derived in [ch. 2] and amongst others were given in table [ch. 2.3, table 3]. The values given in the table below are the design values of the carbon/epoxy unidirectional reinforced composite that are to be used in further calculations.

		60% Carbon M35J 40% Epoxy Toray	70% Carbon M35J 30% Epoxy Toray
ρ	kg/m ³	1.582	1.629
E_L	N/mm ²	207.180	241.135
$E_L(K)$	N/mm ²	196.821	217.022
E_T	N/mm ²	8.860	10.170
ν_{LT}	-	0,260	0,245
G_L	N/mm ²	10.298	12.692
G_T	N/mm ²	9.465	11.677
k^*	N/mm ²	7.165	8.190
$S_{L-tensile}$	N/mm ²	1.680	1.945
$S_{L-compr.}$	N/mm ²	1.277	1.468
α_{fL}	10 ⁻⁶ /K	1,50	1,75
α_{fT}	10 ⁻⁶ /K	25,00	29,2

Table 4: Design values of the mechanical properties of the high performance carbon/epoxy composite with fiber ratios of 60% and 70%.

3.4 DESIGN VALUES OF MECHANICAL PROPERTIES OF THE UNIDIRECTIONALLY REINFORCED COMPOSITE

The Eurocode [NEN-EN 1990: 2002] prescribes the use of ultimate limit states and serviceability limit states. The Dutch CUR96+ FRP composite structures recommendation [CUR96+ Draft April 2012, ch. 2.2, p15] prescribes the following.

- Ultimate limit states relate to the safety of the structure. Ultimate limit states should be used for, among others, the maximum load capacity with regard to strength, stability and fatigue.
- Serviceability limit states relate to the functioning of the structure, the comfort of people, and the appearance of the building works.

For this research this means that the deformation behavior should be carried out in the serviceability limit state and that the maximum stresses and the fatigue behavior should be considered in the ultimate limit state.

. The reason for this lies in the fact that these values have been calculated using more advanced calculation procedures than for the strength values [ch. 2.1.1] [LS, ch. 2.6.2.3, p77]. As described in [LS, ch 2.6.3, p81] and advised by [B01, p98] the calculation values of the stiffness that will be used in further design and analyses on the deformation behavior is $E_L(K)$.

For the ultimate limit state as well as the serviceability limit state it is chosen to use the design values for material and product properties of CUR96+ [CUR96+ Draft April 2012, ch. 2.5.3, p20]. Note that this approach is very similar to that described in the literature study [LS, ch. 2.6.7, p93] [LS, ch. 2.6.7.1, p93] [LS, ch. 2.6.7.2, p94] which was based on the old CUR96 2003 recommendation [CUR96]. Following this approach a reduction factor ($\gamma_m * \gamma_c$) will be used for the design values of the strength and stiffness.

The strength values for tension S_{L-t} and compression S_{L-c} and E_L given in [ch. 3.3, table 4] will be reduced by a number of factors, described below. In this case, the factors are similar for both the strength and stiffness. The first formula gives the general expression for a the design mechanical property of a composites X_d , which is calculated by dividing the initial mechanical property X_k by the material factor γ_m and the conversion factor γ_c .

$$X_d = X_k / (\gamma_m * \gamma_c) \quad (3.1)$$

The material factor γ_m is calculated by the following formula given in [CUR96+ Draft April 2012, ch. 2.5.3.1, p20] , which incorporates uncertainties in obtaining correct material properties ($\gamma_{m,1}$) and uncertainties due to the production method ($\gamma_{m,2}$), as described in the following chapter [ch. 3.5]

$$\gamma_m = \gamma_{m,1} * \gamma_{m,2} = 1,1 * 1,1 = 1,21 \quad (3.2)$$

$$\gamma_{m,1} = 1,1 \text{ for properties derived by testing (manufacturer)}$$

$$\gamma_{m,2} = 1,1 \text{ for pultrusion}$$

The conversion factor is calculated using the following formula given in [CUR96+ Draft April 2012, ch. 2.5.3.2, p21]. For strength and fatigue verifications in the ultimate limit state the CUR96+ recommendation prescribes to use the conversion factors for temperature and humidity only [CUR96+ Draft April 2012, ch. 2.5.3.2, table x, p21].

$$\gamma_c = \gamma_{ct} * \gamma_{cv} = 1,1 * 1,1 = 1,21 \quad (3.3)$$

for ULS strength and fatigue verifications

$\gamma_{ct} = 1,1$ *conversion factor for temperature*

$\gamma_{cv} = 1,1$ *conversion factor for humidity*

The total reduction as described in [eq. 3.1] therefore becomes:

$$X_d = X_k / (\gamma_m * \gamma_c) = X_k / (1,21 * 1,21) = X_k / 1,464 \quad (3.4)$$

Using the reduction method described before, the design values for tensile and compressive strength as well as the longitudinal stiffness and the longitudinal shear stiffness of the 70/30 carbon/epoxy composite thereby become: Note that for the derivation of the longitudinal stiffness the stiffness value $E_L (K)$, which incorporates the fiber misalignment stiffness reduction factor of $\kappa = 0,9$ [ch. 3.3, table 4].

$$S_{L-t-d} = \frac{S_{L-t}}{1,464} = \frac{1.718N/mm^2}{1,464} = 1173,50N/mm^2 \quad (3.5)$$

$$S_{L-c-d} = \frac{S_{L-t}}{1,464} = \frac{1.458N/mm^2}{1,464} = 995,90N/mm^2 \quad (3.6)$$

$$E_{L-d} = \frac{E_L (K)}{1,464} = \frac{229.078N/mm^2}{1,464} = 156.474,0N/mm^2 \quad (3.7)$$

$$G_{L-d} = \frac{G_L}{1,464} = \frac{12.692N/mm^2}{1,464} = 8.669,0N/mm^2 \quad (3.8)$$

Note that these design values, which feature the design reduction for material and product properties dictated by the Dutch CUR96+ [CUR96+ Draft April 2012, ch. 2.5.3, p20] will be used for all further analyses.

3.5 PRODUCTION METHODS

Next to the material wise composition of the fiber reinforced composite that was described in the chapter before, another important characteristic of FRP materials is the production method used for the fabrication of the FRP structural elements. In this chapter a choice on production methods of the different elements of the main load bearing structure will be made, partly based on the demands in fiber volume content as described in [ch. 2.2], partly based on the nature of the different elements that have to be fabricated and partly based on other important characteristics, such as production costs.

In the literature study a lot of information on the different production techniques of fiber reinforced polymer as structural material was given [LS, ch. 2.5.4, p58]. Based on the comparative table [LS, ch. 2.5.4.5, table 19, p71] the production methods were filtered by the needed fiber volume ratio. To achieve the maximum stiffness and strength in the unidirectional reinforced composite, it was chosen to use a fiber volume ratio between 60% and 70% [ch.3.3]. With all of the production methods shown in the table below these high fiber volume ratios can be achieved.

Type	Fiber volume [%]	Size range [m ²]	Processing pressure [bar]	Processing temperature [°C]	Detail tolerance [mm]	Relative production cost [-]
------	------------------	------------------------------	---------------------------	-----------------------------	-----------------------	------------------------------

Open mold processes

Hand lamination	13-50	0,25-2000	ambient	ambient	1,0-5,0	High
Automated tape lamination	20-60	0,25-500	ambient	ambient	0,2-1,0	Moderate/High
Filament winding	55-70	0,1-100	ambient	ambient	1,0-2,0	Moderate/Low

Closed mold processes

Vacuum bag	15-60	0,5-200	ambient	ambient	1,0-3,0	Very High
Pressure bag	20-70	0,5-200	1-3,5	20-70	1,0-3,0	Very High
Autoclave	35-70	0,25-5,0	1-10,0	20-140	0,5-1,0	Very High

Continuous processes

Pultrusion	30-65	Up to 1m width	varies	130-150	0,2-0,5	Low
Continuous filament winding	55-70	Up to 2m diam.	ambient	ambient	1,0-2,0	Low

Table 5: FRP production methods suitable for fabrication of high fiber content FRP elements.

The main cylindrical load bearing structure consists of two primary elements: the circular hollow truss sections and the connections. Because these elements differ greatly, as well in shape and complexity, as also in the flow of forces it is advisable to review both elements separately. It is expected that different production techniques are found to be most suitable for each of the two types of elements of the main cylindrical load bearing structure.

3.5.1 TRUSS MEMBER PRODUCTION

Along the whole structure, the shape of all circular truss members varies very little. Furthermore typical CHS sections are not a very complex shape. They are prismatic and have a constant wall thickness. Therefore these members can and should be produced using automated, mass production and thus more cost-effective production techniques. Hence, continuous processes are the only applicable production techniques for the truss members.

Truss members are primarily loaded in longitudinal compressive- or tensile forces and not in flexure or by shear forces, therefore the unidirectional fiber orientation of pultrusion elements does not pose a disadvantage compared to the multidirectional orientated fibers in continuous filament wound elements. Next to that the pultrusion technique can yield more precise elements at roughly the same cost as continuous filament winding. It is therefore chosen to fabricate the FRP CHS truss elements using the pultrusion production technique.

To recall the basic principle and characteristics of pultrusion from the literature study [LS, ch. 2.5.4.4, p69-70]: In the pultrusion process, the reinforcement is pulled through a resin bath and then through a heated die, which forms it to the final profile shape. It then emerges fully cured from the die and can be directly cut to length. Advantages of the pultrusion process are excellent longitudinal alignment and hence very high and consistent mechanical properties, the high production rate, close tolerances and the high consistency. [LS, ch. 2.5.4.4, p69-70]

3.5.2 CONNECTION PRODUCTION

The connections between the linear CHS truss elements have quite different properties than the truss members. Depending on the truss topology [ch. 7.1], 3 to 10 different members meet at a single connection, thereby inducing multidirectional stresses. Next to that, connecting several members also calls for a specific shape of the connecting element, such that the transition from member into the connection

happens smooth. Finally, depending on the position of the connection in the main load bearing cylinder the shape of the connection element can vary due to the different angles of the members that are to be connected.

Because of the multidirectional character of the stresses in the connections a production method is needed that is able to provide elements with sufficient transverse mechanical properties. In fact a (quasi) isotropic material behavior would be ideal for the connection elements. Next to that a production method is needed for the connections that can yield a multitude of differently shaped connection elements. Therefore mass-productive and automated processes are not suitable in the case of connections.

When comparing the left-over processes in [ch 3.5, table 5], the relatively new process of automated tape lamination or automated fiber placement, as well as robotic filament winding can all achieve a very high level of detail tolerance, comparable to that of the autoclave production method, while also yielding significantly smaller production costs than in the case of the very expensive autoclave production. Both processes have already been used for the production of complex shapes, such as the tee-joint shown in picture below on the left. This joint was produced using a conventional filament winding machine, only adapting the software. This tee joint was already produced in 1989 by 'Cadfil' [WEB, www.cadfil.com].

Since then automated robots, similar to those used in the automotive industry have found their way into the FRP manufacturing market. Another example is the research carried out by J. Scholliers, and H. Van Brussel (1994) at the KU Leuven [P105]. For this research GFRP tee joint was produced using computer-integrated robotic tape-winding. See the picture below on the right for the winding patterns used.

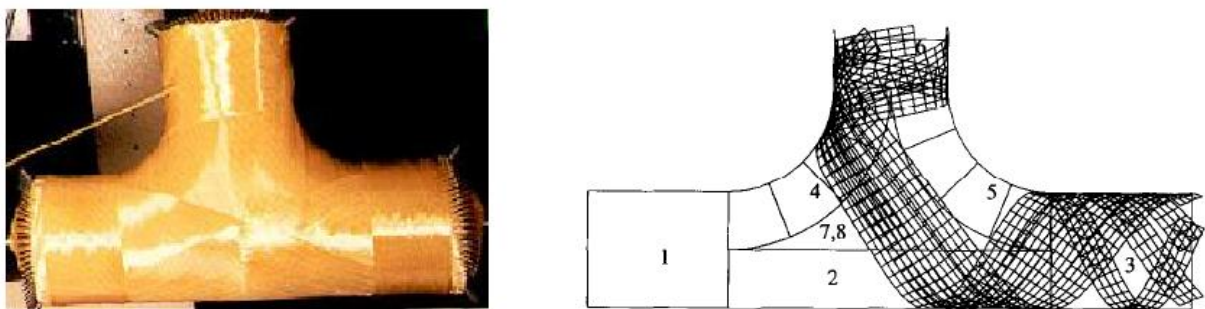


Fig. 2: Left: GFRP tee-joint used for the connection of tubular FRP members. [WEB, www.cadfil.com] Right: Robotic tape-winding patterns for the production of a tee joint [P105, p8]

Before robots entered the market, complex elements such as tee-joints would typically have to be produced using labor-intensive hand-layup combined with very expensive vacuum- or pressure-bag techniques. This made the design and fabrication of structures, such as trusses, with a large number of (complex) connections very costly and infeasible.

However, considering the newly available state-of-the-art computer numerical controlled (CNC) and robotic techniques large (and complex) have become more and more cost-effective and feasible. It is therefore chosen to produce the connection elements by using innovative CNC robotic filament winding techniques. This way, connection elements with several differently oriented UD-fiber layers, varying widths and complex shapes can be produced in a relatively cost-effective manner.

4. FIRE SAFETY FOR FIBER REINFORCED POLYMER COMPOSITES IN BRIDGE ENGINEERING

First general information on the fire safety of bridges and fiber reinforced polymers will be recalled from the literature study [LS, ch. 4, p135] in this chapter. This information is necessary to make appropriate design choices on the type of passive and active fire protection measures that are to be taken. First the goals and demands of fire protection of traffic bridges will be discussed, followed by the characteristics of fire reaction and –resistance. Finally, the available protection measures will be summed up and compared. The most important parts of this chapter might be the choice on the most appropriate fire safety measures, both active and passive, that will find their application in the bridge design.

4.1 SPECIFIC TRAFFIC BRIDGE FIRE SAFETY

In the following the general order of events leading to fire and fire damage for traffic bridges is given. This general flow of actions can be used for most traffic bridges. [P90, p3]

- Initial accident
- Release or spill of fuel or other flammable contents
- Ignition of the flammable materials
- Fire and/or explosion
- Fire exposure of unprotected bridge elements
- Severe damage to the bridge

These actions clearly show that bridges can be damaged, even by little accidents. These accidents can cause the follow up actions such as spill of fuels, and may have devastating consequences on the bridge and its users. [LS, ch. 4.2.2, p140]

To minimize the consequences of the occurring events that are described above it is important to stick to the three principles described below. These reasons also show why sufficient fire protection is always necessary in the case of traffic bridges can be found below: [P90, p8]

Protect people

The fire protection measures are necessary to protect the people, their lives and their health. That means that possibilities of egress should always be provided. Traffic disruption should also be minimized to stop more people from getting hurt in the case of an occurring accident.

Protect assets

The fire protection should always be aimed at maintaining the existing infrastructure. Next to that the threat of elements being exposed to fire should be minimized. Also the fire protection measures should extend the useful life of the bridge and aim at maintaining stable usage, thus not overloading the bridge.

Protect environment

Finally, the fire protection measures should also protect the environment. This means that in the case of fire no excessive smoke or liquid spill should pollute the environment.

Extensive research on different codes and regulations in the literature study showed that there is very little prescribed on the fire safety of bridges. The only way of achieving sufficient fire safety is thus to revert to the performance based design. This means that the fire safety engineer has to choose specific needs of the fire design. This can mean a fire safety period of 30 minutes for example, which means that the structural integrity must be fully guaranteed in the first 30 minutes of a fire. This means that the fire safety engineer has to choose specific needs of the fire design. This can mean a fire safety period of 30 minutes for example, which means that the structural integrity must be fully guaranteed in the first 30 minutes of a fire. [LS, ch. 4.2.2, p140]

4.1.1 METHODS OF PROTECTING TRAFFIC BRIDGES

In the following, general fire protection measures for traffic bridges of any material are given. These were derived in the literature study [LS, ch. 4.2.2.1, p141-142]. In the most general notion active- and passive fire protection methods can be discerned as well as methods that are based on limiting use of the bridge by vehicles carrying hazardous materials. Active fire protection measures are mechanisms that actively fight fire with for example water, foam, CO₂ and others. Passive fire protection measures rely on shielding the vulnerable structural materials from fire and heat, limiting the spreading rate of fire and reducing toxic emissions.

The most obvious measures are also most hard to realize in an environment with set design parameters and boundary conditions. These are the methods that rely on limiting the use of the bridge by vehicles carrying hazardous materials: First, the under-passing traffic should be limited to low-limit vehicles, e.g. no tankers. Secondly, the over-passing height of the bridge should be increased, thereby reducing the proximity of the bridge to possible under-passing fire sources. [P90, p9]

The perhaps most often used method of fire protection is the utilization of passive fire protection measures such as for example the application of inorganic, gypsum, silicate or magnesium oxychloride panels that are inflammable and are very heat resistant. One can imagine that the option of providing protective panels is not very applicable in the case of curved trusses composed of circular hollow sections. The added cost of such panel systems is generally mediocre. [P90, p10-12]

The next method of passive fire protection is the application of formed in place materials, such as added layers of concrete, which have the disadvantage of being thick and heavy and having only a limited corrosion resistance. The formed in place materials are at about the same magnitude of cost as the panel systems. [P90, p13] In the same family of protection measures are the spray applied materials, which are mostly thinner and lighter than the former method. Often they consist of sprayed fibers and cementitious lightweight materials such as cement/sand/vermiculite mixtures. They have the great advantage of low cost. Both methods described in this section are not very useful to be applied on smooth circular hollow sections that are always visible and are supposed to be visible and visually attractive to the user of the bridge. [P90, p14]

The last method of passive fire protection to be described here is the intumescent coating fire protection, where structural elements are coated in a thin (max. 1-2mm) layer of so called intumescent materials. These materials foam up during fire and swell up to about 40-100 times of their initial thickness, thereby protecting the underlying structural material. These coating are very well suited to protect structural elements without being visibly obstructive [P90, p15]. In [ch. 5.3] on FRP specific fire protection these coatings will be discussed in more detail.

The last bridge protection method to be discussed is that of active fire suppression. Measures such as sprinklers; CO₂ gas installations and foam sprinklers can be installed on traffic bridges in general. The cylindrical shape of the main load bearing system of the bridge is especially suitable for the installment of sprinkles high above the bridge deck. [P90, p9]

4.2 FIBER REINFORCED POLYMER SPECIFIC FIRE PROPERTIES

In the literature study the most important drawback of fiber reinforced polymer in structural applications was already discussed [LS, ch. 4.3, p143-144], here this disadvantage will be recalled. The performance of FRP's in fire is generally very poor. When composites are exposed to high temperatures, above 300°C, the organic matrix quickly decomposes with the release of heat, smoke, soot and toxic volatiles. When organic fibers such as aramid or polyethylene are used as reinforcement, the fibers also decompose and contribute to the heat and smoke release. [B07, p3]

Next to that, composites also soften, creep and distort at even lower temperatures, above 100°C-200°C, which can result in buckling and eventually failure of load-bearing structures. Due to the release of heat, smoke and gases firefighting becomes extremely hazardous during FRP fires. This disadvantageous property of fiber reinforced polymers is the main reason for the very infrequent application of this material in the infrastructure sector. [B07, p3]

However, in the aerospace industry, high tech plastic composites are often used as heat shields for spacecrafts re-entering the earth's atmosphere. This somewhat contradicts to the earlier statement that FRP composites behave very poorly under elevated temperature conditions. Composites have excellent thermal insulation properties and conduct heat much slower than steel or other metals. Next to that FRP can be tailor-made to have and improved resistance against pyrolysis. Properties that can be improved with alteration of matrix composition include ignition time, heat release rate, heat of combustion, smoke production and toxic potency of gas products. An added fact is the availability of thousands of different matrix compositions which all have very different fire properties. Some burn quick and violent whilst others can withstand temperatures over 1.300°C. [B07, p3] [B23, p406]

4.2.1 BEHAVIOR OF FIBER REINFORCED POLYMER COMPOSITES IN FIRE

When a fiber reinforced polymer composite is exposed to a sufficiently large heat flux the (polymer) matrix and the organic fibers will decompose and yield volatile gases, carbonaceous char and airborne soot particles (smoke). This process is shown in the scheme below. Note that the heat release caused by the decomposition can accelerate this decomposition process, thus forming a circular flow. The decomposition usually starts at temperatures in the range of 250°C - 400°C. [B07, p135]

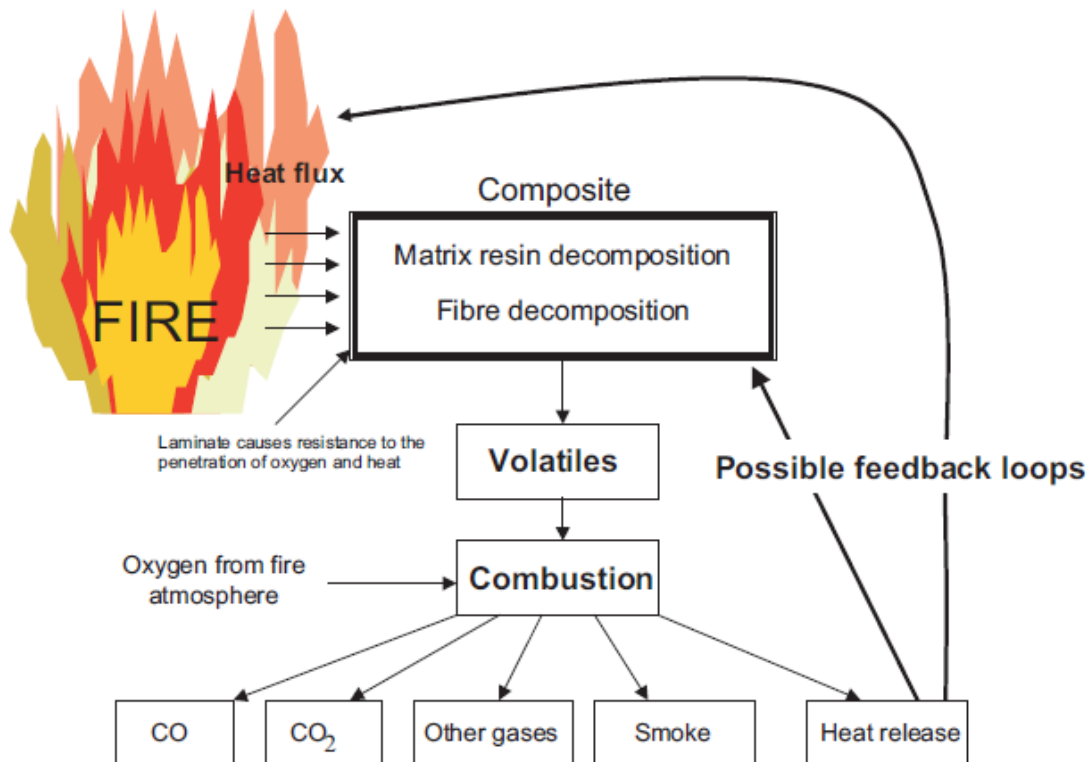


Fig. 3: Scheme depicting the composite decomposition during fire [B07, p21]

The volatile gases consist of a variety of vapors and substances, both flammable (e.g. carbon monoxide, methane, low molecular organics) and non-flammable (carbon dioxide, water). The gases diffuse into the flame zone, where they react with oxygen leading to the final combustion products, such as water, carbon dioxide, smoke particles and small amounts of carbon monoxide, of course accompanied by heat release, thus forming a self-sustaining process. [B07, p20] [LS, ch. 4.3.2, p146]

4.2.1.1 CHAR FORMATION

A process that occurs in fiber reinforced polymer under fire load is the formation of char, which can cause significant flame retardation, similar to timber char formation under fire load. Polymers with high char yield generally possess longer ignition times, lower heat release rates, slower flame spread rates, and generate less smoke and toxic gases than low char-forming polymers. [LS, ch. 4.3.3.1, p147]

This beneficial property of the char production in composites has several reasons: Firstly, the char often acts as a thermal insulation layer because the thermal conductivity of char is mostly lower than the conductivity of the virgin composite material. [B07, p48] Secondly, char can also improve fire resistance by limiting the access of oxygen from the atmosphere to the region of the composite undergoing decomposition, which slows down the combustion rate. Thirdly, char can act as a barrier against the flow of volatiles from the decomposition zone, thereby delaying ignition, slowing flame spread, and reducing the heat release rate. [B07, p50] Finally, char can help retaining the structural integrity of a fire-damaged composite by holding the fibers in place after the polymer matrix has been degraded.

However, for char to be effective in providing fire retardation it must form a continuous network structure that possesses low thermal conductivity and gas transportation properties. Furthermore the char must adhere strongly to the underlying composite; otherwise it can flake off and expose virgin material directly to the fire. A discontinuous char structure will enable the escape of flammable volatiles into the flame, and thereby reduces the effectiveness of the char layer to provide fire protection. [B07, p51]

4.2.1.2 DELAMINATION DAMAGE

Delamination cracking between the ply layers and matrix cracking within the plies often occurs ahead of the char zone when composites are exposed to fire. This damage may be confined solely to the reaction zone, or may spread through the reaction zone and underlying virgin material. It is believed that the cracking is in part due to the internal pressure build-up in the material due to volatile formation and, in some cases, vaporization of trapped moisture. The temperature in the delamination cracking region is well above the glass transition temperature in most polymer systems used in composites, so the phenomenon can be readily explained by the combination of pressure build-up and matrix softening. [B07, p53] [LS, ch. 4.3.3.2, p148]

Delamination, and to a certain extent matrix cracking, can be expected to have a significant effect on fire behavior due to the formation of non-bonded interfaces between plies. Matrix cracks can also provide pathways for the rapid release of combustion gases. Furthermore, when laminates are located above a fire source or in a vertical orientation, delamination can cause plies to fall off, thereby exposing fresh material to fire. [B07, p53]

4.2.2 FIRE PROPERTIES OF SELECTED FIBER REINFORCED POLYMER COMPOSITES

In this chapter the information derived in the literature study on the fire properties of matrix- and reinforcement materials as well as common composites will be recalled for the most important materials. [LS, ch. 4.3.3.3-4.3.6, p149-165] Three different matrix materials will be covered: epoxy, (unsaturated) polyester and phenolic. Next to that three reinforcement materials will be described: glass fiber, carbon fiber and aramid (Kevlar) fiber.

4.2.2.1 POLYESTER

Unsaturated polyester resins are the most used in the fiber reinforced polymer industry. The reason for this lays in their moderate cost, good mechanical properties, reasonable environmental durability, low viscosity at room temperature and good low-temperature cure properties. [B07, p25-26]

The thermal decomposition process of all unsaturated polyesters results in a variety of low molecular weight volatiles. Among these volatiles molecules such as CO, CO₂, methane and others can be found. 90%-95% of the original mass of the unsaturated polyester matrix is decomposed into the mentioned volatiles, rather than char. This is the main reason for the relatively high flammability and heat release of polyester composites. [B07, p32]

In addition to flammability and heat release, another disadvantage of polyester resin systems in fire is that the styrene component tends to produce smoke. Furthermore these resins tend, during decomposition, to pass through a 'liquid' or low viscosity stage that can result in the formation of flaming droplets. These disadvantages can be somewhat alleviated by applying high reinforcement- or filler content. [B07, p33]

Unsaturated polyester resins are often made more fire resistant by addition of halogen fillers to the resin. Despite environmental concerns, this method is highly effective in reducing flammability and is still the main measure by which low-flammability general-purpose resins are realized.

4.2.2.2 EPOXY

Decomposition of most epoxies occurs via molecular random chain scission reactions over the temperature range of about 380°C to 450°C. The scission reactions decompose 80- 90% of the original polymer weight into almost 100 different volatile, partly flammable compounds. These substances provide a fuel source for the decomposition reaction to continue until the epoxy is completely degraded. Only 10% to 20% of the original polymer weight is transformed into a highly porous char. As with polyester composites, the high

yield of flammable volatiles produced in the decomposition reaction is the main reason for the relatively poor fire performance of epoxy matrix composites. [B07, p38]

4.2.2.3 PHENOLIC

Unlike the other resins discussed earlier, the retained mass of phenolic resins decreases with increasing temperature in several stages which is indicative of a multiple-order decomposition process. Above 300°C the scission process commences, which mainly involves scission reactions along the chain, with elimination of some volatile byproducts. The reaction rate reaches a maximum in the second stage, and a variety of volatile gases are produced including CO, methane and phenol.

In contrast to many other thermosetting systems, much of the higher molecular weight aromatic material remaining after the scission reactions is able to condense to form a solid material. When a phenolic matrix composite is exposed to fire then the char formation temperature will decrease quickly with distance below the hot surface. 40%-60% of the original mass of phenolic resins is transformed into char, resulting in a much lower yield of flammable volatiles compared to other polymers (only 10% to 20% char formation in the case of epoxy and polyester): hence the superior fire performance and low flammability of phenolic composites. [B07, p40-41]

4.2.2.4 GLASS FIBER

E-glass fiber, which is the most used type of glass fiber, remains unaffected by fire until temperatures of about 830°C (1050°C for S-glass), when softening and viscous flow starts. Melting occurs at 1070°C (1500°C for S-glass). However, the mechanical properties such as strength and creep resistance decrease over a range of temperatures well below the softening temperature. Since the temperature of most fires is typically in the range of 500°C-1.100°C, common glass fibers have excellent fire resistance properties. Upon cooling the molten glass can fuse, which can slow the rate of heat conduction and acts as a barrier against the release of flammable volatile gases. Under these conditions, fused glass fibers can even reduce the flammability of composite materials. [B07, p44]

4.2.2.5 CARBON FIBER

Oxidation of carbon fibers starts at temperatures of 350°C-450°C. In that case impurities and irregularities in the fibers can cause axial splitting other fibers into small fibrils under fire load, which can become a health hazard when released from a burning composite into the smoke plume where they can be inhaled. However, in most types of fire the extent of oxidation is small because most carbon fibers within a composite are protected by char. It is usually only fibers at the hot composite surface are directly exposed to the fire. Only in oxygen-rich environment carbon fibers experience significant oxidation, and this is the only case, when the heat flux is high. [B07, p44]

4.2.2.6 ARAMID FIBER

Decomposition of aramid fibers starts quite rapidly at temperatures of 450°C-500°C in air and nitrogen, respectively, involving a substantial break-down of the main polymer network structure by a random scission process. The fibers yield a high amount of char of 40% of the original mass, as a by-product of the decomposition reaction when heated in nitrogen. Despite the thermal instability, aramid fibers are inherently flame resistant with very good oxygen limit value. [B07, p45]

4.2.2.7 ASSEMBLED FIBER REINFORCED POLYMER COMPOSITES

Heat Release Rate

The "Heat Release Rate" (HRR) is the single most important fire reaction parameter for composites; it also influences other parameters such as the surface spread of flame, smoke generation, and carbon monoxide emission. In composites the heat release rate is not constant but has a clear path of development. In the induction period no heat is released, because the exposure time to external heat is insufficient to heat the composite up to decomposition reaction temperature. After this initial period the heat release rate rapidly

increases in only a few seconds. This increase is caused by a sudden, short-term release of heat from the ignition of flammable volatiles from the resin-rich surface of the composite. The curve continues to rise to a peak HRR, after which the heat release is slowed down due to the formation and growth of char at the hot surface. After a certain amount of burning time the HRR becomes negligibly small due to the complete depletion of flammable fuels. At this stage the polymer matrix is completely depleted. The graph below, on the left shows the different stages of the heat release process for a glass vinyl-ester composite under a constant heat flux of 50kW/m^2 . [B07, p72-73]

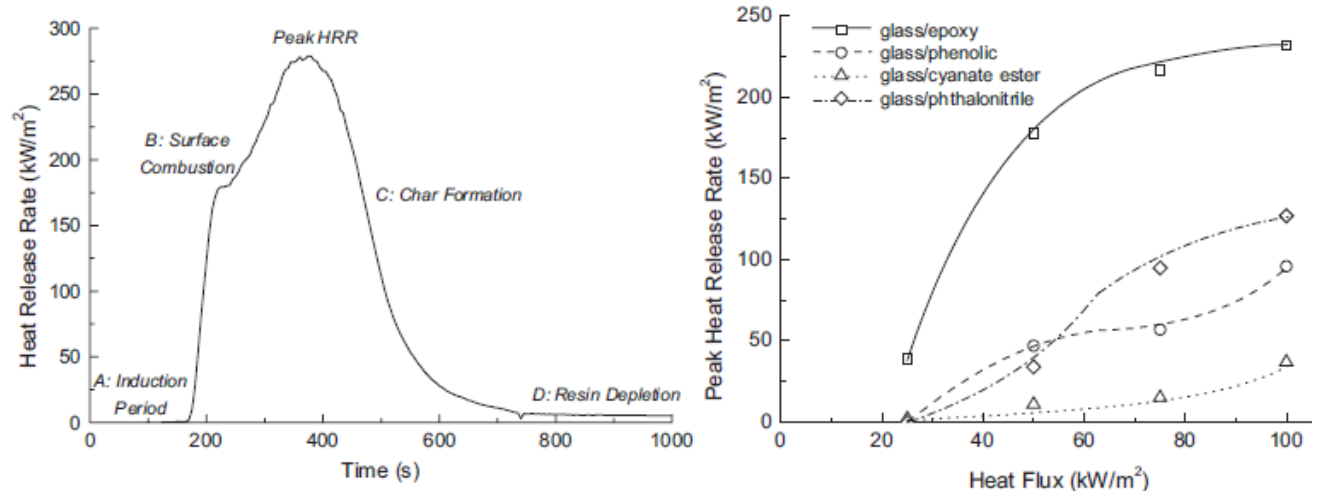


Fig. 4: Left: Typical heat release process for glass vinyl ester composites under constant heat flux of 50kW/m^2 . Right: Comparison of HRR's of normal and high fire performance composites. [B07, p72-73]

Time-To-Ignition

Most resins do not ignite when the initial external heat flux lies under a certain value. This value is called the threshold heat flux and lies at about 13 kW/m^2 for polyester, vinyl ester and epoxy composites. Phenolic laminates have a higher threshold heat flux of 25kW/m^2 . [B07, p60]

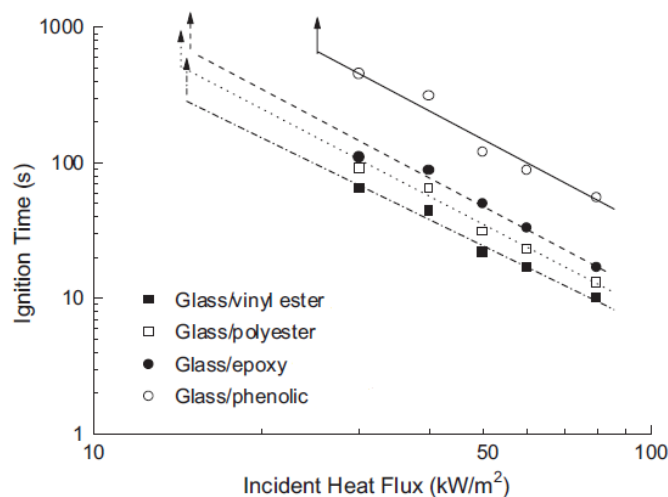


Fig. 5: Time-to-ignition of different thermoset (left) and thermoplastic (right) resin based composites. [B07, p61,62]

The fiber reinforcement in composites can also influence the ignition time, although glass and carbon fibers are inert to fire when the heat flux is below $100\text{-}125\text{ kW/m}^2$. Therefore, the amount of reinforcement present in the composite (the fiber content) substantially increases the ignition time. However the binders and coatings which are often used to for reinforcement fibers can have an adverse effect on the ignition time, since they are mostly organic and thus not inert to fire. Chopped Strand Mats for example, which are heavily coated/impregnated by nature decrease the ignition time drastically, particularly at low to mediate heat fluxes ($< 50\text{ kW/m}^2$). The difference in ignition time of CSM glass fiber/polyester composite compared to woven glass fiber/polyester composite is about 40%. [B07, p63-65]

Surface Spread of Flames

In flame spread tests it can be observed that the flame propagates readily down the surface of glass/polyester and glass/epoxy laminates, and this is caused by the high flammability of these materials. However, the flame is unable to spread down the glass/phenolic laminate, and this material can be regarded as self-extinguishing. Phenolic laminates thus again have excellent resistance of flame spread, and this is another outstanding fire reaction property of these materials that makes them suited for many high fire risk applications. The greatest influence on the flame spread rate of composite materials is their heat release rate. The higher the peak HRR, the higher the flame spread speed. The graph below on the left shows the flame spread distance over time for three different thermoset based composites. Note that phenolic composite allows no flame spread at all, thus, as mentioned before, can be considered self-extinguishing. [B07, p94]

Limiting Oxygen Index

The LOI index values shown in the graph, below left, were determined at room temperature. However, a composite material will reach much higher temperatures in a fire. Different studies have shown the LOI-values of composites are dependent on the test temperature. The values can change dramatically with temperature, usually decreasing with increasing temperature, and often changing the relative ranking of some materials. It is therefore questionable to use LOI values measured at room temperature to assess the flammability of composite materials. The LOI index values of glass phenolic and glass epoxy composite increase with temperature up to 100°C, but at higher temperatures there is a steady reduction in the values because less heat is needed to sustain decomposition and burning. [B07, p91]

Smoke generation and -toxicity

The graph below shows the correlation between external heat flux and the average smoke density. Although smoke density increases with growing heat fluxes, the increase is not so dramatic as with the heat release rate for example. [B07, p88]

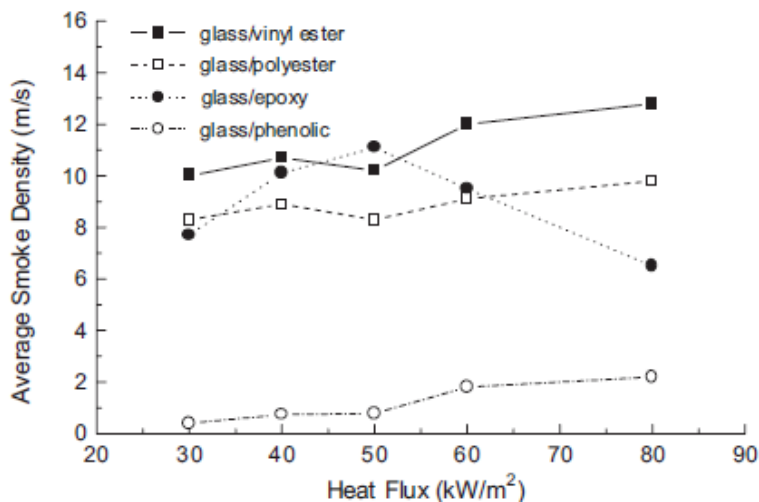


Fig. 6: Correlation between heat flux and average smoke density for different thermoset polymer composites [B07, p88]

The table below shows typical values for the emission of CO, CO₂, HCN and HCl gases. It is interesting to see that even a high fire performance thermoset like phenolic does not perform better than other thermosets. [B07, p90]

Composite	CO (ppm)	CO ₂ (vol%)	HCN (ppm)	HCl (ppm)
Glass/ Epoxy	283	1,5	5	not detected
Glass/ Phenolic	300	1,0	1	1
Glass/ Polyimide	200	1,0	trace	2

Table 6: Emission of toxic gases of different fiber reinforced composites [B07, p90]

Another table is presented which compares the toxicity of different gases. It can be seen that the exposure limits for Carbon Monoxide and Carbon Dioxide are much higher than the limits for the other toxic gases.

Type of toxic gas	Chemical	Exposure limit [ppm]
Carbon Monoxide	CO	1.500
Carbon Dioxide	CO ₂	50.000
Hydrogen Cyanide	HCN	50
Hydrogen Chloride	HCl	30
Sulfure Dioxide	SO ₂	30
Nitrogen Oxides	NO _x	30

Table 7: Toxic gas exposure limit [B07, p367]

The amount of CO produced is also very much influenced by the heat release rate properties of a composite. The CO-level correlates linearly with the heat release rate, which suggests that the toxic hazard caused by the release of CO can be minimized by using composites with low heat release rates.

Back-face Temperature Build-up

In fire resistance one of the most important parameters used is the general build-up of the back-face (unexposed face) temperature and specifically the time taken for the back-face temperature to reach 160°C, at which point the fire is likely to spread from one compartment to another. The graph below on the left shows the back-face temperature build-up for glass polyester and glass phenolic composites exposed to the standard cellulosic fire curve. It is seen that the temperature rise at the back-face of the phenolic laminate over the initial 30-40 minutes is lower than the polyester composite. At longer times the temperature of the phenolic increases faster. This is due mainly to explosive delamination damage caused by the internal pressure build-up from the vaporization of entrapped water in the phenolic matrix. [B07, p96-97]

The graph below, on the right shows a more important value for the back-face temperature, it correlates the thickness of different composite laminates with the time to reach 160°C at the back-face. To obtain this graph the more common (and severe) hydrocarbon fire curve was used. The time to reach 160°C rapidly increases with growing thickness of the test specimens. It is clearly visible that unprotected FRP composites reach the critical back-face temperature in very short times, mostly under 20 minutes. It can be seen that phenolic behaves much better than polyester resin. [B07, p97]

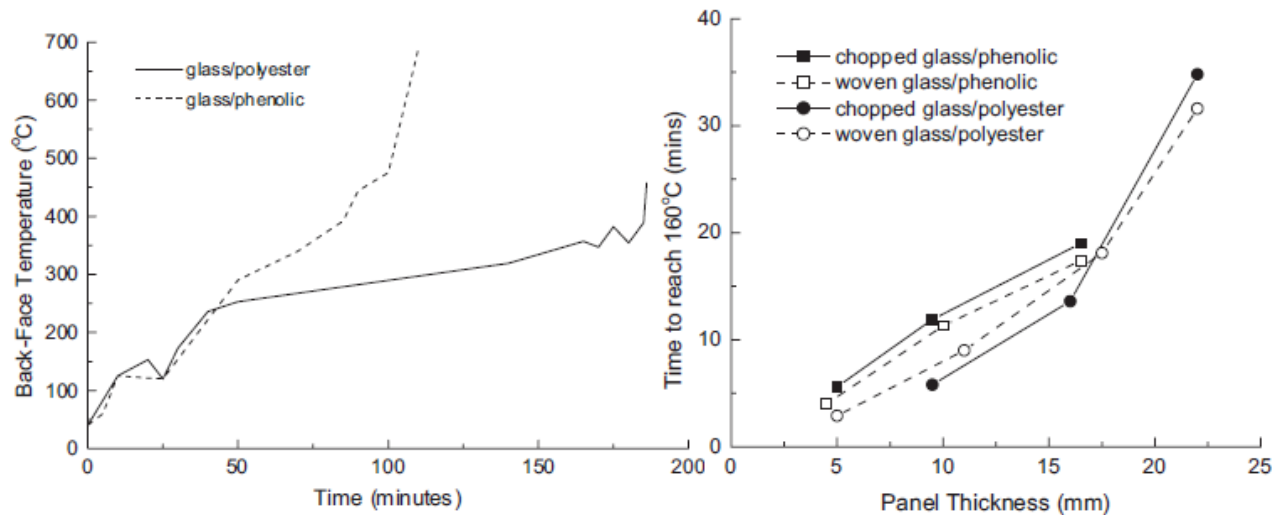


Fig. 7: Left: Back-face temperature build-up in cellulosic fire conditions. Right: Comparison of time to reach a back-face temperature of 160°C correlated to the member thickness for different composites. [B07, p96,97]

Mechanical properties of FRP composites under fire load

As described in the literature study [LS, ch. 4.3.5, p159-162], the available theoretical models on the structural performance of fiber reinforced composites are still in an experimental phase, therefore this chapter will concentrate on some available experimental data. The graph below, on the left shows the temperature dependence of the elastic modulus of an unidirectional reinforced glass polyester pultrusion and its components. The unidirectional core comprises about 60% by volume of the total section; the other

parts are foremost comprised by the random swirl mats. It can be seen that the modulus declines with about 40% up to 200°C, where the decline flattens out. The most rapid drop of modulus can be found in the temperature range of 75°C to 175°C [B07, p182, 183]. Note also that most predictive models use the modulus as a basis for the prediction of the decline of other mechanical properties as well. [B07, p175]

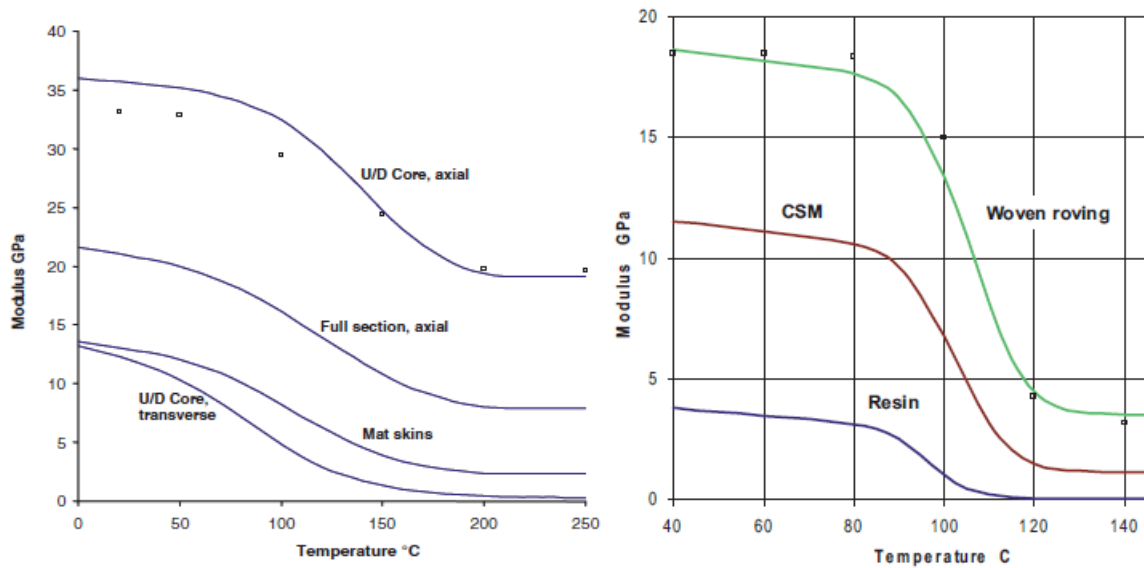


Fig. 8: Left: Young's modulus of UD- 60% reinforced glass polyester pultruded section (including its components) and random swirl mat correlated to the temperature. Right: Young's modulus of woven glass vinyl ester laminate and its parts correlated to the temperature [B07, p183, 185]

The graph above, on the right shows a similar relationship as the previously described graph. However it describes several vinyl ester resin based composites. It can be seen that decrease of modulus for vinyl ester resins is even bigger than for polyester resins. The modulus of the isolated resin drops to zero at about 120°C. [B07, p185]

The graphs above compare the normalized tensile (left) and compressive stresses (right) of vinyl ester (top) and phenolic (bottom) glass resins under different fire loads. The failure times of the phenolic laminate are the shortest, which is interesting considering its lower flammability. The less favorable performance of the phenolic laminate was attributed to heat-induced delamination and matrix cracking, which is more extensive than for the vinyl ester laminate. Comparison of the tensile failure curves with those for compression loading underlines the significantly longer failure times for the tensile case. [B07, 191-197]

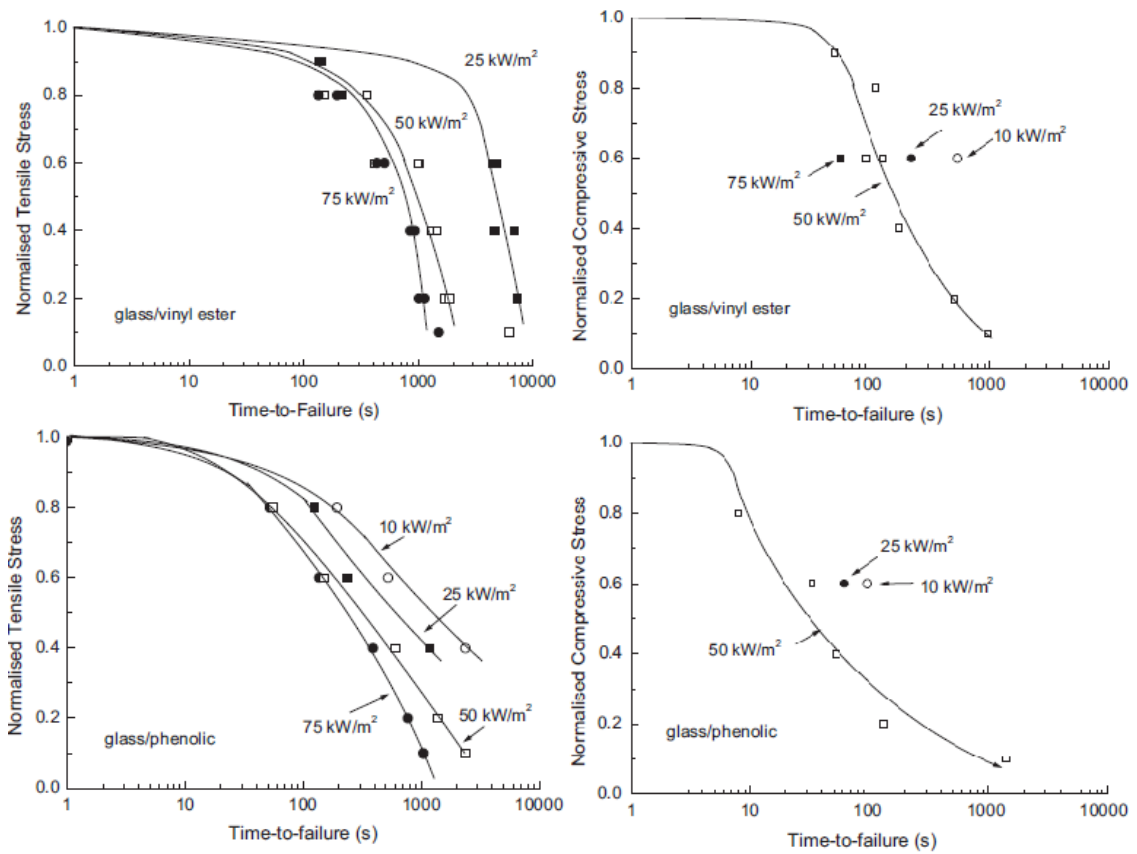


Fig. 9: Failure times under normalized tensile (left) or compressive (right) stresses of different resins [B07, p195, 196]

Post-fire Properties of composites

The graphs below show the post-fire flexural strength of different thermoset (left) and thermoplastic- and epoxy composites (right). The test specimens were loaded with a constant 25 kW/m² heat flux for twenty minutes. For the thermoset composites a generally very high reduction in strength can be seen. A disturbing feature is that the post-fire strength of epoxy based composites diminishes very rapidly, due to the flammability of the epoxy matrix. This is a large problem because epoxy is often used for high strength applications such as bridge engineering. [B07, p217] The thermoplastic resins (right) are able to retain a much higher strength than the thermoset resins. Most probably this is due to the higher decomposition temperature. [B07, p225]

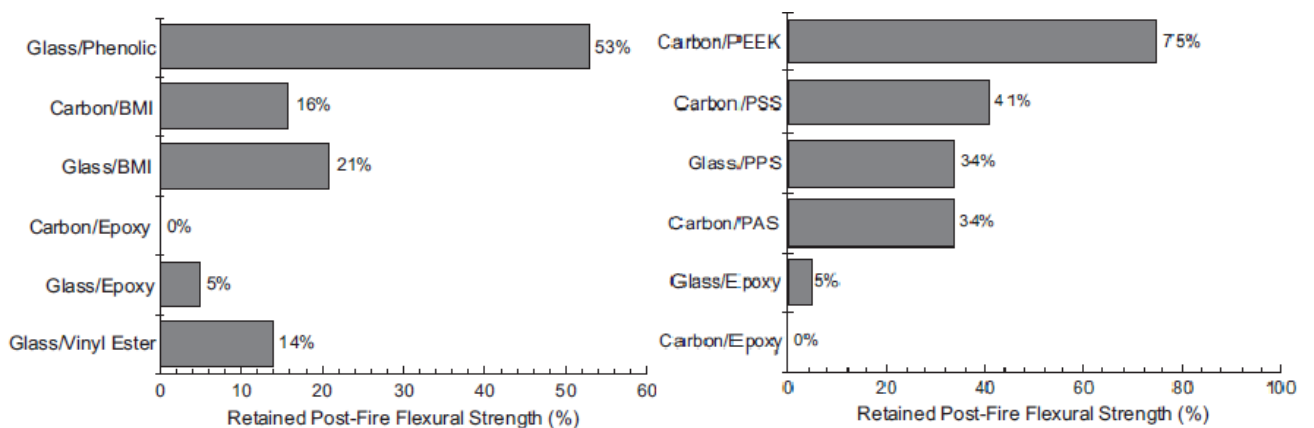


Fig. 10: Retained post-fire flexural strength of different thermoset (left) and thermoplastic (right) composites [B07, p217, 226]

4.2.2.8 CONCLUSION ON THE FIRE PROPERTIES OF VIRGIN ASSEMBLED COMPOSITES

One very important conclusion of this chapter is that the matrix is the governing factor for the fire behavior of FRP composites. The reinforcement fibers exhibit much better fire resistance properties, therefore high fiber contents in excess of 60%, as needed for structural application in bridge engineering are advantageous for the fire behavior.

Next to that thickness of composite laminate is another governing factor in the fire resistance and – reaction. Laminates with thicknesses in excess of 10mm to 15mm have a much better fire resistance than laminates with thicknesses under 5mm.

Another important conclusion of this chapter is that the fire behavior of ‘virgin’ FRP composites, thus composites without added fire protection measures, have insufficient capacity to provide a structurally safe bridge, even after small fires.

Just considering the fire behavior of ‘virgin’ fiber reinforced polymer composites, glass fiber phenolic composites with high glass fiber contents in excess of 60% would be the most fitting material. However, even this material only retains 53% of its flexural strength after 20 minutes of exposure to a 25kW/m^2 heat flux [ch. 4.2.2.7, Fig. 10]. Also, the back face temperature buildup behavior and the failure times under constant heat flux of phenolic matrices can be even worse than that of other matrix systems, leading to a fast spread of fire and/or high temperatures and sudden failure: Typical failure times of FRP composites for medium heat fluxes of 75 kW/m^2 are not bigger than 100 seconds. Next to that the FRP composites compared in [ch. 4.2.2.7, Fig. 3, right] all show very large heat release rates for the maximum heat flux of 100 kW/m^2 . The heat release rate of glass phenolic composite is about 100kW/m^2 , which is still about 40% of glass epoxy composite with a heat release rate of 250kW/m^2 . The latter composite is considered to be amongst the most flammable FRP composite materials available.

This chapter made clear that the use of ‘virgin’ FRP composites in traffic bridge engineering is not possible when application of traffic fire safety standards is obligatory. Therefore it is inevitable that fire protection measures have to be taken, both passive, to protect the ‘virgin’ FRP material and active, to quickly contain and eliminate occurring fires.

4.3 POSSIBLE FIRE PROTECTION MEASURES

As described in the chapter before, passive fire protection methods are of obligatory need when designing large structures such as traffic bridges made of fiber reinforced polymers. In this chapter the available protection measures are recalled from the literature study [LS, ch. 4.3.7, p165] in a somewhat abbreviated form. Furthermore they will also be compared and quantified, whenever possible. The measures described here mostly concern the matrix, since this is the main source for the poor structural performance of composites under fire load, as described in the conclusion of the chapter before. Although applications of nano-composites for fire protection of FRP composites are starting to emerge in the market, they are not considered here as fire protection measure that can be applied in practice in such a large scale. For more information see [LS, ch. 4.3.7.6, p181-183]. Other (highly efficient) methods described here function by encasing the composite.

4.3.1 FLAME RETARDANT FILLERS

In this chapter the information collected and presented in the literature study [LS, ch. 4.3.7.1, p167-171] will be summarized. The most important parts of this section of the literature study that will influence the design choice on the passive fire protection measures will be given here.

Fillers are inorganic non-reactive compounds that are added to the polymer during the final stages of processing to reduce the flammability of the finished product. The filler particles are under $10\text{ }\mu\text{m}$ in diameter, and often in the submicron range. The particles are blended into the liquid resin. Most polymers

require a high loading of filler to show an appreciable improvement to their flammability resistance, and the minimum volume content is usually about 20% and the average content is typically 50 to 60%. Fillers are often used because of their low cost, relatively easy addition into the polymer, and high fire resistance. It is important to note that fillers are rarely used alone, but instead are used in combination with other flame retardants to achieve a high level of flammability resistance. There are two classes of fillers – inert- and active flame retardants – which are distinguished by their mode of action. [B07, p241]

The main mechanism of inert flame retardant fillers is the reduction of the fuel load by diluting the mass fraction of organic material in a composite by the addition of a non-combustible filler. Obviously, for this mechanism large filler loadings of 50% to 60% are needed. The most commonly used composites are silica, calcium carbonate and carbon black. Sometimes simple hydrated clay silicates such as talc, gypsum or pumice are used.

Active fillers are more effective than inert fillers because they do not only operate as flammable mass reducer and heat sink, they also function in the condensed phase by decomposing at elevated temperature via an endothermic reaction that can absorb large amounts of heat. The decomposition of the filler also yields a large amount of inert gases, such as water vapor and carbon dioxide, which diffuse into the flame where they dilute the concentration of flammable volatiles. To achieve a substantial reduction in flame retardancy, medium to high filler loadings of 20% to 60% are needed. A diverse range of metal oxides and metal hydroxides are used as active flame retardant filler, although the most common is aluminum trihydroxide, $Al(OH)_3$ or 'ATH'.

A general problem with flame retardant fillers is the high loading level required. High loads of filler also depreciate the mechanical properties of the composites, thus are not very suitable for high strength applications. However, when ATH is used in combination with phenolic resin systems very good results can be gained with lower loading levels. The graph below shows some of the improvements on fire reaction properties due 30% fill ratio of ATH in glass phenolic composite subjected to a heat flux of $50kW/m^2$.

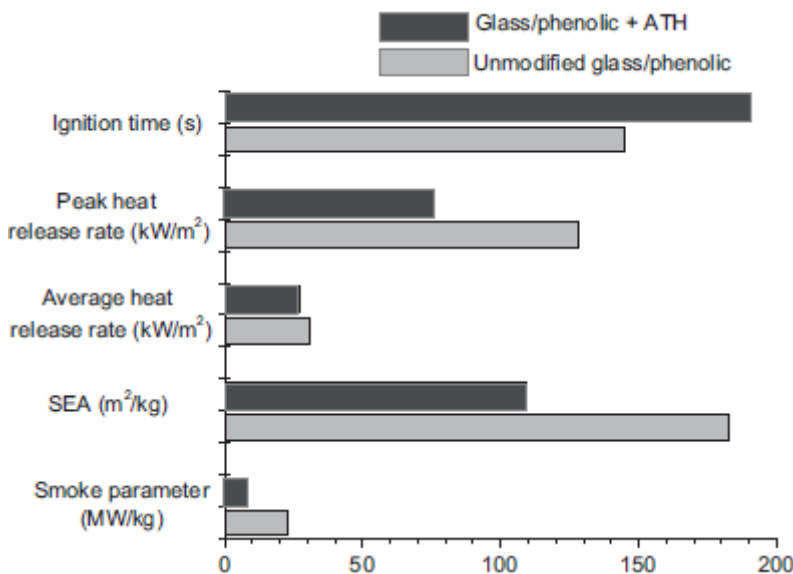


Fig. 11: Effect of 30% ATH fill on the fire reaction properties of a glass phenolic composite subjected to a heat flux of $50kW/m^2$ [B07, p248]

4.3.2 FLAME RETARDANT POLYMERS

In this chapter the information collected and presented in the literature study [LS, ch. 4.3.7.2, p171-175] will be summarized. The most important parts of this section of the literature study that will influence the design choice on the passive fire protection measures will be given here.

Flame retardant polymers are available in two main groups, organic and inorganic polymers. Both function by structurally modifying the polymer chains and thereby increasing the thermal stability by incorporating aromatic and heterocyclic ring structures into the main chain, and minimizing the presence of H, N and O and thus increasing the strength of the molecular chain bonds. Not only is the decomposition temperature of a polymer increased by this modification, but the mass fraction of flammable volatiles is reduced which lowers the heat release rate: thus an effective technique for improving flammability resistance.

The most common organic flame retardant polymers are halogenated polymers, made by incorporating halogen into the molecular network structure of the resin via co-polymerisation. As an example, flame retardant epoxy can be produced using a brominated monomer derivative of bisphenol A. Ignition time, heat release rate and smoke parameter all drastically improve due to bromination of the polymer. Generally improvements are better than when using flame retardant fillers. Note that for good flame retardant properties the bromine content in the polymer must be over 20%. [B07, p261] An exemption for these high loading rates is the use of phosphorous, for a loading rate of only 3%, this method reduced the peak heat release rate of carbon epoxy composite by 25% and the average heat release rate by 55%.

Inorganic flame retardant polymers such as geopolymer, POSS, and 'FyreRoc' have even more promising characteristics, they can reduce flammability and fire reaction by almost 100% while not negatively affecting the mechanical properties of the 'virgin' FRP composite material [LS, ch. 4.3.7.3, p174-175]. However these so-called ceramic composites have only been applied in small scale, high cost applications. Therefore application in large civil structures such as bridges is very unlikely and expensive.

4.3.3 FIRE PROTECTIVE SURFACE COATINGS

In this chapter the information collected and presented in the literature study [LS, ch. 4.3.7.5, p175-181] will be summarized. The most important parts of this section of the literature study that will influence the design choice on the passive fire protection measures will be given here.

A common method to protect composites from fire is to use an insulating coating. This method has the general advantage of not negatively affecting the mechanical properties of the 'virgin' FRP material. There are three major classes of insulating coatings: flame retardant polymer coatings, thermal barriers, and intumescent coatings. Flame retardant polymer coatings are inherently fire resistant organic resins or inorganic materials, applied as thin film. The most used coatings are phenolic, brominated resins and alkyd resin. A limitation of these coatings is the maximum coating thickness of 2mm to 3mm, limiting their protection period to short time spans. It is also possible to apply inorganic polymer coatings such as the already described geopolymer and POSS, these can be applied with thicknesses up to 8mm to 10mm.

Thermal barriers are usually ceramic-based materials that are non-flammable and have low heat conducting properties. Examples are silica and Rockwool mats and sprayed films such as zirconia. These materials can drastically reduce the minimum incident heat flux needed to ignite a composite from 15kW/m^2 to 35kW/m^2 . An unprotected glass polyester composite starts to char after about 30 seconds and completely burnt through after 17 minutes. Using a thermal coating as protective layer leads to delaying the charring moment to about 11 minutes after ignition and postponing burn through well after 30 minutes. However to obtain substantial long-term fire protection with thermal (ceramic) coatings, thicknesses of about 10mm to 20mm are needed. [B07, p279] This adds to the weight and dimensions of the structure and is not advantageous in the case of a truss traffic bridge with a lot of surface area. Next to that, the price of most ceramic coatings is also very high, making large-scale application costly.

Intumescent materials provide fire protection by foaming and swelling under elevated temperatures. Intumescent coatings consist of a multitude of compounds. The four main types of compounds are carbon-rich (carbonific) compound, inorganic acid or acid salt, organic amine or amide and a blowing agent

(spumific). These compounds undergo a series of decomposition reaction and physical processes almost simultaneously in order to function well as fire retardant. Having very small coating thickness under 3mm, good intumescent coatings expand to 50 to 200 times of their original volume under fire load. They thereby form a fine-scale multicellular network with cell sizes of 20 μm to 50 μm and a wall thickness of 6 μm to 8 μm . A recent development in the field of intumescent is the addition of graphite flakes, which expand up to 100 times on heating and improve the effectiveness of the insulating layer. Several additives can be incorporated into the intumescent mix, including agents that control the cell thickness, antioxidants, thickeners, pigments and milled fibers for structural reinforcement. The pictures below show an intumescent of 0,8 mm thickness (left) which has expanded about 65 times to a thickness of 52 mm after fire load (right) [B07, p281-282]



Fig. 12: Intumescent coating before (left, thickness = 0,8 mm) and after (right, thickness = 52 mm) fire loading [B07, p282]

Intumescent coatings are excellent heat insulators that slow the rate of heat transfer into composite laminates in fire. They can also be extremely effective in delaying combustion, suppressing flame spread, reducing the heat release rate, and lowering the smoke density of composite materials. The graph below on the left compares the temperature rise in a composite panel with and without such a coating. The temperature was measured at the back-face of the panel. The results are impressive, even after an exposure time of 60 minutes the intumescent protected composite temperature does not rise over 200°C (compared to furnace temperature of almost 1000°C. The graph below, on the right shows the effect of incident heat flux on the ignition time of glass polyester composite with and without an intumescent coating. Ignition was delayed considerably by the intumescent coating, with the thick mat providing greater protection because it was able to swell more than the film. [B07, p282]

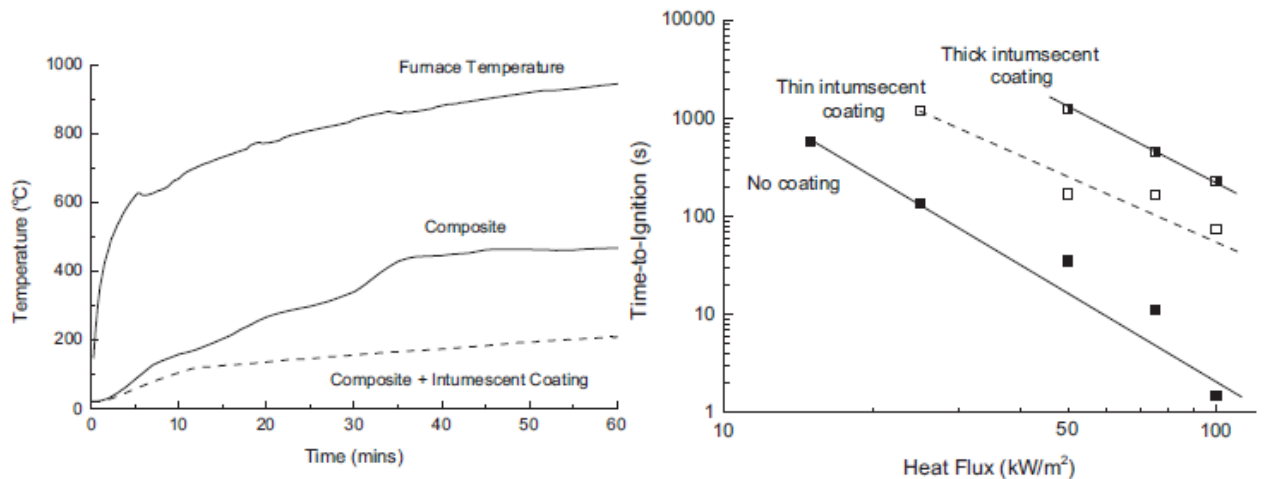


Fig. 13: Left: Back-face-temperature of an intumescent protected composite panel. Right: Ignition time of a glass polyester composite protected with thin and thick intumescent coatings at different heat fluxes [B07, p283]

The graphs below show the impressive results that can be achieved with fire protective surface coatings. The left graph shows the post-fire flexural strength of glass polyester composite with different surface coatings. Note that under a heat flux of 100 kW/m² the normalized flexural strength of the composite even exceeds 1,0 due to the excessive swelling. The right graph shows the correlation between heating time and post-fire flexural strength of protected and unprotected glass polyester composite. It can be seen that a protective intumescent layer drastically improves the post-fire strength. [B07, p234, 273-274]

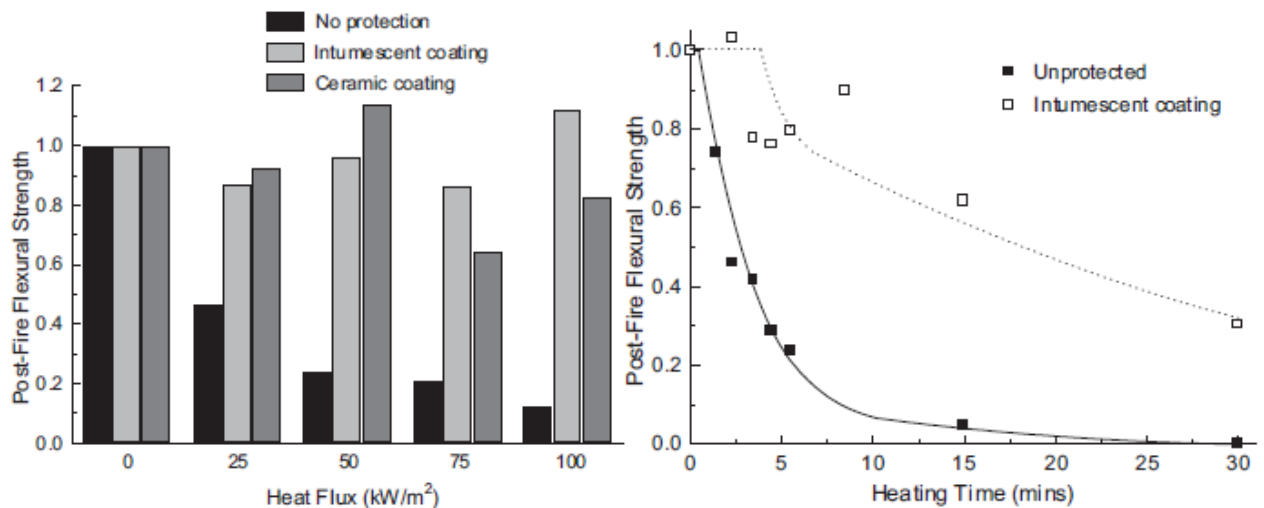


Fig. 14: Post-fire flexural strength of glass polyester composites with different coatings. Right: Correlation between heating time and post-fire flexural strength of protected and un-protected glass polyester composite. [B07, p234]

4.4 DESIGN FIRE

In this chapter the choices for the design fire that is to be used will be made and explained, these include the performance criterion that was chosen, the fire curve that is applicable to this bridge design and the maximum fire load that is expected to be present on the bridge.

4.4.1 PERFORMANCE CRITERION TO BE USED

The performance criteria for construction products and building elements are prescribed in 'NEN-EN13501, Fire Classification of construction products and building elements – Part 2: Classification using data from fire resistance tests, excluding ventilation services.' [NEN-EN 13501-2:2007+A1:2009] For the classification of load bearing elements without a fire separating function, as is the case with all structural elements of the bridge, since the bridge only has one compartment. The relevant performance criterion for load bearing elements is R. The following classes are defined: R15, R20, R30, R45, R60, R90, R120, R180, R 240 and R360, wherein the numbers behind R stand for the time in minutes that the element can resist a fire without losing its structural function.

The loadbearing capacity R is thus the ability of the element of construction to withstand fire exposure under specified mechanical actions, on one or more faces, for a period of time, without any loss of structural stability. The criteria which provide for assessment of imminent collapse will vary as a function of the type of loadbearing element. For flexurally loaded elements e.g. floors, roofs this shall be a rate of deformation (rate of deflection) and a limit state for the actual deformation (deflection). [NEN-EN 13501-2:2007+A1:2009, ch. 5.2.1]

Since performance criteria in excess of R60 are only used for buildings, in which users have to cover large distances in order to escape fire hazard, such as high rise buildings where classes higher than R120 are not uncommon, it is clear that the resistance criteria for a bridge with a maximum span of 49m, see [ch. 5.3] are much less severe. The only similar reference project in respect to fire safety is the 'Bridge Pavilion in Zaragoza, built for the EXPO2008, described in the literature study [LS, ch. 6.3.2, p207]. Here a resistance criterion of R45 was applied for the parts of the bridge that were used for pedestrian thoroughfare only. These parts of the bridge are much more complex than the bridge to be designed; they feature two decks with varying width. With two spans of 185m and 85m they furthermore have much larger spans than the bridge to be designed. Finally, these bridge parts are also used for a far larger number of pedestrian users and escape is only possible by foot.

All these differences lead to the conclusion that a fire resistance of R45 is not necessary for the bridge that is to be designed. The background on the time that is included in the structural fire resistance is the time needed for evacuation of all users to safety, thus in this case, of the bridge. Due to the limited span of the bridge, the large width of the emergency escapes (equal to the width of the bridge deck), and the fact that two emergency escapes are always provided (at both ends of the bridge), it is reasonable to use a lighter fire resistance class than in the reference project [LS, ch. 6.3.2, p207]. It is therefore chosen to use the R30 fire resistance class as the performance criterion for all structural elements of the bridge.

4.4.2 FIRE CURVE TO BE USED

The hydrocarbon fire curve is the designated fire curve for more severe fires, involving flammable materials like petrol gas, chemical, gasoline etc. [NEN-EN 13501-2:2007+A1:2009, ch. 4.1, p13] The hydrocarbon curve is applicable when petrol fires could occur, such as for example car fires, petrol or oil tankers and chemical tankers. It is thus the only applicable fire curve for a semi-enclosed heavy traffic bridge, since tanker trucks can always be present during the service-life of the bridge. The hydrocarbon fire curve reaches its maximum temperature of 1100°C just under 30 minutes, making it the most severe fire loading curve of [NEN-EN-1991-1-2].

$$\theta_g = 1080(1 - 0,325e^{-0,176t} - 0,675e^{-2,5t}) + 20 \quad (4.1)$$

$$\theta_g = \text{gas temperature } [^{\circ}\text{C}], t = \text{time } [\text{min}]$$

$$\alpha_c = 50 \text{ W/m}^2\text{K coefficient of heat transfer} \quad (4.2)$$

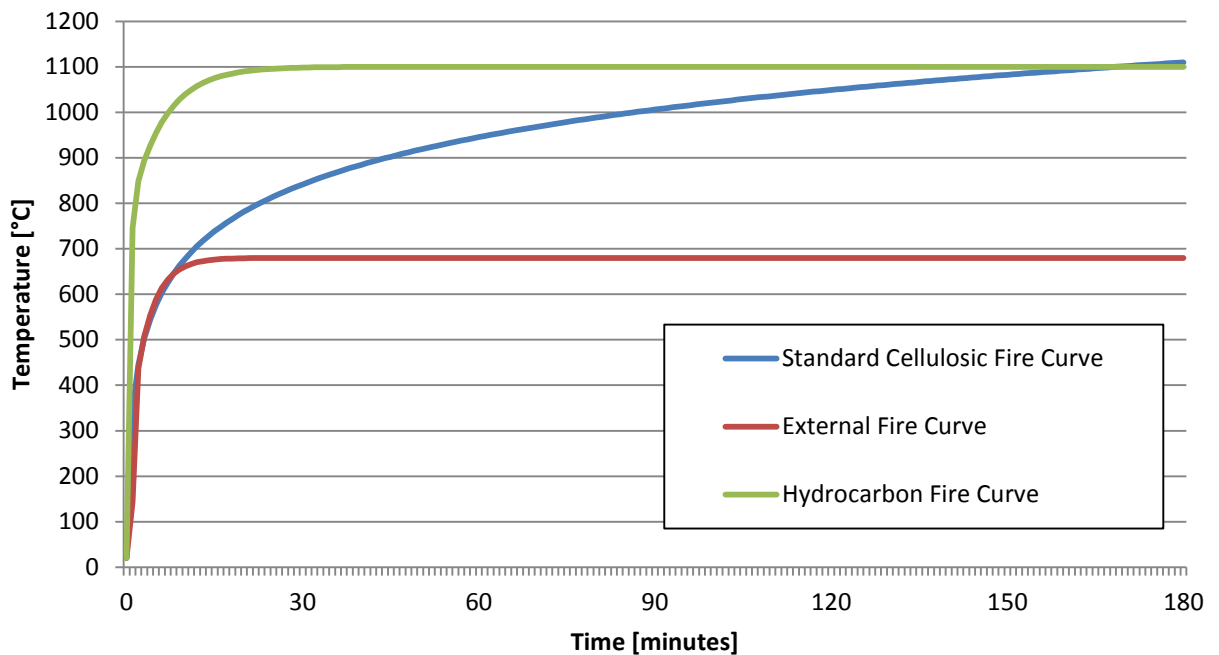


Fig. 15: Standard fire curves, including the hydrocarbon fire curve [NEN-1991-1-2-2002, p23]

Using the performance criterion of R30 derived before, and inserting this value into the hydrocarbon fire curve equation yields a maximum temperature at $t = 30 \text{ min}$ of $T(30) = 1100^{\circ}\text{C}$.

4.4.3 MAXIMUM FIRE LOAD AND FIRE SCENARIO

The maximum fire load that has to be dealt with on traffic bridges, parallel to the demanded hydrocarbon fire curve, is a fire occurring in or around a gasoline tanker truck. This is the most severe fire scenario that

can occur during regular service life. The accompanying size of an equivalent gasoline pool, heat release rate, smoke generation and maximum temperature can be found in the table below [LS, ch. 4.2.2.2, table 34, p143] that was taken from the American infrastructure fire safety code [NFPA502, p19]. The maximum temperature of 1000°C correlates very well with the hydrocarbon fire curve.

Cause of fire	Equivalent size of gasoline pool [m ²]	Heat Release Rate [MW]	Smoke Generation Rate [m ³ /sec]	Maximum Temperature [°C]
Passenger Car	2	8	20	400
Van	5	15	40	550
Bus or Truck	10	30	60	700
Gasoline Tanker	30-100	120	100-200	1000



Table 8: Fire loads due to different road vehicles fires [NFPA502, p19]

4.5 CHOICE ON FIRE SAFETY MEASURES

In this chapter a choice on the application of fire safety and protection measures will be made. Although some researchers have performed many tests on the fire safety of FRP composites, for example A.P Mouritz et al. in 'Fire Properties of Polymer Composite Materials' (2006) [B07], there is no unambiguous theoretical methodology to exactly quantify the fire resistance of particular measures such as for example the added fire resistance time of a FRP composite when an intumescent coating of certain type and thickness is applied.

It is therefore chosen to base the choice of fire protection measures not on calculated quantities as normally done in the engineering practice but furthermore on qualitative observations, thoroughly backed by applicable literature, such as described before. Normally, when insufficient data is available, an engineer reverts to lab-tests to investigate the unknown behavior and quantify the outcomes. Based on these tests, design choices are made. If the time and resources for testing, or in this case excessive fire lab-testing of FRP composites, is not available a qualitative analysis of the available information is the next best choice. In this case the design choices are based on that analysis, which was carried out in the literature study [LS, ch. 4, p135-183] and recalled and refined in this chapter [ch. 4].

4.5.1 MEASURES CONCERNING THE BRIDGE

Concerning the fire safety, an important feature of a traffic bridge and its bridge deck is the ability to drain spilled liquids such as flammable fuels in a fast and efficient way. That way spilled fuel cannot accumulate on the bridge deck in a large pool and pose a potential source for a disastrous fire. In order to achieve this, the first measure that is taken is the providence of a drainage system.

In the chapter on the design requirements for traffic bridges [ch. 5.1] it will be shown that the Dutch codes prescribe a perpendicular slope of at least 2%. [RWS-SATO2005, ch. 2.4.2.2, p70] [ch. 6.1.1] The main reason to prescribe this slope is the flow off of rainwater. However, this slope also poses a good mechanism to drain flammable fuels in the case of a spill of liquids.

The perpendicular slope of the bridge deck surface to be applied is 2% and the direction of flow-off will be from the centerline of the bridge to the sides. At the sides of the main road there will be drains that will let rainwater as well as fuels flow off through a network of pipes under the bridge deck.

In building design it is advised to use an active fire suppression system or sprinkler system for buildings higher than 70m, fire compartments larger than 1.000 m² or to lower the fire retardancy material demands but still achieve the same fire resistance class. [NEN-Praktijkids Brandveiligheid, ch. 5.9, p223-224] Since there are no fire proof dividing walls present on the bridge the complete inside of the cylindrical bridge has to be considered as a single fire compartment. Most probably the size of this compartment will be bigger

than 1.000 m², thereby making a sprinkler system necessary. However, the bridge to be designed does not completely separate the inside of the bridge from the outside. That way natural ventilation is provided, leading to a much better heat dissipation than in typical enclosed buildings.

This is one reason why it is chosen not to use active sprinkler systems. The second reason is that the passive fire protection measures described in the chapter below, concerning the fire resistance of the structural elements are abundant to achieve the desired fire safety level in case of the design fire described in [ch. 4.4] The third reason not to choose a sprinkler system as active fire protection measure is the high cost associated with systems of this kind. Research into the application of sprinkler systems for road tunnels and even for bridges has only recently been initiated and is certainly not widely used for the fire suppression in infrastructure projects. [P103, p8-9]

For the application and placement of fire extinguishers again a comparison is made with the rules for building design. The Dutch code 'NEN 4001, Fire protection – Planning of portable and mobile fire extinguishers' [NEN 4001] prescribes that a building has to be divided in zones of a particular size, in which at least one fire extinguisher of a certain size needs to be present. [NEN 4001, table 2, p11-12] Furthermore the type of fire extinguisher is also prescribed [NEN 4001, table 1, p8]. In the case of LPG or gasoline fire, which are also the substances considered in the design fire for the bridge before [ch. 4.4.3], the code prescribes fire class C (gasses) and thus the use of powder fire extinguishers.

Since bridges are not covered in the Dutch code, the most severe scenario of the code is used for the bridge. For fires in industrial rooms the code prescribes one fire extinguisher of 9kg-12kg per zone of 150 m². Estimating the size of the bridge deck as prescribed below, this leads to a total number of 8 powder fire extinguishers of 9kg-12kg, for width and span values see [ch. 8.3]

$$A_{bridgedeck} = l_{span} * b_{bridgedeck} = 49 * 24,82 = 1218,8m^2 \quad (4.3)$$

$$N_{fire-extinguisher} = \frac{A_{bridgedeck}}{A_{firezone}} = \frac{1151,5}{150} = 8,1 \cong 10 \quad (4.4)$$

Since the code [NEN 4001] also prescribes that the maximum distance from every part of the bridge deck cannot exceed 20m [NEN 4001, ch. 4.4.1.3, p12] these 8 fire extinguishers need to be evenly distributed alongside the bridge. The fire extinguishers will be placed next to heavy traffic roads, thus between the main road and the bicycle paths, leading to two rows of 5 fire extinguishers with a spacing of $\sqrt[4]{9/5} = 9,8m$. For more information on the determination of the exact layout of the bridge deck and span of the bridge see [ch. 5.2] [ch. 5.3] [ch. 8.3]

4.5.2 MEASURES CONCERNING THE MATERIAL

The choice for passive material protection was made using the following guideline: using fire protection that can easily assure the R30 fire resistance performance criterion whilst not largely negatively affecting the mechanical properties of the 'virgin' material, the building costs and the overall appearance of the bridge.

Using this guideline a combination of an intumescent coating fire protection layer and a low load filler system is chosen. Amongst all coating systems, the intumescent coating is the one which can achieve very high levels of protection while also having a very small thickness, smaller than 3mm. Next to that intumescent coatings have been applied very often in steel structures and even for the increase of the fire safety of bridges with a steel load bearing system as in the case of the 'Hafenstrassenunterfuehrung Bridge', in Frankfurt, Germany [LS, ch. 6.3.1, p205]. Here a total surface of 34.000 m² was coated with a 0,5mm to 2mm thick layer of 'Permatex' 'Unitherm ESA 38092' intumescent steel coating. The total added weight due to the coating is only 40.000 kg. Thereby this bridge could maintain a R30 fire resistance performance criterion.

Another great advantage of an intumescent coating system is the ease of application in the production process of the fiber reinforced polymer structural elements. The layer can easily be applied in a gel-coat layer that is used to shield not only the 'virgin' material from environmental influences but also to protect to intumescent layer from the same influences.

Next to the intumescent layer it is chosen to use a fire retardant protective filler system for an added degree of fire retardancy. As described in the literature study [LS, ch. 4.3.7.2, p 173-174] addition of small loading levels of phosphorous can drastically improve the fire performance of composites. It is therefore chosen to use the phosphorous filler system as fire retardant filler. The most common method for adding phosphorus is blending phosphorous filler compound into a polymer during processing. The most common types are elemental phosphorus, ammonium polyphosphates and triallylphosphates. Phosphorus can also be incorporated into the molecular structure by copolymerization of the resin with a reactive organic phosphorous monomer or halogenated phosphate. The flame retardant efficiency of phosphorous increases with the oxygen content of the polymer. [B07, p266-267] Very small amounts of phosphorous lead to the best results, the vertical burn time does not substantially reduce for more than 3% phosphorous content. The heat release rate shows best results for about the same amount of phosphorous. [B07, p267-268]

As described before [ch. 4.4.1], the main performance criterion for general load bearing systems in structures is the time that the structure can maintain its structural load bearing capacity under fire load. However the appropriate code [NEN-EN 13501-2:2007+A1:2009] also prescribed the so-called integrity criterion for certain elements of structure: 'Integrity E is the ability of the element of construction that has a separating function, to withstand fire exposure on one side only, without the transmission of fire to the unexposed side as a result of the passage of flames or hot gases.' [NEN-EN 13501-2:2007+A1:2009, ch. 5.2.2, p16]

In the case of the traffic bridge that is to be designed, the bridge deck is the part of the structure that not only needs to retain its load bearing capacity but also needs to retain its integrity for the same amount of time in order to be able to provide all users with safe means of escape and evacuation. Therefore, the bridge not only has the performance criterion R30, but also RI30, wherein I stands for 'integrity'. Since these demands are somewhat stricter than the demands for all other parts of the structure, and foaming up of the bridge deck surface is not very helpful in the case of an emergency evacuation it is chosen to use another system for the bridge deck.

The bridge deck surface will be covered with a thicker thermal barrier, such as a silica mat or fabric with a thickness of about 10-15mm, as described before [ch.4.3.3]. That way integrity as well as structural load bearing capacity of the bridge deck is secured for a period of at least 30 minutes. This barrier can be applied during production of the bridge deck elements as described later on, or after the placement of the whole bridge deck, but before the application of the wearing surface [ch. 11.1.6].

4.5.3 VALIDATION OF FIRE PROTECTION MEASURES

After choosing the passive protection measures described before, an effort was made to validate this choice by using other reference studies on this subject. Therefore one recent and renowned PhD research was chosen, in which the fire safety of FRP structural systems for buildings was investigated. This research was carried out by C.D. Tracy (2005) for the EFPL Lausanne, Switzerland under the supervision of the FRP expert Prof. T. Keller [T16]. In this research a fire resistant FRP building system was developed. For the fire resistance this system uses an active water cooling pipe network inside of the FRP structural elements. Although the demands for buildings as well as the active fire protection system differ somewhat from the fire safety for traffic bridges, in some parts both subjects share similar fire resistance measures.

An important conclusion of the research on fire resistant FRP building system by C.D Tracy, was that of all passive FRP fire resistance measures, as described in [ch. 4.3] and [LS, ch. 4.3.7, p165] the "best methods for promoting char production involve the use of phosphorous-based fire retardants, intumescent surface layers, phenolic resins or nano composites" [T16, p99]. This is exactly the same conclusion as drawn in the theoretical research given in the chapter before. Of these measures the phenolic resin dropped out because of the limitation in freedom-of-choice on the matrix material to be used, see also [ch. 3.2]. The nano-

composites are not chosen because of their early stage of development and high price, see also [ch. 4.3] and [LS, ch. 4.3.7.6, p181-183].

Furthermore C.D. Tracy also states that: “[...] while these methods are effective for short durations (<30 min), they make little difference in the range of exposure times that load-bearing building components are expected to withstand. [T16, p99] Since a performance criterion of a fire resistance of R30 was chosen before [ch. 4.4.1] this does not pose a serious disadvantage for the passive measures that were chosen. In other words: since the design fire resistance of the bridge to be designed is 30 minutes or less, sufficient fire protection is provided by the passive fire protection measures as described in [ch. 4.5.2]. For fire resistance times in excess of 30 minutes, which are customary in (high rise) buildings, where performance criteria of R90-R120 are certainly no exception, passive FRP fire protection measures are not sufficient. Here, active fire suppression systems such as sprinkler installations or inert water cooling circulation systems have to be provided. [T16, p99-100]

Finally the described research also gives a recommendation on the simultaneous use of multiple (passive) fire protection measures: “[...] no passive or active method is without weaknesses or compromises. For this reason a combination of methods is usually employed. [...] a component may be fire retarded using a combination of ATH and res phosphorous, and then covered with an intumescent layer [...]. [T16, p100] This recommendation correlates very well with the choice of using a low-volume of a phosphorous filler system combined with an intumescent surface protection layer, as described in [ch. 4.5.2].

In conclusion it can be said that the chosen fire safety and fire retardancy measures are sufficient to achieve a fire resistance of R30. This conclusion is backed by other scientific researches, mainly [T16] by C.D Tracy. By also providing a quick run-off of flammable fuels on the bridge deck and sufficient fire extinguishers, as described in [ch. 4.5.1] the level of fire safety is further increased.

Part B

Design study & Parameter study

5. GEOMETRIC REQUIREMENTS OF THE BRIDGE

As described before in the literature study [LS, ch. 1.2, ch. 3.1] and in the introduction [ch. 1.1] the choice was made to design the fiber reinforced polymer bridge as a cylindrical truss bridge. The reasons are described again below. This structural shape combines the high bearing capacities of trusses with the slenderness of tube girders by transforming the traditional 2D truss bridge concept into a 3D cylindrical truss where the occurring forces are more evenly distributed between the members. Until now it has been used mostly in the case of pedestrian bridges, as described in the examples in the literature study [LS, ch. 6.1.1-6.1.8]. Because new developments in bridge engineering and –design usually occur first in the field of pedestrian bridges due to less stringent load demands, it is very promising to investigate whether this structural shape can be used for traffic bridges with higher load demands.

Next to the mechanical advantages of a cylindrical truss, it is also very slender and appealing, modern, innovative and futuristic, thus making it a perfect example of the cooperation of architect and engineer. Since this striking shape fits very well in modern architecture, and forms a real challenge for the engineer, it makes up a very interesting shape to study and analyze. Very little research has been done on cylindrical trusses as a load bearing system for heavy traffic bridges.

The next reason for the choice of this shape lies in the mechanical properties of fiber reinforced polymers. Currently all cylindrical truss bridges are made of steel; by nature steel has a very high modulus of elasticity, thus making it very deformation resistant, even with smaller cross-sections. To achieve the same stiffness as steel elements, which is the product of modulus and the element's second moment of area, fiber reinforced plastic elements need a higher second moment of area, and thus larger element dimensions. This is caused by the inherently lower modulus of elasticity which fiber reinforced polymers generally exhibit. A cylindrical truss bridge can be seen as a large diameter tube, which makes it a perfect shape for the application of fiber reinforced plastic as building material.

Also, Rijkswaterstaat expressed one of their future visions of so-called "traffic tubes". [P23, p28, p33] In this vision future highways will be placed inside large tubes or cylinders made of light weight structural materials such as fiber reinforced plastics. These tubes are both used as a load bearing system and as containment for noise and emissions, enabling highways through urban, densely populated areas without any disturbance. Tubular trusses could very well be a suitable solution to the traffic tube vision. The voids between the structural members can be filled up, or the whole tube can be covered by impermeable, sound insulating layers.

In the literature study all existing bridge types were investigated [LS, ch. 3.1] Among the arch bridges, the suspension bridges, the cable-stayed bridges, the girder bridges and the truss bridges, the last two bridge types seemed to be most suitable for the proposed span of 30-50m. The shape that is therefore most applicable for a design of this kind is a hybrid between a girder bridge and a truss bridge. Since even for this "simple" type of girder-bridge the use of fiber reinforced polymers has not been thoroughly investigated it should hopefully be a suitable material for efficient and feasible design and construction of heavy traffic truss-girder bridges.

5.1 SPATIAL DEMANDS OF THE BRIDGE USERS

To determine the dimensions of the bridge that is to be designed it is necessary to investigate the space demands for trucks, cars, bicyclists and pedestrians obliged by law in The Netherlands. Furthermore the size of the safety buffer zones needs to be quantified. In this chapter Dutch codes and rules will be investigated to obtain the needed free width and height for each user.

5.1.1 ROAD CATEGORY AND DESIGN SPEED

The Dutch legislating document “Rijkswaterstaat, Specifieke Aspecten Tunnel Ontwerp” (in English: specific aspects of tunnel design) [RWS-SATO2005], hereafter called SATO gives rules for different road types in tunnels. Since the bridge that is to be designed in the course of this research is in fact a tunnel-tube placed on pillars, because it fully encloses the bridge deck, this document is most applicable. First the road type for the bridge needs to be specified. In the scheme below the chosen road profile is marked by the orange arrow. The name of this road category is: “Buiten bebouwde kom, Hoofdcategorie B, Hoofdwegennet, III, 100 km/h, enkelbaans, weg met functie voor lange-afstands-verkeer [RWS-SATO2005, table 2.4.1, p70]. In short this means that the road that the bridge has to carry is meant for 2x1 lanes of traffic with a design speed of 100 km/h.

The corresponding perpendicular slope of the pavement has to be at least 2%, in order to let rainwater flow off. [RWS-SATO2005, ch. 2.4.2.2, p70]

5.1.2 HEAVY TRAFFIC REQUIREMENTS

The corresponding lane-width for roads of the above category with a design speed of 100 km/h is 3,25m. This value is measured between the lines and does not include them. Since the design width of a typical European lorry is set to 2,50m this value was chosen.[RWS-SATO2005, ch. 2.4.3.2, p83]

ONTWERPER						
BENAMING	Autoweg				Weg met geheel of gedeeltelijk geslotenverklaring voor langzaam verkeer (in elk geval gesloten voor (brom)fietsers)	
	Hoofdcategorie B				Hoofdcategorie C	
	Hoofdwegennet		Niet-hoofdwegennet		Niet-hoofdwegennet	
CATEGORIE	III	IV	III	IV	V	VI
WEG-OMGEVING	Alle situaties	Urbaan	Alle situaties	Alle situaties	Alle situaties	Alle situaties
ONTWERP-SNELHEID	100 km/h	80 km/h	100 km/h	100 km/h	80 km/h	60 km/h
DWARS-PROFIEL	Enkelbaans	Dubbelbaans	Enkelbaans	Dubbelbaans	Enkelbaans	Enkelbaans
KRUISPUNTVORM	Gelijkvloers ^a	Gelijkvloers	Gelijkvloers ^b	Gelijkvloers	Gelijkvloers	Gelijkvloers
KRUISINGSVORM	Ongelijkvloers	Ongelijkvloers	Ongelijkvloers	Ongelijkvloers	Gelijkvloers	Gelijkvloers
INDICATIE NETWERKFUNCTIE	Weg met een functie voor het langeafstandsverkeer	Weg met een belangrijke ontsluitingsfunctie voor een stad of agglomeratie	Wegverbinding tussen belangrijke kernen in een regio	Een belangrijke verbinding tussen kernen in een regio	Weg met een functie voor het middel-lange afstandsverkeer of ontsluitingsweg voor een regio	Weg van overwegend lokaal belang met een beperkte verkeersfunctie

Fig. 16: Road categories according to Rijkswaterstaat [RWS-SATO2005, table 2.4.1, p70]

The advised width for the lines that enclose the road to the side is 0,15m. The so called “kantstrook”, the strip of pavement between the line and the safety barrier has to be at least 0,45m wide. This value includes the width of the line. [RWS-SATO2005, ch. 2.4.3.2, p84]

The needed free height for trucks is set to 4,50m. This value is a combination of the design height of the vehicle, which is 4,00m; vertical movement of the vehicle, which is 0,20m and a safety margin of 0,30m. [RWS-SATO2005, ch. 2.4.4.2, p89] Since the design height of typical passenger vehicles is only 2,06m, the free height needed for passenger vehicles is significantly lower than that of trucks. The free height for the trucks needs to be guaranteed for the total width of the lane, the line width and the strip between the line and the safety barriers; in short, for the total width between the safety barriers at each side of the lane.

Furthermore the SATO also specifies a minimum ‘objectafstandsmarge’ of 1,50m for roads with a design-speed of 100 km/h. This value describes the minimum horizontal distance, measured from the inside of the right boundary of the lane, which all objects next to the road must have in respect to any object [RWS-SATO2005, ch. 2.4.4.1, p87]. Next to the use for emergency stops, this is also the reason for the provision of a small hard shoulder with a width of 1,50m. Due to the space restraints in a fully enclosed cylindrical load-bearing structure it was chosen not to provide a full hard shoulder, or emergency lane. The SATO only prescribes a compulsory emergency lane for highways.

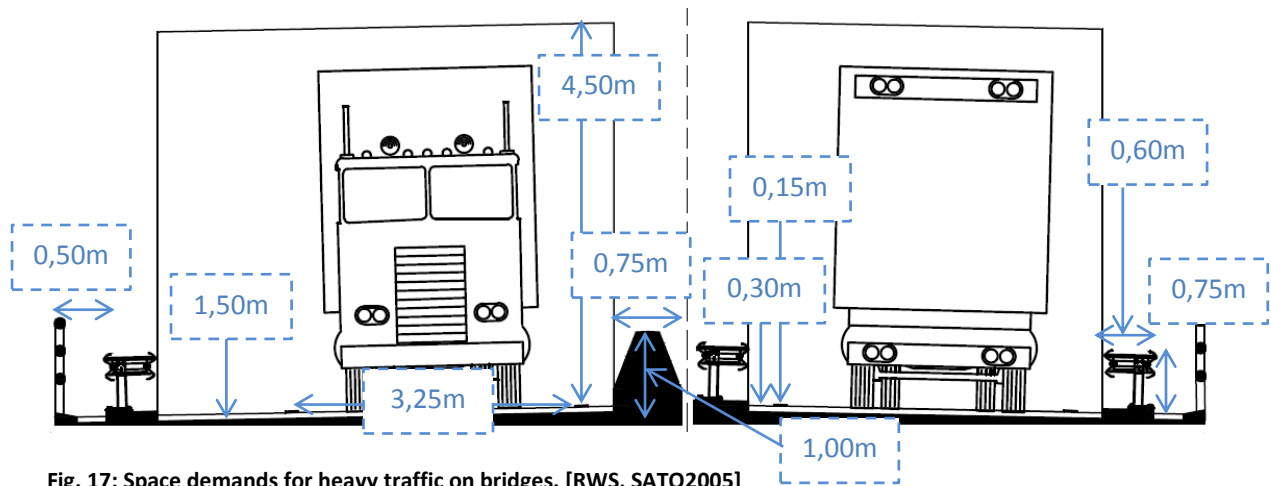


Fig. 17: Space demands for heavy traffic on bridges. [RWS, SATO2005]

In the layout of the heavy traffic road safety barriers are needed to prevent cars and trucks from escaping their dedicated space in the event of an accident. In this research two different kinds of safety barriers are used. The first safety barrier is the so-called ‘Stepbarrier’, which is of the type ‘geleidebarriere’ (guidance barrier) as defined by Rijkswaterstaat [RWS-SATO, ch. 5.4.2.1, p606]. The ‘Stepbarrier’ is used to separate the two driving lanes. It is placed longitudinally at the center of the bridge over the full length of the structure. See the drawing below for exact specification of the free-standing ‘Stepbarrier’.

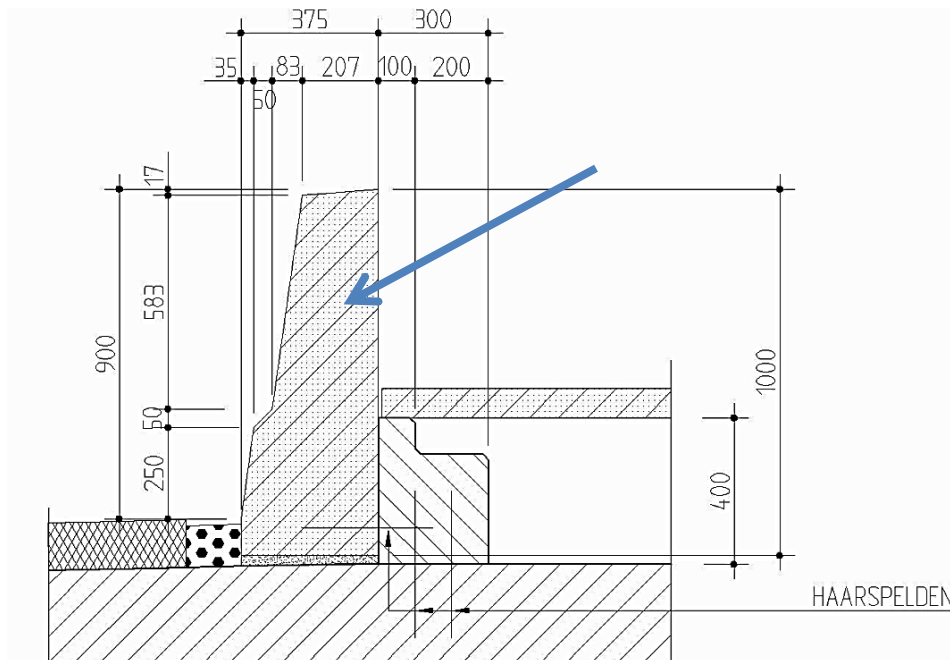


Fig. 18: Dimensions of the free-standing guidance barrier ‘Stepbarrier’ as defined by Rijkswaterstaat [RWS-SATO, ch. 5.4.2.1, p606]

The second kind of safety barrier is the ‘VLP 1LV 133-60’, which is of the type ‘geleiderail’ (guidance rail) as defined by the ‘Richtlijn voor het ontwerpen van autosnelwegen 1989, chapter 6, veilige inrichting van bermen’ (Dutch design guide for highway design 1989, chapter 6, safe layout of berms) [RWS-ROA1989, ch. 6] is used to protect the right side of both driving directions. That way it is prevented that trucks and cars loose track and collide with bicyclists, pedestrians or even the bridge load-bearing structure itself. This safety barrier type is most often used on traffic bridges in the Netherlands. The ‘VLP 1LV 133-60’ safety barrier has a relatively stiff behavior, in case of collision the maximum lateral deformation is limited to 0,30m-0,50m [RWS-ROA1989, ch. 6.4.2.4, p48-49]. The dimensions of this safety barrier are depicted below.

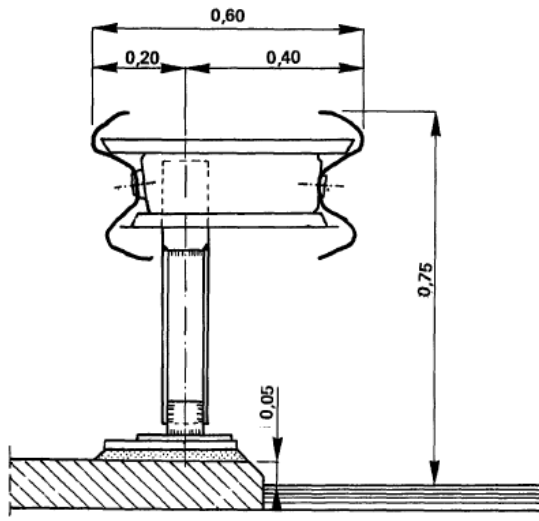


Fig. 19: Dimensions of the guidance rail 'VLP 1LV 133-60' as defined by Rijkswaterstaat [RWS-ROA1989, ch. 6.4.2.4, p49]

The last important rule for the design of heavy traffic lanes on bridges is the minimum asphalt cover thickness. This thickness is required to be at least 70,00mm by the 'SATO' [RWS-SATO2005, ch. 2.4.4.2, p89]. For uniformity reasons this cover thickness will also be applied for the bicycle- and foot paths. In obtaining a correct height-profile and in fitting all needed functions in the confined bridge space it is important to take this into account as well.

5.1.3 PEDESTRIAN REQUIREMENTS

The Dutch document for minimum free height and width requirements of footpaths is the 'Richtlijn voor het ontwerpen van niet-autosnelwegen' (in English: Regulations for the design of non-highways) [RWS-RONA1986], hereafter called 'RONA'. In this document the minimum width for footpaths on bridges is set to 1,50m, when being next to a bicycle path. Furthermore it is prescribed that between the bicycle path and the footpath a buffer zone of 0,50m needs to exist, with a slightly elevated surface [RWS-RONA 1986, ch. 2.1, p2]. The free height above the footpath is set to at least 2,25m. [RWS-RONA1986, ch. 1.2, p1] Since the demand for the free height is a bare minimum, it was chosen to set the free height for footpaths to 2,50m. This poses minor additional space demands, since the free height of the neighboring bicycle path is set to a minimum of 2,50m [ch. 5.1.4]. However it does increase the spacious feeling of pedestrian users significantly and is therefore an advisable adaptation of the free height.

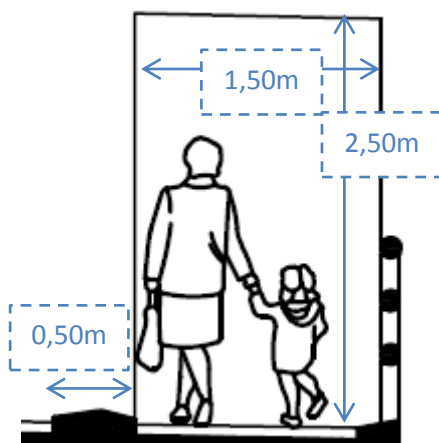


Fig. 20: Space demands for footpaths on bridges [RONA1986, ch. 1.2, p1, ch. 2.1, p2]

5.1.4 BICYCLIST REQUIREMENTS

The same document as for pedestrians also holds for bicyclists in the Netherlands. The RONA gives a minimum width 2,50m for bicycle paths that are used in one driving direction only. The minimum width for a bicycle path used in two driving direction is 3,5m. [RONA1986, ch. 2.1, p2] The free height that is to be provided for bicycle paths according to RONA is 2,5m. [RONA1986, ch. 1.2, p1]

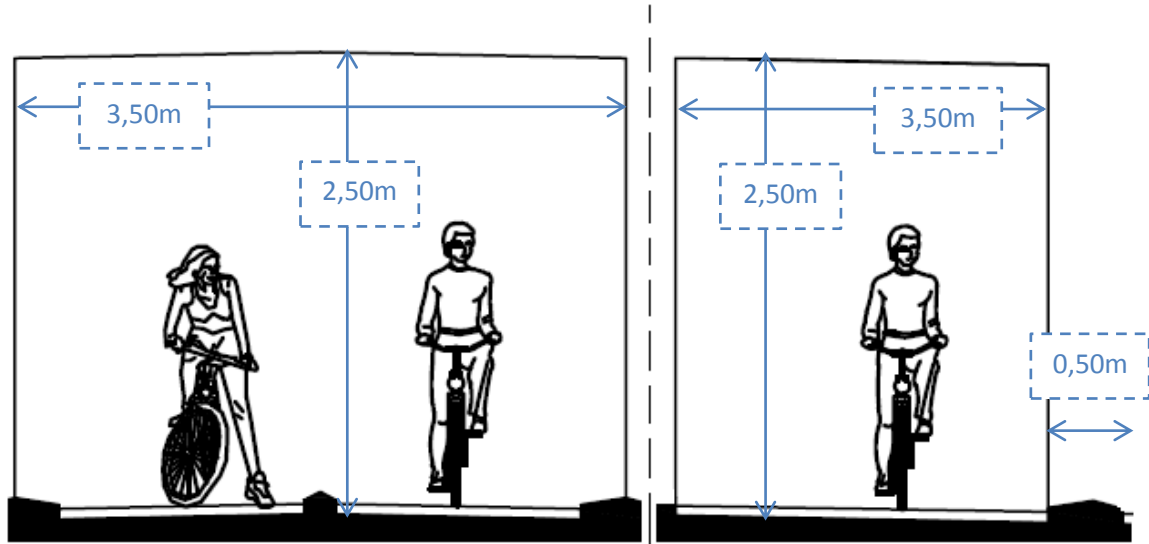


Fig. 21: Space demands for bicycle paths on bridges [RONA1986, ch. 1.2, p1, ch. 2.1, p2]

5.2 GENERATION OF BRIDGE DECK LAYOUT VARIANTS

In the preceding chapter the space requirements for all users were derived. Knowing these, it is possible to generate a number of different variants of bridge cross sections. Following the general shape outline described in [ch. 1.1] [ch. 5], the two geometrical shapes that were used for these variants are the circle and the ellipse. In the following, 5 variants will be given and described. Each of these variants has an elliptical- and a circular sub-variant, denoted 'A' and 'B'. The total number of variants becomes 10 that way.

The goal of this chapter is to derive the most optimal solution in terms of space- and material-usage, based solely on the space demands for the traffic users. Mechanical behavior is explicitly not considered here. The variants will be compared by the use of material in m^2 for the outer shell, assumed that this shell is made up of continuous plate material. This assumption is a simplification of the final design, where truss elements will be used. Furthermore the ratio between used- and 'empty'-space inside the tube will be calculated. This can be seen in the following drawings wherein the blue part denotes the 'used space' which is assumed to be of a trapezium shape. That way the efficiency of space usage inside the tube is derived, as well as the total material usage for the outer shell.

Below the variants will be described. Furthermore a drawing of every sub-variant is provided in which the used space is shown, as described before. Next to that a table is provided in which the input values needed for the space-efficiency and material usage are given. All used formulae used for these calculations, are trivial geometric formulas, except for one: the formula for the circumference of an ellipse, which is given below. [WEB: en.wikipedia.org/Ellipse] This chapter will be concluded with a table that compares the most important features of all variants.

$$C_{ellipse} \cong \pi(a + b) \left(1 + \frac{3 \left(\frac{a-b}{a+b} \right)^2}{10 + \sqrt{4 - 3 \left(\frac{a-b}{a+b} \right)^2}} \right) \quad (5.1)$$

$a = \text{First radius (R1)}$

$b = \text{Second radius (R2)}$

5.2.1 LAYOUT VARIANT 1

This variant yields the smallest possible cross-section. In this variant the bridge only houses two lanes for cars and lorries with a design speed of 100 km/h, see [ch. 5.1.1]. Furthermore there is no hard shoulder for emergency stops. The only added functionality that this variant has, next to the two driving lanes, is a narrow walking strip with a width of 0,50m, next to the safety barrier. This strip is needed because of the deformation capacity demands of the safety barrier [ch. 5.1.2] Of course; this strip may also be used as walking path for inspection and emergencies.

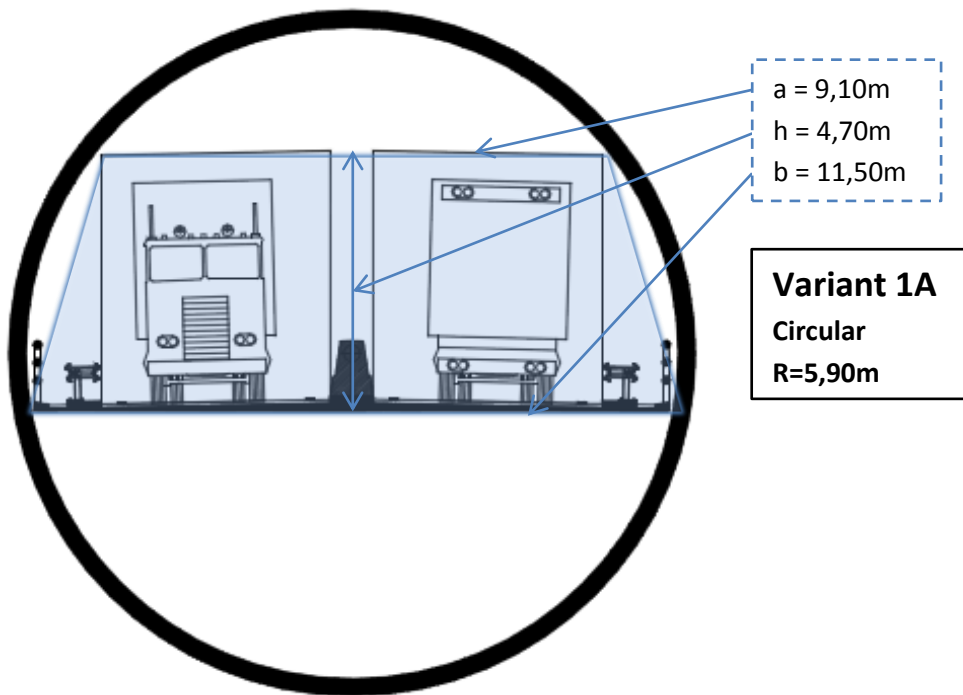


Fig. 22: Variant 1A (circular) for the bridge cross section size determination.

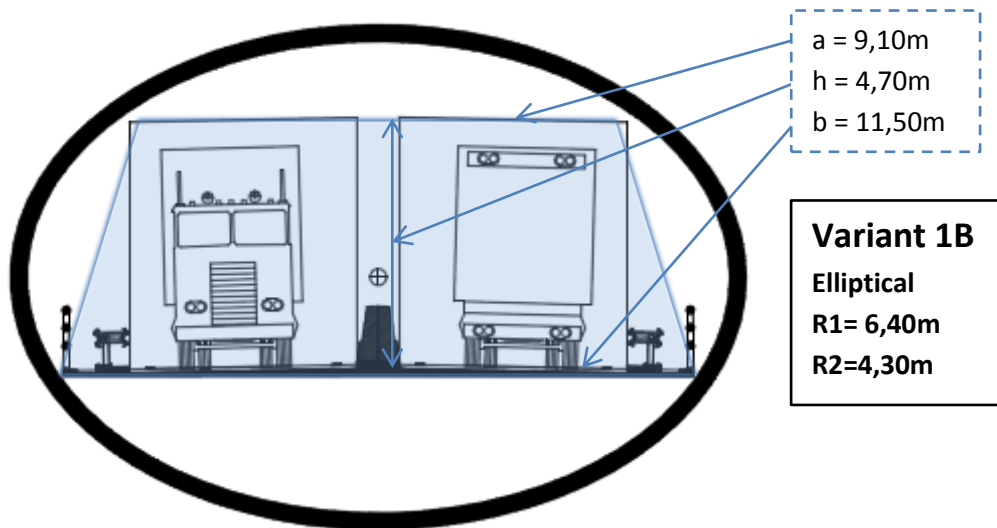


Fig. 23: Variant 1B (elliptical) for the bridge cross section size determination.

Property	Symbol	1A	1B
Description	-	1x circular cross section	1x elliptical cross section
Users	-	Trucks, cars	Trucks, cars
Radius 1	R1 [m]	5,90	6,40
Radius 2	R2 [m]	-	4,30
Circumference	S [m]	37,07	33,94
Cross-sectional area	A_c [m ²]	109,36	86,46
Used space	A_u [m ²]	48,41	48,41
Ratio A_u/A_c	-	44,27%	55,99%
Total Area	A_{tot} [m ²]	1853,54	1696,98

Table 9: Most important characteristics of sub-variants 1A and 1B

5.2.2 LAYOUT VARIANT 2

The second variant is based on the first variant, but is equipped with additional means to facilitate pedestrians as well as bicyclists in both directions. Next to that the road for heavy traffic also features a small hard shoulder for emergency stops, with a width of 1,50m; as prescribed by the SATO [RWS-SATO2005, ch. 2.4.4.1, p87]. This type of configuration is much more typical for modern heavy traffic bridges than the configuration of 'variant 1', yet it leads to a much bigger cross-section than in the case of 'variant 1'.

This variant clearly show that for typical cross-sectional configurations of heavy traffic bridges a circular tube leads to a very disadvantageous A_c/A_u -ratio of about 25%. Adaption of the shape into an ellipse improves this ratio almost by two times to 46%. The reason for this most certainly lies in the very wide and low layout of the different elements on the bridge. A narrow ellipse mimics such a shape much better than a circle with a single diameter.

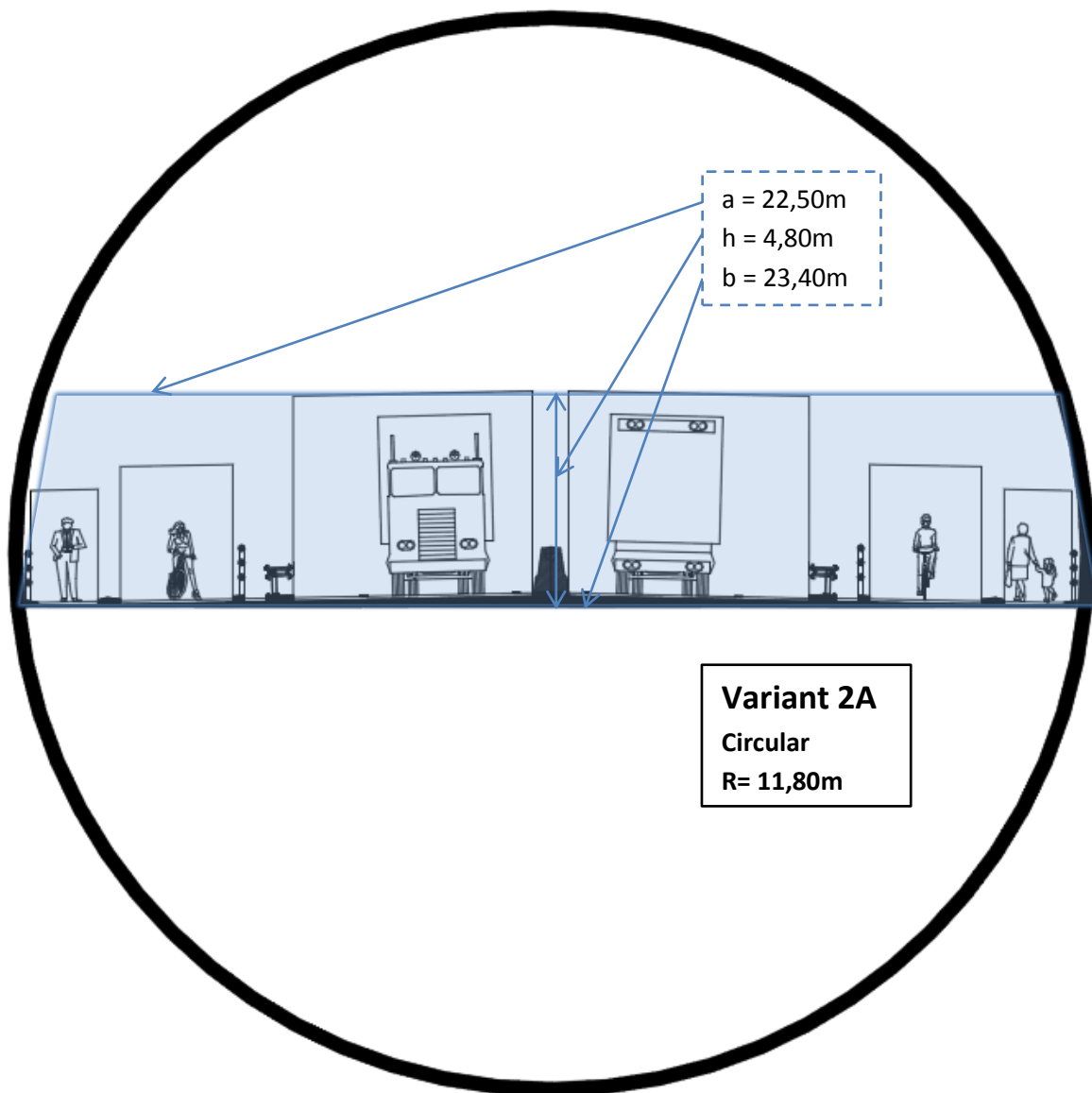


Fig. 24: Variant 2A (circular) for the bridge cross section size determination.

Property	Symbol	2A	2B
Description	-	1x circular cross section	1x elliptical cross section
Users	-	Trucks, cars, bikes, pedestrians	Trucks, cars, bikes, pedestrians
Radius 1	R1 [m]	11,80	12,00
Radius 2	R2 [m]	-	6,30
Circumference	S [m]	74,14	58,89
Cross-sectional area	A_c [m ²]	437,44	237,50
Used space	A_u [m ²]	110,16	110,16
Ratio A_u/A_c	-	25,18%	46,38%
Total Area	A_{tot} [m ²]	3707,08	2944,71

Table 10: Most important characteristics of sub-variants 2A and 2B

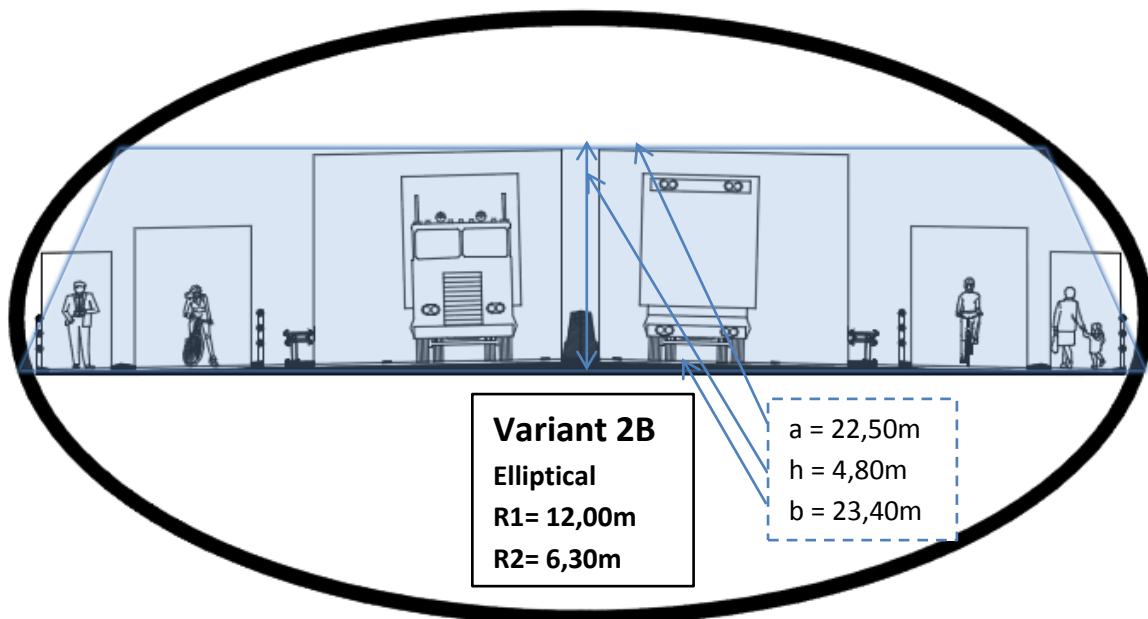


Fig. 25: Variant 2B (elliptical) for the bridge cross section size determination.

5.2.3 LAYOUT VARIANT 3

This variant facilitates the same users as ‘variant 2’, thus trucks, cars, bicyclists and pedestrians in both directions. In order to increase the A_c/A_u -ratio, the bicyclists and pedestrians are not placed on the same bridge deck as the heavy traffic. Instead, these users have their own bridge deck, placed beneath the heavy traffic bridge deck. As shown in the table below, both sub-variants have a very high space-efficiency of 55% and 58%. Due to the two stacked bridge decks, application of an elliptical cross-section instead of a circular cross-section yields only marginal space-efficiency yield.

Property	Symbol	3A	3B
Description	-	1x circular cross section, split level	1x elliptical cross section, split level
Users	-	Trucks, cars, bikes, pedestrians	Trucks, cars, bikes, pedestrians
Radius 1	R1 [m]	7,00	7,10
Radius 2	R2 [m]	-	6,50
Circumference	S [m]	43,98	42,75
Cross-sectional area	A_c [m ²]	153,94	144,98
Used space	A_u [m ²]	84,01	84,01
Ratio A_u/A_c	-	54,57%	57,94%
Total Area	A_{tot} [m ²]	2199,11	2137,32

Table 11: Most important characteristics of sub-variants 3A and 3B

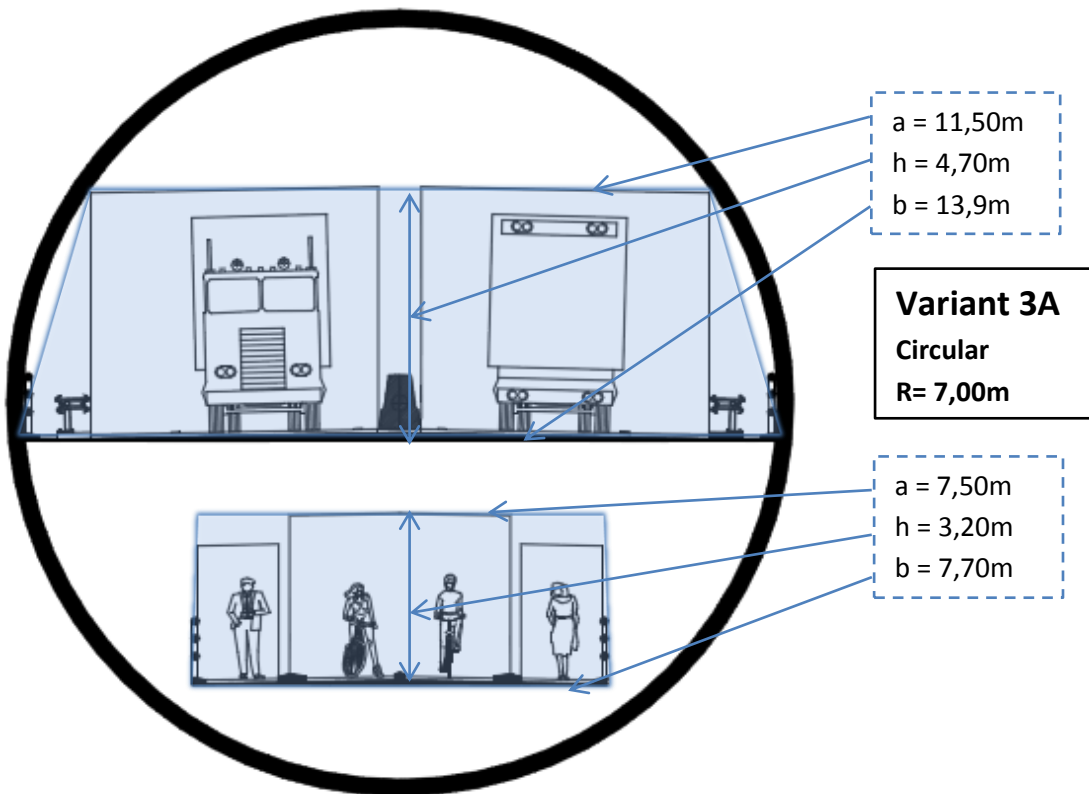


Fig. 26: Variant 3A (circular) for the bridge cross section size determination.

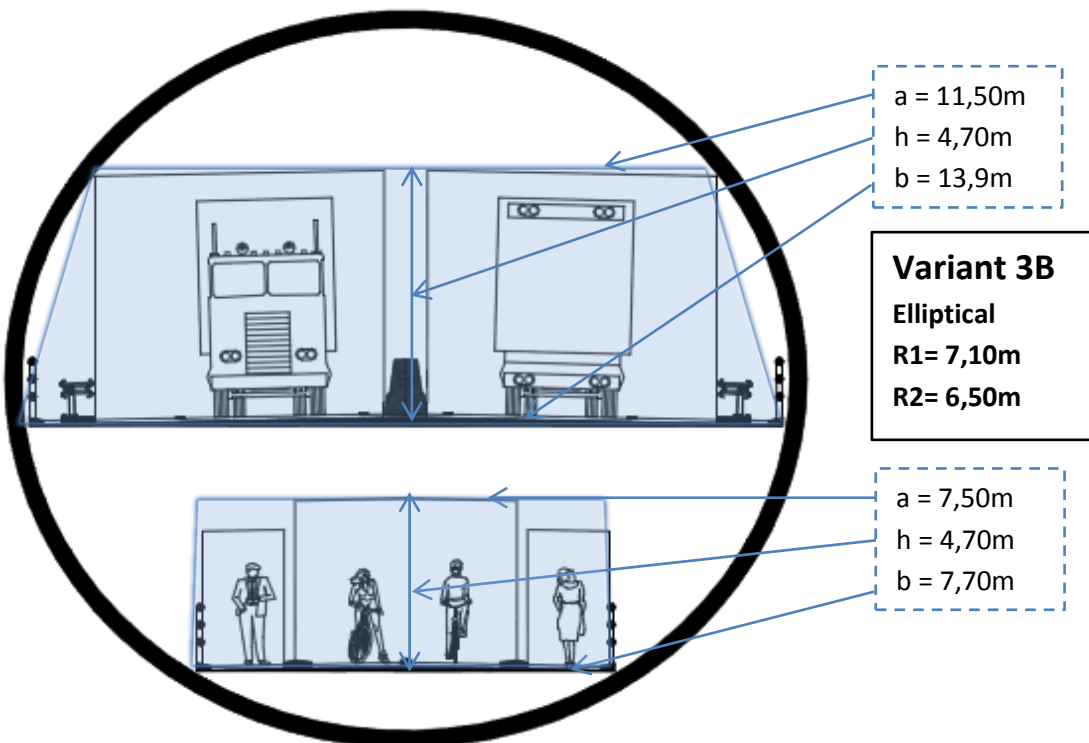


Fig. 27: Variant 3B (elliptical) for the bridge cross section size determination.

5.2.4 LAYOUT VARIANT 4

In contrast to the variants described before, where a single cylindrical tube was used, this variant features two tubes. Both cylindrical tubes have exactly the same dimensions. Combined, both tubes house the same provisions for users as 'variant 2' and 'variant 3'. The split in two separate tubes improve the space-efficiency of the circular variant ('variant 4A' compared to 'variant 2A') from 25% to 43%. However, using two smaller tubes instead of one large tube also increases the needed shell material from 3700 m² to 4000m² in the case of a circular cross section. Constructing two tubes of course also means that two substructures and foundations have to be built.

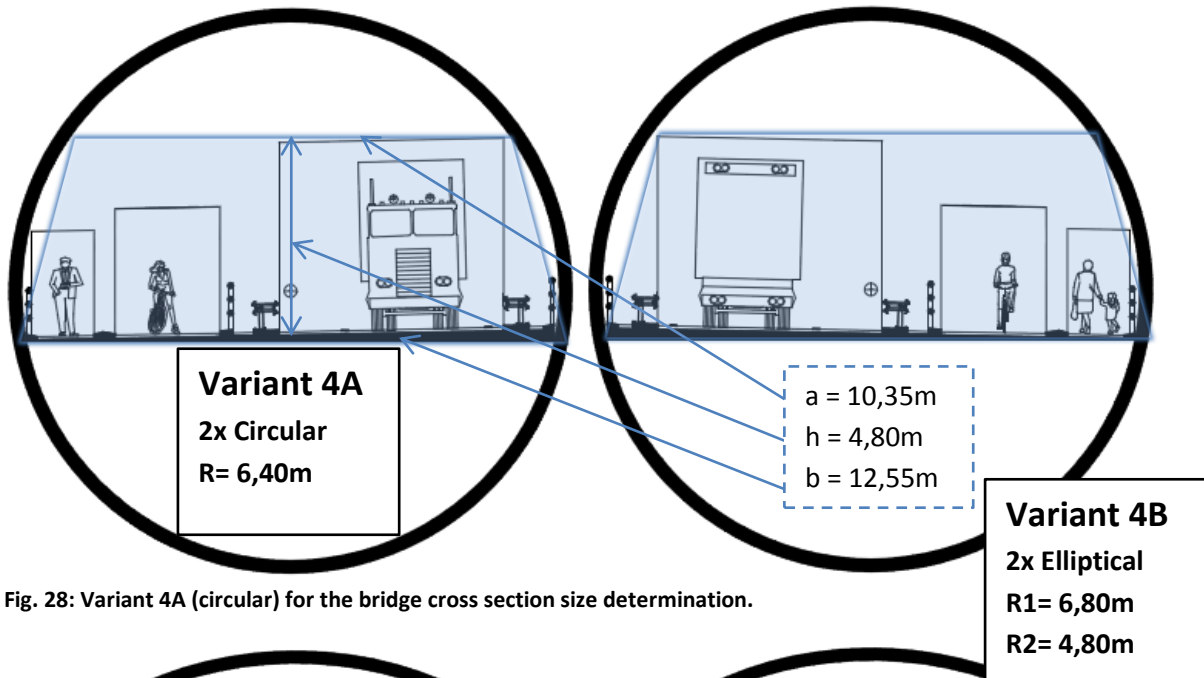


Fig. 28: Variant 4A (circular) for the bridge cross section size determination.

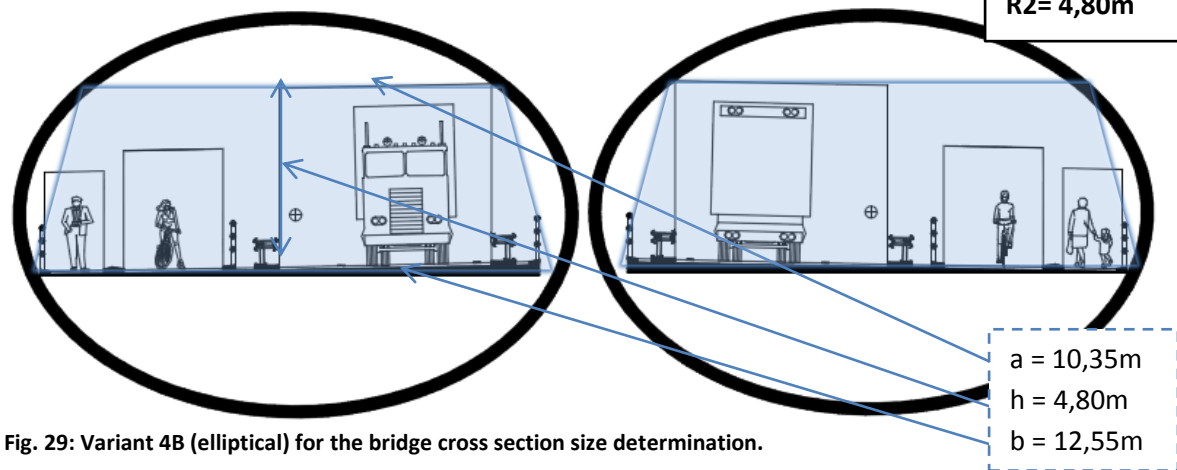


Fig. 29: Variant 4B (elliptical) for the bridge cross section size determination.

Property	Symbol	4A	4B
Description	-	2x circular cross section	2x elliptical cross section
Users	-	Trucks, cars, bikes, pedestrians	Trucks, cars, bikes, pedestrians
Radius 1	R1 [m]	6,40	6,80
Radius 2	R2 [m]	-	4,80
Circumference	S [m]	80,42	73,43
Cross-sectional area	A_c [m ²]	257,36	205,08
Used space	A_u [m ²]	109,92	109,92
Ratio A_u/A_c	-	42,71%	53,60%
Total Area	A_{tot} [m ²]	4021,24	3671,38

Table 12: Most important characteristics of sub-variants 4A and 4B

5.2.5 LAYOUT VARIANT 5

This variant is similar to 'variant 4'; it also uses two different cylindrical tubes. In contrast to this variant, however both tubes have differing sizes. One tube houses the bicycle and pedestrian paths and one tube houses the 2-lane road. Sub-variant 'variant 5B' yields a very high space efficiency of about 55%, while also having the advantage of protecting the 'vulnerable' users (bicyclists and pedestrians) from the other users by placing them in their own cylindrical tube. The extra material usage induced by using two tubes is limited, for 'variant 5B' it is 3100 m², which is only marginally higher than that of 'variant 2B', which is 2950 m².

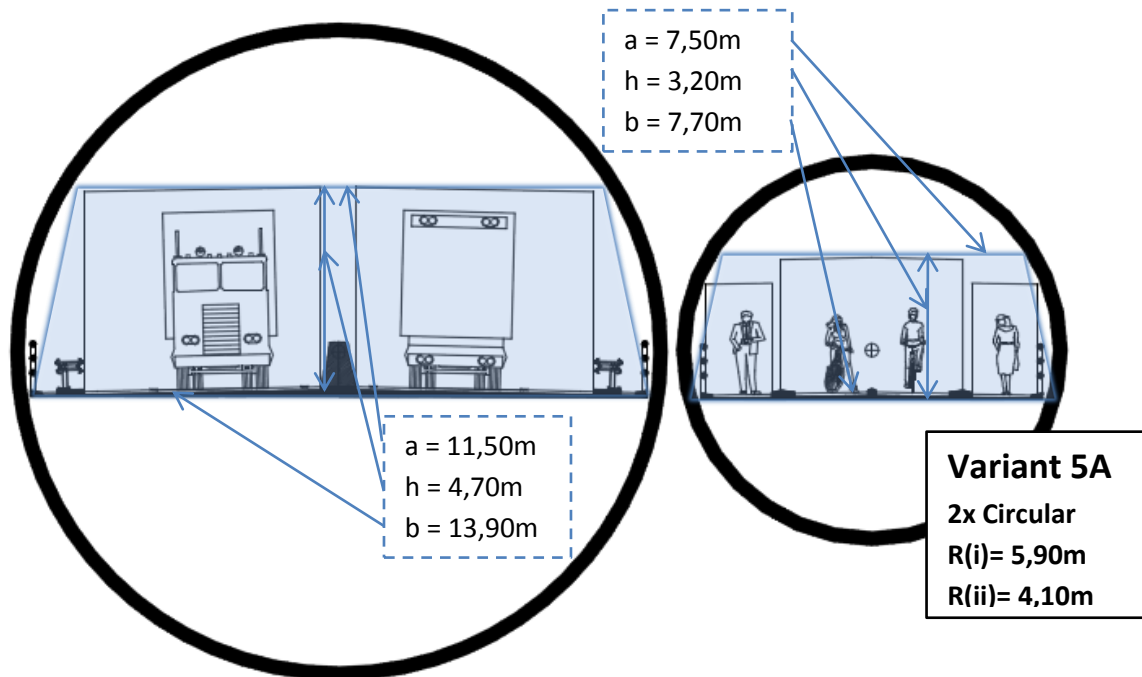


Fig. 30: Variant 5A (circular) for the bridge cross section size determination.

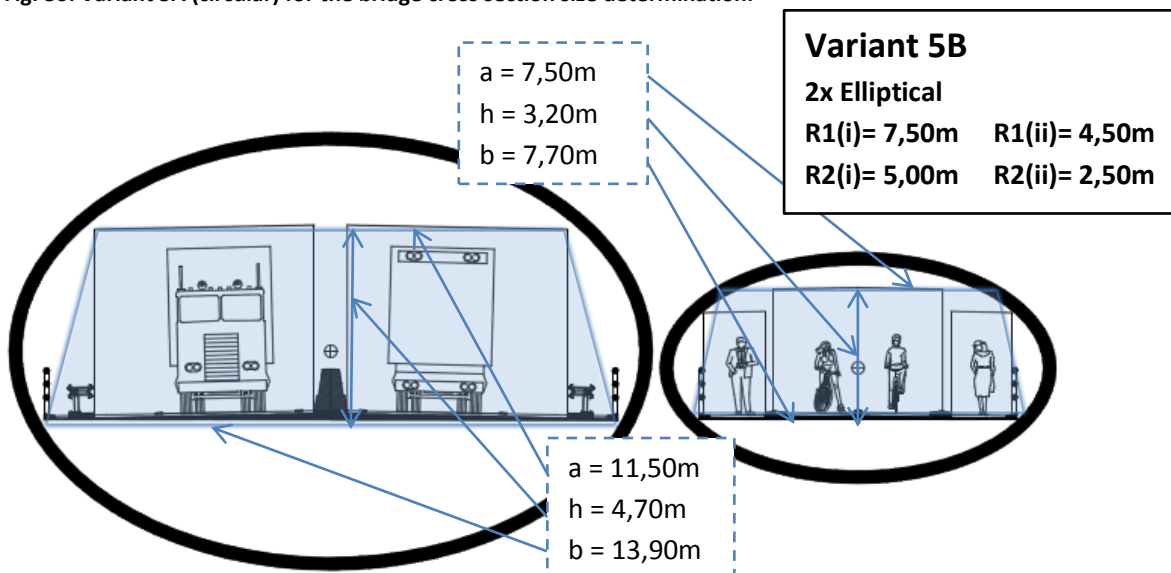


Fig. 31: Variant 5B (elliptical) for the bridge cross section size determination.

Tube 1 (Trucks, Cars)

Property	Symbol	5A (1 of 2)	5B (1 of 2)
Description	-	2 different circular cross sections	2 different elliptical cross sections
Users	-	Trucks, cars	Trucks, cars
Radius 1	R1 [m]	7,10	7,50
Radius 2	R2 [m]	-	5,00
Circumference	S [m]	44,61	39,66
Cross-sectional area	A_c [m ²]	158,37	117,81
Used space	A_u [m ²]	59,69	59,69

Tube 2 (Bicyclists, Pedestrians)

Property	Symbol	5A (2 of 2)	5B (2 of 2)
Description	-	2 different circular cross sections	2 different elliptical cross sections
Users	-	Bikes, pedestrians	Bikes, pedestrians
Radius 1	R1 [m]	4,10	4,50
Radius 2	R2 [m]	-	2,50
Circumference	S [m]	25,76	22,44
Cross-sectional area	A_c [m ²]	52,81	35,34
Used space	A_u [m ²]	24,32	24,32

Ratio A_u/A_c	-	39,78%	54,85%
Total Area	A_{tot} [m ²]	3518,58	3105,29

Table 13: Most important characteristics of sub-variants 5A and 5B

5.2.6 LAYOUT VARIANT 6

To compare the self-generated variants with an existing structure, it was chosen to add the 'Light-rail Viaduct Beatrixkwartier' in The Hague, The Netherlands [LS, ch. 6.1.3, p192] as additional variant. This structure houses two light-rail tracks, with a standard track-width of 1435mm. The cars have a height of 3,65m and a width of 2,65m [A54, p2]. The tracks run on elliptical concrete girders with a width of 2,40m. The main load-bearing structure is comprised of a dia-grid ellipse with a major radius of 5,00m and a minor radius of 3,75m. The steel CHS-sections that make up the dia-grid have a diameter of 323,9mm. They are supported by an additional set of steel plate rings with a thickness of 40mm. The span of this structure is similar to the span of the bridge to be designed; it is in the order of 40-50m. In a later chapter this existing steel cylindrical truss bridge is compared to the final design [ch. 12].

For investigation purposes another sub-variant is added, a circular version of the existing structure.

Property	Symbol	6A	6B
Description	-	1x Circular cross section	1x elliptical cross section
Users	-	2x Light-rail track	2x Light-rail track
Radius 1	R1 [m]	4,50	5,00
Radius 2	R2 [m]	-	3,75
Circumference	S [m]	28,27	27,63
Cross-sectional area	A_c [m ²]	63,62	58,90
Used space	A_u [m ²]	35,40	35,40
Ratio A_u/A_c	-	55,65%	60,10%
Total Area	A_{tot} [m ²]	1413,72	1381,47

Table 14: : Most important characteristics of sub-variants 5A and 5B

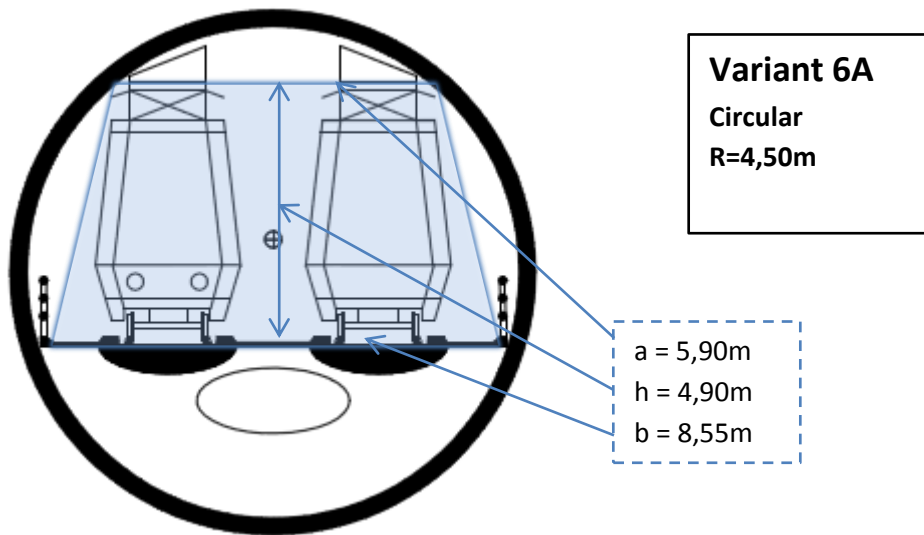


Fig. 32: Variant 6A (circular) for the bridge cross section size determination. This variant is a circular version of the existing 'Light-rail Viaduct Beatrixkwartier' in The Hague, The Netherlands [LS, ch. 6.1.3, p192]

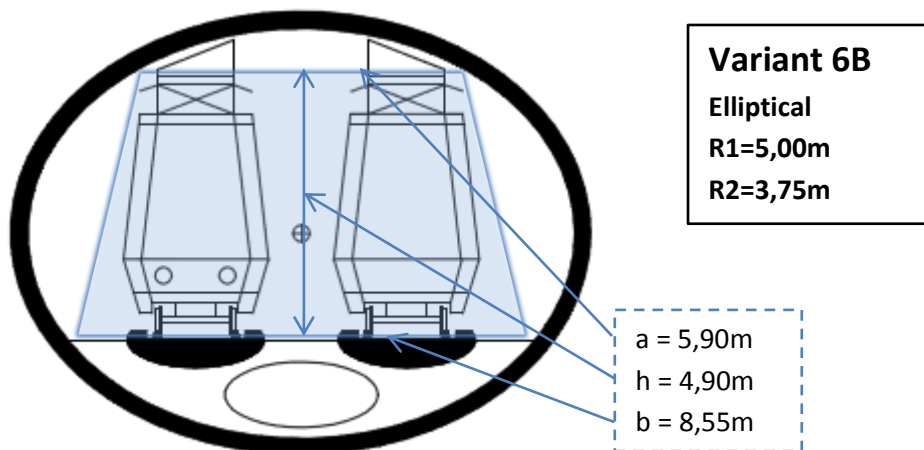


Fig. 33: Variant 6B (elliptical) for the bridge cross section size determination. This variant is a replica of the existing 'Light-rail Viaduct Beatrixkwartier' in The Hague, The Netherlands [LS, ch. 6.1.3, p192]

5.2.7 COMPARISON OF THE VARIANTS

The table below shows the A_c/A_u -ratio, as well as the total area of plate material that would be hypothetically used for the (elliptical) cylinder for each variant. 'Variant 1' uses the least material, but this is caused by the fact that it only houses trucks and cars and does not provide space for other users. All other variants also house bicycle- and footpaths. Of the other variants, 'variant 3' uses the least material. The most probable reason for this is that this variant features two bridge decks. This way most space inside of the cylinder is used for the function a bridge is intended for. However, two bridge decks stacked on top of each other also need more complex provisions to connect the bridge to existing infrastructure.

In terms of the other important parameter, the A_c/A_u -ratio, 'variant 3' and 'variant 5' yield the best ratio, with values between 50% and 60%. However, 'variant 5' also uses two separate cylindrical tubes, which leads to higher material demands. Next to that, this variant does not feature a small hard shoulder for emergency stops as described before. Adapting the variant to house such a hard shoulder as well would increase material usage and decrease the space-efficiency.

To conclude, in terms of space-efficiency and material usage ‘variant 4’ yields the best values. However, stacking bridge decks poses other added costs and engineering challenges. When one would prefer to choose a classic heavy traffic bridge deck configuration, ‘variant 2’ would be most suitable, since its material usage is limited and for the elliptical sub-variant ‘variant 2B’ it yields an acceptable space-efficiency value of about 50%. This leads to another conclusion, which is that elliptical cross-sections are generally found to yield better A_c/A_u -ratios than circular cross-sections. However they also reduce the overall height of the bridge cross-section, possibly negatively affecting structural bearing capacity.

When the choice is made to divide the bridge into two separate cylindrical tubes it is advisable to split by user-groups as in ‘variant 5’ and not simply into two-halves, as is the case in ‘variant 4’. Splitting by user-groups not only logically separates the vulnerable slow bridge-users from the faster heavy traffic, but also causes reduced material usage and increased space-efficiency .

Comparing the self-generated variants to ‘variant 6’ which is based on the existing ‘Light-rail Viaduct Beatrixkwartier’ in The Hague, The Netherlands, it becomes clear that the space-efficiency of the existing structures (‘sub-variant 6B’) has a particularly high efficiency of about 60%. This can only be matched applying two stacked bridge decks (‘variant 3’) and thereby achieving a space-efficiency of 58% or by splitting the bridge into two separate bridges with different dimensions (‘variant 5’) and thereby achieving a space-efficiency of about 55%.

In terms of material usage, ‘variant 6’ uses clearly less material than all other variants. The material usage of ‘variant 6’ lies at about 1400m² per span of 50m. The only variant which comes close to this value is ‘variant 1’, which is the minimum variant and still has a material usage of about 1750m². However it does not house the functions that the other self-generated variants house, such as foot- and bicycle-paths in two directions as well as small hard shoulders for emergency stops. A modern heavy traffic-bridge needs to house these functions as well, so it is not possible to achieve material usage values that are as low as those of ‘variant 1’ or even ‘variant 6’.

Property	Symbol	1A	1B	2A	2B	3A	3B
Description	-	1xCirc.	1xElli.	1xCirc.	1xElli.	1xCirc.	1xElli.
Users	-	Lorries	Lorries	All	All	All	All
Radius 1	R1 [m]	5,90	6,40	11,80	12,00	7,00	7,10
Radius 2	R2 [m]	-	4,30	-	6,30	-	6,50
Radius 1	R1 (ii) [m]	-	-	-	-	-	-
Radius 2	R2 (ii) [m]	-	-	-	-	-	-
Ratio A_u/A_c	-	44,3%	56,0%	25,2%	46,4%	54,6%	57,9%
Total Area	A_{tot} [m ²]	1854	1697	3707	2945	2199	2137

Property	Symbol	4A	4B	5A	5B	6A	6B
Description	-	2xCirc.	2xElli.	2xCirc.	2xElli.	1xCirc.	1xElli.
Users	-	All	All	All	All	Light-rail	Light-rail
Radius 1	R1 [m]	6,40	6,80	7,10	7,50	4,50	5,00
Radius 2	R2 [m]	-	4,80	-	5,00	-	3,75
Radius 1	R1 (ii) [m]	-	-	4,10	4,50	-	Au
Radius 2	R2 (ii) [m]	-	-	-	2,50	-	0,00
Ratio A_u/A_c	-	42,7%	53,6%	39,8%	54,9%	55,6%	60,1%
Total Area	A_{tot} [m ²]	4021	3671	3519	3105	1414	1381

Table 15: Comparison of the most important characteristics of the different sub-variants

After generating all variants and comparing them, as described before it turned out that the efficiency in terms of the usage of the space inside the cylinder is generally only mediocre. The same holds for the material usage, in terms of the amount of material in m², needed to cover the whole cylindrical truss. Since the efficiency and material usage of the existing structure, the ‘Light-rail viaduct in The Hague, The Netherlands’ are significantly better than that of the shapes generated, after shape generation several ideas

came up to increase the efficiency, while not using two separate tubes, thereby drastically decreasing the material usage.

5.2.8 CANTILEVER VARIANT

The single most appealing and interesting idea that was generated in the process of finding more efficient shapes with a minimized amount of material usage is the idea of placing the 'slower' users, thus the pedestrians and bicyclists outside of the main cylindrical tube by constructing a cantilevering truss. This way the slow and vulnerable traffic is logically and physically separated and protected from the fast and heavy traffic inside the cylinder. The main cylindrical load bearing structure, which houses the heavy traffic has the same dimensions as the heavy traffic part of 'Variant 5B' [ch. 6.2.5], thus two radii of 7,50m and 5,00m.

Whether this idea can be realized has to be investigated through finite elements analysis, since the load on the main cylindrical load bearing structure significantly increases and the cantilever itself is heavily loaded due to the large cantilever of about 5000mm. Furthermore, the cantilever also induces transverse moments in the cylindrical truss, which could be disadvantageous. Next to that the extra material usage of the cantilevering truss would also have to be considered. To give an impression, below a drawing of the 'cantilever variant' can be found.

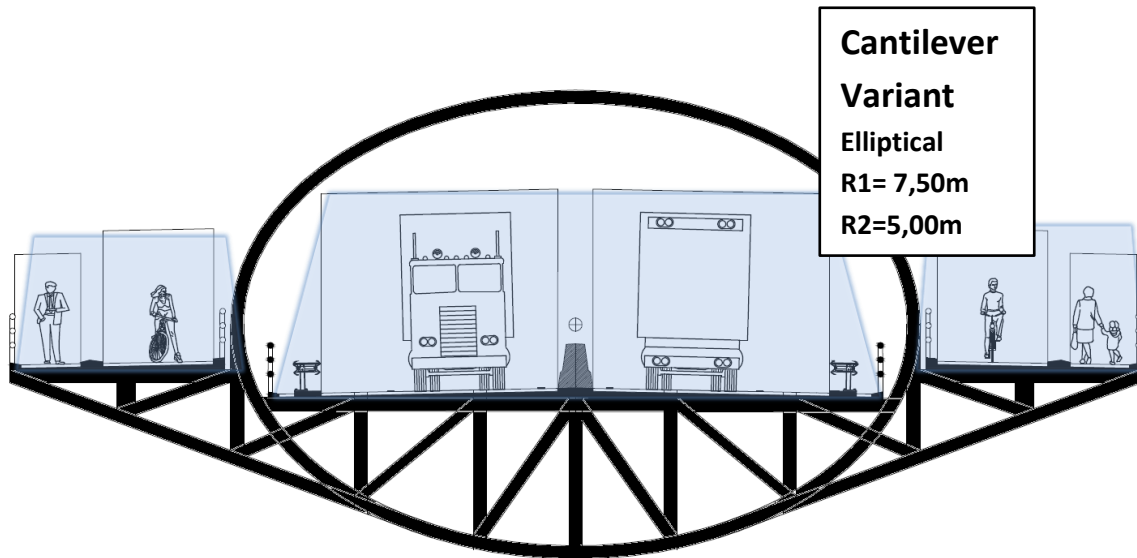


Fig. 34: Drawing of the 'Cantilever variant'. The cylindrical shape of this variant is similar to the heavy traffic part of 'Variant 5B'. A cantilevering truss structure is used to house the pedestrians and bicyclists, while keeping them physically separated from the fast, heavy traffic.

5.3 REQUIREMENTS FOR THE DESIGN SPAN OF THE BRIDGE

In order to determine the required span of the bridge it is necessary to know the exact characteristics of the road that the bridge will span. To take account of the largest roads, the assumption is made that the bridge has to span a highway. The Dutch highway characteristics are prescribed by 'Rijkswaterstaat' in the 'Nieuwe Ontwerprichtlijn Autosnelwegen' or 'NOA' in short (New Design Guide for Highways) [RWS-NOA2007]. This document gives several demands for the width and height of all road elements, as well as the free space next to and above the road.

The examples given by the NOA [RWS-NOA2007, ch. 4.2.5, p90] give most necessary values for the road. The lane width is uniformly set to 3,30m. The emergency lane on the right side of each driving direction has a width of 3,15m. The lining between the driving lanes has a width of 0,15m and at both sides of every driving direction 0,20m. Furthermore safety barriers are placed, surrounding each driving direction at the sides. These barriers are of a similar type as described in [ch. 5.1.2]. The middle berm has a width of 4,00m, measured from barrier to barrier. It can thus accommodate an intermediate support or bridge pillar. The side berms have a width of 2,50m, measured from the barrier to the bridge pillar. That way there is room for special safety barriers that encase the bridge pillars, for example a 'Rimob' ('Rimpelbuis-obstakelbeschermer') as described in [RWS-ROA1989, ch. 6.5.4, p89] Of course this type of object-protection can also be used in the middle berm. The picture below shows the 'Rimob' safety barrier as prescribed by the ROA.

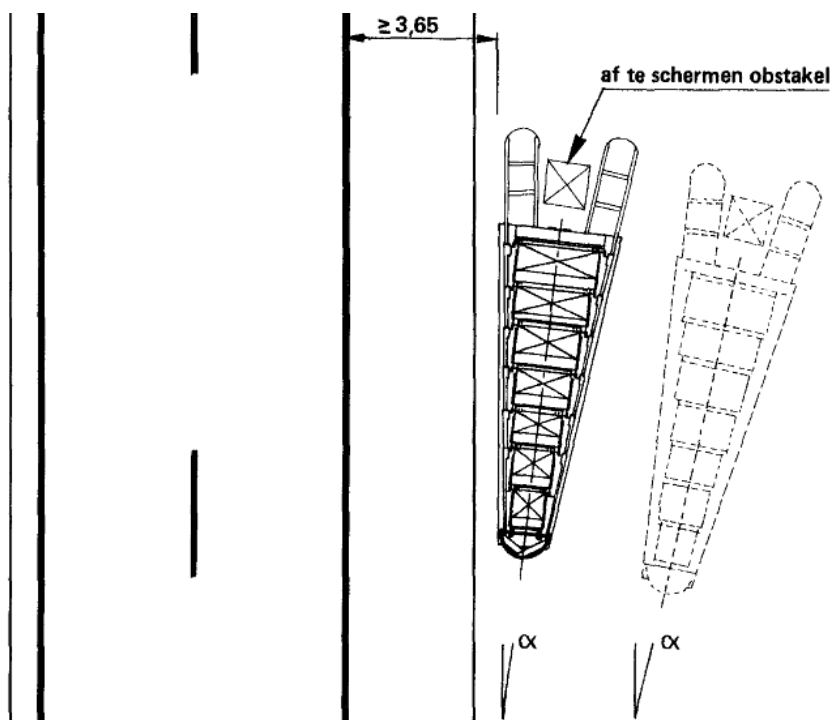


Fig. 35: Safety barrier of the 'Rimob' type to protect bridge pillars. [RWS-ROA1989, ch. 6.5.4, p92]

Taking into account all needed widths and free height as described before, it is possible to generate several highway cross-sections. Below three common cross-sections were generated, based on [RWS-NOA2007, ch. 4.2.5, p90]. The first cross-section is the 2x2 lane highway. As all other variants this cross-section features a free height of 5,00m and a full emergency lane. The total span of a bridge, spanning a 2x2 lane highway of this type, would be 35,20m. Since there is enough space in the middle berm, it would also be possible to divide the total span into two smaller spans of 2x17,60m.

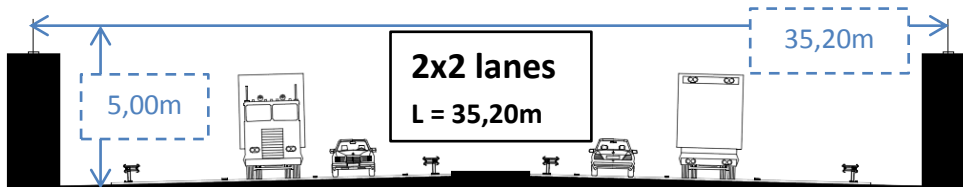


Fig. 36: Profile of the 2x2 lane highway that the bridge could span. The single span would be 35,20 m, if an intermediate support is used, the span would be 2x17,60 m.

The second cross-section that was generated is slightly larger than the first one. It features another driving lane in both directions. This is the only difference compared to the first 2x2 cross section. In the case of this 2x3 lane highway, the total length to be spanned would be 42,10m. Dividing the span into two halves would yield two smaller spans of 2x21,05m. 2x3 lane highways are very common in the Netherlands. Most highways in the ‘Randstad’ (the area containing around the major cities) are of this type or even larger.



Fig. 37: Profile of the 2x3 lane highway that the bridge could span. The single span would be 42,10 m, if an intermediate support is used, the span would be 2x21,05 m.

Finally a cross-section was generated with 2x4 lanes. A highway of this kind is used for very high amounts of traffic, though close to the big cities of the Netherlands such as The Hague, Amsterdam, Utrecht and Rotterdam. Adding another driving line gives a width of 49,00m that has to be spanned. Of course this is caused by the increased number of lanes. One can thus conclude that for an increasing number of lanes it becomes more likely that the span will be divided in for example two equal spans. In the case of this 2x4 lane highway this would mean two spans of 2x 24,50m

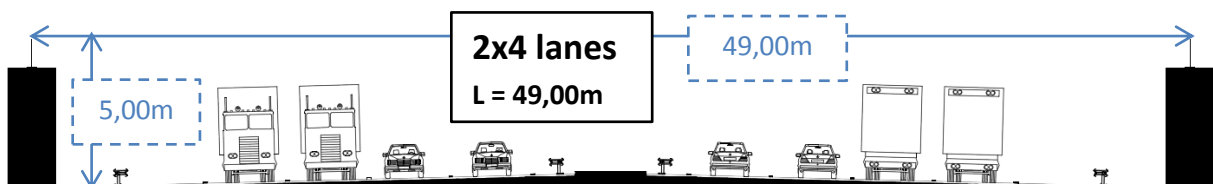


Fig. 38: Profile of the 2x4 lane highway that the bridge could span. The single span would be 49,00 m, if an intermediate support is used, the span would be 2x24,50 m.

To summarize all information on the possible span length of the bridge a small table is presented made in which all given information is depicted. Generally said, all possible design spans are well within the expected values of 30-50m [LS, ch. 3.1.6, p111]. Directly spanning a large 2x4 lane highway should not pose a problem, since the maximum span would be 49,00m. In the densely populated areas of the Netherlands 2x4 lane highways are very common nowadays, it is therefore chosen to use a span of 49m as design span of the cylindrical truss bridge.

Property	2x2	2x3	2x4
Description	2x2 lane highway	2x3 lane highway	2x4 lane highway
Emergency lane in both directions	Yes	Yes	Yes
Single Span	35,20m	42,10m	49,00m
Two Equal Spans	2x17,60m	2x21,05m	2x24,50m

Table 16: Comparison of different span options

5.4 GENERATION OF CYLINDRICAL TRUSS TOPOLOGY VARIANTS

To derive several truss topology variants for the cylindrical truss, the next phase of the design of the main load bearing structure is the mesh generation. In the preceding chapter the overall shape was defined, based on the demands of the different users. In this chapter computer-aided modeling tools will be used to make a fully parametric geometric model of the main load bearing structure of the bridge. It was chosen to make a dynamic parametric geometric model in which all design parameters can be continuously altered during the design, instead of a static model, which has to be rebuilt after every design-change due to complexity of the design. In the following it will be described how this model is generated and what the outcome of this stage is.

5.4.1 CHOOSING SUITABLE SOFTWARE

As described in the above introduction, for complex shapes like cylindrical truss girders it is necessary to take an extra step before being able to do FEM-calculations on the geometrically defined structure. This step is the generation of a dynamic parametric geometric model from which the needed geometric variants can be extracted and inserted into software FEM-FEA to start the calculation process.

To generate such a dynamic parametric geometric model, it was chosen to use a so-called NURBS (Non-rational B-splines) 3D-modeling tool. Although this software package called 'Rhino' by 'Robert McNeel & Associates', hereafter called 'Rhino' was not mentioned in the literature study before [LS, ch. 5] it turned out during design that use of parametric modeling was indispensable. 'Rhino' is often used by architects and graphic designers to make 3D-models of complex structures.

Because for this design generative algorithms are used for geometry generation it was further chosen to use a special plugin for 'Rhino', called 'Grasshopper'. This plugin is a graphical algorithm editor that is tightly integrated with Rhino's 3-D modeling tools. It allows designers to build form generators from a basic level to the more advanced shapes.

5.4.2 PARAMETRIC MODEL OF THE CYLINDRICAL TRUSS

In the following the method of generating the parametric model in 'Rhino' 'Grasshopper' will be described. All steps that were used in the 'Grasshopper' interface will be given and explained. In general, a 'Grasshopper' model consists of elements that are connected by lines. An element can be data such as single integer number, a vector, a particular function or anything like it. The lines represent the connection between these elements, showing that one element influences another, when connected. In other words a line generally transfers an output value of one element to the input element of another.

5.4.2.1 BASIC CYLINDRICAL SHAPE

The first step of building the model is to define the basic shape. In this case the basic (cross-sectional) shape is an ellipse, defined by the two radii R_1 and R_2 . In the case that $R_1 = R_2$ this ellipse becomes a circle, such that all variants described in [chapter 5.2] can easily be generated in the same model. The accompanying step in the model below is [Step 1], wherein via two sliders the radii are generated, in this case $R_1 = 12m$ and $R_2 = 6m$. Then two ellipses are created [Step 2], one on the base point $[0,0,0]$ in the YZ-plane [Step 3], and one [Step 4] parallel to the 'start ellipse' with a perpendicular distance defined by [Step 5], in this case $L = 50m$.

Then a surface is created between these two ellipses [Step 6], which is then divided into a number of segments in all directions [Step 7]. This produces an evenly spaced or uniform grid. The number of divisions is controlled by [Step 8]. In this example the number of divisions is set to 10 for all directions. It is also possible to use different numbers of divisions for the X- and YZ-directions. Finally, at each line intersection on the surface, points are generated. [Step 9]

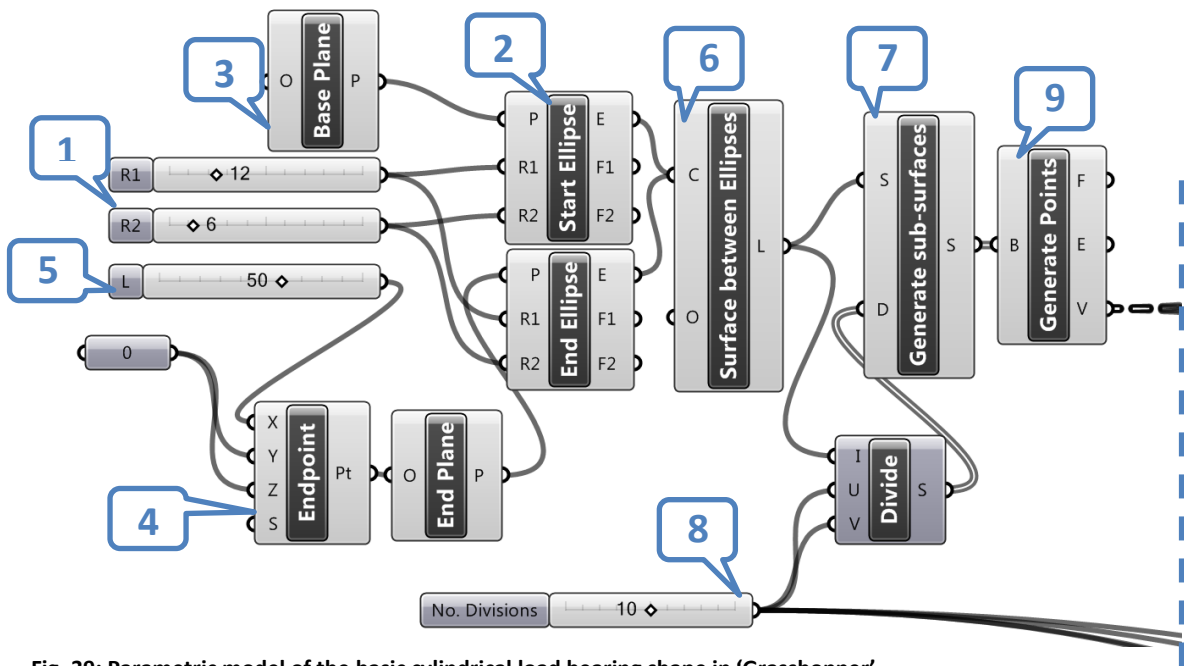


Fig. 39: Parametric model of the basic cylindrical load bearing shape in 'Grasshopper'

Using the steps described and depicted above, the following geometry is obtained. Note that the basic shape of the cylindrical load bearing system is clearly visible. However this shape still only consists of surfaces that are cut by lines. In the drawing below the numbers correspond to the numbers of the steps described before [Step 1- Step 9]

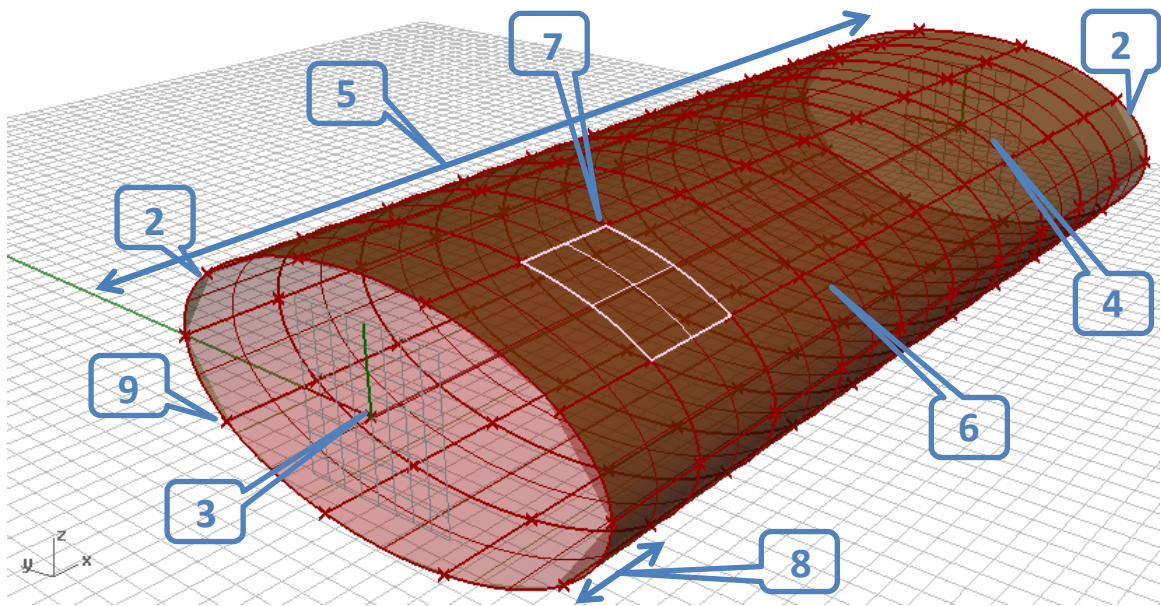


Fig. 40: Model of the basic shape of the cylindrical load bearing shape in 'Rhino'

The function in 'Grasshopper' that generates sub-surfaces from a bigger surface has the disadvantage that it divides the surface in double-curved sub-surfaces. Therefore [Step 9] is really important, since by connecting these points by direct lines, the double-curved sub-surfaces are omitted. The creation of the lines or members between these points will be the subject of the next steps in the parametric geometric model generation process. By creating them, a network of members will be created, which will together form the cylindrical truss, which the basis of the main load bearing structure.

5.4.2.2 GENERATION OF THE HORIZONTAL AND VERTICAL MEMBERS

Before continuing with the generation of the linear members, first the point generation process needs to be explained. 'Grasshopper' generates all points as shown in the list below. The numbers '0, 1, 2, 3' on the left

side of the yellow rectangle denote the points with their corresponding X-, Y-, Z-coordinates. These points are grouped into sets of 4 points, denoted by (0;0;0) on the right side, each defining the corner points of the sub-surfaces generated in [Step 7]. Thus when connecting point 0 of the first set (0;0;0) with point 1 of the same (0;0;0) and continuing in that manner up until the last set (0;0;n) one can generate a specific set of lines. Of course it is also possible to connect 'point 0' with 'point 2' or 'point 2' with 'point 3' etc. This is exactly the method used in 'Grasshopper' to generate all linear members.

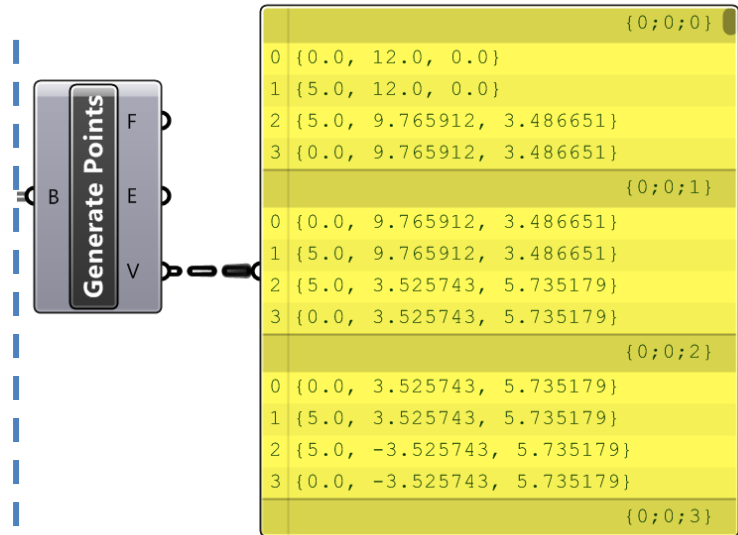


Fig. 41: Details of the point generation in Grasshopper

The corresponding function in 'Grasshopper' is shown in the picture below. The input for this function is the total matrix of points generated in [Step 9], as shown above. By defining which element of the total matrix and thus of every sub-surface or set of points is to be extracted, in this case 'point 0' and 'point 1', 'Grasshopper' now produces a set of only 'point 0' and 'point 1' of every sub-surface. Connecting these points via a line-function, thus setting 'A' and 'B' of this function to 'point 0' and 'point 1' produces horizontal members. The corresponding 'Grasshopper' code is shown below.

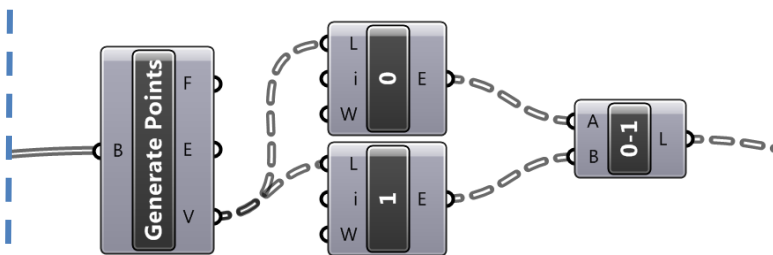


Fig. 42: Generation of linear horizontal members in 'Grasshopper'

For a better visualization the lines were cosmetically altered in the picture below, giving them a distinct color and a radius. The gray horizontal members can be clearly seen in the picture below.

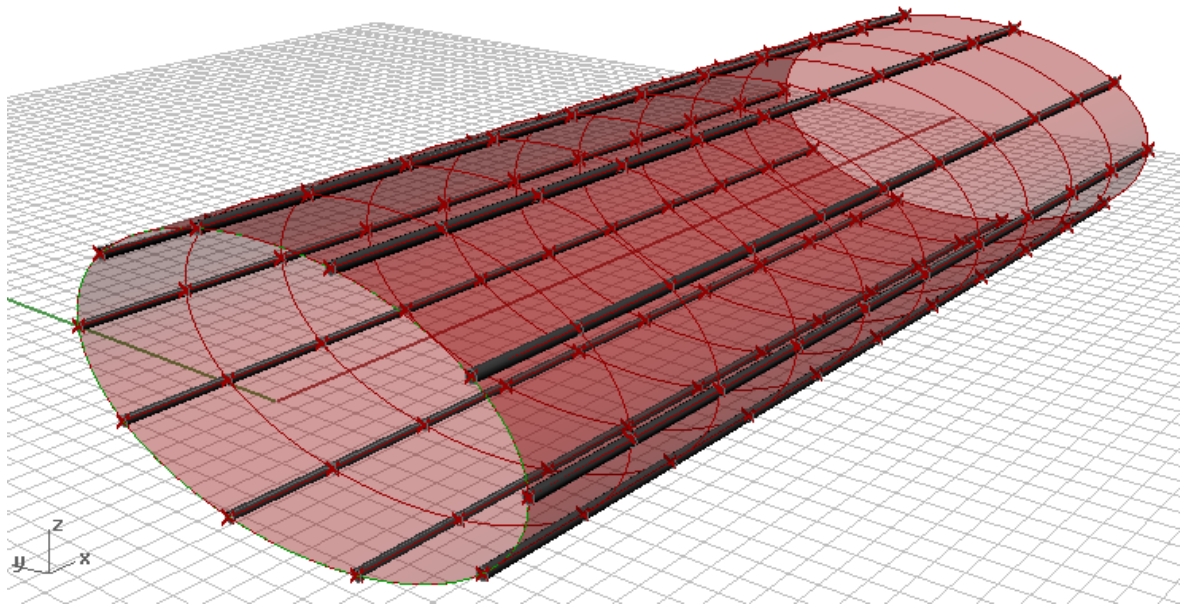


Fig. 43: Horizontal members parametrically generated in 'Grasshopper' by connecting 'point 0' and point 1' of every sub-surface

After that, proceeding in the same way, but now connecting 'point 0 and 'point 3' of every sub-surface yields all 'vertical' members or the elliptical rings of the cylindrical truss structure.

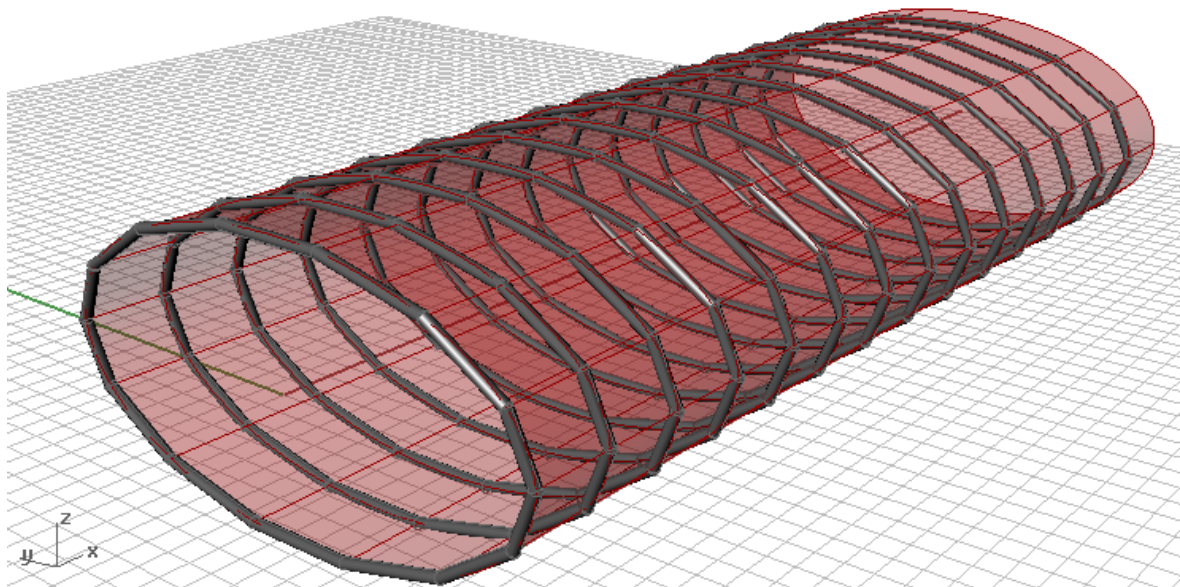


Fig. 44: Vertical members or elliptical rings parametrically generated in 'Grasshopper' by connecting 'point 0 and 'point 3' of every sub-surface.

Combining the two shapes yields a cylindrical Vierendeel-truss, where all member intersections are simple connections with an angle of 90° . This cylindrical Vierendeel-truss can already be used as a cylindrical load-bearing system. However, typical trusses also feature diagonal members. The generation of those members will be the subject of the next chapter.

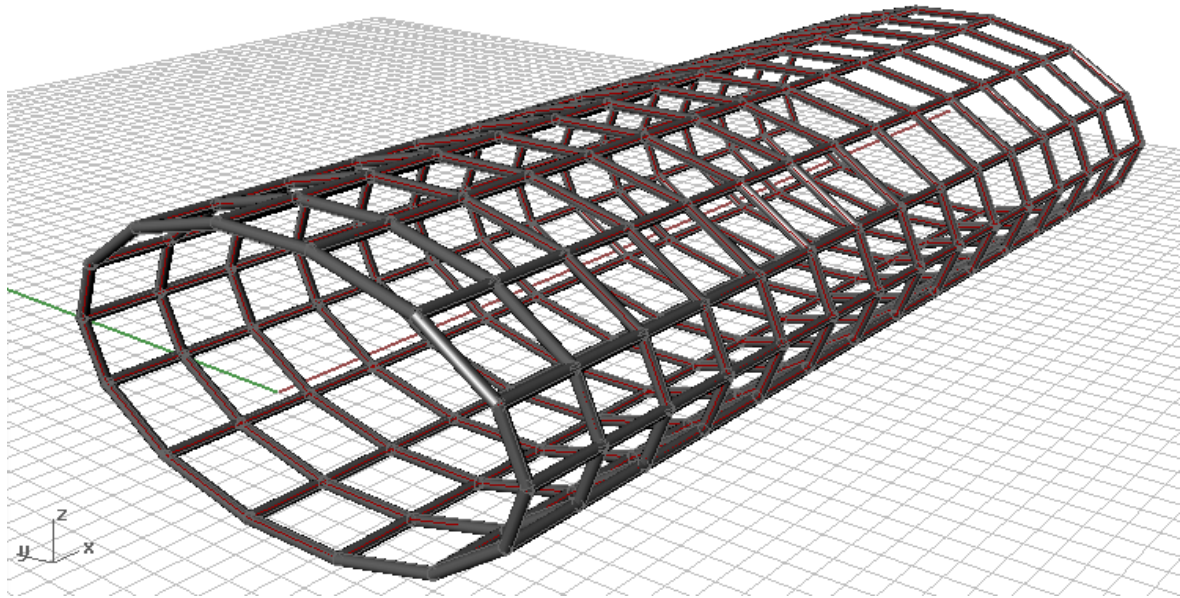


Fig. 45: Horizontal and vertical members parametrically generated in 'Grasshopper' by connecting 'point 0 and 'point 1' as well as 'point 0 and 'point 3' of every sub-surface.

5.4.2.3 GENERATION OF THE DIAGONAL MEMBERS

Following the same procedure as for the horizontal and vertical members of the cylindrical truss, the diagonal members can also be generated. Connecting 'point 0' and 'point 2' of every subsurface yields the diagonal members in one direction. Combined with horizontal and vertical members generated before as described above, yields the following cylindrical truss-layout.

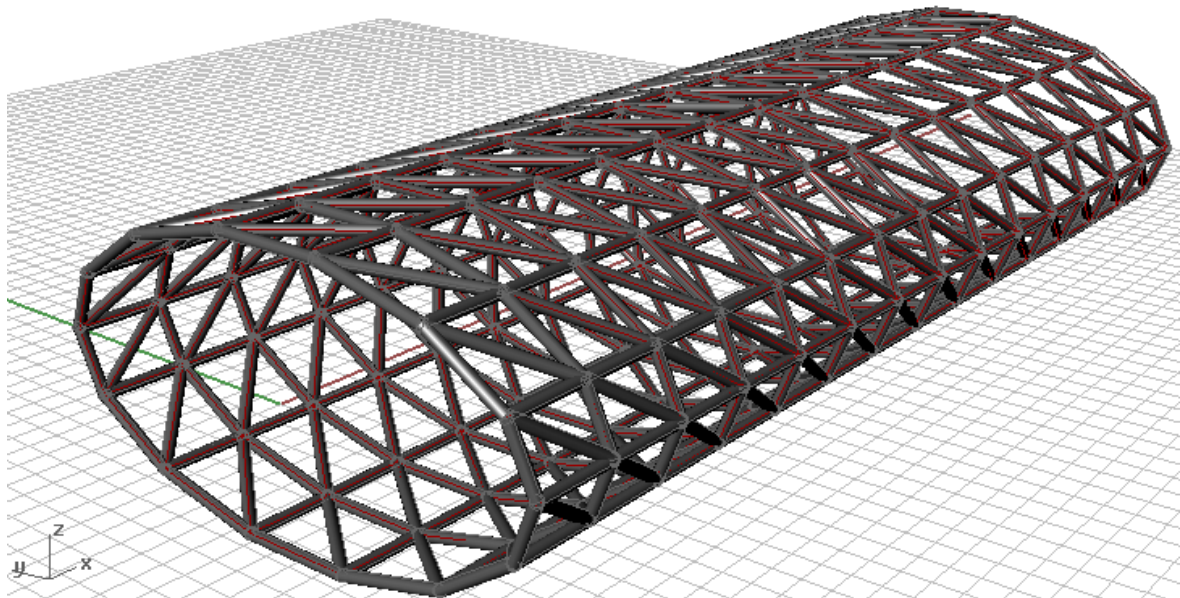


Fig. 46: Parametrically generated 'Grasshopper' model with horizontal-, vertical- and diagonal members. This result is achieved by connecting 'point 0 and 'point 1', 'point 0 and 'point 3' as well as 'point 0 and 'point 2' of every sub-surface.

Further extending this model with the diagonals in the other directions leads to the following model. This model is the stiffest truss configuration possible because it features diagonals in two directions as well as horizontal and vertical members. A disadvantage of this model is the complexity of the connection points: Every node has to connect eight elements; wherein for the model with a single diagonal only six members have to be connected in the nodes.

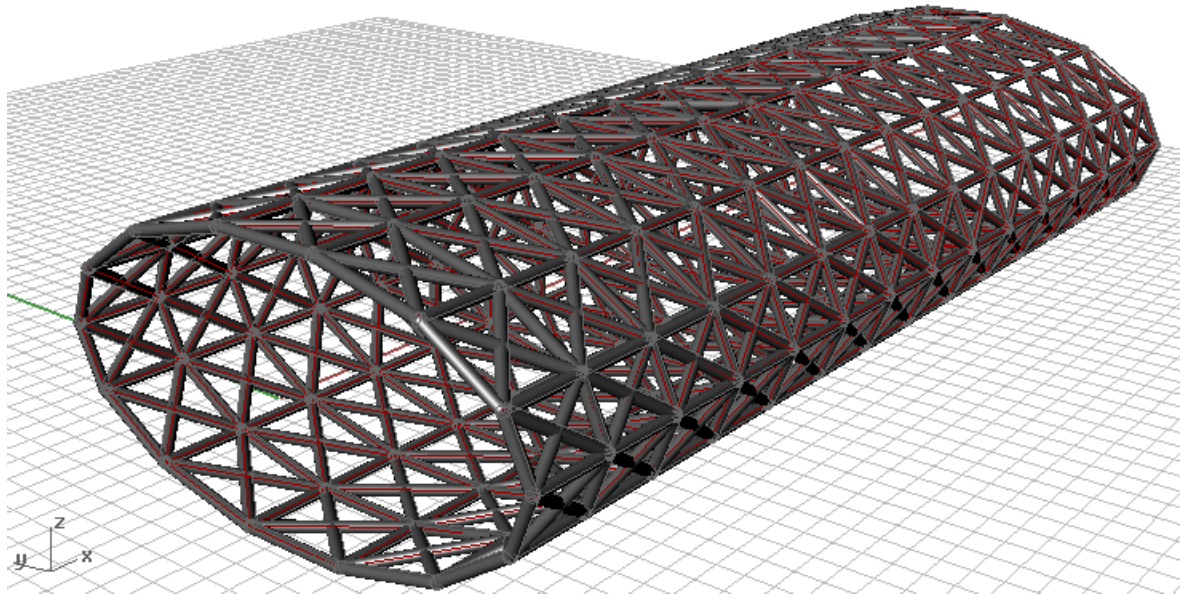


Fig. 47: Parametrically generated 'Grasshopper' model with horizontal-, vertical- and diagonal members in two directions. This result is achieved by connecting 'point 0 and 'point 1', 'point 0 and 'point 3', 'point 0 and 'point 2' as well as 'point 1 and 'point 3' of every sub-surface.

By leaving out the horizontal and vertical linear members, thus not connecting 'point 0 and 'point 1' as well as 'point 0 and 'point 3' with each other, a much lighter truss structure is obtained; the so-called diagrid. This type of structure is very often used in modern structures, such as for example the 'Light Rail Viaduct Beatrixkwartier' in The Hague, The Netherlands. [LS, ch. 6.1.3, p192] The picture below shows this configuration. Also, the connections of a diagrid are much simpler than that of truss with one or even two diagonals. The nodes only have to connect 4 members.

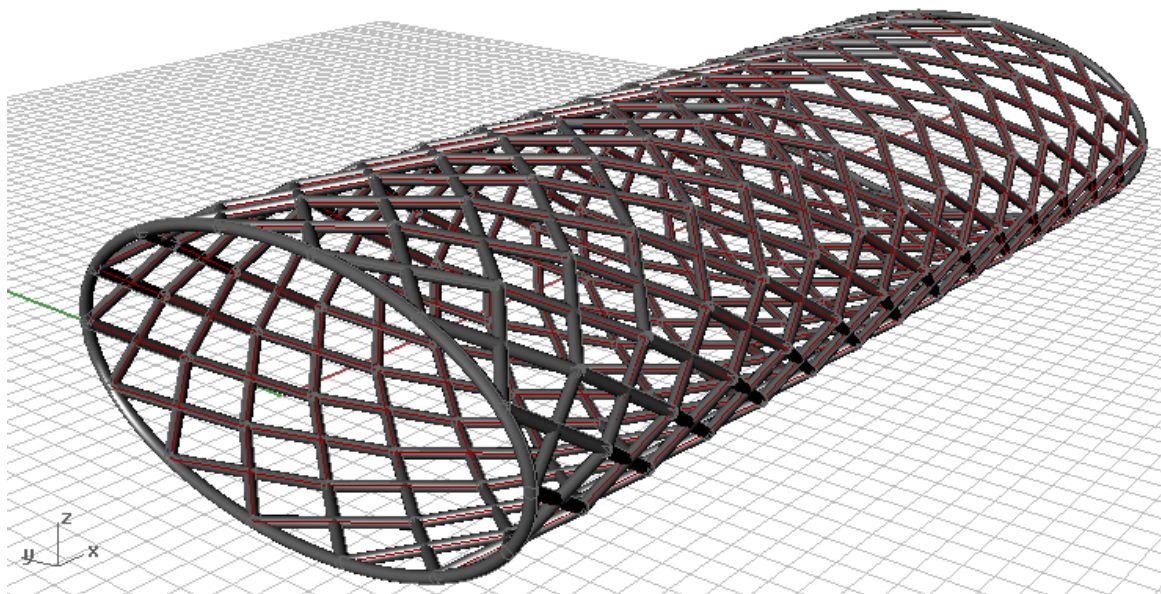


Fig. 48: Parametrically generated 'Grasshopper' model with diagonal members in two directions. This result is achieved by connecting 'point 0 and 'point 2' as well as 'point 1 and 'point 3' of every sub-surface.

5.4.2.4 GENERATION OF OTHER GRID TYPES

Because of the strength and of dynamic parametric geometric modeling, it was chosen to add some additional possible mesh layouts that are to be investigated. The picture below shows the three only possible regular 'tessellations', meaning that these are the only grid-layouts that symmetrically divide a plane into regular polygons. The middle type is the 'Vierendeel' truss that has already been described in [ch. 5.4.2.2]. Herein each polygon has 4 sides and each node connects 4 members. The left type is the hexagonal

tessellation, each hexagon has 6 sides and each node connects 3 members. The right type is the triangular tessellation, each polygon has 3 sides and each node connects 6 members. Along with some other grid layouts these 2 grid types will be briefly described below.

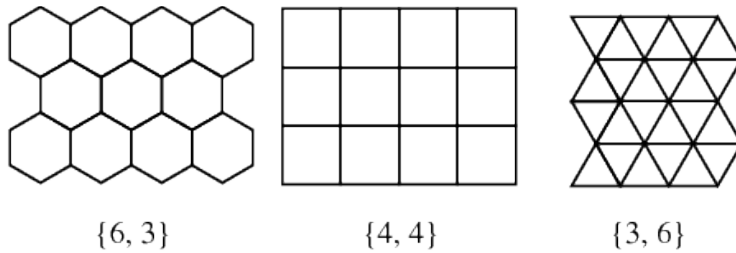


Fig. 49: The three regular tessellations dividing a plane into equal hexagons, squares or triangles [WEB, mathworld.wolfram.com/Tessellation]

Hexagonal grid

The hexagonal grid is another grid-type that can be generated through ‘Grasshopper’, often also referred to as ‘honeycomb’. This grid type has the advantage that the nodes are relatively simple; they only have to connect three members. Furthermore the length of the members is smaller than in the earlier described configurations, reducing the buckling length. Next to that the length of all members used in this grid is similar.

The hexagonal grid is also used for many natural structures, such as the honeycomb or engineered materials such carbon Nano-tubes, as described and depicted before in the literature study [LS, ch. 4.3.7.6, p182]. Since Nano-tubes are considered to be among the strongest and stiffest materials available, it is interesting to investigate whether a similar grid will also function on a much larger scale.

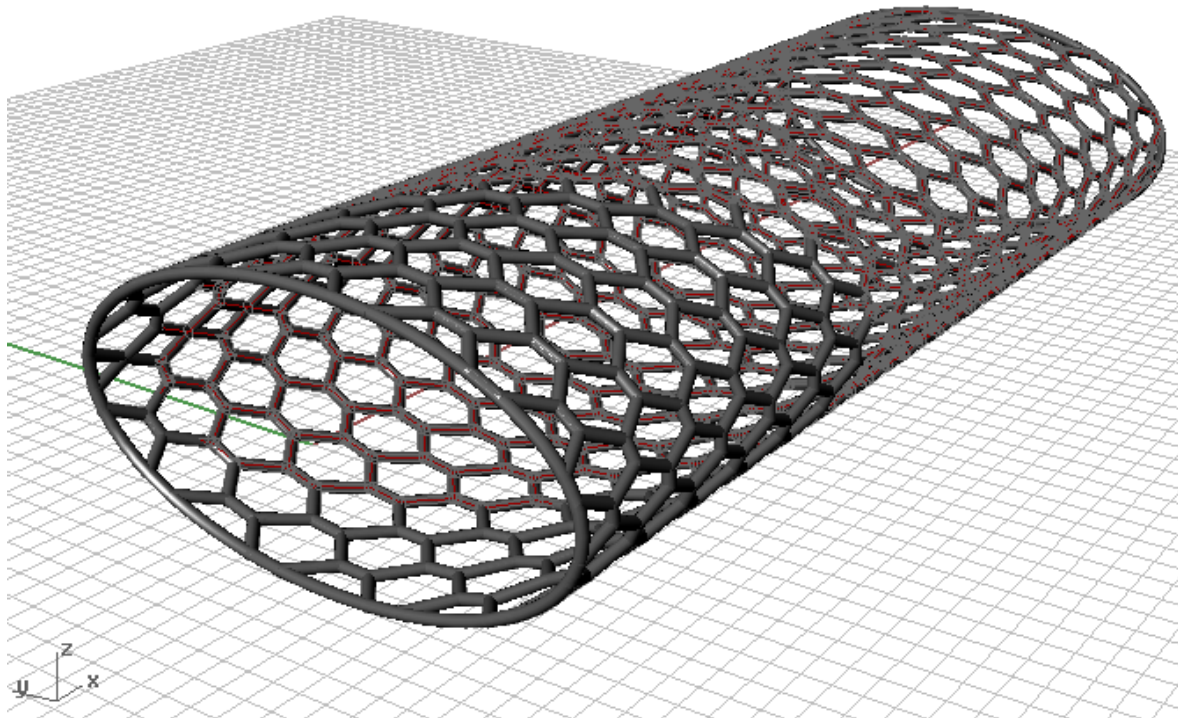


Fig. 50: Parametrically generated ‘Grasshopper’ model of the hexagonal grid type cylindrical truss bridge.

The above picture shows the parametric ‘Grasshopper’ model that was generated. In this model the cell size can be adapted as well as their aspect-ratio. Cells can be stretched in in x, y, z- directions.

Triangular grid

The triangular grid is very often used in modern lattice shell structures. A recent example is the courtyard of the British Museum in London where a double-curved, single-layer steel triangular grid with glass panels was used to provide a roof for the courtyard of this museum. The picture below shows this structure.



Fig. 51: A triangular grid-shell made of steel provides the roof structure for the courtyard of the British Museum in London

The same grid layout can also be used for the cylindrical truss bridge, which is to be designed. The picture below shows the 'Grasshopper' model of this structure. In the parametric model the angle of the triangles as well as their density along the grid can be controlled.

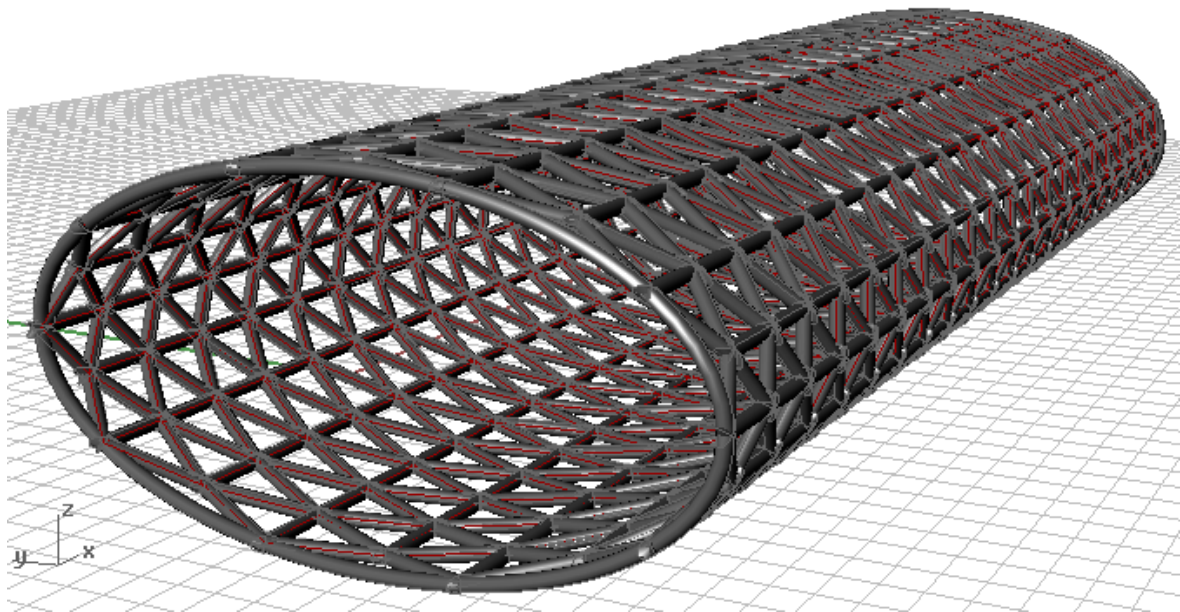


Fig. 52 : Parametrically generated 'Grasshopper' model of the triangular grid type cylindrical truss bridge.

Non-uniform grids

The grids covered until now all share a uniform distribution of members; the grid is exactly the same for every x-coordinate. It is known that occurring stresses are not uniform along the length of a girder. In this sub-chapter a method is given that shows that through 'Grasshopper' the generation of non-uniform grids is possible. However, due to the added set of parameters that these non-uniform grids would introduce during the final FE-analysis, it is expected that these advanced grid shapes will not be used for the final design.

To cope with these non-uniform stresses a 'Grasshopper' model is needed which can produce non-uniform grids as well as uniform grids. Because the generation of such code is slightly more complex than that of the other uniform grid, the code is shown in the scheme below and briefly described in the following.

Normally [Step 7] and [Step 8] of [ch. 5.4.2.1] would create an evenly spaced, uniform grid. Now, the evenly spaced intervals are decomposed into two lists, where the x- and yz-divisions can be separately controlled [Step A]. In 'Grasshopper' the divisions are not called x- and yz-divisions but U- and V-divisions. That is why the components used in the 'Grasshopper' code all have U- and V-inputs or -outputs instead of x- and y-z-values. In this explanation they will be exclusively referred to as x- and y-z-divisions or -components.

The x-components are fed into a 'Graph-mapping component' [Step B]. Here a Bezier-type graph is used to control their division intervals. Of course other graph-types can also be used. Since the list previously had been split to affect only the x-division intervals, afterwards the x- and y-z-component lists have to be re-assembled again [Step C]. If necessary the x-y-division can also be unevenly distributed by adding another 'Graph-mapping component' for the y-z-division intervals between [Step A] and [Step C]. In the code depicted below the y-z-output lines run straight from the initial domain component to the new re-assembled domain, without having been altered.

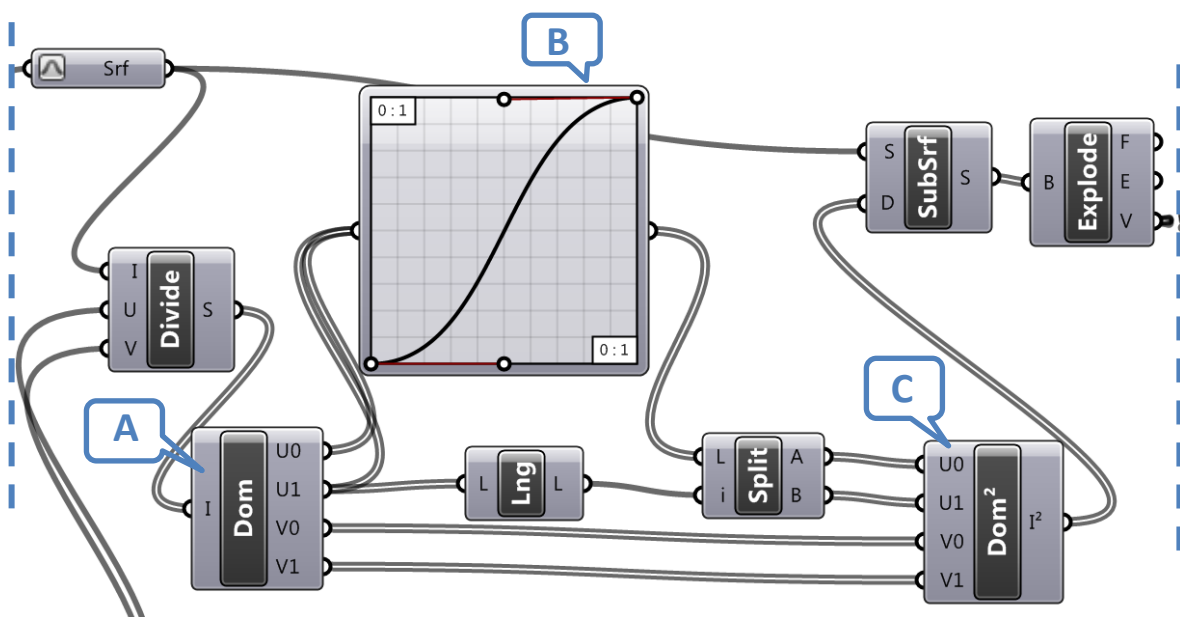


Fig. 53: 'Grasshopper' code to generate a non-uniform grid

The picture below shows the result of the 'Grasshopper' code described above. The two-diagonal truss was adapted in such a way that towards the edges of the cylindrical truss the truss grid becomes gradually more dense. The rate-of-change of this density can be adapted through the curve in the 'Grasshopper' code.

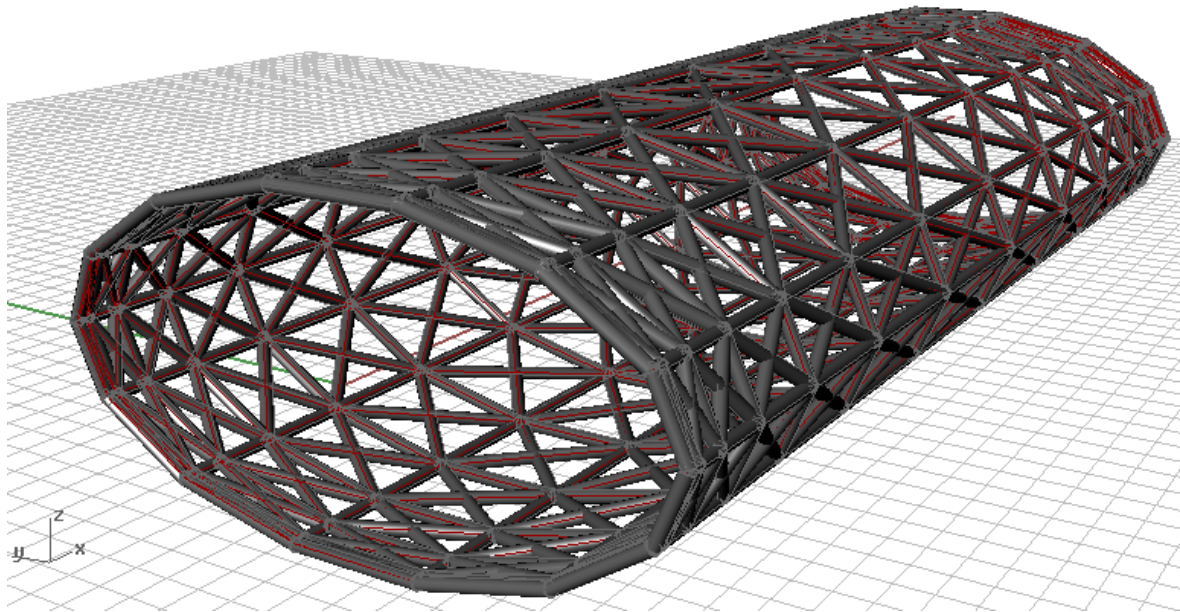


Fig. 54: Parametrically generated ‘Grasshopper’ model of the non-uniform grid type cylindrical truss bridge. This model is based on the two-diagonal truss, described in [ch. 5.7.2.3] adapted by a ‘Bezier-curve’.

Double layer space frame grid

All previously described mesh layouts share one property: They are single-layered. In other structures, such as large-span roofs, multi-layered truss structures are often used. These so-called space frames have the advantage that they possess a structural height, leading to smaller perpendicular-to-the-plane deformations. Applying such a space frame to the cylindrical truss bridge is an interesting option that has to be called out. Similar to the non-uniform grids described before, the double layer space frame grid will be described here, but it is not expected that it will be used in the final design, due to high overall complexity, as well as the added material usage and the complexity of the nodes in particular. Here it is described for the sake of completeness and to show that generation of such complex grids is possible, when using ‘Grasshopper’.

The picture below shows the dynamic parametric geometric model of the space frame cylindrical truss bridge. This height of the space frame and the type perpendicular members can be adjusted through ‘Grasshopper’, in this example it was set to 1,00m. Of course, a structure of this type is much more complex than a single-layer mesh layout. It also uses about 2x times as much material as the single-layer structure. Whether the advantages of the second layer weigh up against the added material costs and the drastically increased complexity of the connections still has to be investigated.

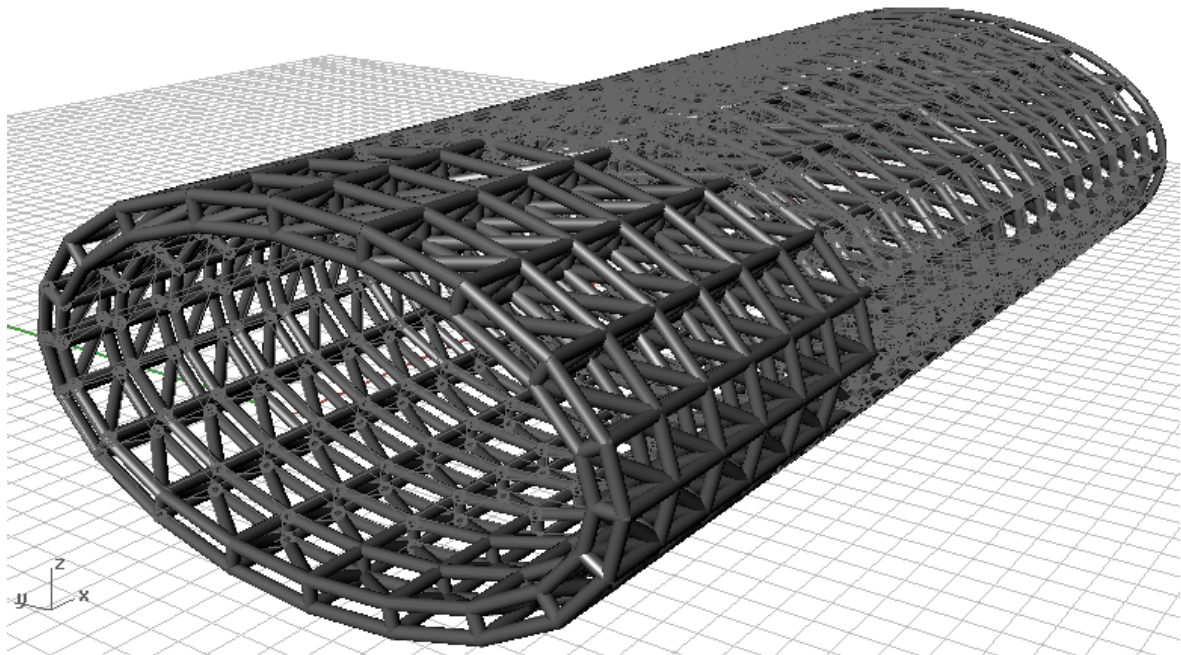


Fig. 55: Parametrically generated 'Grasshopper' model of the double-layered space frame grid type cylindrical truss bridge.

6. LOAD & DEFLECTION REQUIREMENTS OF THE HEAVY TRAFFIC BRIDGE

In this chapter the rules that were found to be applicable for a heavy traffic bridge in the literature study [LS, ch. 3.3, p118] are recalled and quantified for the specific bridge. In the Netherlands, as in the rest of the EU, the Eurocode is the code that has to be followed by any bridge designer, in specific this is 'Eurocode 1: Actions on structures'.

6.1 ENVIRONMENTAL- & DEAD LOADS

In this chapter the normal loads that act on all kinds of structures built in an outside environment are considered. These include the snow loads, the wind loads and the dead load by own weight.

6.1.1 SNOW LOAD

In the literature study [LS, ch. 3.3.2, p123], the rules for the snow load on structures were already given, these were found in the following code: 'Eurocode 1 - Actions on structures – Part 1-3 – General Actions – Snow loads and the Dutch national annex' [NEN-EN 1991-1-3:2003/NB:2007]. For an open tube type truss bridge, meaning the truss cells surrounding the bridge deck are not covered, it is assumed that the snow loads on traffic bridges can be assessed as snow loads on the ground according to. [NEN-EN 1991-1-3:2003, chapter 4.3, p15]:

$$s_{Ad} = C_{est} s_k \quad (6.1a)$$

Wherein s_{Ad} is the calculation value of the snow-load on the ground for the considered location, C_{est} is the coefficient for special snow loads and s_k is the characteristic value of the snow load on the ground for a specific location. In the Netherlands, according to [NEN-EN 1991-1-3/NB:2007, chapter 4.1, p3] the characteristic value for the snow load on the ground for all Dutch regions and provinces has to be taken as $s_k = 0,7 \text{ kN/m}^2$. The coefficient for special snow loads C_{est} is given by [NEN-EN 1991-1-3:2003, chapter 4.3, p15] by: $C_{est} = 2,0$. This yields the following design snow load (without any safety factors) that has to be applied on the total bridge deck surface, calculated by multiplying the width of the bridge by the span.

$$q_{snow} = C_{est} s_k = 2,0 * 0,7 = 1,4 \text{ kN/m}^2 \quad (6.1b)$$

6.1.2 WIND LOAD

As stated in the literature study before [LS, ch. 3.3.1, p118] the lateral wind load on traffic bridges has to be calculated according to 'Eurocode 1991-1-4, Actions on structures – General actions – Wind actions' and the Dutch national annex of this code [NEN-EN 1991-1-4:2005/NB:2007]. Since the type of bridge structure that is used here is not considered in the chapter of this code on bridges [NEN-EN 1991-1-4:2005, ch. 8, p75], here the normal procedure for buildings is used. For the structure that is considered here, the wind load is

cannot be neglected because of the substantial height of the structure. Due to this height a large surface is susceptible to wind loads. The normal wind load F_w can be calculated using the following formula [NEN-EN 1991-1-4:2005, p27] :

$$F_w = c_f c_s c_d q_{wind} A_{ref} = \quad (6.2)$$

$$F_w = 2,1 * 1 * \frac{4,084 \text{ kN}}{\text{m}^2} * 230,128 \text{ m}^2 = 1973,670 \text{ kN}$$

In this formula, q_{wind} is the wind pressure, A_{ref} is the reference surface of the structure, c_f is the force coefficient of the element and $c_s c_d$ is the building factor. The calculation of this coefficient is time-consuming and requires knowledge on the structure, such as Eigen frequencies and mass per unit length, which can only be derived in a later design-stage. In this report the design value of the building coefficient will therefore be taken as $c_s c_d = 1$. The normal wind load is a point load. For a (linear) bridge a line load is the more realistic choice, this load can be calculated by:

$$q_{wind \text{ per } m \text{ span}} = F_w / l_{bridge} \quad (6.3)$$

$$q_{wind \text{ per } m \text{ span}} = 1973,670 / 49,0 = 40,28 \text{ kN/m}$$

The general formula for extreme wind pressure is given by [NEN-EN 1991-1-4:2005, p24]

$$q_{wind}(z) = \frac{\rho}{2} (v_m)^2 (1 + 7I_v) = c_e(z) * q_{base-wind} \quad (6.4)$$

$$q_{wind}(z) = \frac{0,0125}{2} (16,579)^2 (1 + 7 * 0,1968) =$$

$$q_{wind}(z) = 4,084 \text{ kN/m}^2$$

Wherein: $\rho = 1,25 \text{ kg/m}^3$, which is the air-density at a temperature of about 10°C according to [NEN-EN 1991-1-4,NB:2007, p9]. v_b is the base wind speed, and I_v is the turbulence intensity. Before the wind pressure can be calculated, first the 'base wind speed', the 'roughness factor', the 'terrain factor' and the 'turbulence intensity' need to be calculated. In the following the formulae for these parameters will be given. The premise for the procedure below is that the site for the bridge lies in The Netherlands, South Holland Province (Wind area II) in urban terrain (Terrain roughness III).

In the following the calculation procedure for the wind load on the structure will be given in more detail. According to the Eurocode a number of characteristic values have to be calculated in order to be able to derive the design wind load. These characteristic values include the base wind speed, the roughness factor, the terrain factor, the turbulence intensity, the reference surface area and the force coefficient.

Base wind speed

The base wind speed can be calculated by the following formula: [NEN-EN 1991-1-4:2005, p21]

$$v_m(z) = c_r(z) c_o(z) v_b = \quad (6.5a)$$

$$v_m(z) = 0,614 * 1 * 27,0 =$$

$$v_m(z) = 16,579$$

Wherein: $c_r(z)$ is the roughness factor, calculated by the formula below, $c_o(z)$ is the orographic factor, which is set to $c_o(z) = 1$, for the Dutch flatlands. [NEN-EN 1991-1-4:2005, p21] The base wind speed $v_b = v_{b,0} = 27 \text{ m/s}$ for the Dutch province of South Holland, wind area II, according to [NEN-EN 1991-1-4,NB:2007, p3,4].

Roughness factor

In the case of a height above 7m (= z_{min}) above sea level and, in the case of terrain roughness III, urban area, $z_0 = 0,5m$ according to [NEN-EN 1991-1-4,NB:2007, p5]. The formula for the roughness factor $c_r(z)$ then becomes [NEN-EN 1991-1-4:2005, p21] as described below. The median height z of the bridge is defined by: $z = h_{free} + 0,5 * R2_{var2B} = 5,00m + 2,5m = 7,50m$ [ch. 5.2.2] [ch. 5.3]

$$c_r(z) = k_r \ln\left(\frac{z}{z_0}\right) \text{ for } z_{min} \leq z < z_{max} \quad (6. 5b)$$

$$c_r(z) = 0,22 \ln\left(\frac{7,50}{0,5}\right) =$$

$$c_r(z) = 0,614$$

In this formula k_r is the terrain factor, dependent on the roughness length z_0 .

Terrain factor

The terrain factor k_r is given by the following formula: [NEN-EN 1991-1-4:2005, p21]:

$$k_r = 0,19 \left(\frac{z_0}{z_{0,II}}\right)^{0,07} = \quad (6. 5c)$$

$$k_r = 0,19 \left(\frac{0,5}{0,05}\right)^{0,07} =$$

$$k_r = 0,22$$

Wherein $z_{0,II} = 0,05m$, the roughness length of terrain roughness category II, given by [NEN-EN 1991-1-4:2005, p22]

Turbulence intensity

The turbulence intensity I_v can be calculated using the following formula, according to [NEN-EN 1991-1-4:2005, p24]

$$I_v(z) = \frac{\sigma_v}{v_m(z)} = \frac{k_l}{c_o(z) * \ln(z/z_0)} \text{ for } z_{min} \leq z < z_{max} \quad (6. 5d)$$

$$I_v = \frac{1}{1 * \ln(8,15/0,05)} =$$

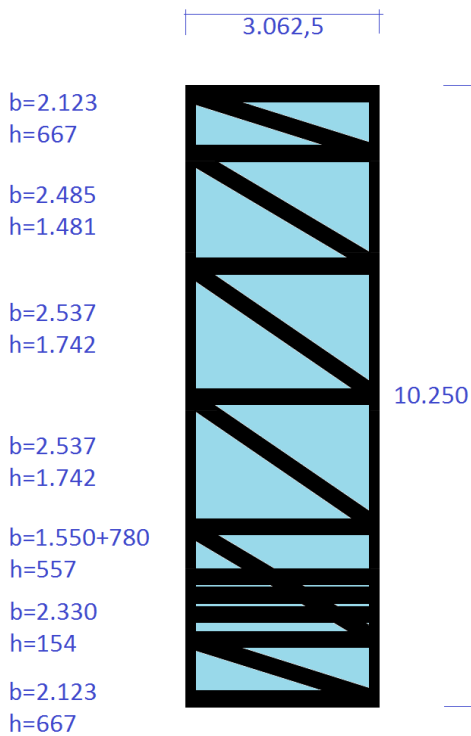
$$I_v = 0,1968$$

Herein σ_v is the standard deviation of the turbulence component of the wind speed. The standard deviation can be calculated using the value $k_l = 1$ for the turbulence factor according to [NEN-EN 1991-1-4:2005, p24]. The term $\ln(z/z_0)$ is the same as used in the calculation of the roughness factor. $c_o(z)$ is the orographic factor, which is set to $c_o(z) = 1$, for the Dutch flatlands. [NEN-EN 1991-1-4:2005, p21]

Reference surface area

The reference surface area A_{ref} of the structure is the surface area of the truss bridge and can be calculated by the summation of the projected surfaces of all truss members in the vertical lateral plane of the bridge. In the form of a formula this is equal to: [NEN-EN 1991-1-4:2005, p72]

$$A_{ref} = \sum_0^n d_n l_n \quad (6. 5e)$$



The reference area can only be calculated when the exact dimensions of all bridge members are known. Therefore here the final design is used, that is described in a later chapter [ch. 8]. The reference surface area A_{ref} is calculated according to the scheme of the final bridge design given below. This scheme shows a section of the bridge only. Since the bridge is completely prismatic, the reference surface area factor of the section is also valid for the whole bridge.

In the following formula, A_c is the total surface area enclosed by the outer bridge edges, laterally and vertically projected. Another important value used in this formula is the solidity ratio φ which denotes the ratio of reference surface area to total surface area. This ratio is needed in the calculation procedure of the force coefficient. [NEN-EN 1991-1-4:2005, p72]

Fig. 56: Scheme of a section of the final design of the bridge for the calculation of the reference surface area.

$$A_c = 3,0625m * 10,250m * 16 = 16 * 31,391m^2 = 502,256m^2$$

$$A_{ref} = A_c - 16(2 * 2,123m * 0,667m + 2,485m * 1,481m + 2 * 2,537m * 1,742m + (1,550m + 0,780m) * 0,557m + 2,330m * 0,154m) = 16 * 14,383m^2 = 230,128m^2$$

$$\varphi = \frac{A_{ref}}{A_c} = \frac{230,128m^2}{502,256m^2} \cong 0,458 \quad (6. 5f)$$

Force coefficient

The force coefficient c_f is given by the following formula [NEN-EN 1991-1-4:2005, p70]:

$$c_f = c_{f,0} \psi_\lambda \quad (6. 5g)$$

Wherein $c_{f,0}$ is the force coefficient of the truss without the so called end effects, $c_{f,0}$ can be derived from the design graph below for spatial trusses as a function of the solidity ratio φ : [NEN-EN 1991-1-4:2005, p71]:

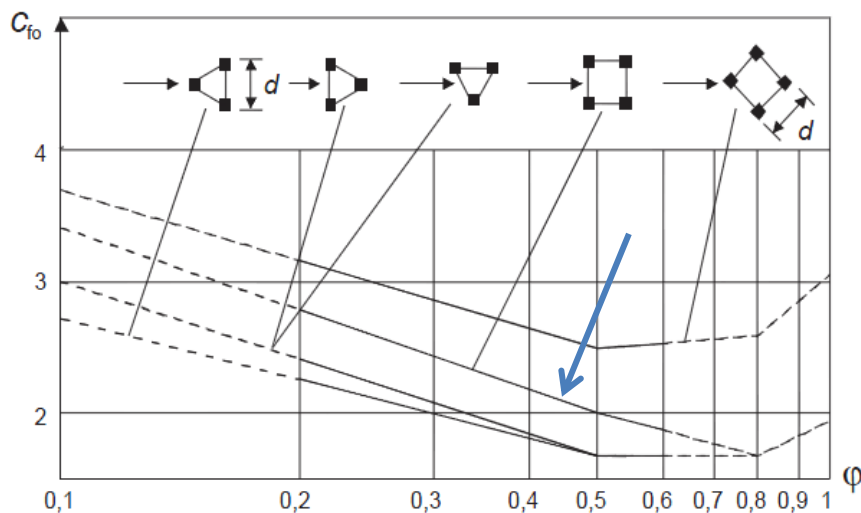


Fig. 57: Force coefficient for trusses without end effects as a function of the solidity factor [NEN-EN 1991-1-4:2005, p71]

The end effect factor ψ_λ for trusses as a function of the structure slenderness of the structure takes the smaller wind resistance of the structure at the ends into account. A conservative and safe value for this factor is $\psi_\lambda = 1$, assuming that there is no wind resistance reduction at the ends of the structure (See also [T09, p28] [NEN-EN 1991-1-4, Table 7.16, p74])

$$c_f = c_{f,0} \psi_\lambda$$

$$c_f = 2,1 \tag{6.5h}$$

6.1.3 SELF-WEIGHT

The self-weight of the structure itself also has to be considered. Since the exact dimensions of the bridge have not yet been chosen the total self-weight cannot be quantified yet. Therefore in this chapter the main elements will be summed up that contribute to the total dead load.

- Main load bearing cylindrical truss structure: Self-weight of truss members, self-weight of connections.
- Bridge deck substructure: self-weight of inner bridge supporting trusses, self-weight of outer bridge supporting trusses.
- Bridge deck panels: weight of the panels of the bridge deck as supplied by the manufacturer.
- Fire safety protection measures: It is decided to account for the weight of the fire safety coatings and fillers, as described in [ch. 4.5.2] by increasing the weight of the structural sections by 5%.

6.1.4 THERMAL LOAD

To take into account the stresses that are induced by daily and seasonal changes in air temperature and solar radiation the Eurocode prescribes several rules [NEN-EN1991-1-5:2003]. In this research only the uniform temperature components will be taken into account to model the change in air temperature and thus the uniform temperature change of the structural members over the course of certain time period.

Normally, for the bridge deck, a linearly varying temperature difference component in z-direction is also taken into account to model the change in temperature of the bridge deck due to solar radiation. However,

since the bridge deck is not the main part of this research, it is chosen not to use this thermal load as a design load.

For the derivation of the thermal effects, the Eurocode prescribes to use the coefficient of linear expansion. [NEN-EN1991-1-5:2003, Sec.4, par. 5, p15] For the unidirectional reinforced FRP carbon/epoxy composite used, this coefficient was already described in [ch. 3.3, table 4]. The minimum and maximum shade air temperature T_{min}, T_{max} dictated by the national annex of the Eurocode [NEN-EN1991-1-5:2003, NB: 2011, ch.5.2, table 5.2,p3] are:

$$\begin{aligned} T_{min} &= -25^{\circ}\text{C} \\ T_{max} &= 30^{\circ}\text{C} \end{aligned} \quad (6.6)$$

According to [NEN-EN1991-1-5:2003, table 5.2, p18] [NEN-EN1991-1-5:2003, NB:2011, ch.5.3, p3] the value for T_{out} , the surface temperature of structural materials in an outside environment has to be calculated by the following formulae.

$$\begin{aligned} T_{out-min} &= T_{min} = -25^{\circ}\text{C} \\ T_{out-max} &= T_{max} + T_4 = 30^{\circ}\text{C} + 30^{\circ}\text{C} = 60^{\circ}\text{C} \end{aligned} \quad (6.7)$$

Herein the effects of the surface color of the structural material are taken into account by the additional temperature T_4 . T_4 is used for a 'light surface color', which is assumed to be about the surface color of the finished bridge.

For the heat-up of bridge decks, the Eurocode does not give specific data. However specific data on the heat up of FRP composite bridge decks is not included. Therefore in this research the data for steel plate bridge decks is used. The Eurocode national annex [NEN-EN1991-1-5:2003, NB:2011, ch.5.3, p3] prescribes the following minimum and maximum temperatures for the uniform heat up of steel bridge decks, which are also used for FRP bridge decks here:

$$\begin{aligned} T_{e,min} &= T_{out-min} - 3^{\circ}\text{C} = -25^{\circ}\text{C} - 3^{\circ}\text{C} = -28^{\circ}\text{C} \\ T_{e,max} &= T_{out-max} + 16^{\circ}\text{C} = 60^{\circ}\text{C} + 16^{\circ}\text{C} = 76^{\circ}\text{C} \end{aligned} \quad (6.8a)$$

The uniform temperature component ΔT_N that has to be taken into account therefore becomes:

$$\Delta T_N = T_{e,max} - T_{e,min} = 76^{\circ}\text{C} + 28^{\circ}\text{C} = 104^{\circ}\text{C} \quad (6.8b)$$

This uniform temperature component will be used together with the coefficient of linear expansion to calculate the maximum elongation/contraction of the FRP-structural members of the bridge. Because this elongation or contraction cannot always happen freely in a bridge structure, the restrained movement will induce stresses on the members and thereby on the bridge.

6.2 VERTICAL HEAVY TRAFFIC LOADS

The vertical traffic loads are the most important loads for any traffic bridge. In the literature study [LS, ch. 3.3, p124] all load models prescribed by the Eurocode [NEN-EN 1991-2:2003, ch. 4.3, p35] were already discussed. In this chapter only the two most applicable load models will be covered.

'Load model 1' (LM1) features concentrated and uniformly distributed loads and covers most of the effects of the traffic of trucks and cars. According to the Eurocode [NEN-EN 1991-2:2003, ch. 4.3.1.2 (a), p35] it is the model that should be used for general and local verifications.

'Load model 2' (LM2) only features a single axle load on specific tire contact areas. It covers the dynamic effects of the normal traffic on short structural members with a loaded length up to 3,0m up to 7,0m.

For the possibility of crowd loading, a third load model is used: 'Load model 4' (LM4). This load model should only be used for some transient design situations, if specifically asked for by the authorities or if a crowd loading is expected.

6.2.1 LOAD MODEL 1 (LM1)

As described before in the literature study [LS, ch. 3.3.3.1, p124], this model consists of two partial systems: the double-axle concentrated loads system (tandem system) as well as uniformly distributed loads system (UDL system). Both systems have to be applied simultaneously. The denoted adjustment factors α are specified by the Dutch national annex [NEN-EN1991-2:2003/NB:2009, table NB.4.1, p6] They are dependent on the number of trucks per lane per year and the span of the bridge. Since the traffic intensity is not known the most conservative value is chosen: $\alpha_Q = 1$

The definition of LM1 is directly taken from Eurocode 1 [NEN-EN 1991-2:2003, ch. 4.3.2, p35-38] For bridges with only one notional lane the tandem system consists of two axles with two wheels each. Each axle load has the following magnitude F_{axle} . Since every axle has two wheels the load per wheel is defined by F_{wheel} :

$$F_{LM1-axle} = \alpha_Q Q_k = 1,0 * 300,0 = 300,0kN \quad (6.9)$$

One tandem has to be used per notional lane. They should be placed centrally on the appropriate lane. The weight of the axle should be uniformly distributed between the wheels, defined by:

$$F_{LM1-wheel} = 0,5 * F_{LM1-axle} = 0,5 * 300,0 = 150,0kN \quad (6.10)$$

This tandem has to be applied on each notional lane (defined by the orange squares in the picture below). The contact surface of the wheels is square and $A_{LM1-wheel} = 0,4m * 0,4m$ (represented by the black squares in the picture below). The wheels, thus two of these squares should be placed with a 2,0m distance centrally in the lane with 2,00m distance to the other axle.

Since the number of notional lanes per driving direction is one, the uniformly distributed loads system prescribes a uniformly distributed load for this notional lane with a width of $w_{nLane} = 3,0m$ of q_{LM1-1} for the first (and only) notional lane and of q_{LM1-R} for the rest of the bridge deck surface between the two outermost safety barriers .

$$q_{LM1-1} = \alpha_q q_{LM1-1} = 1,0 * 9,0 = 9,0 kN/m^2 \quad (6.11)$$

$$q_{LM1-R} = \alpha_q q_{LM1-1} = 1,0 * 2,5 = 2,5 kN/m^2$$

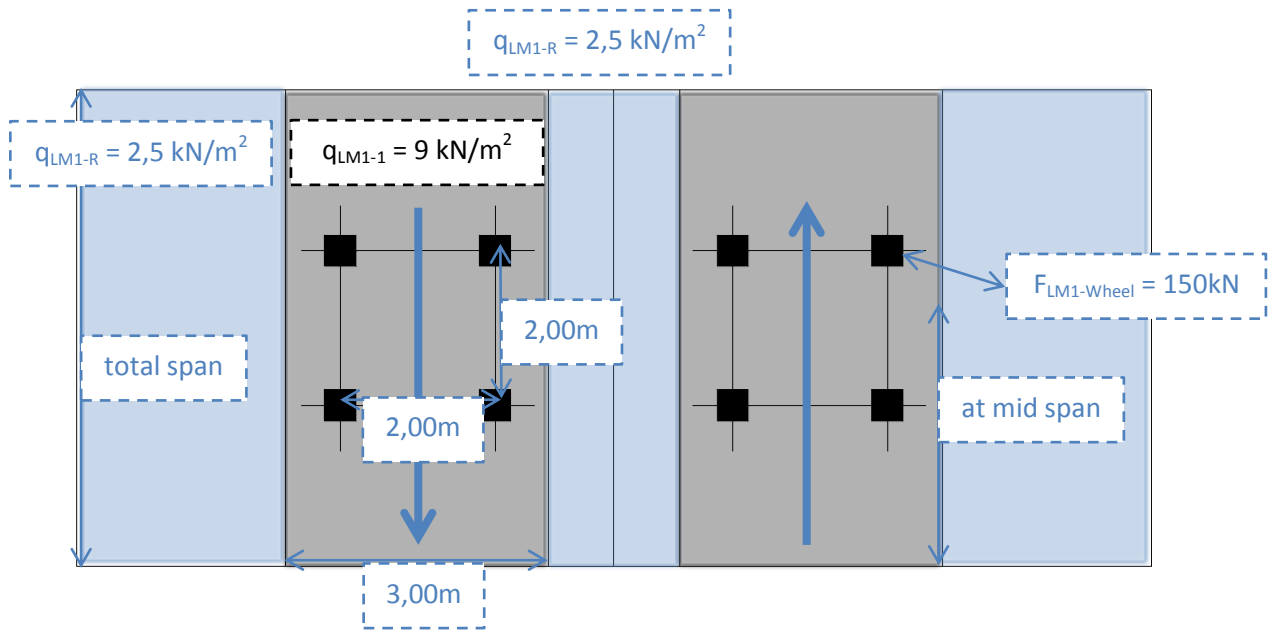


Fig. 58: Definition of LM1 for the bridge to be designed, as prescribed by Eurocode 1 [NEN-EN 1991-2:2003, ch. 4.3.2, p35-38]

6.2.2 LOAD MODEL 2 (LM2)

In the literature study LM2 was already covered [LS, ch. 3.3.3.2, p125]. It prescribes a single axle load applied on specific tire contact areas which covers the dynamic effects of the normal traffic on short structural members with loading length up to 3,00m up to 7,00m.

According to the Dutch national annex the value for the adjustment is $\beta_Q = \alpha_{Q1} = 1$ [NEN-EN1991-2:2003/NB:2009, Par. 4.3.3 (2)]. The information on LM2 was directly derived from Eurocode 1 [NEN-EN 1991-2:2003, ch. 4.3.3, p38-39]

$$F_{LM2-axle} = \beta_Q Q_k = 1,0 * 400,0 = 400,0kN \quad (6.12)$$

$$F_{LM2-wheel} = 0,5 * F_{LM2-axle} = 0,5 * 400,0 = 200,0kN \quad (6.13)$$

This load should be applied at any location on the carriageway. When relevant only one wheel of $200\beta_Q kN$ may be taken into account. The contact surfaces of the wheel (black squares in the picture below) should be set to $A_{LM2-wheel} = 0,35m * 0,6m$. These tire surfaces are different than in LM1, due to a different model. LM2 is normally the preferred model for orthotropic decks.

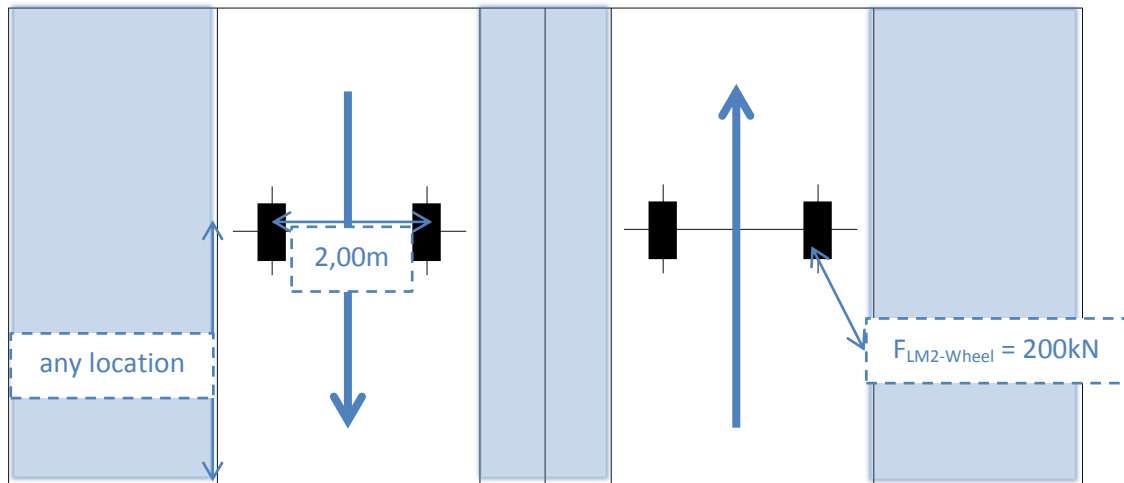


Fig. 59: Definition of LM2 for the bridge to be designed, as prescribed by Eurocode 1 [NEN-EN 1991-2:2003, ch. 4.3.3, p38-39]

6.2.3 LOAD MODEL 4 (LM4)

As described in the literature study before [LS, ch. 3.3.3.4, p126], LM4 is used to anticipate crowd loading in special occasions. It is intended only for general verifications. The load is defined as a uniformly distributed load of. This load includes dynamic amplification. It should be placed on all relevant parts of the bridge [NEN-EN 1991-2:2003, ch. 4.3.3, p39-40]. This load model should only be used for some transient design situations, if specifically asked for by the authorities or if a crowd loading is expected. Since this possibility is still left open, this load case has to be taken into consideration. The magnitude of the uniformly distributed load is defined by the national annex of the Eurocode: [NEN-EN 1991-2:2003/NB: 2009, ch. 4.3.5, eq. NB4.1, p7]

$$\begin{aligned}
 q_{LM4} &= 2,0 + \frac{120}{L + 30} \text{ kN/m}^2 & (6.14) \\
 &= 2,0 + \frac{120}{49 + 30} \text{ kN/m}^2 \\
 q_{LM4} &= 3,52 \text{ kN/m}^2
 \end{aligned}$$

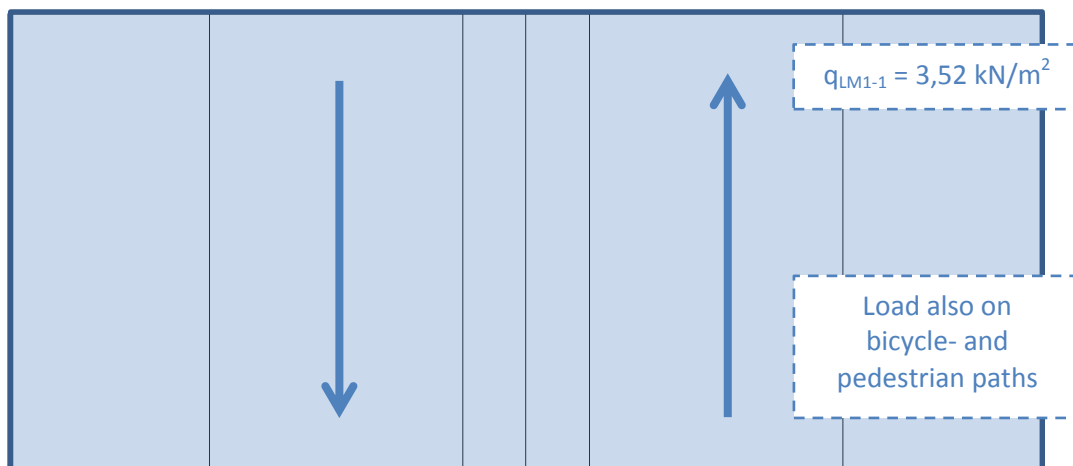


Fig. 60: Definition of LM4 for the bridge to be designed, as prescribed by Eurocode 1 [NEN-EN 1991-2:2003, ch. 4.3.5, p39-40]

6.3 BICYCLE AND PEDESTRIAN LOADS

The loads that the Eurocode 1 [NEN-EN 1991-2:2003, ch. 5, p59] prescribes for bicycle- as well as pedestrian paths on bridges have already been given in the literature study [LS, ch. 3.3.7.4, p134]. Since the bridge to be designed is primarily intended for heavy traffic and the light traffic is only secondary, it is chosen not to use the specialized requirements for pedestrian and bicycle bridges, dictated by the [HIVOSS, Human induced vibrations of steel bridges, design of footbridges guideline, 2008]. The loads given by the Eurocode are expected to be sufficient in this case. The Eurocode bicycle and pedestrian load model has to be used for the remaining area of the bridge that was not covered in [ch. 7.2].

The load model for bicycles and pedestrians is similar to LM1, it features a combination of a uniformly distributed load q_{bp} as well as a point load F_{bp} . The distributed load q_{bp} should only be applied in the unfavorable parts of the influence surface, longitudinally and transversally. The value for the uniformly distributed load is lower than that derived in [ch. 6.2.3], therefore this value can only be used if the full load of the crowd loading model LM4 is not used. F_{bp} has to be applied on a rectangular surface of $A_{bd} = 0,1m * 0,1m$.

$$q_{bp} = 2,0 + \frac{120}{L + 30} kN/m^2 \quad (6.15)$$

$$= 2,0 + \frac{120}{49 + 30} kN/m^2$$

$$q_{bp} = 3,52 kN/m^2$$

$$F_{bp} = 7,0kN \quad (6.16)$$

Next to the loads induced by pedestrians and bicyclists, the Eurocode also prescribes to also take the load induced by a service vehicle F_{serv} into account.

$$F_{serv-axle} = 25,0kN \quad (6.17)$$

$$F_{serv-wheel} = 0,5 * F_{serv-axle} = 12,5kN \quad (6.18)$$

The axles of the service vehicle should have a distance of 3m, each axle having two wheels spaced at 1,75m. The contact surface for each wheel should be set to $A_{service-wheel} = 0,25m * 0,25m$. In the case of a traffic bridge, horizontal forces due to pedestrian or cyclists do not have to be taken into account.

6.4 HORIZONTAL TRAFFIC FORCES

Next to the mostly vertical traffic loads on road bridges, horizontal forces can also occur. In this research several types of horizontal traffic loads will be considered: Braking- and acceleration forces as well as collision forces as centrifugal forces.

6.4.1 BRAKING AND ACCELERATION

As described in the literature study [LS, ch. 3.3.7.1, p132] a braking and acceleration force F_{ba} shall be taken as a longitudinal force acting at the surface level of the carriageway. The braking and acceleration force is limited to 900 kN for the total width of the bridge. It should be calculated as follows:

$$F_{ba} = 0,6(2F_{LM1-axle}) + 0,10q_{LM1-1}w_nLaneL \quad (6.19)$$

$$F_{ba} = 0,6 * (2 * 300) + 0,10 * 9,0 * 3,0 * 49$$

$$F_{ba} = 492,3kN$$

6.4.2 COLLISION

Since the carriageways is enclosed by safety barriers on all sides, the collision forces on the vehicle restraint system have to be taken into account as described in the literature study [LS, ch. 3.3.7.3, p133], given by the Dutch national annex of the Eurocode [NEN-EN 1991-2:2003/NB:2009, ch. 4.7.2.2, p43] by applying certain horizontal load $F_{col-hor}$.

This load $F_{col-hor}$ depends mainly on the energy take-up of the restraining system. It has been derived from measurements during collision tests. In this research a typically used steel safety barrier [ch. 5.1.2] is used for the containment of the carriageway. Therefore the second most ductile safety class B is used [NEN-EN 1991-2:2003, ch. 4.7.3.3, p56]. The load has to be applied as vertical line load a height 0,1m below the top of the restraining system with a length of 0,5m. An additional vertical load $F_{col-vert}$ has to be applied simultaneously.

$$F_{col-hor} = 200kN \text{ for class B} \quad (6.20a)$$

$$F_{col-vert} = 0,5 * F_{LM1-axle} = 150kN \quad (6.20b)$$

6.4.3 CENTRIFUGAL FORCES

According to the Eurocode [NEN-EN1991-2:2003, ch. 4.4.2, table 4.3] the transverse centrifugal force that has to be taken into account is dependant on the horizontal radius of the carriageway centerline. Since the bridge that is designed here has a radius of $r_{carriageway} = 0$, the value of the transverse centrifugal force becomes

$$Q_{tk} = 0 \text{ for } r_{carriageway} = 0 \quad (6.21)$$

For this research it is assumed that additional lateral forces from skew braking or skidding do not have to be separately taken into account. This is in accordance with [NEN-EN1991-2:2003, ch. 4.4.2, par. 4], where the Eurocode states that the loading due to wind effects mostly also includes the transverse traffic loading effects.

6.4.4 VEHICULAR IMPACT

The Eurocode [NEN-EN-1991-1-7:2006, ch. 4.3, p21] prescribes that the substructure of every bridge which spans a roadway, specific static vehicular impact forces must be taken into account that act directly on the substructure of a bridge (e.g. pillars). The values of these vehicular impact forces are given in the national

annex of the Eurocode [NEN-EN-1991-1-7:2006/NB:2011, table NB.1-4.1, p5]. This table (in Dutch) is shown below:

Verkeerscategorie		F_{dx}^a kN	F_{dy}^a kN	d_b m
Autosnelwegen, provinciale wegen en hoofdwegen		2 000	1 000	20
Rijkswegen in landelijke gebieden		1 500	750	15
Wegen in stedelijke gebieden		1 000	500	10
Binnenplaatsen en parkeergarages met toegang voor:	auto's	100	50	4
	vrachtwagens (> 3,5 ton)	200	100	5
^a x = normale rijrichting, y = loodrecht op de normale rijrichting.				

Fig. 61: Vehicular impact forces on the substructure prescribed by the Eurocode Dutch National annex [NEN-EN-1991-1-7:2006/NB: 2011, table NB.1-4.1, p5]

This impact forces must be act at a height of 1,20m of the bridge substructure. For the full-FRP, which is designed to span a 2x4 lane motorway the first row must be used for the forces (highlighted in blue).

Next to the vehicular load on the substructure, the national annex of the Eurocode [NEN-EN-1991-1-7:2006/NB: 2011, table NB.2-4.2, p6] also prescribe vehicular impact forces on the superstructure of the bridge. The following table prescribes the values of these impact forces. Again the first row (highlighted in blue) must be used for the bridge that is to be designed in the course of this research.

Verkeerscategorie		F_{dx}^a kN	$F_{a,\beta}$ kN
Autosnelwegen, provinciale wegen en hoofdwegen		2 000	600
Rijkswegen in landelijke gebieden		1 500	450
Wegen in stedelijke gebieden		1 000	450
Binnenplaatsen en parkeergarages met toegang voor:	auto's	100	
	vrachtwagens (> 3,5 ton)	200	
^a x = normale rijrichting			

Fig. 62: Vehicular impact forces on the superstructure prescribed by the Eurocode Dutch National annex [NEN-EN-1991-1-7:2006/NB: 2011, table NB.2-4.2, p6]

Particularly the vehicular impact load on the superstructure will be considered in the course of this research, since the superstructure is the main design objective. Therefore the two loads F_{dx} and F_{ab} will be placed as a nodal load on the lowest node at mid span. This node which is closest to the surface of the motorway that is spanned is most likely to be hit first by a moving vehicle.

6.5 COMBINATION OF TRAFFIC LOADS

Next to the single traffic load components which are prescribed by the Eurocode, the multi component action is another important load that has to be taken into account. This way the simultaneity of the loading systems as described in [ch. 6.2.1-6.4.3] is taken into account.

The Eurocode prescribes the following combination groups of single traffic load components for the derivation of the characteristic multi component action [NEN-EN1991-2-22003/NB: 2009, table 4.4a, p10]. Of the 6 combination groups, only 4 are used in this research. Gr3 and Gr5 are not taken into consideration, since Gr4 is used and since special vehicles are not part of the design load spectrum of the bridge.

Each of the combination groups, which are mutually exclusive, should be considered as defining a characteristic action for combination with non-traffic loads.

Traffic Load Combination Case	Description
Gr1a	1 * LM1 + 0,4 * (Bicycle & Pedestrian Loads)
Gr1b	1 * LM2
Gr2	0,8 * LM1 + 1 * (Accidental & Collision Loads)
Gr3	not applicable if Gr4 is used
Gr4	1 * LM4
Gr5	only applicable for special vehicles

Table 17: Combination of single traffic load components according to [NEN-EN1991-2003/NB: 2009, table 4.4a, p10]

6.6 COMBINATION OF TRAFFIC LOADS WITH OTHER LOADS

Next to the combination of traffic loads, the combination of traffic loads with other loads such as self-weight, wind, snow and thermal load is also prescribed by the Eurocode [NEN-EN1990:2003/A2, ch. A2.2.2, p9-10, table A2.1, p13]. Here the following important rules are given:

- Gr1b does not need to be combined with any other variable non traffic action [NEN-EN1990:2003/A2, ch. A2.2.2, par. 2]
- Snow- and wind loads do not need to be combined with braking, acceleration and centrifugal forces or Gr2 or Gr4 [NEN-EN1990:2003/A2, ch. A2.2.2, par. 3]
- Snow loads do not need to be combined with Gr1a or Gr1b [NEN-EN1990:2003/A2, ch. A2.2.2, par. 4]
- No wind load greater than the smallest of F_{Wk} OR F_{W}^* (see table) should be combined with Gr1a [NEN-EN1990:2003/A2, ch. A2.2.2, par. 5]
- Wind- thermal loads need not to be combined. [NEN-EN1990:2003/A2, ch. A2.2.2, par. 6]

For the derivation of the load combination values these rules as well as the rules dictated by the table below [NEN-EN1990:2003/A2, ch. A2.2.2, table A2.1, p13], need to be followed:

Action	Symbol	ψ_0	ψ_1	ψ_2	
Traffic loads (see EN 1991-2, Table 4.4)	gr1a (LM1+pedestrian or cycle-track loads) ¹⁾	TS	0,75	0,75	0
		UDL	0,40	0,40	0
		Pedestrian+cycle-track loads ²⁾	0,40	0,40	0
	gr1b (Single axle)		0	0,75	0
	gr2 (Horizontal forces)		0	0	0
	gr3 (Pedestrian loads)		0	0	0
	gr4 (LM4 – Crowd loading))		0	0,75	0
gr5 (LM3 – Special vehicles))		0	0	0	
Wind forces	F_{Wk}				
	- Persistent design situations	0,6	0,2	0	
	- Execution	0,8	-	0	
	F_W^*	1,0	-	-	
Thermal actions	T_k	0,6 ³⁾	0,6	0,5	
Snow loads	$Q_{sr,k}$ (during execution)	0,8	-	-	
Construction loads	Q_c	1,0	-	1,0	

Table 18: Recommended values of Ψ factors for road bridges [NEN-EN1990:2003/A2, ch. A2.2.2, table A2.1, p13]

Combined with the traffic loads with the normal loads, such as self-weight, wind-, snow-, thermal- and vehicle impact loads yields the following combination cases that need to be examined during final design:

Combination Case	Description
LCC1	1 * Self-weight + 1 * Gr1a + 0,6 * Wind
LCC2	1 * Self-weight + 1 * Gr1b
LCC3	1 * Self-weight + 1 * Gr2
LCC4	1 * Self-weight + 1 * Gr4
LCC5	1 * Self-weight + 1 * Wind + 0,8 * Snow
LCC6	1 * Self-weight + 1 * Gr1a + 0,6 * Thermal
LCC7	1 * Self-weight + 1 * Gr2 + 0,6 * Thermal
LCC8	1 * Self-weight + 1 * Gr4 + 0,6 * Thermal
LCC9	1 * Self-weight + 1 * Vehicle Impact

Table 19: Combination of traffic loads with other loads according to [NEN-EN1990:2003/A2, ch. A2.2.2, table A2.1, p13]

6.7 FATIGUE & VIBRATION LOADS

For traffic bridges fatigue is an indispensable load case that has to be considered, as described in the literature study [LS, ch. 3.3.4.3, p127], is fatigue loading. For general fatigue verifications fatigue load model 1 or FLM1 is used in the Netherlands as prescribed by the Eurocode [NEN-EN 1991-2:2003, ch. 4.6, p45] [NEN-EN 1991-2:2003, ch. 4.6.2, p48]

The stress spectrum (minimum stress to maximum stress) produced by traffic running on bridges has to be calculated according to the fatigue load models. FLM1 is very similar to 'Load Model 1' (LM1) as described in [ch. 6.2.1]. However, the values used for the axle loads and uniformly distributed loads in FLM1 are only 0,7x times the axle load of LM1 and 0,3x times the uniformly distributed loads LM1. [NEN-EN 1991-2:2003, ch. 4.6.2, par. 1, p48]

Using the values for LM1, described in [ch. 6.2.1], the values of the axle loads of FLM1 therefore become,

$$F_{FLM1-axle} = 0,7 * F_{LM1-axle} = 0,7 * 300,0 = 210,00kN \quad (6.22)$$

$$F_{FLM1-wheel} = 0,5 * F_{FLM1-axle} = 0,5 * 210,0 = 105,00kN$$

Similarly the values of the uniformly distributed loads of FLM1 are calculated using the previously derived values for LM1 [ch. 6.2.1].

$$q_{LM1-1} = 0,3 * q_{LM1-1} = 0,3 * 9,0 = 2,70 kN/m^2 \quad (6.23)$$

$$q_{LM1-R} = 0,3 * q_{LM1-R} = 0,3 * 2,5 = 0,75 kN/m^2$$

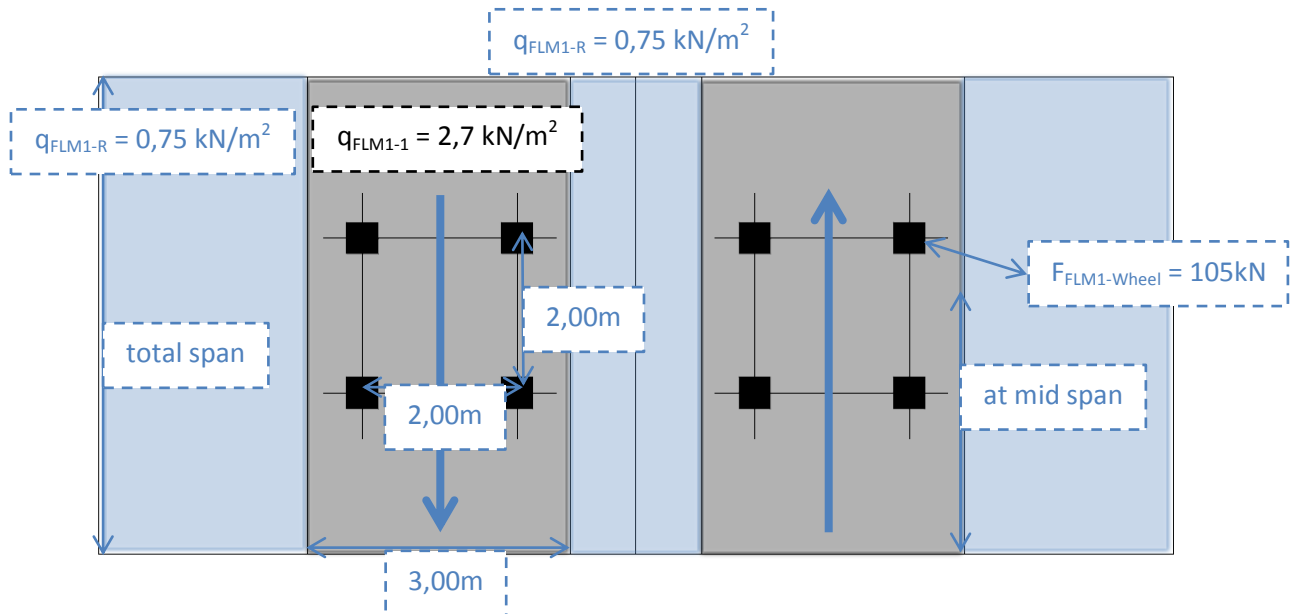


Fig. 63: Definition of FLM1 for the bridge to be designed, as prescribed by Eurocode 1 [NEN-EN 1991-2:2003, ch. 4.6.2, p48]

When the occurring minimum and maximum stresses have been calculated, the number of cycles to failure N_f needs to be calculated according to [CUR96, ch. 9.4.2, p33-34] [CUR96, ch. 9.4.3, p35]

$$N_f = \left(\frac{\sigma_{amp} * \gamma_m * \gamma_c}{\sigma_{Rk}} \right)^k \quad (6.24a)$$

$$N_f = \left(\frac{\sigma_{amp}}{\sigma_{t,RD} \left[1 - \frac{\sigma_{mean}}{\sigma_{t,RD}} \right]} \right)^k \quad \text{for } \sigma_{mean} > 0 \quad (6.24b)$$

$$N_f = \left(\frac{\sigma_{amp}}{\sigma_{c,RD} \left[1 - \frac{\sigma_{mean}}{\sigma_{c,RD}} \right]} \right)^k \quad \text{for } \sigma_{mean} < 0 \quad (6.24c)$$

This number of cycles should then be compared to the table in the Eurocode Dutch National Annex [NEN-EN 1991-2:2003/NB:2009, table 4.5(n).NB, p11]. In this table the number of expected 'single vehicles' per notional driving lane per year for several road classes is given. In order to use this table, first the traffic category of the bridge has to be chosen.

For this bridge a medium flow rate assumption is chosen. This yields category 2 and an expected number $N_{obs} = 0,5 * 10^6$ of FLM1 load inductions per year. For the Dutch road system this means that the bridge

will carry a 'Lokale weg of autoweg met gemiddeld vrachtverkeer (N-wegen)'. Furthermore, the national annex states that for bridges with one lane per direction only the total number of N_{obs} is not $2 * N_{obs}$, as could be expected for two directions, but $1,2 * N_{obs}$ [NEN-EN 1991-2:2003/NB:2009, par.3, p11]. See the table below for the values for other traffic categories:

Traffic categories		N_{obs} per year and per slow lane
1	Roads and motorways with 2 or more lanes per direction with high flow rates of lorries (Dutch A-roads)	$2,0 \times 10^6$
2	Roads and motorways with medium flow rates of lorries (Dutch N-roads)	$0,5 \times 10^6$
3	All other roads	$0,125 \times 10^6$

Fig. 64: Expected number of 'single vehicles' per notional driving lane per year according to the Eurocode [EN1991-2:2003, table 4.5(n), p46]

The life expectancy in years for the heavy traffic bridge then can be calculated by the following relationship:

$$N_{FLM1-years} = \frac{N_f}{N_{obs}} \quad (6.25)$$

The value of $N_{FLM1-years}$ should exceed 100 years, since the Eurocode 0 [NEN-EN1990:2000, ch.2.3, table 2.1, p29] prescribes a design life of 100 years for all bridges. This coincides with the design life category 4 of [NEN-EN1990:2000, ch.2.3, table 2.1, p29], which is the strictest design life criterion prescribed by the Eurocode.

6.7.1 VIBRATION BEHAVIOR

Vibrations are another common load that traffic bridges have to cope with, generally three types of vibrations can be distinguished, human induced vibrations with a frequency of 1H-4Hz [LS, ch. 3.3.5.2, p129], vehicle induced vibrations with a frequency of 5H-25Hz [LS, ch. 3.3.5.3, p130] and wind induced vibrations [LS, ch. 3.3.5.4, p130].

Since the natural frequency analysis and –determination for a large and complex bridge design cannot be done by hand, it has to be done using finite element analysis. Here, for every type of vibration the limiting value for the natural frequency of the traffic bridge is given. These values are prescribed by the Eurocode [NEN-EN 1990+A1+A1/C2:2011, ch. A2.4.3.2, p76] [B21, p141] [NEN-EN 1991-1-4:2005, p31]. The vibration criterion horizontal for human induced vibration as well as the criterion for wind induced vibration (both shown below) concern the horizontal natural frequency of the bridge.

When the conditions below are satisfied, no additional investigations and measures to counteract on vibrations are necessary. During the finite element analysis these conditions will be checked. Note that the Eurocode explicitly does not prescribe vibration checks [NEN-EN 1990+A1+A1/C2:2011, ch. A2.4.2, remark 1, p75]. However, since here a lightweight structure is used, it is chosen to check the natural frequencies of the bridge and to check that the two most critical types of vibrations are excluded.

$$L_{human-vert} > 5,0 \text{ Hz} \quad (6.26a)$$

$$L_{human-hor} > 2,5 \text{ Hz} \quad (6.26b)$$

$$L_{wind-hor} > 1,0 \text{ Hz} \quad (6.26c)$$

6.8 LIGHT RAIL LOADS

In this chapter the loads needed for light rail traffic are described. These are mentioned here for the sake of completeness and for the case that they will be needed during the final design stage. Neither the Eurocode [NEN-EN 1991-2:2003, ch. 6.1(3), p66] nor the Dutch national annex of this code [NEN-EN 1991-2:2003/NB:2009, 6.1(3), p17] prescribe design loads for light-rail traffic. To gain access to the design loads that are to be used during design, manufacturers have to be directly consulted. In the case of the light rail network of the 'The Hague area' in the Netherlands the type of railways that are used is manufactured by 'Alstom'. The rolling stock used here are the 'Alstom, Regio Citadis' 3-car trams. The dimensions of these trams can be found below; they have been directly derived from the manufacturer [A54, p2]:

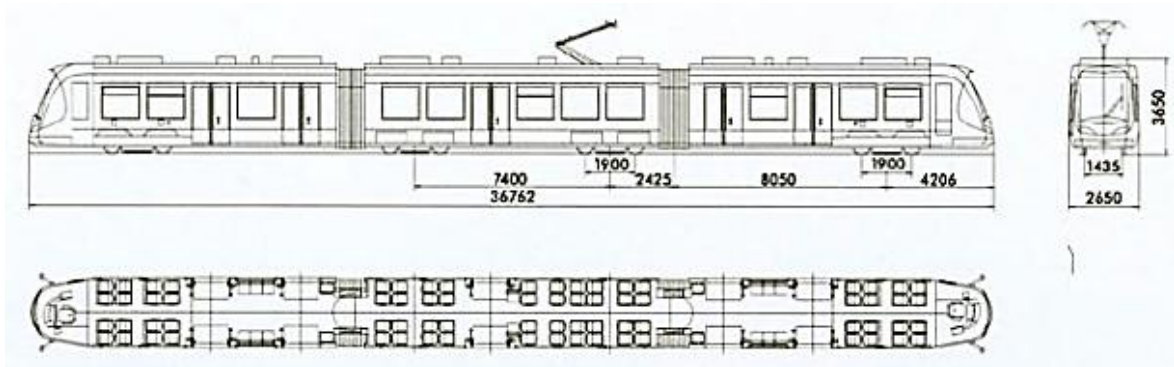


Fig. 65: Dimensions of the light rail tram 'Alstom, Regio Citadis 3-car' [A54, p2]

Using the dimensions displayed before, together with the maximum axle load that was also derived from information of the manufacturer [A53, p4] yields the design loads that have to be applied for a bridge design for light rail traffic.

$$F_{LR-3car-tram} = 920,0 \text{ kN} \quad (6.27a)$$

$$F_{LR-bogie} = 0,25 * F_{LR-3car-tram} = 230,0 \text{ kN} \quad (6.27b)$$

$$F_{LR-axle} = 0,5 * F_{LR-bogie} = 115,0 \text{ kN} \quad (6.27c)$$

$$F_{LR-wheel} = 0,5 * F_{LR-axle} = 57,5 \text{ kN} \quad (6.27d)$$

The 'Regio Citadis' has 4 bogies in total, with 2 axles with 2 wheels each. The picture below shows the light rail loading scheme that was derived using the information from the manufacturer [A53] [A54]. Since the bridge to be designed would have two rail-tracks, one in each direction as described in [ch. 5.2.6] the loading scheme also has to feature two trams. The black squares represent a single wheel; each group of four wheels represents one bogie.

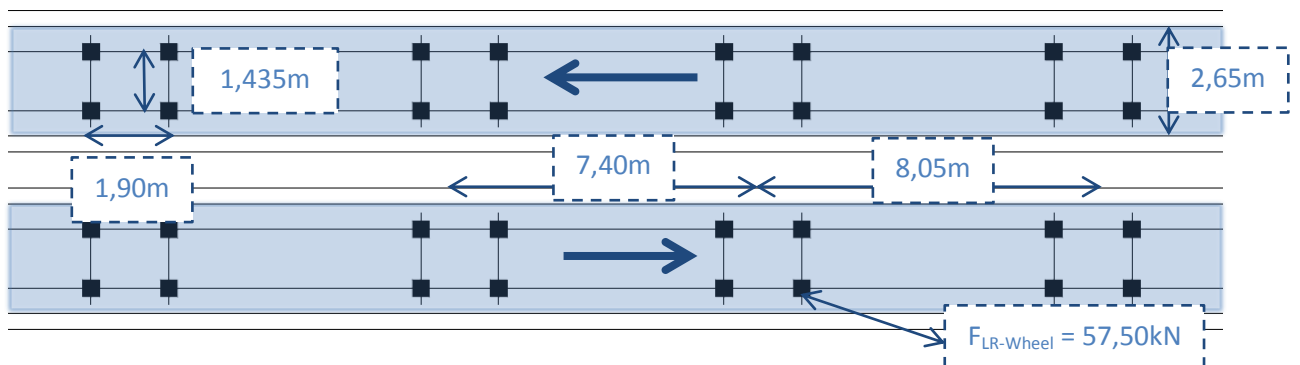


Fig. 66: Loading scheme for the Alstom light rail tram 'Alstom, Regio Citadis 3-car' [A53] [A54]

Because the codified information on light rail tracks is very scarce or even not available, and the loading due to light rail vehicles is not the design load of most interest, vertical forces due to e.g. braking, acceleration, collisions etc. are explicitly not considered in this research. Also, the contact areas of each wheel are not known, when needed a sound assumption on their dimension will be made.

6.9 DEFLECTION LIMITS

Since fiber reinforced polymer is a material which has not been used very often in bridge engineering, codes that prescribe a certain deflection maximum for this material do not exist. Hence the Eurocode advises to limit the occurring vibrations on traffic bridges, using the so-called 'human comfort criteria' to limit the vibration and acceleration of bridge parts [NEN-EN 1990/A1:2005, p24]. Due the complexity of such a vibration limit, in this research, a maximum deflection based estimation will be used. The American code AASHTO [AASHTO-LFRD 1998] gives the following general deflection limits. [LS, ch. 3.3.6, p131-132]

- Deflection limit due to vehicular load, general, on two-support span: $L/800$
- Deflection limit due to vehicular and/or pedestrian load, on two-support span: $L/1000$
- Deflection limit due to vehicular load on cantilever arm: $L/300$
- Deflection limit due to vehicular and/or pedestrian load on cantilever arm: $L/375$
-

It has to be mentioned though, that the AASHTO deflection limits are also based on the limitation of unwanted bridge vibrations. Deflection limits are comfort criteria, meaning that limiting the maximum deflection has the primary goal to meet the comfort needs of the bridge users. They are thus not safety-related. Of course excessive vibration can cause other damages caused by for example fatigue and should therefore also be limited.

Further research on deflection limits of fiber reinforced polymer traffic bridges was carried out by J.R. Demitz et al. [P102]. In his paper he describes that in nearly all FRP bridge designs, -researches, and -papers, deflection limits of $L/425$ to $L/1000$ where used [P102, p4]. This is similar to what was found out in the literature study [LS, ch. 3.3.6, p131-132]. To further investigate whether these limits are indeed correct and safe to use, J.R. Demitz et al. compared three E-glass vinyl-ester composite sandwich traffic bridge designs with a span of approximately 20,0m to steel, reinforced concrete and timber designs. One FRP-design was based on the $L/400$ deflection criterion, one on $L/600$ and one on $L/800$. Without going into detail, it turned out that the $L/400$ design did not meet several acceleration- and vibration limits for speeds above 100 km/h [P102, p9] Using the other two deflection limits was found to be safe, and met all acceleration- and vibration limits.

Of the $L/600$ and the $L/800$ limit the $L/600$ limit should therefore yield sufficiently comfortable bridge designs and meet all acceleration- and vibration limits. It is therefore chosen to use this limit for general bridge deflections.

Quantifying the deflection limit for the design span of the bridge 49,00m, it becomes

$$u_{max} = L_{span} * \frac{L_{span}}{600} = \frac{49.000mm}{600} = 81,667mm \quad (6.28)$$

7. CYLINDRICAL TRUSS PARAMETER STUDY

In this chapter an optimized shape of the cylindrical load bearing structure will be derived. In a first step, the different truss topologies that were obtained in [ch. 5.4.2] are adapted, such that they can be compared in FEA software. Afterwards all of these topologies will be compared using unity loads only. That way the most efficient truss topology will be found. The next step will be the further optimization of this chosen truss topology. The grid size of the truss topology will be varied with the goal of finding the most efficient grid size for this bridge. The last optimization step in the process will be the investigation on the most efficient member cross section dimensions. For this purpose several combinations of CHS diameters and wall thicknesses will be compared to find the most efficient cross section dimensions. The final product of this chapter will be an optimized main cylindrical load bearing structure, which will be used in [ch. 8] for the final design complete with bridge deck [ch. 11.1] and bridge deck substructures [ch. 8.1] [ch. 8.2] as well as all loads prescribed by the Eurocode [ch. 6].

7.1 COMPARISON OF TRUSS TOPOLOGIES

The truss topologies that were described in [ch. 5.4.2] will be compared regarding primarily occurring deformations and stresses in this chapter. Furthermore other important decision points will be called out, such as for example the complexity of the connections for each topology variant. The final result of this chapter will be a comparative table from which the most efficient choice on the truss topology for the cylindrical truss can be derived based on multiple criteria. In conclusion a choice on the truss topology will be made. From then on further calculations and alterations will be based on the truss topology chosen in this chapter.

7.1.1 ADAPTING THE GRASSHOPPER MODELS

Before the different truss topologies can be compared to each other, first the earlier Grasshopper models need to be adapted in such a way that comparison can be done in fair and correct way. Therefore all models have to share their basic dimensions, such as type and radii of the cross-section shape and span. All of these values can be easily controlled with the sliders as described in [ch. 6.4.2.1]. A decision on the span has already been made in [ch. 5.3]. For all variants the span is therefore set to $l_{span} = 49,0m$. For the radii of the cross section a preliminary choice for the elliptical cross section of 'variant 2B' [ch. 5.2.2] is made. Note that this choice is not definitive, here it is only used for the comparison between the truss topology variants. The basic dimension that are used for all truss topology variants are given in the following formulae. The circumference $c_{el.rings}$ of the ellipse was calculated using [eq. 6.1, ch. 6.2].

basic shape = elliptical cylinder (7.1)

$$l_{span} = 49,0m$$

$$c_{el.rings} = 58,89m$$

$$R_1 = 12,0\text{m}$$

$$R_2 = 6,3\text{m}$$

Another important parameter that has to be set equal for all topology variants is the total material usage. This is necessary because a truss that is using substantially larger amounts of material than another will subsequently also behave substantially stiffer and stronger than a truss with less material. In this research it is chosen to measure the amount of material used in total meters of tubular truss members used. An underlying assumption for this method is that all variants use similar CHS sections of constant thickness and radius. In the following the procedure used to measure the total amount of meters of section per topology variant will be described. All topology variants have to be adapted using the 'Grasshopper' code shown in the scheme below. In [Step 1] the curves that represent the totality of all truss members are used as input by the function in [Step 2]. This function calculates the length of each single curve elements as shown in [Step 3]. A very long list of elements is displayed in the yellow 'dialog box'. All elements of this list are added up, using the 'Mass addition function [Step 4]. This 'Mass addition' yields a single number [Step 5], which represents the total length of truss members used, measured in meters.

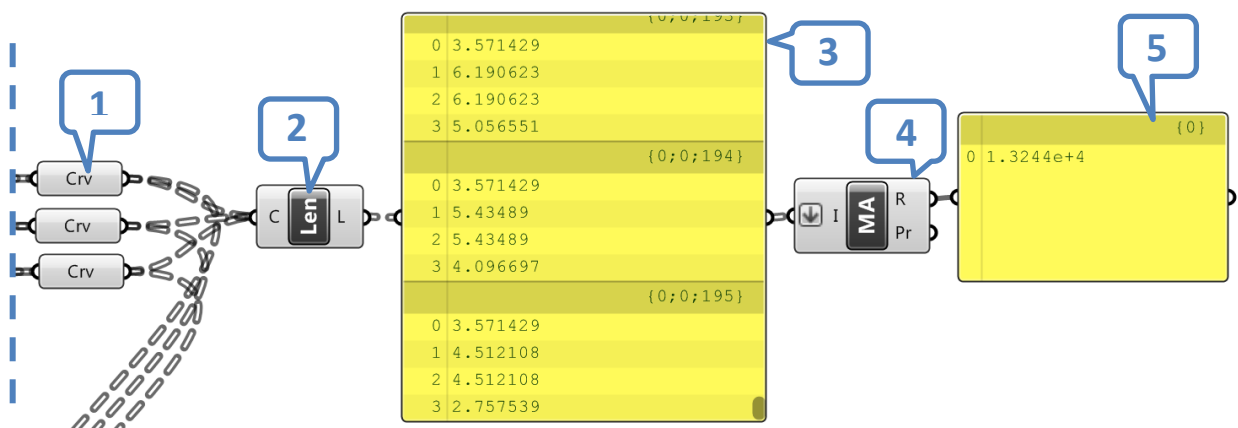


Fig. 67: Deriving the total material usage of all topology variants using 'Grasshopper' code.

For now a choice on the value of material usage for the truss topology variant must be made. In this case the 'Square Vierendeel' truss topology was chosen to be used for the derivation of the material usage. The following definition gives the material usage for the combined length of the truss members used for the 'Square Vierendeel' variant.

$$l_{material} = 4.982,45\text{m} \cong 5000\text{m} \quad (7.2)$$

$$N_{el.rings} = 42$$

$$N_{horiz.lin.memb} = 50$$

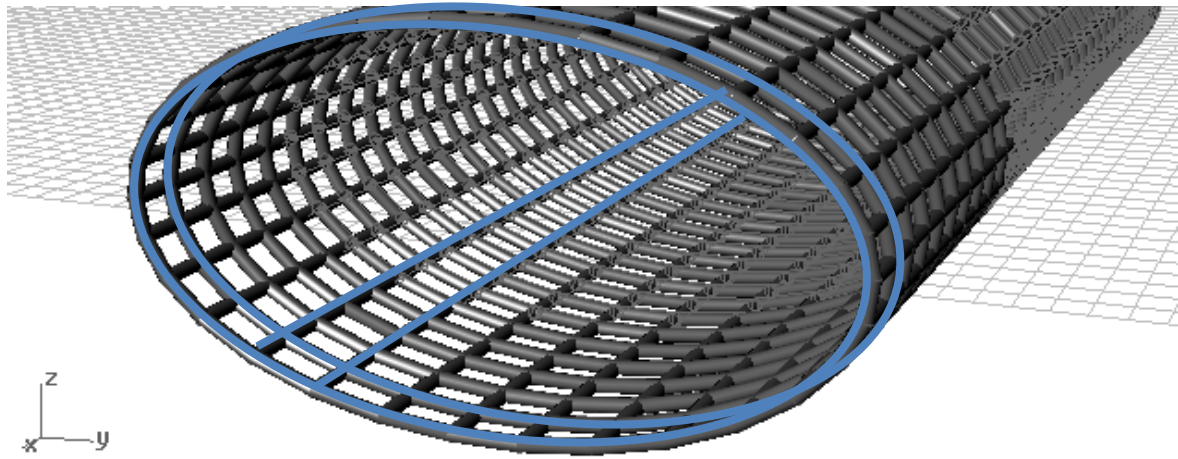


Fig. 68: Definition of elliptical rings and horizontal linear members and their mutual distance for the ‘Square Vierendeel’ variant.

To give an idea of the real-world dimensions of the mesh that is used for this comparison. The horizontal distance of the elliptical rings $l_{el.rings}$ (distance between the blue ellipses in the picture below) and the average distance between the horizontal linear members $l_{horiz.lin.memb}$ (distance between the straight blue lines in the picture below) is:

$$l_{el.rings} = \frac{l_{span}}{N_{el.rings}} = 49/42 = 1,167m \quad (7.3)$$

$$l_{el.rings} = \frac{c_{el.rings}}{N_{horiz.lin.memb}} = 58,89/50 = 1,177m$$

In the following table the most important parameters of all variants that were used in [ch. 5.4.2] are given. The table shows the parameters of all variants after they were adapted, as described in this chapter. In the following FEA these adapted variants will be compared. Note that the number of variants in the table below is significantly larger than that of the variants in [ch. 5.4.2]. This is due to the fact that next to the square truss layouts described in that chapter; in this chapter two rectangular layouts were added to each variant. These layouts are shown in the graphic below. The goal of these layouts was to investigate the influence of the longitudinal/lateral ratio. Therefore the three ratios were aimed to be 1:1 (square), 1:2 (rectangular lateral) and 2:1 (rectangular longitudinal). The ratio is shown in the 8th column of the table below.

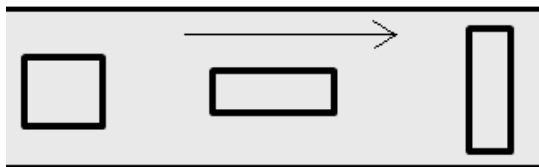


Fig. 69: Additional truss layout variants used for the adaption of the original topology; left: original square layout; middle: longitudinal rectangular layout; right: lateral square layout.

In total 6 groups of variants, the main variants with 3 sub variants each are investigated, leading to a total number of 18 FE-analyses.

#	Topology Variant	# long. divisions	# lat. divisions	# diagonals	Cell size long. [m]	Cell size lat. [m]	long./lat. ratio	Avg. length of Diagonals	Total material usage [m]	Deviation from 5000
0A	Vierendeel square	42	50	-	1,167	1,178	0,990	-	4982,451	-0,351%
0B	Vierendeel rectangular lateral	60	29	-	0,817	2,031	0,402	-	5013,547	0,271%
0C	Vierendeel rectangular longitudinal	29	66	-	1,690	0,892	1,894	-	5000,827	0,017%
1A	TrussOneD square	24	30	720	2,042	1,963	1,040	2,832	4981,662	-0,367%
1B	TrussOneD rectangular lateral	33	18	594	1,485	3,272	0,454	3,593	5018,684	0,374%
1C	TrussOneD rectangular longitudinal	17	38	646	2,882	1,550	1,860	3,273	5036,203	0,724%
2A	TrussTwoD square	17	21	714	2,882	2,804	1,028	4,022	4960,504	-0,790%
2B	TrussTwoD rectangular lateral	22	14	616	2,227	4,207	0,529	4,760	4972,709	-0,546%
2C	TrussTwoD rectangular longitudinal	13	26	676	3,769	2,265	1,664	4,398	5071,233	1,425%
3A	Diagrid square	30	34	2040	1,633	1,732	0,943	2,381	4974,632	-0,507%
3B	Diagrid rectangular lateral	37	23	1702	1,324	2,561	0,517	2,883	5024,333	0,487%
3C	Diagrid rectangular longitudinal	20	44	1760	2,450	1,339	1,830	2,792	5031,340	0,627%
4A	Trigrig square	39	40	3120	1,256	1,472	0,853	1,601	5032,868	0,657%
4B	Trigrig rectangular lateral	64	20	2560	0,766	2,945	0,260	2,969	4965,038	-0,699%
4C	Trigrig rectangular longitudinal	21	48	2016	2,333	1,227	1,902	1,693	4936,828	-1,263%
5A	Hexgrid square	84	96	-	0,583	0,613	0,951	-	4980,040	-0,399%
5B	Hexgrid rectangular lateral	98	56	-	0,500	1,052	0,475	-	5000,319	0,006%
5C	Hexgrid rectangular longitudinal	52	148	-	0,942	0,398	2,368	-	4928,609	-1,428%

Table 20: Material usage for all adapted 18 sub variants. These adapted models were used for further analysis

7.1.2 TRANSFORMING THE GRASSHOPPER MODELS TO FEA MODELS

All sub variants that were prepared in the preceding chapter are compared using the FEA suite 'Oasys GSA'. This might be surprising, since this software was not mentioned in the literature study. However it is a very powerful FEA/FEM software which is often used in the building and bridge design industry. The program was originally developed by the renowned engineering firm 'Arup'.

The flow chart below depicts the methodology that was used to use the initial geometry for the derivation of FEA-results. The geometry of all variants was parametrically defined using 'Rhinceros' and 'Grasshopper'. Of the bridge deck layout variants described in [ch. 5.2] it was chosen to use 'variant 2B' with a span of 49m for the initial comparative FE-analysis. The coordinates of the nodes and elements was imported into 'GSA' using the 'DWG' format, a digital format for 2D and 3D drawing originally developed by 'Autodesk' for 'Autocad'. The next steps in the process are definition of the material properties, the cross-section size and -type, the support conditions and the loading. These were all defined in 'GSA'.

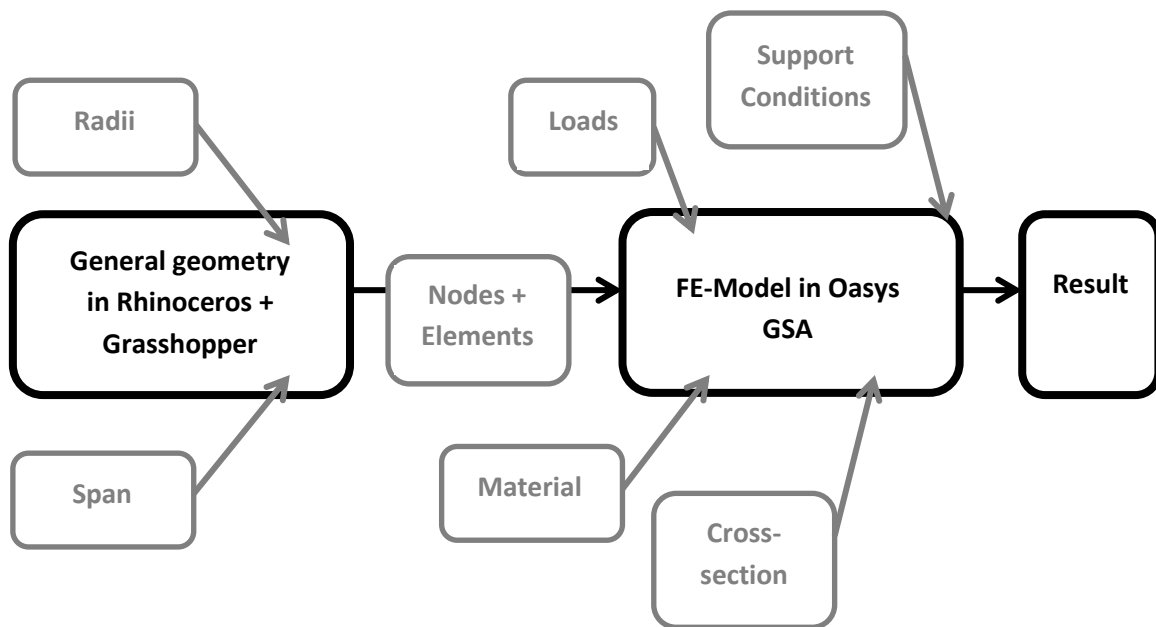


Fig. 70: Flow chart for the transformation of the initial geometry to a fully functional FE-model.

7.1.2.1 MATERIAL & CROSS-SECTION

For this research the FRP composite material is assumed to behave quasi-isotropic. This is a simplification, which is only acceptable since exclusively truss members are used in the design and these are primarily axially loaded, as already described in [ch. 3.5.1]. These properties are based on the Carbon/Epoxy 70/30 unidirectional reinforced composite as described in [ch. 3.4]. The values of the longitudinal properties are also used for the transverse properties.

		70% Carbon M35J
		30% Epoxy 0
ρ	kg/m ³	1.629
$E_{L-d} = E_{T-d}$	N/mm ²	148.239
$\nu_{LT} = \nu_{TL}$	-	0,245
$G_L = G_T$	N/mm ²	8.669

Table 21: Simplified isotropic material properties for the initial comparative FE-analysis, based on [ch. 3.3, table 4]

Furthermore it was chosen to use a single cross-section for all elements of the main cylindrical load bearing structure. The type of this cross section is a circular hollow section with a diameter of 300mm and a wall thickness of 30mm. Note that these dimensions are again only used for the comparison of topology variants. These dimensions are bound to change during further analysis.

7.1.2.2 SUPPORT CONDITIONS

In order for any FE-analysis to function support conditions and boundary conditions must be defined for all members. In this case it was chosen to model the connections between the members as fully fixed nodes; thus being able to transfer moments. Although the exact (spring) stiffness of the connection elements is not known, this comes closer to reality than assuming fully hinged truss elements. Furthermore it was chosen to model the elements as simple beam elements.

Another important choice to be made before the FE-analysis can be started is the type of support conditions for the main load bearing structure of the bridge. In this research two general support conditions were used: Firstly all edge nodes were fully fixed. This support condition models the presence of a large elliptical edge beam on both ends of the bridge. Similar edge beams have been used for other bridges with a cylindrical cross section, such as the 'Calatrava Peace Bridge', Calgary, Canada, described in the literature study [LS, ch. 6.1.4, p193]



Fig. 71: First support condition: Fully fixed edge nodes. This support condition models the often used edge beam, as is the case with the Calatrava Peace Bridge, Calgary, Canada, March 2012 that is shown in the picture [WEB: www.broccolocity.com]

The second support condition that is used for the initial FE-analysis, the pinned support of the bottom half of the edge nodes of the cylindrical load bearing structure. With this support condition a more common support of the bridge through concrete and sand embankments is simulated. Hereby the truss cylinder is supported by two embankment structures, one at each side. The scheme below shows this support condition.

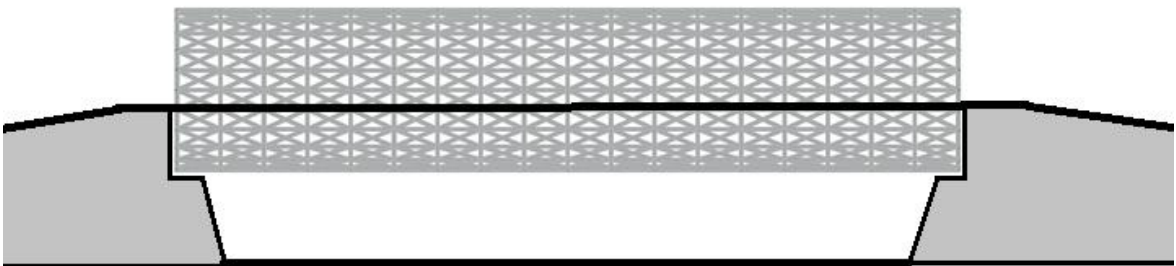


Fig. 72: Second support condition: Bottom half of the edge nodes pinned on concrete/sand embankment.

Finally an extract from 'GSA' is shown below that shows the nodes in the FE-models that were fixed or pinned. Which exact support condition will be used for the final design will be decided following the initial analyses. Next to the two shown support condition it is also possible that other support conditions will also be considered in the follow up.

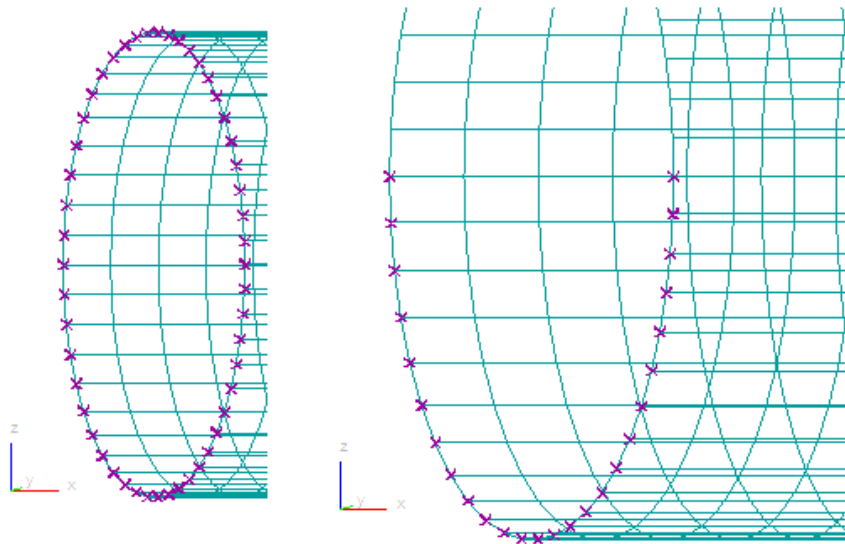


Fig. 73: General support conditions of the initial FE-models. Left: Fully fixed edge nodes. Right: Bottom half of the edge nodes pinned.

7.1.2.3 LOADS & LOAD CASES

For the first FE-analyses 3 load cases were used to be able to compare the different truss topologies as accurately as possible. These load cases are defined below:

- **Self-weight:** In this load case the only load applied on the structure is the self-weight of the structure.
- **Line load of 10kN/m:** In this load case a line load of 10kN/m was placed centrally over the whole length of the bridge. A line load resembles a real-world traffic load much better than the uniform loading of the self-weight of the structure. Topologies like the hexagonal grid do not feature continuous horizontal members. In that case the line load was distributed along in-line nodes.
- **Point load of 100kN:** In this load case a point load was applied centrally at mid-span of the bridge. The load was placed at a single node. Since real-world traffic load models also use point loads next to line loads, see [ch. 6.2], it was chosen to incorporate a point load model as well.

Load Cases for the Truss Topology Variants

Combining the load cases and the two support conditions, a total of four load cases were used for the comparison of the truss topology:

- **LC1:** Fully fixed edge nodes + Self-weight
- **LC2:** Pinned bottom half edge nodes + Self-weight
- **LC3:** Pinned bottom half edge nodes + Line load of 10kN/m
- **LC4:** Pinned bottom half edge nodes + Point load of 100kN.

7.1.3 COMPARING THE TRUSS TOPOLOGIES

Knowing all needed prerequisites for the initial finite element analysis, the analysis can be carried out. In total, all 6 main topology variants, thus 18 sub variants were analyzed for 4 analysis cases each are compared. The main parameter that is used for the comparison of the variants is the maximum deflection. The maximum deflection was derived for all $18 \times 4 = 72$ analyses.

Below an overview of all analyzed truss topologies is given. The models shown below represent the exact models used for FE-analysis in 'GSA'. Next to that a detail scheme of one grid cell is depicted for every sub-variant.

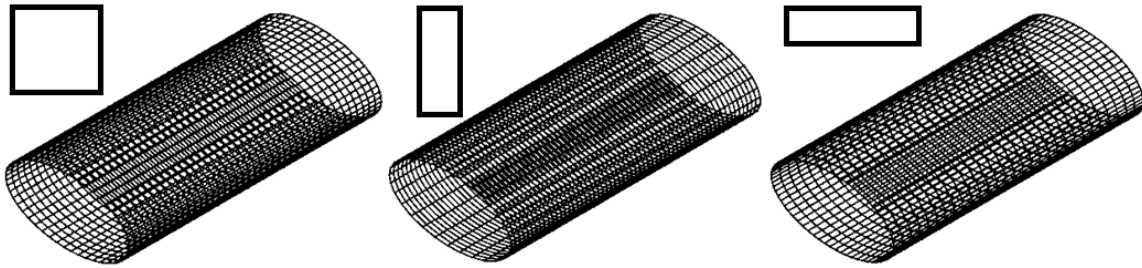


Fig. 74: Truss topology variant 0A, 0B, 0C: Vierendeel square, -rectangular lateral and -rectangular longitudinal

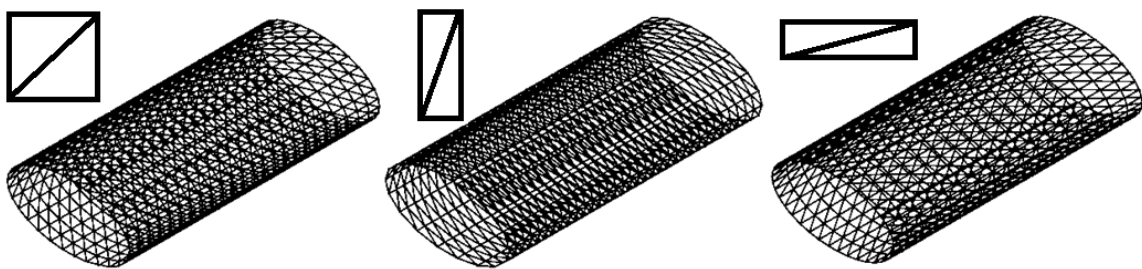


Fig. 75: Truss topology variant 1A, 1B, 1C: Truss One Diagonal square, -rectangular lateral and -rectangular longitudinal

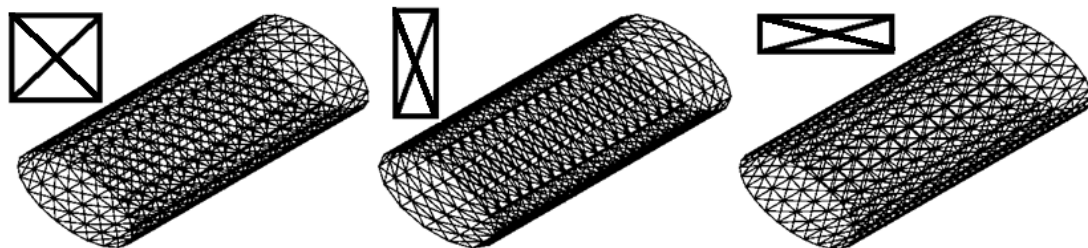


Fig. 76: Truss topology variant 2A, 2B, 2C: Truss Two Diagonals square, -rectangular lateral and -rectangular longitudinal

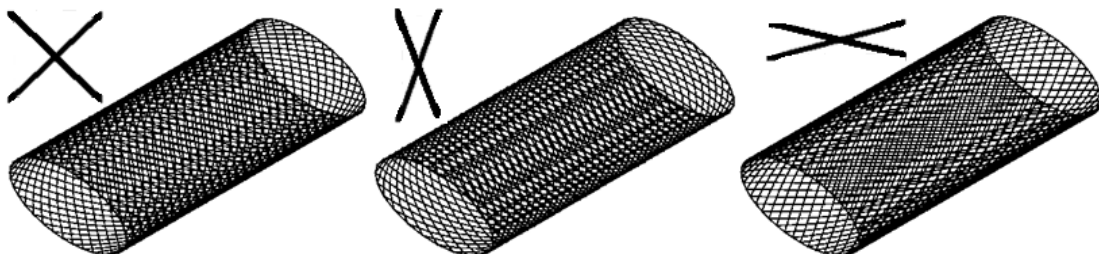


Fig. 77: Truss topology variant 3A, 3B, 3C: Diagrid square, -rectangular lateral and -rectangular longitudinal

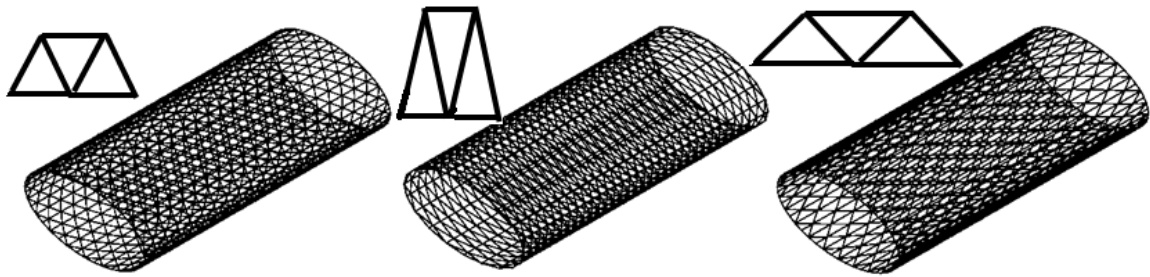


Fig. 78: Truss topology variant 4A, 4B, 4C: Triangular grid square, -rectangular lateral and -rectangular longitudinal

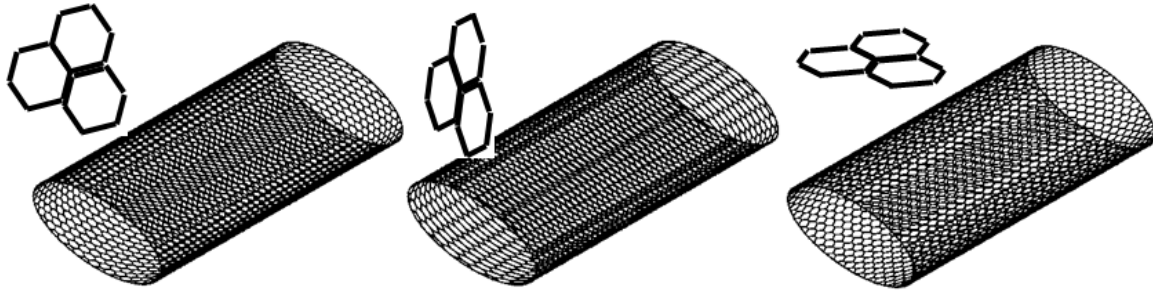


Fig. 79: Truss topology variant 5A, 5B, 5C: Hexagonal grid square, -rectangular lateral and -rectangular longitudinal

To give a general idea of the type of deflections that arise in the structure due to the four analysis cases, here the square truss topology variant with one diagonal (variant 1A) is used. Below four pictures of this variant are shown; one for each analysis case. It can be seen that the magnitude of nodal deflection is lowest for the first analysis case LC1, thus the case under self-weight only with fully fixed nodes on both edges of the cylinder. The second support condition, pinned nodes at the bottom half of the edges is a more realistic scenario for a traffic bridge. Here larger deflections arise due to self-weight only (LC2). Particularly the upper half of the cylinder deforms about 3x times more than in the fully fixed case.

However, line loads and point loads are the main loading type for general traffic bridges. The last two analysis cases (LC3 and LC4) represent these load types, yielding deflections in the order of 8mm over a span of 49m for a considerably large line load of 10kN/m and deflections in the order of 6mm for a substantial point load (nodal load) of 100kN.

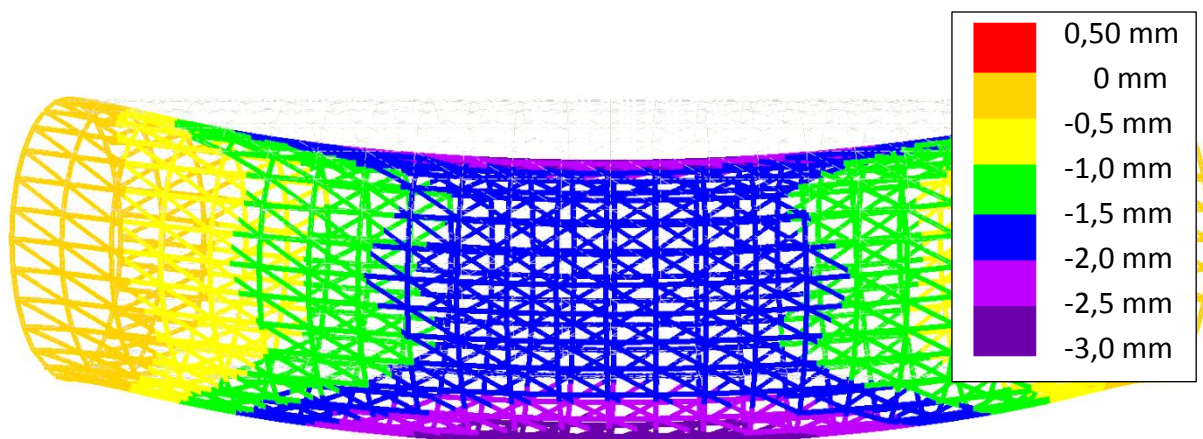


Fig. 80: Deformation of variant 1A, a truss with one diagonal, due to loading by self-weight. All nodes on both cylinder edges are fully fixed.

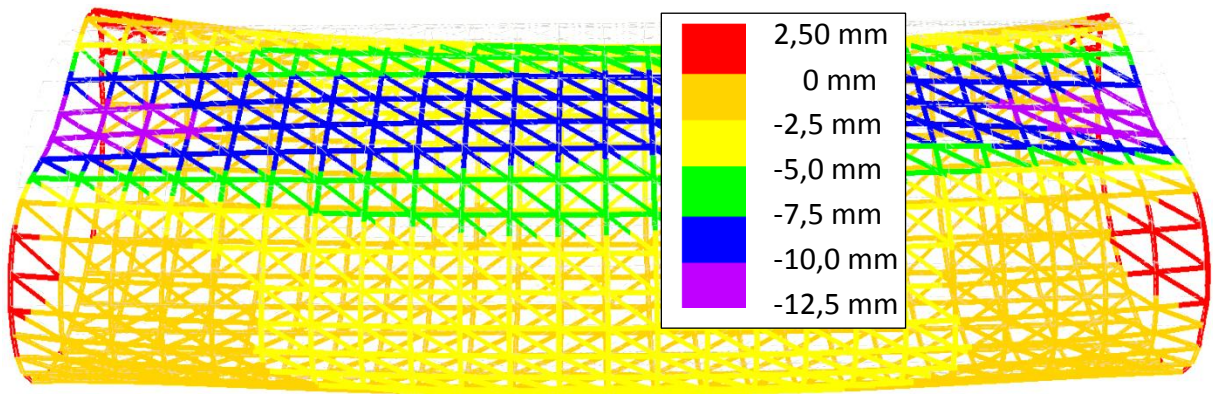


Fig. 81: Deformation of variant 1A, a truss with one diagonal, due to loading by self-weight. The bottom half of the edge nodes is pinned.

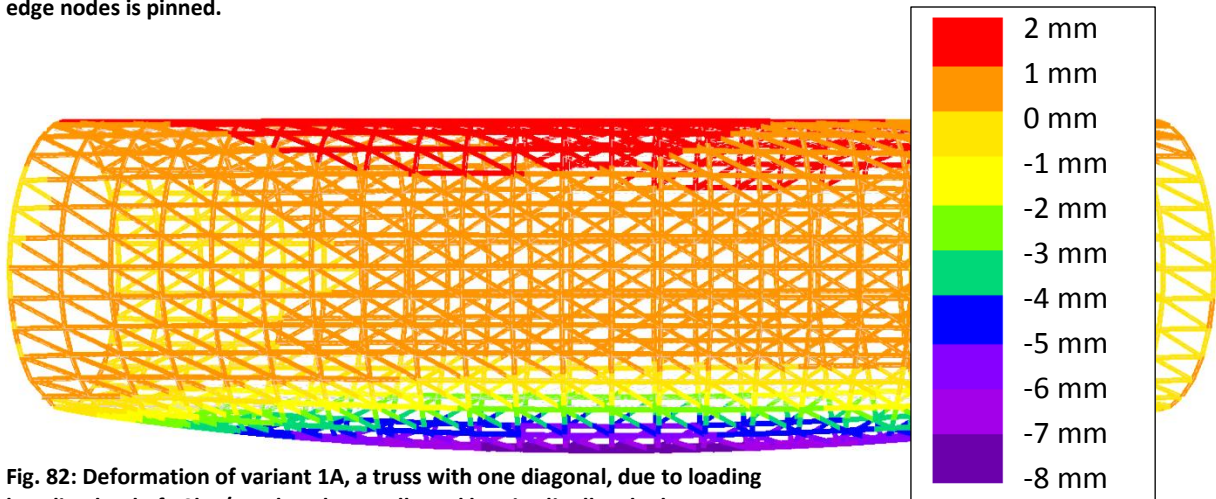


Fig. 82: Deformation of variant 1A, a truss with one diagonal, due to loading by a line load of 10kN/m, placed centrally and longitudinally. The bottom half of the edge nodes is pinned.

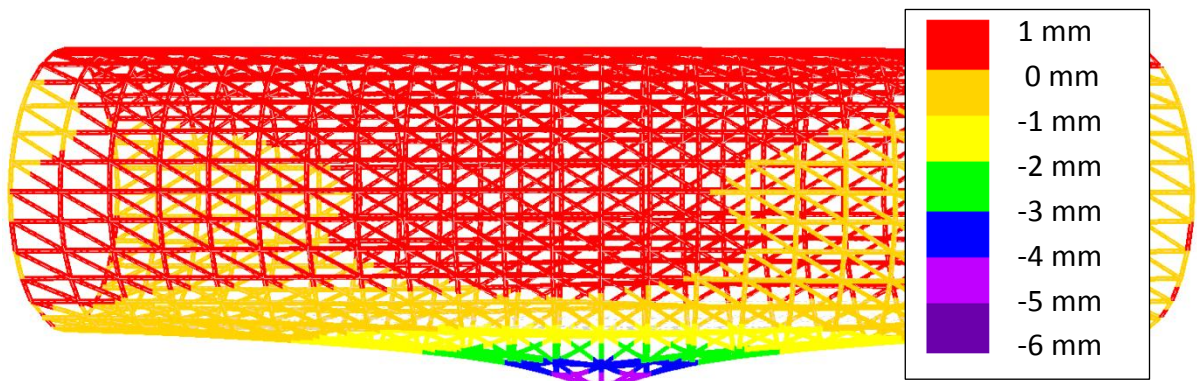


Fig. 83: Deformation of variant 1A, a truss with one diagonal, due to loading by a point load of 100kN, placed centrally at mid=span. The bottom half of the edge nodes is pinned.

After all analyses are carried out the maximum deflection of each sub variant is known for each analysis case. The goal of the initial FE-analysis is finding the most efficient truss topology for the cylindrical load bearing structure. Therefore the results must be compared in such a way that a choice on the truss topology can be made. Firstly the most efficient sub-variant is defined.

7.1.3.1 GENERAL RESULTS

In this first result chapter the general results of all load cases (LC1-LC4) for all sub variants (0A, 0B, 0C – 5A, 5B, 5C) are briefly discussed. The table below gives the most important data of all these load cases. From left to right, the number of members and nodes is given, then the order of nodes, describing the number of members that are connected by one node. Afterwards the minimum- and maximum member length is given, defining the range of length of the linear members. Another important parameter given in the next

column is the longitudinal/lateral ratio, which was already described in [ch. 7.1.1, table 20]. Finally the results of the FE-analysis on the maximum nodal deformation of the cylindrical truss due to all load cases are given and the variants are ranked based on this sum of deflections.

In the table below the two best deflection values for each load case are marked in green, the 2 worst deflection values are marked in red. Furthermore the ranking is marked green for sub variants among the 9 lowest deflections. The ranking column is marked red for the sub variants with the 9 highest deflections.

Variant	# members	# nodes	Order of Nodes	Min. Member length [m]	Max. Member length [m]	long./lat. ratio	LC1 [mm]	LC2 [mm]	LC3 [mm]	LC4 [mm]	Sum of LC1-LC4 [mm]	Rank based on sum
0A	4251	2151	4	0,584	1,448	0,990	8,738	12,680	14,410	8,289	44,117	11.
0B	3509	1769	4	0,816	2,491	0,402	10,820	13,920	31,070	8,266	64,076	16.
0C	3894	1980	4	0,551	1,690	1,894	10,470	15,150	18,710	10,050	54,380	14.
1A	2189	759	6	1,245	4,671	1,040	2,899	11,840	7,411	5,175	27,325	6.
1B	1800	612	6	1,484	4,265	0,454	4,074	9,220	7,194	5,390	25,878	4.
1C	1976	684	6	0,972	3,456	1,860	3,809	15,130	9,915	6,402	35,256	8.
2A	1449	378	8	1,738	4,482	1,028	1,845	9,804	6,820	4,476	22,945	2.
2B	1246	322	8	2,227	5,538	0,529	2,223	8,248	4,869	4,145	19,485	1.
2C	1378	364	8	1,450	4,675	1,664	2,065	13,780	7,041	5,216	28,102	7.
3A	2108	1054	4	1,092	2,683	0,943	4,433	21,310	13,740	15,760	55,243	15.
3B	1749	875	4	1,059	3,407	0,517	27,300	58,340	22,770	26,560	134,970	18.
3C	1851	927	4	0,810	2,952	1,830	3,032	17,830	11,720	17,330	49,912	13.
4A	2503	863	6	0,754	2,450	0,853	1,874	12,340	7,629	4,793	26,636	5.
4B	2003	683	6	0,754	3,640	0,260	3,398	8,742	7,872	5,094	25,106	3.
4C	1709	605	6	2,228	4,455	1,902	2,949	20,160	14,550	9,005	46,664	12.
5A	6217	4177	3	0,376	1,219	0,951	4,959	16,120	13,510	7,969	42,558	9.
5B	4216	2830	3	0,353	1,484	0,475	19,270	46,390	22,480	13,630	101,770	17.
5C	6035	4074	3	0,140	1,082	2,368	4,029	17,320	13,730	8,596	43,675	10.

Table 22: General deflection results due to load cases LC1-LC4 for all 18 sub variants

Reading this rather complex table leaves a lot of room for discussion. The choice for the most efficient truss topology variant cannot only be based on the deflections due to a variety of load cases, the sum of all these cases can also be considered. Furthermore the number of members and nodes can also be an important parameter for this choice. Considering constructability and make-ability, a perhaps even more important parameter is the order of the nodes. A node that connects only three members is a lot easier to construct than a node that connects 8 members. Next to these parameters the two last parameters that can be used for a choice is the range of member lengths and finally the architectural appearance. Although the last parameter cannot be put into numerical terms it tends to have a large influence on real-world design problems.

Returning to the deflection due to the various load cases shows that the Vierendeel main variant (0A, 0B, 0C) as well as the diagrid main variant (3A, 3B, 3C) overall yield the highest deflections. The hexagonal grid main variant closely follows them. It is rather interesting to see that these three main variants also feature the lowest order of nodes (the order of nodes of these variants is 3 or 4). The truss with two diagonals main variant has the highest order of nodes (8 connected members per node), but the square variant also yields the lowest sum of all deflections, being only 15% of the main variant with the highest deflections. Since all variants have the same material usage [ch. 7.1.1, table 20], the conclusion can be drawn, that the order of the connections has a large influence on the deflection behavior.

Basing the decision only on this deflection behavior would lead to the choice of the truss topology with two diagonals, closely followed by the truss with one diagonal and the triangular grid. The latter two main variants are very similar, not only in the layout itself, but also in the majority of deflection values.

Below a graph can be found in which the deflection data shown in the table below is represented in another way. Here all load cases are compared for each sub variant individually. The large deflection values for the Vierendeel main variant and foremost the diagrid main variant and the hexagonal main variant can be clearly seen as three spikes along the x-axis.

The deflections per load case were already described in [ch. 7.1.3, table 22], this deflection behavior can also be traced back in the graph below. Load case LC2 (red line) generally yields the highest deflection whereas analysis case LC1 (blue line) yields the lowest deflections.

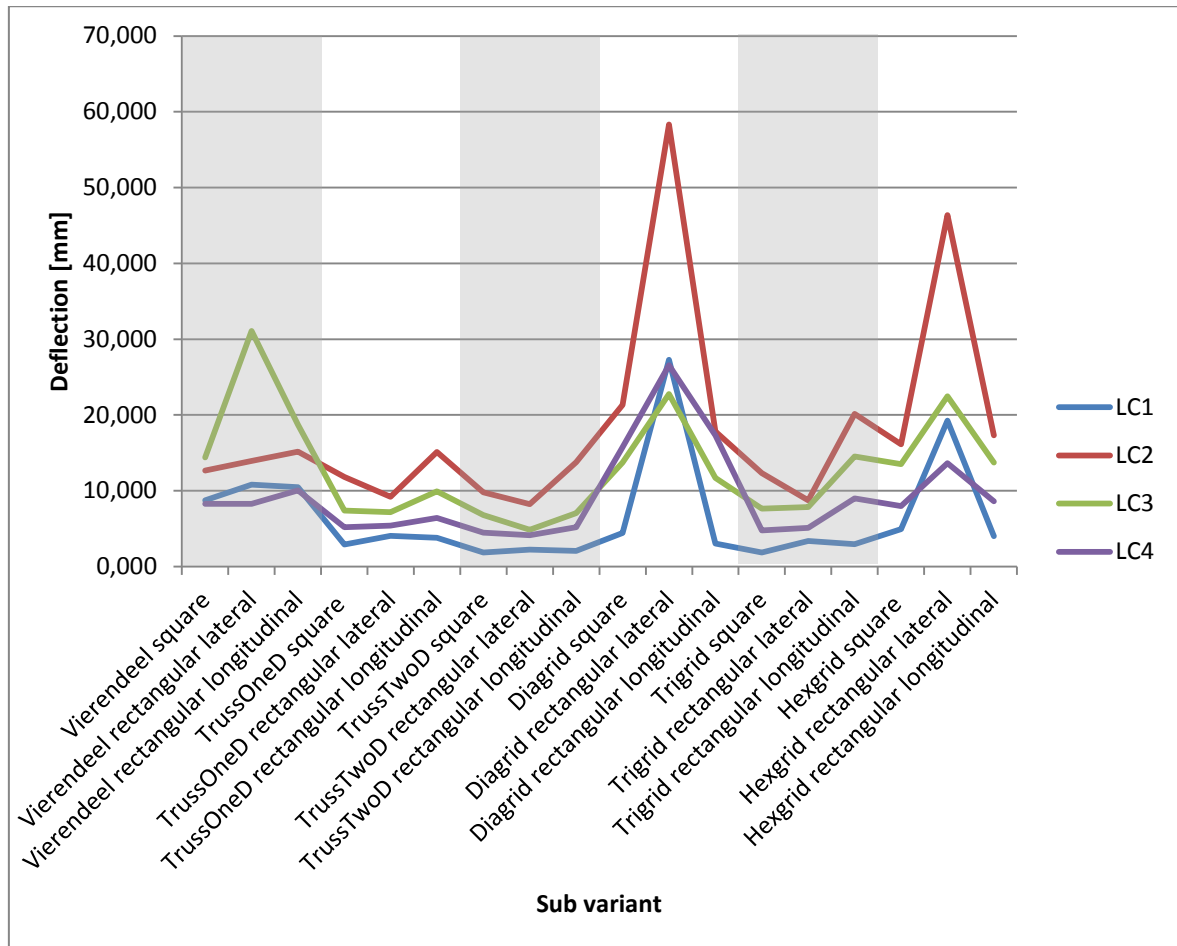


Fig. 84: Graph of general deflection results due to load cases LC1-LC4 for all 18 sub variants

7.1.3.2 CHOICE OF SUB VARIANT BASED ON DEFLECTION

Following the general results described in the chapter before, the large table can be broken down into several parts: To determine which sub variant behaves most efficient, the results of all main variants are grouped by sub variants, resulting in deflection data for each sub variant group as described in [ch. 7.1.1]: square, rectangular lateral, rectangular longitudinal.

The graph below is the result of the summation of the maximum deflection of all main variants, grouped by sub variants. It can be clearly seen that the deflection of the rectangular lateral sub variants is notably higher for all load cases. Of the two remaining sub variants the square sub variant shows about 15%-20% smaller deflections than the rectangular longitudinal variant.

From the initial FE-analyses it can therefore be concluded that a truss topology based on squares rather than on rectangles yields smaller deflections under uniform loads, line loads as well as point loads. In the following, only square variants will be investigated, leaving only the 6 main variants: Vierendeel, truss with one diagonal, truss with two diagonals, diagrid, triangular grid and hexagonal grid. Since the choice of sub-variant has no influence on the order of nodes and the influence on the other parameters such as

architectural appearance is limited it can be concluded that the decision on most efficient sub variant based on deflection behavior does not conflict with the other parameters.

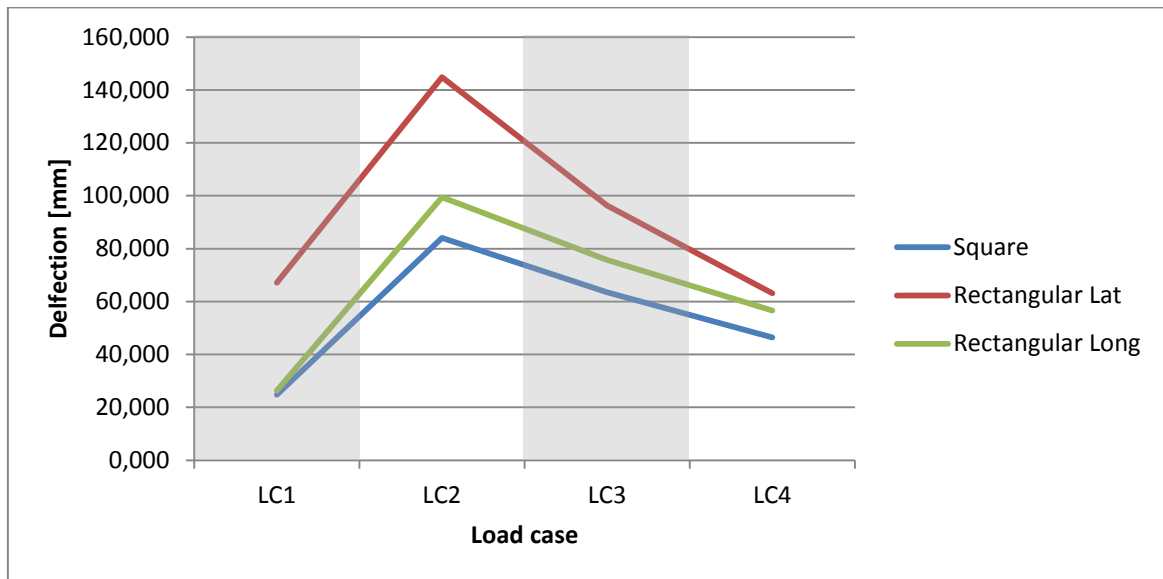


Fig. 85: Graph for the comparison of the summation of all sub-variant deflections for all load cases.

7.1.3.3 CHOICE OF MAIN VARIANT BASED ON DEFLECTION

After choosing the sub variant which yields the lowest overall deflections for all analysis cases, 6 main variants remain that were already described in the general results in [ch. 7.1.3.1]. They need to be compared more in-depth. The first comparison between the Vierendeel, truss with one diagonal, truss with two diagonals, diagrid, triangular grid and hexagonal grid is based on deflection behavior only. For this purpose all results are filtered, such that only the square sub variants remain.

Doing so, and placing the data in a similar graph as shown in [Fig. 81] yields the graph shown below. It is clearly visible that the diagrid, the vierendeel grid and the hexagonal grid deform significantly more over nearly the complete range of analysis cases. This result is the same as derived before in [ch. 7.1.3.1]. This leads to the conclusion that the other three main variants, the truss with one and with two diagonal as well as the triangular grid have a better deflection behavior than the other three main variants.

For the all fixed + self-weight analysis case the truss with two diagonal yields similar values as the triangular grid. The same holds for the half pinned + point load at mid-span analysis case, for which the differences in deflection are very small (<10%). The main differences lie in the half pinned + self-weight analysis case. Here the triangular grid, as well as the truss with one diagonal deflect almost 20% more than the truss with two diagonal.

Considering only the maximum deflection of the main cylindrical load bearing structure, from the initial FE-analysis it can be concluded that of all main truss topology variants the truss with two diagonal behaves best. However, it also has to be stated that the truss with one diagonal as well as the triangular grid both yield results that are nearly as good as that of the truss with two diagonals.

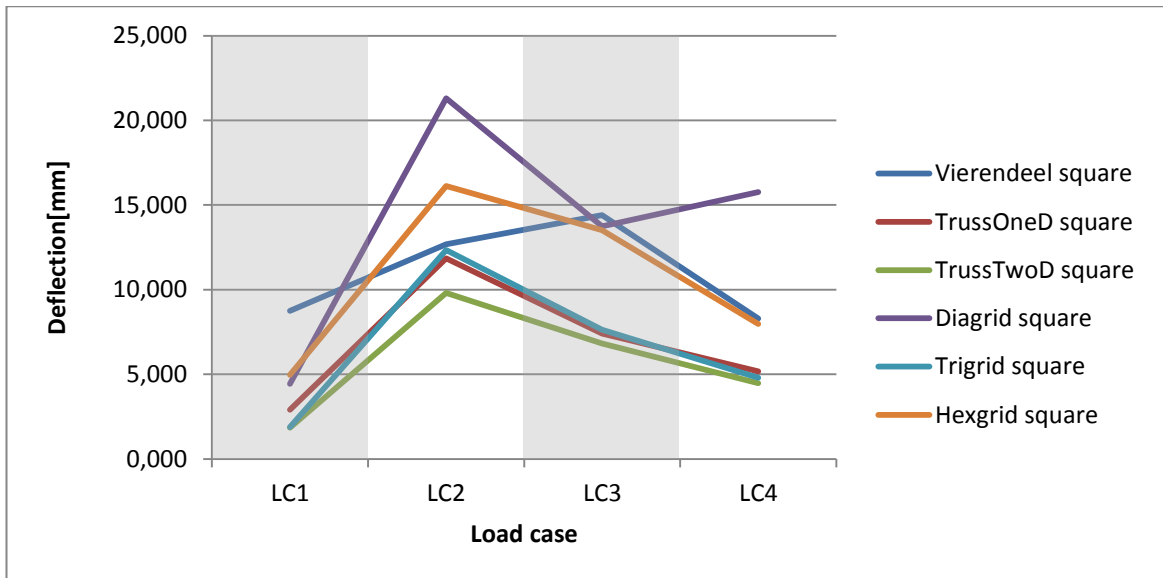


Fig. 86: Graph of the deflection of all square sub variants for the determination of the stiffest main variant

For comparison, in the graph below the results for all sub variants are given as well. The graph below was derived similar to that above. However, in the graph below the results of all sub variants were summated to yield one deflection value for each main variant. This graph backs up the choice of stiffest truss topology, given before, because the summation of all deflections is similar to the deflections of the square sub variants only.

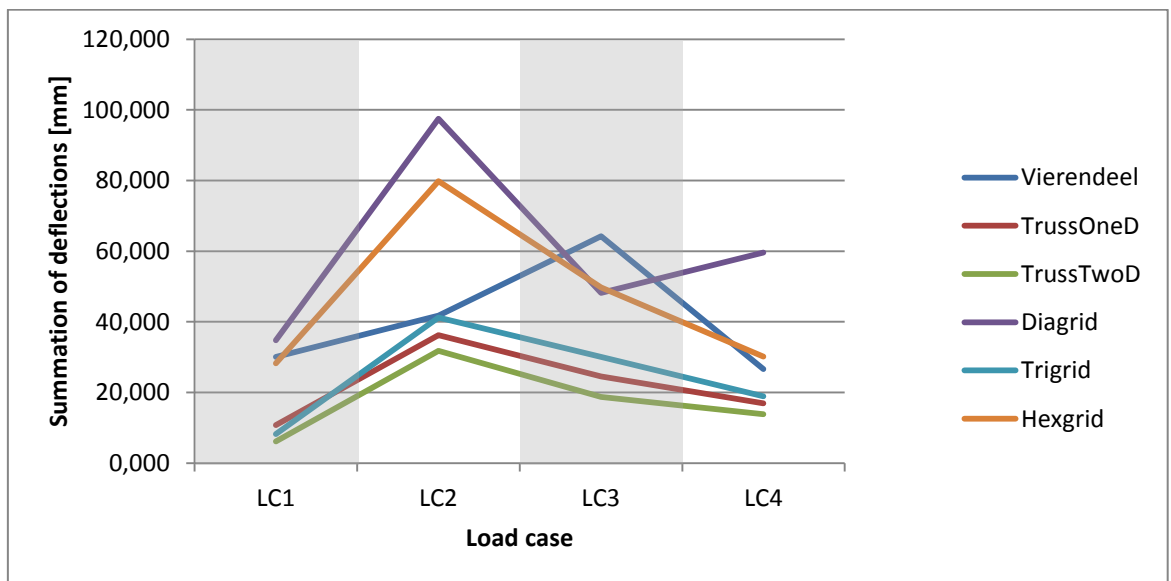


Fig. 87: Graph of the deflection of the summation of the sub variants for each main variant for the determination of the stiffest main variant

7.1.3.4 CHOICE OF MAIN VARIANT BASED ON OTHER PARAMETERS

Next to the deflection parameter two other parameters are essential for the constructability of the cylindrical truss: One is the order of nodes and the other is the total number of nodes in the structure. It is expected that the nodes are the most costly elements in the structure and their layout and number should therefore be thoroughly analyzed.

The table below gives all parameters of the square sub variants except for the deflection due to the four load cases. It can be seen that the truss topology with two diagonals (variant 2A) features the lowest number of members and nodes. However, this variant also features the highest order of nodes by far, with a total of 8 members to be connected per node.

In reverse, the hexagonal grid topology (variant 5A) has the lowest order of nodes, with a total of only 3 members to be connected per node. The problem of the hexagonal grid is that the number of nodes is by far the largest for this variant, being about 10x bigger than the number of nodes in case of the truss topology with two diagonals.

Therefore another parameter has been introduced: the 'node parameter', which is the product of the number of nodes and the order of nodes. That way comparison of the main variants becomes clearer. In the 'node parameter' column the three best variants are marked green and the three worst variants are marked red.

#		# members	# nodes	Order of Nodes	Node parameter	Min. Member length [m]	Max. Member length [m]
0A	Vierendeel square	4251	2151	4	8604	0,584	1,448
1A	TrussOneD square	2189	759	6	4554	1,245	4,671
2A	TrussTwoD square	1449	378	8	3024	1,738	4,482
3A	Diagrid square	2108	1054	4	4216	1,092	2,683
4A	Trigrig square	2503	863	6	5178	0,754	2,450
5A	Hexgrid square	6217	4177	3	12531	0,376	1,219

Table 23: Number- and order of nodes as design parameter of the cylindrical truss topologies

Ordered from best to worst the topology variants become: TrussTwoD, Diagrid, TrussOneD, Trigrig, Vierendeel, Hexgrid. A further important point of interest is the complexity of the nodes, described by the order of nodes in the above table. Given the recent developments, particularly in the offshore industry, for steel circular hollow sections and pre-fabricated connections with 8 members might not pose a big problem in terms of constructability. However when using fiber reinforced polymer as stand-alone structural material such connections deserve special attention.

As described before in [ch. 3.5.2] connections of CHS FRP members have been developed and tested for up to 3 members only. Despite the fact that these researches were carried out more than 15 years ago, it still is a fact to be taken into account. It is therefore chosen to exclude the most complex connection from further analysis. This means that the truss with two diagonals topology variant will be not be considered because the connections with 8 members to be connected are expected to be too complex to fabricate in FRP material.

7.1.3.5 FINAL CHOICE ON TRUSS TOPOLOGY

Combining the outcome of the chapter before [ch. 7.1.3.4] with the very good deflection behavior of the TrussTwoD, TrussOneD and triangular grid topologies as described in [ch. 7.1.3.3] shows that the truss with one diagonal and the triangular grid topologies are most suitable for the use in the main cylindrical load bearing structure. This choice is not purely based on the deflection behavior for all four load cases but also incorporates the number of nodes and the complexity/order of the nodes. To compare between the best two variants: the truss with one diagonal has a better 'node parameter' of 4554 compared to 5178 of that of the triangular and the order of the nodes is similar, with 6 connecting members each. Furthermore the

deflection behavior of both variants is very similar, although the truss with one diagonal yields slightly lower deflection values, both for the square sub variant [Fig. 86] as well as for the summation of all sub variants [Fig. 87]. It is therefore chosen to use the square truss with one diagonal topology for the main cylindrical load bearing structure of the FRP traffic bridge. Following the analyses performed and described in the chapters before this is the most efficient choice for the truss topology.

7.2 LOAD CASES FOR FURTHER ANALYSIS

For further optimization a new set of load cases will be used that are closer to the loads described by the Load Model 1 of the Eurocode [ch. 6.2.1]. The reason for this is to get a better insight in the behavior of the main load bearing structure under real-world traffic loads. Furthermore only the second support condition of [ch. 7.1.2.2] will be used. It is expected that this support condition of a simple pinned support is more likely to be built than the first support condition, the fixed end-ring.

In the further analyses prior to the final bridge design the following load cases will be used:

- **LC1:** Pinned bottom half edge nodes + Self-weight
- **LC2:** Pinned bottom half edge nodes + Distributed line load of 54kN/m
This load was derived by multiplying the by 'Load Model 1' prescribed load of 9kN/m² by the prescribed width of nominal lane of 3,00m by the number of nominal lanes of 2 [ch. 6.2.1], such that

$$LC2 = 9\text{kN/m}^2 * 3,00\text{m} * 2 = 54 \text{ kN/m} \quad (7.4)$$

- **LC3:** Pinned bottom half edge nodes + Point load of 1200kN.
This load was directly derived from 'Load Model 1', as described in [ch. 6.2.1]. Here a set of 4 point loads of 150kN each is prescribed for each driving direction. For two driving directions the load becomes:

$$LC3 = 150\text{kN} * 4 * 2 = 1200\text{kN} \quad (7.5)$$

Note that this load is conservative, since in a real-world scenario this load will always be spread to multiple loads by the bridge deck and its supporting structure. However, LC3 should give a good estimation on how the different grid size variants deform under heavy point loads.

7.3 INFLUENCE OF BRIDGE DECK SUBSTRUCTURE ON OVERALL BRIDGE STIFFNESS

Knowing the most efficient truss topology, before proceeding with the grid-size- and cross-section-optimization, it is important to know the influence of the bridge deck substructure on the stiffness of the overall main load bearing structure. It is expected that the main load bearing structure complete with an inner network of bridge deck supporting lateral and longitudinal trusses has a much larger stiffness than the 'hollow' main load bearing structure without added inner trusses.

The goal of this chapter is to find a factor of increase of stiffness of the main load bearing structure with bridge deck supporting trusses compared to that of the main load bearing structure without bridge deck supporting trusses. For this cause the geometry obtained in the preceding chapter is used and the inner trusses are added as described in the chapter below.

The main radii for the elliptical main load bearing structure used for the analyses in this chapter are that of bridge cross section variant 5B, [ch. 5.2.5]:

$$R1 = 7,50m \quad (7.6a)$$

$$R2 = 5,00m \quad (7.6b)$$

7.3.1 ADDITION OF INNER BRIDGE DECK SUBSTRUCTURE TO THE MAIN LOAD BEARING STRUCTURE

The inner bridge deck was modeled in the following way. First a lateral truss was placed in each ring of the main load bearing structure. A total of 19 lateral trusses are placed in the main load bearing cylinder. For the total span of 49m, these trusses have a c.t.c distance of $49m/(19-1)=2,722m$. The picture below shows the topology of these lateral trusses.

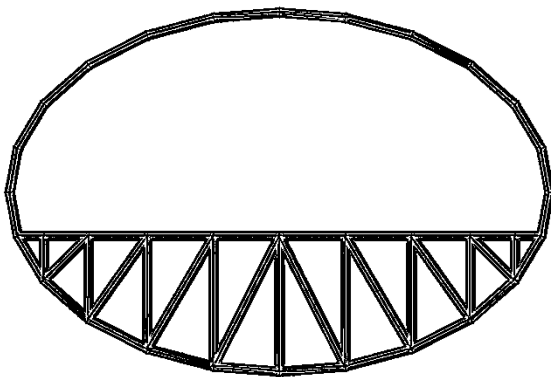


Fig. 88: Topology of the lateral trusses that act as substructure for the inner bridge deck.

In the longitudinal direction the trusses were again placed in line with the main cylindrical load bearing structure. This results in a total of 9 truss longitudinal trusses of which the following picture gives an overview. Note that, due to the symmetry along the central truss, of the 9 trusses only 5 are unique. These are displayed below. Because of the varying height of the cylinder along the y-axis the trusses have different heights as well. The top truss in the picture is the longitudinal truss that has the largest distance from the centerline of the bridge. The lowest truss is the central longitudinal truss of the bridge. The height of these trusses varies from 1,2m for the outer most trusses to 3,78m for the central truss.

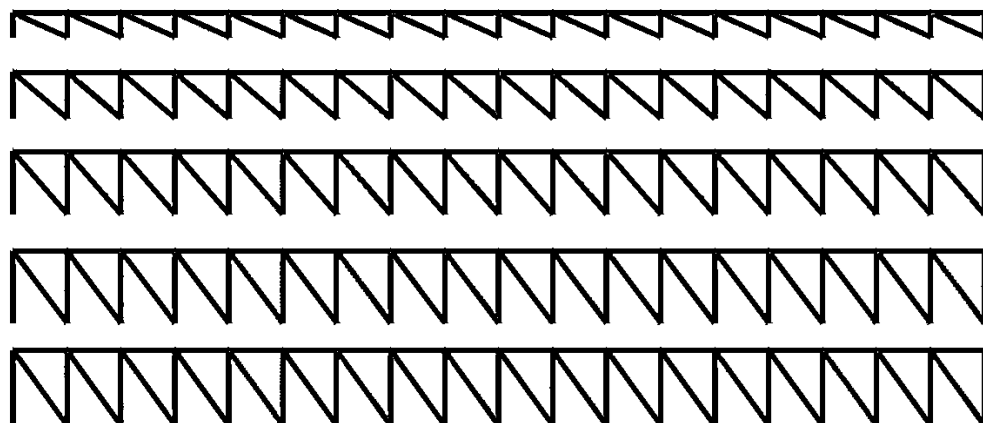


Fig. 89: Topology of the longitudinal truss that act as substructure for the inner bridge deck.

Combining the lateral- and longitudinal trusses with the main cylindrical load bearing structure yields the following FE-model of the bridge with the inner bridge deck and its substructure.

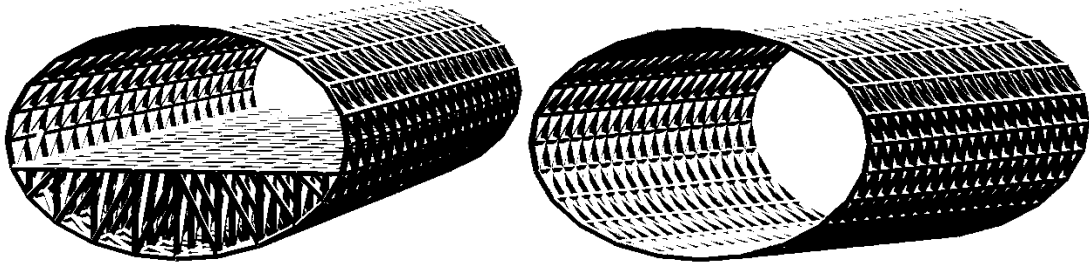


Fig. 90: Main load bearing structure with (left) and without (right) inner substructure for bridge deck.

7.3.2 COMPARITIVE FINITE ELEMENT ANALYSIS FOR THE DETERMINATION OF THE STIFFNESS INFLUENCE OF THE BRIDGE DECK SUBSTRUCTURE

For the two variants shown in the picture above an FE-analysis will be made for LC1-LC3, as described in [ch. 7.2]. The results of these analyses are shown in the table below:

Variant	LC1 Max. Deformation	LC2 Max. Deformation	LC3 Max. Deformation	Sum of max. Deformations	L/600 Deflection Limit
No inner truss	4,439	14,710	44,530	63,679	81,667
Inner truss	5,849	6,116	6,570	18,535	81,667
Factor	0,759	2,405	6,778	3,436	

Table 24: Deformations of the main load bearing structure with and without inner truss structure for all load cases

The last row of the above table shows the factor that represents the added stiffness of the variant with added inner truss. The deformation of the variant with inner truss is for example 3,436x times lower for the sum of all load cases than for the variant without inner truss. This also means that the structure with added inner truss behaves 3,436x times stiffer than that without.

Particularly the results for LC3, the point load case are striking; here the inner truss variant behaves 6,778x times stiffer. For LC2, the distributed load case, the difference is a lot smaller, but with a factor of 2,405 still significant. LC1, the self-weight only load case shows little difference between the two variants, although the variant without inner truss even behaves slightly stiffer than that with inner trusses. The graph below shows the difference between the two variants for all load cases as well as the sum of all load cases.

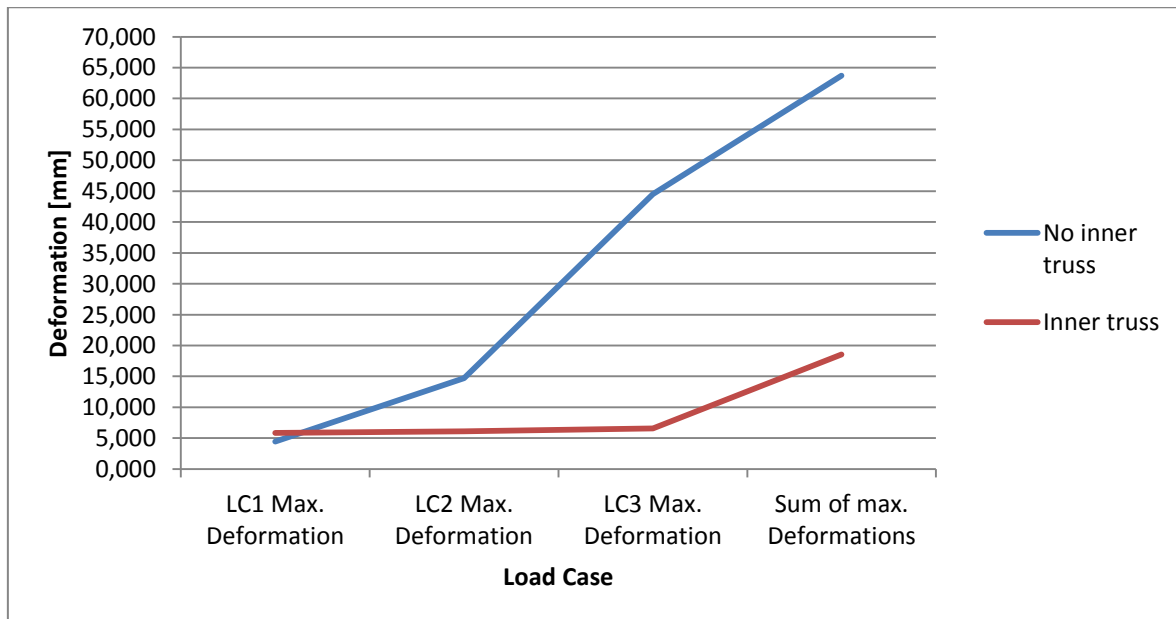


Fig. 91: Deformation caused by LC1-LC3 for the main load bearing structure with and without inner supporting trusses.

During the analyses described above, the maximum occurring tensile and compressive axial stresses were also compared for the variant with and without inner truss. The results showed that the differences between the variants are much smaller than for the deflections. Therefore the results are not discussed here; in the table below they are shown without further comments.

Tensile stress	Variant	LC1 Max. Stress	LC2 Max. Stress	LC3 Max. Stress	Sum of max. Stress
	No inner truss	6,966	12,750	36,290	56,006
Inner truss	10,200	18,060	25,370	53,630	
Factor	0,683	0,706	1,430	1,044	
Compressive stress	Variant	LC1 Max. Stress	LC2 Max. Stress	LC3 Max. Stress	Sum of max. Stress
	No inner truss	5,317	11,380	14,700	31,397
Inner truss	9,197	14,280	14,490	37,967	
Factor	0,578	0,797	1,014	0,827	

Table 25: Maximum tensile and compressive axial stresses caused by LC1-LC3 for the main load bearing structure with and without inner supporting trusses.

7.4 DETERMINATION OF MOST EFFICIENT GRID SIZE

After the choice on the most efficient truss topology that was the subject of the preceding chapter, the next step in finding the most suitable grid size for this truss topology. In [ch. 7.1.1] the grid size was chosen such that the material usage had a particular value. The main reason to investigate the influence of the grid size is to obtain the maximum grid size for which the deflection- and stress-demands are still fulfilled. By using this maximum grid size during final design the number of connections as well as the overall material usage is minimized, leading to a more efficient and easier to construct bridge structure.

The factor that describes the influence of the inner bridge deck sub structure on the overall stiffness of the main load bearing structure will not be applied in this stage of optimization. It will be applied in the next stage, in [ch. 7.5] where the cross section size will be optimized.

In contrast to the earlier chapter [ch. 7.1.3], where cross section variant 2B was used for the two main radii of the main load bearing structure to determine the most efficient truss topology; in this chapter the main dimensions (first- and second radii) of the cantilever variant will be used [ch. 5.2.8] because it is most likely to be used for the final layout of the bridge, see [ch. 7.6.3] for a more detailed explanation on this choice. To recall, the radii of the cantilever variant are radii are $R_1 = 7,50m$ and $R_2 = 5,00m$.

The table below shows the most important geometric parameter of all grid size variants, in a similar way as the truss topology variant table [ch. 7.1.1, table 20].

Grid Variant	Size	# long. divisions	# lat. divisions	# diagonals	Cell size long. [m]	Cell size lat. [m]	long./lat. ratio	Avg. length of Diagonals	Total material usage [m]
1		10	8	80	4,900	4,958	1,012	6,971	1385,959
2		12	10	120	4,083	3,966	0,971	5,693	1688,738
3		14	12	168	3,500	3,305	0,944	4,814	1991,713
4		16	14	224	3,063	2,833	0,925	4,172	2294,805
5		18	16	288	2,722	2,479	0,911	3,682	2597,973
6		20	18	360	2,450	2,204	0,899	3,295	2901,192

Table 26: Main geometric parameters for all 6 grid size variants

The material and cross section are kept similar to that described in [ch. 7.1.2.1]. In [ch. 7.5] further research on the most efficient cross section dimensions will be carried out.

7.4.1 FINITE ELEMENT ANALYSIS FOR THE GRID SIZE DETERMINATION

The 6 different grid size variants are inserted into GSA and compared using the deflections due to LC1-LC3. The pictures below show the varying material usage of 'grid variant 1' to 'grid variant 6'. In the following tables the results of this FE-analysis will be discussed.

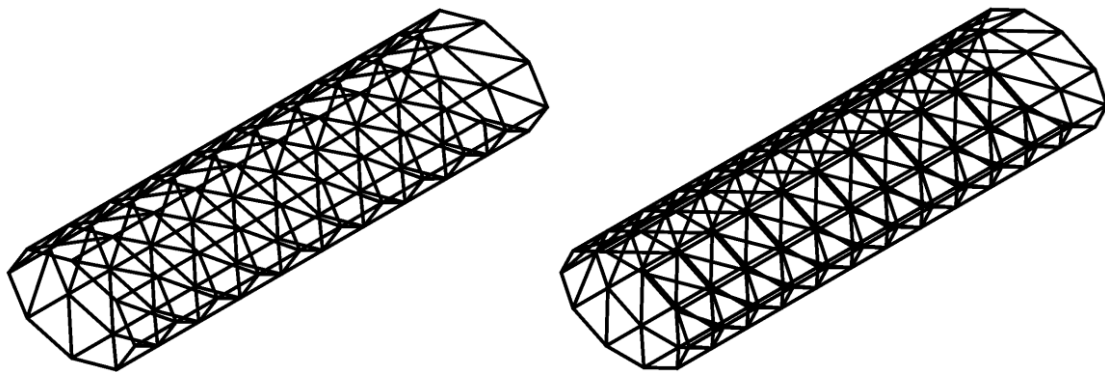


Fig. 92: 'Grid Size Variant 1' (left) and 'Grid Size Variant 2' (right)

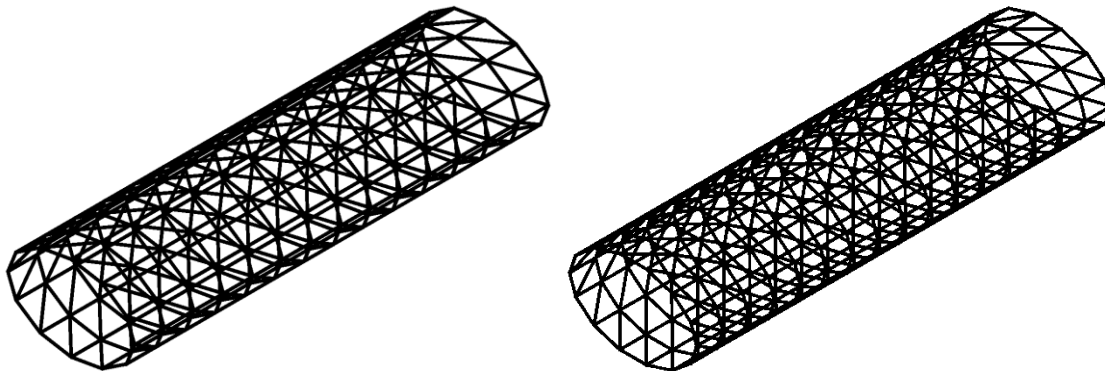


Fig. 93: 'Grid Size Variant 3' (left) and 'Grid Size Variant 4' (right)

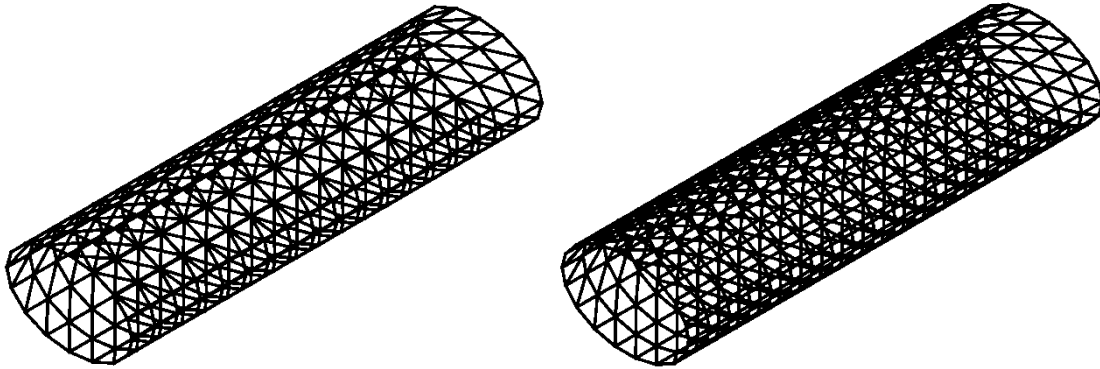


Fig. 94: 'Grid Size Variant 5' (left) and 'Grid Size Variant 6' (right)

7.4.1.1 MATERIAL USAGE OF THE GRID SIZE VARIANTS

In the following table, the material usage and number of connections and elements is shown for each grid size variant. Afterwards a graph is presented which graphically depicts this table. The grid size variants were chosen in such a way that the overall material usage linearly increases with the grid size variant number. It can be seen that both the number of connections as well as the number of elements both show a similar behavior. It can thus be concluded that the difficulty to fabricate the different variants increases with the number of grid size variant.

Grid Size Variant	Cell size long. [m]	Total material usage [m]	Number of elements	Number of nodes
1	4,900	1385,959	248	88
2	4,083	1688,738	370	130
3	3,500	1991,713	517	181
4	3,063	2294,805	686	238
5	2,722	2597,973	880	304
6	2,450	2901,192	1098	378

Table 27: Extended geometric properties of the grid size variants

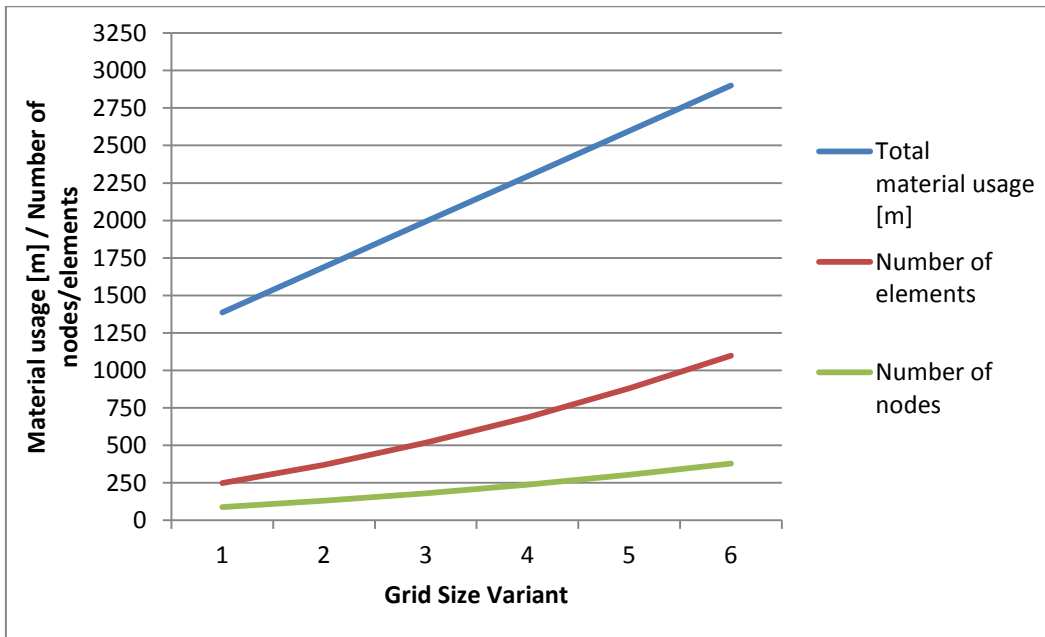


Fig. 95: Graph showing the material usage as well as the number of connections and truss elements for each grid size variant

7.4.1.2 MAXIMUM DEFLECTION OF THE GRID SIZE VARIANTS

The goal of this chapter is to find a variant that has a minimum number of elements and connections, a minimal material usage while complying with the deflection limit of $L/600$, further described in [ch. 6.9]. To find the deflections for each of the six grid size variants, FE-analyses were carried out for each load case. The table and graph below show the results and compare the sum of deflections due to all load cases with the deflection limit.

Grid Variant	Size	LC1 Max. Deformation	LC2 Max. Deformation	LC3 Max. Deformation	Sum of max. Deformations	L/600 Deflection Limit
1		3,542	26,430	66,740	96,712	81,667
2		3,566	20,360	58,720	82,646	81,667
3		3,771	18,860	57,760	80,391	81,667
4		3,777	15,770	50,750	70,297	81,667
5		3,882	14,460	47,750	66,092	81,667
6		3,879	12,620	42,510	59,009	81,667

Table 28: Results of the deflections FE-analysis for all grid size variants and load cases.

The graph below shows that magnitude of deflections decreases with increasing material usage. This follows the general expectation of an increase in overall stiffness for more used material. It can also be seen that grid size variants 1, 2 and 3 do not (or barely) suffice the $L/600$ criterion (represented by the black dashed line). This means that these variants simply lack the material to achieve an abundantly stiff behavior.

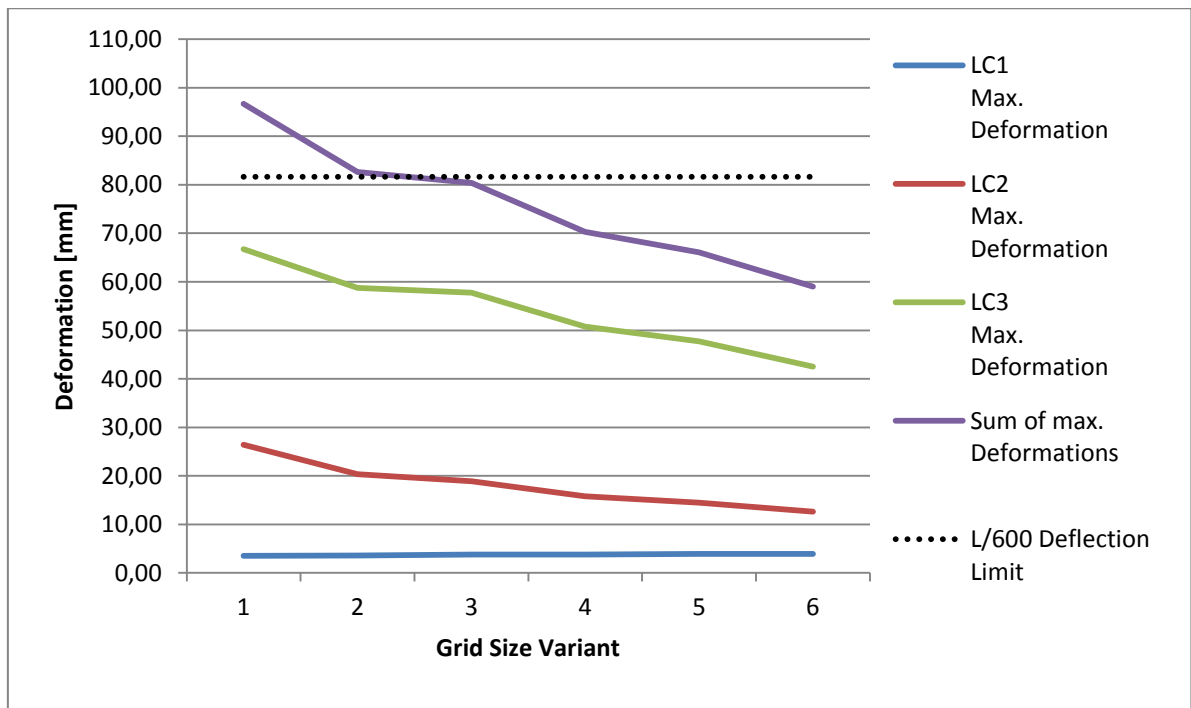


Fig. 96: Graph showing the results for the deflections of the FE-analysis for all grid size variants and all three load cases.

It is also interesting to see that the self-weight load case (LC1) induces a nearly constant deflection of under 5,00mm, thereby not being of much importance. The distributed load case (LC2) also has a surprisingly low influence on the maximum deflection. The largest values induced by this load case lie at a maximum of 26,43mm. The point load case (LC3) produces the largest deflections by far. Here maximum values of 66,74mm are reached for grid size variant 1. Of course it also has to be mentioned that the values for LC3 are conservative, because load-spreading has not yet been taken into account and whole system of 8 point loads of 'Load Model 1' was placed at a single node at bottom mid-span of the main load bearing structure.

7.4.1.3 MAXIMUM COMPRESSIVE AND TENSILE STRESSES OF THE GRID SIZE VARIANTS

The next point of interest in the FE-analyses is the magnitude of the maximum occurring compressive- and tensile stresses in the main load bearing structure, caused by the three load cases. The following table and graph show these values.

Grid Size Variant	LC1 Max. tensile Stress	LC1 Max. compr. Stress	LC2 Max. tensile Stress	LC2 Max compr. Stress	LC3 Max. tensile Stress	LC3 Max compr. Stress	Sum of tensile stresses	Sum of compr. stresses
1	4,722	4,349	33,780	28,610	53,220	36,740	91,722	69,699
2	5,172	4,489	27,990	25,670	51,270	32,930	84,432	63,089
3	5,560	4,714	24,100	21,180	44,060	24,900	73,720	50,794
4	5,915	4,837	21,290	19,470	40,660	22,900	67,865	47,207
5	6,237	4,892	19,710	17,270	36,650	19,290	62,597	41,452
6	6,534	4,900	18,400	15,480	35,940	18,070	60,874	38,450

Table 29: Maximum compressive- and tensile stresses found in the FE-analysis for all grid size variants and load cases.

In the graph below the stress results for the compressive stresses are shown in dashed lines, whereas the results for the tensile stresses are shown in solid lines. It can be seen that the maximum combined tensile stresses lie at about 92,0N/mm² for grid size variant 1. The maximum combined compressive stresses lie significantly lower at about 70,0N/mm², also for grid size variant 1. These values are very low and certainly much less decisive on the final design than the deflection values described earlier.

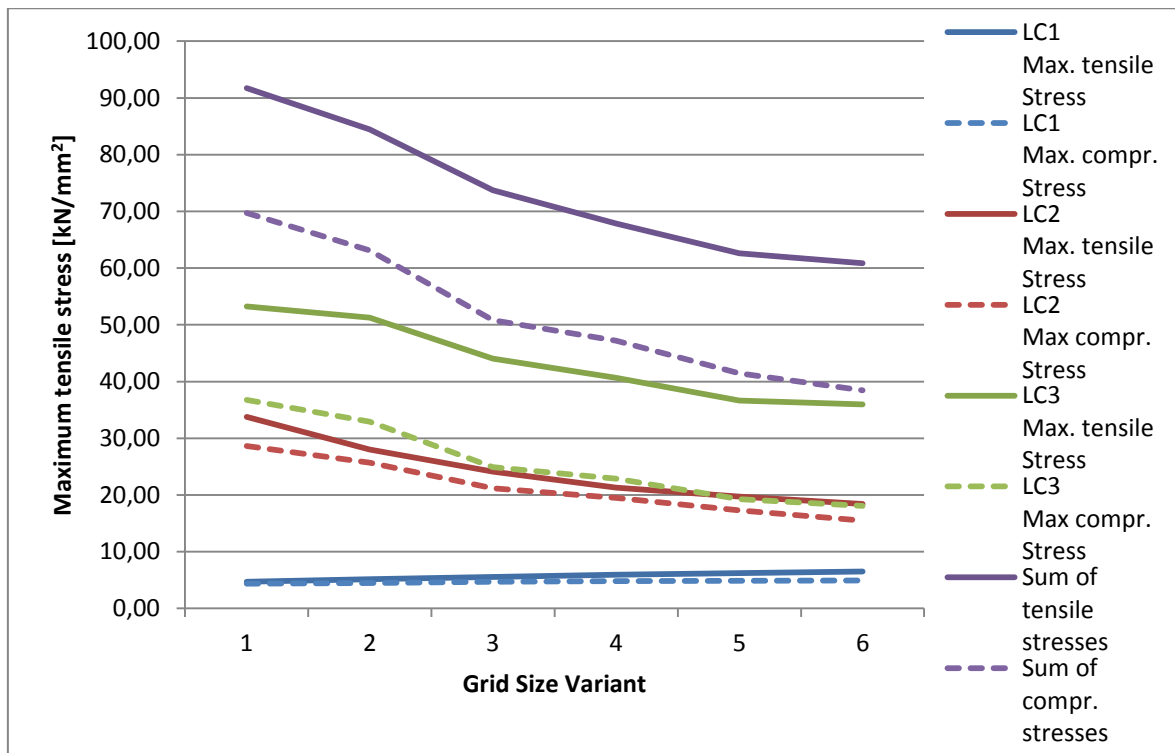


Fig. 97: Results for the maximum compressive- and tensile stresses, following the FE-analysis for all grid size variants and all three load cases.

The difference between the maximum tensile and compressive stress lies mainly in the results for the stresses due to LC3. In this point-load case the structure is primarily loaded under tension because the bottom-most node at mid-span is loaded. Would the top-most node at mid-span be subjected by the same point load, the compression stresses would be much higher than the tensile stresses.

Comparing the magnitude of the stresses arising with the design strength, both in compression and tension in the region of 900-1.200 N/mm², described in [ch. 3.4] leads to the conclusion that application of all variants lead to very low stress levels, and structural design should therefore be focused on deflection behavior. This deflection-driven approach was already described in the literature study [LS, ch. 3.2.3, p113, ch. 3.2.4, p115] and is caused by the relatively low stiffness of FRP-composites compared to their strength. For more information on strength-and stiffness-values of UD-composites, see [ch. 3.3]

7.4.1.4 CHOICE ON THE MOST EFFICIENT GRID SIZE VARIANT

After having shown that the choice on the most efficient grid size variant is stiffness-driven, now the comparison between material usage and stiffness has to be made. For this cause, the total material usage has to be directly compared to the maximum deflection of each grid size variant. In order to do this, both parameters have to be normalized first. The table below shows the normalized deformation due to LC1-LC3 as well as the sum of deformations and the normalized material usage and number of nodes.

Grid Variant	LC1 Max. Deformation	LC2 Max. Deformation	LC3 Max. Deformation	Sum of max. Deformations	Total material usage [m]	Number of nodes
1	0,158	0,244	0,206	0,212	0,108	0,067
2	0,159	0,188	0,181	0,182	0,131	0,099
3	0,168	0,174	0,178	0,177	0,155	0,137
4	0,168	0,145	0,157	0,154	0,178	0,180
5	0,173	0,133	0,147	0,145	0,202	0,230
6	0,173	0,116	0,131	0,130	0,226	0,287

Table 30: Normalized maximum deformations and normalized material usage and number of nodes for all grid size variant

In the two graphs below the results are represented in a clear way. The first graph compares the normalized deflections to the normalized material usage for each grid size variant. The second graph compares the normalized deflections with the normalized number of nodes, again for each grid size variant. Both graphs show very similar outcomes. The line of material usage in the first graph (black dotted line) crosses the deflection lines between 'grid size variant 3' and 'grid size variant 4' (vertical grey band). In the second graph the crossing point between the line of number of nodes and the deflection lines has slightly shifted toward 'grid size variant 4'.

Since this crossing point represents the point where both the material usage and the number of nodes as well as the maximum deformation are equally at their lowest values it can be concluded that of the 6 grid size variants, 'grid size variant 3' and 'grid size variant 4' are both the most efficient grid size variants. However comparing the two the graph below shows that in terms of number of nodes compared to maximum deformations there is a slight preference for 'grid size variant 4'. Furthermore, 'grid size variant 4' yields deformation values that are lower and safer than that of 'grid size variant 3', but also more conservative regarding the maximum $L/600$ deformation limit.

After thorough analyses it can be therefore be concluded that 'grid size variant 3' and 'grid size variant 4' are the most efficient choice when the maximum deformation as well as the overall material usage and total number of nodes are considered.

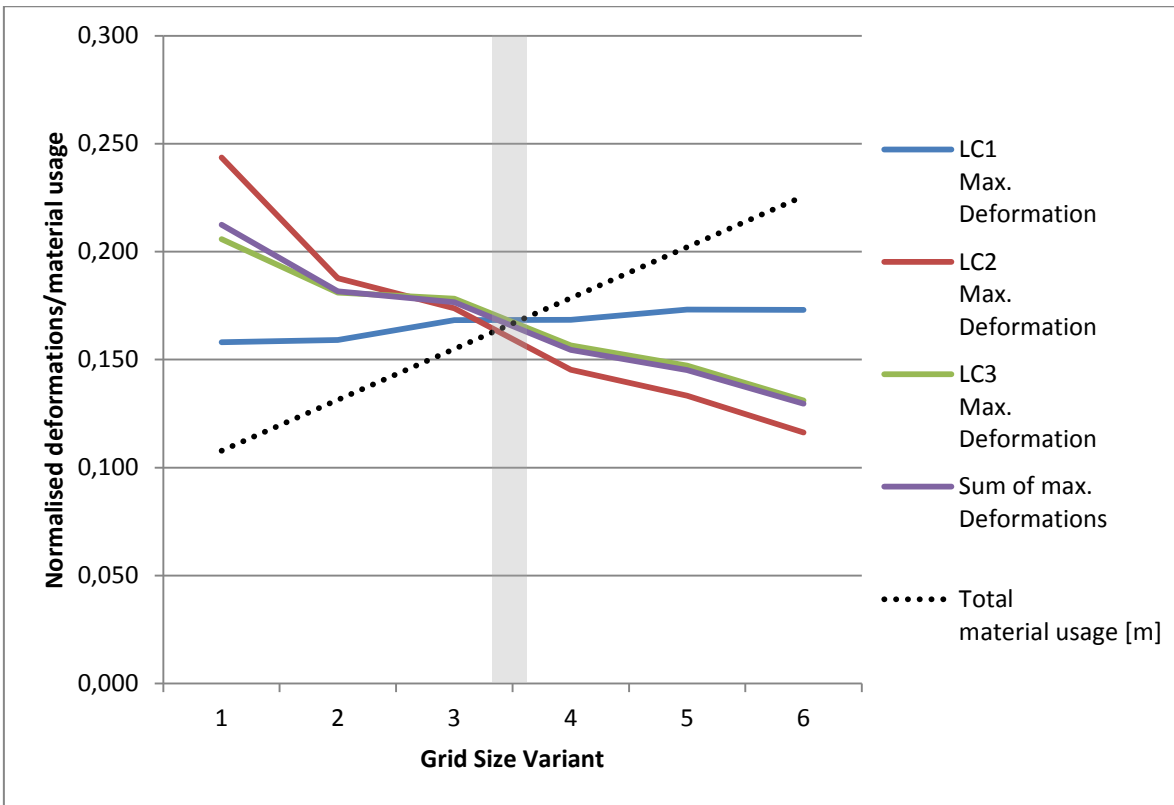


Fig. 98: Normalized maximum deformations and normalized material usage for all grid size variants, leading to a choice the most efficient variant.

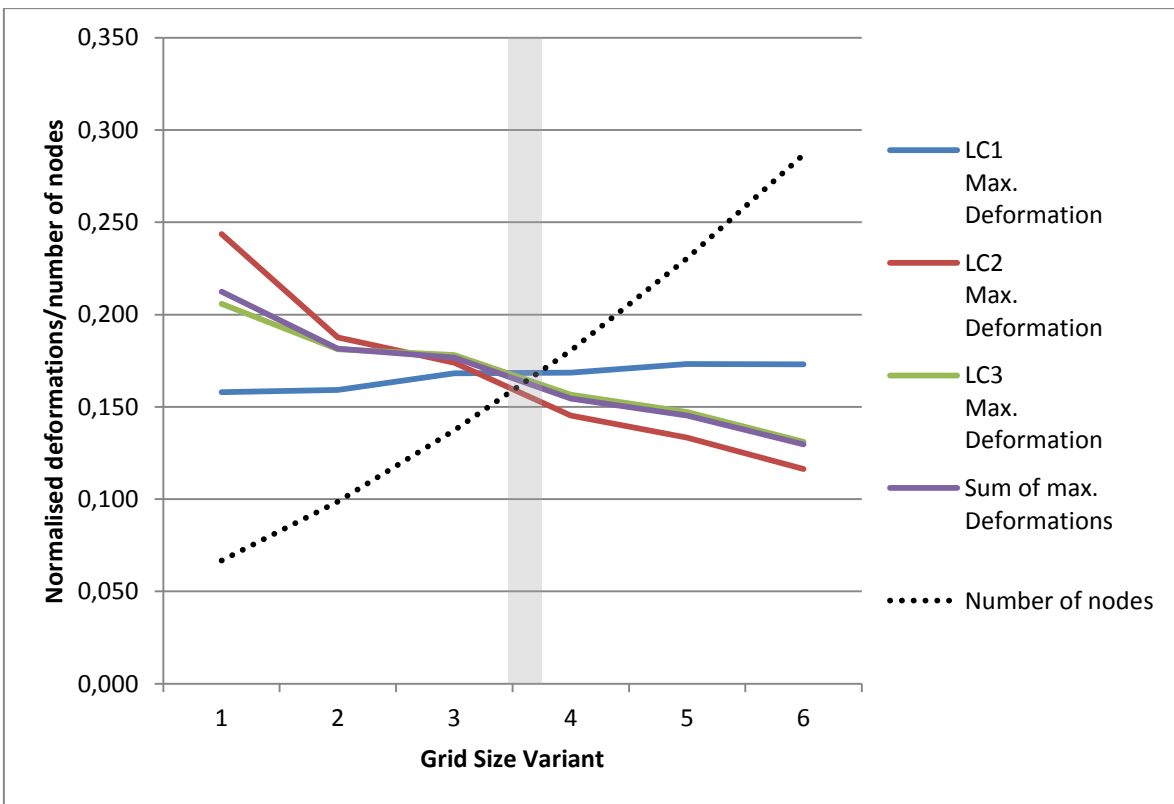


Fig. 99: Normalized maximum deformations and normalized number of nodes for all grid size variants, leading to a choice the most efficient variant.

7.5 DETERMINATION OF MOST EFFICIENT CROSS SECTION DIMENSIONS

In this chapter a number of different cross sections will be analyzed in a similar way as described before. A total of 20 different cross sections were used. It was chosen to use 'grid size variant 4', see [ch. 7.4], for the analyses of the cross sections. For all 20 cross section variants the maximum deflections and stresses were analyzed, for all three load cases LC1-LC3, as described in [ch. 7.2]. The table below shows the main parameters such as diameter, wall thickness, cross sectional area, moment of inertia and weight per meter for all 20 cross section variants.

Cross Section Variant	Diameter [mm]	Wall thickness [mm]	Cross Section [mm ²]	I[x10 ⁶ mm ⁴]	Weight (60/40) [kg/m]
150x10	150,000	10,000	4398,230	10,830	6,958
150x15	150,000	15,000	6361,725	14,670	10,064
150x20	150,000	20,000	8168,141	17,660	12,922
150x25	150,000	25,000	9817,477	19,940	15,531
150x30	150,000	30,000	11309,734	21,630	17,892

200x10	200,000	10,000	5969,026	27,010	9,443
200x15	200,000	15,000	8717,920	37,540	13,792
200x20	200,000	20,000	11309,734	46,370	17,892
200x25	200,000	25,000	13744,468	53,690	21,744
200x30	200,000	30,000	16022,123	59,680	25,347

250x10	250,000	10,000	7539,822	54,380	11,928
250x15	250,000	15,000	11074,114	76,760	17,519
250x20	250,000	20,000	14451,326	96,280	22,862
250x25	250,000	25,000	17671,459	113,200	27,956
250x30	250,000	30,000	20734,512	127,800	32,802

300x10	300,000	10,000	9110,619	95,890	14,413
300x15	300,000	15,000	13430,309	136,700	21,247
300x20	300,000	20,000	17592,919	173,300	27,832
300x25	300,000	25,000	21598,449	205,900	34,169
300x30	300,000	30,000	25446,900	234,700	40,257

Table 31: Main parameters of all 20 cross section variants.

The table below shows the maximum deformation results of the FE-analyses that were performed for all cross section variants and load cases in 'Oasys GSA'. It is important to mention that next to the deformations directly derived from the analysis another deformation column was added here (light blue shade). This column shows the adapted deformation, taking into account the added stiffness of the inner truss structure, used to support the bridge deck. This factor was derived separately for each load case in [ch. 7.3] as well as for the sum of all deformations. The value of the factors is also shown in the table. Note that the value of the factor was conservatively rounded from the values shown in [ch. 7.3.2, table 24]

Cross Section Variant	LC1 Max. Deformation	LC1 Factor 0,75	LC2 Max. Deformation	LC2 Factor 2,0	LC3 Max. Deformation	LC3 Factor 6,0	Sum of max. Deformations	Sum of max. Deformations Factor 3,0	L/600 Deflection Limit
150x10	7,966	10,621	120,400	60,200	579,600	96,600	778,787	259,596	81,667
150x15	8,391	11,188	84,020	42,010	413,900	68,983	559,509	186,503	81,667
150x20	8,831	11,775	65,990	32,995	332,800	55,467	452,391	150,797	81,667
150x25	9,279	12,372	55,340	27,670	285,500	47,583	390,161	130,054	81,667
150x30	9,730	12,973	48,380	24,190	255,300	42,550	350,573	116,858	81,667
200x10	4,890	6,520	79,870	39,935	314,500	52,417	445,715	148,572	81,667
200x15	5,090	6,787	55,240	27,620	220,900	36,817	315,637	105,212	81,667
200x20	5,295	7,060	43,000	21,500	174,600	29,100	251,455	83,818	81,667
200x25	5,506	7,341	35,710	17,855	147,200	24,533	213,612	71,204	81,667
200x30	5,720	7,627	30,910	15,455	129,400	21,567	189,112	63,037	81,667
250x10	4,089	5,452	56,800	28,400	195,400	32,567	290,141	96,714	81,667
250x15	4,146	5,528	39,060	19,530	135,800	22,633	204,064	68,021	81,667
250x20	4,204	5,605	30,230	15,115	106,300	17,717	161,454	53,818	81,667
250x25	4,263	5,684	24,960	12,480	88,720	14,787	136,107	45,369	81,667
250x30	4,323	5,764	21,470	10,735	77,170	12,862	119,462	39,821	81,667
300x10	3,630	4,840	42,450	21,225	132,000	22,000	204,145	68,048	81,667
300x15	3,666	4,888	29,070	14,535	91,170	15,195	143,329	47,776	81,667
300x20	3,703	4,937	22,400	11,200	70,860	11,810	113,100	37,700	81,667
300x25	3,740	4,987	18,410	9,205	58,750	9,792	95,092	31,697	81,667
300x30	3,777	5,036	15,770	7,885	50,750	8,458	83,218	27,739	81,667

Table 32: Results on the deflection of all cross section variants directly derived from FE-analysis and adapted for influence of the bridge deck substructure (light blue shaded)

Plotting the results shown in the above table yields the following two tables. The first table shows the directly from FE-analysis derived results and the second table shows the deflection results adapted for the expected stiffness influence of an added bridge deck substructure.

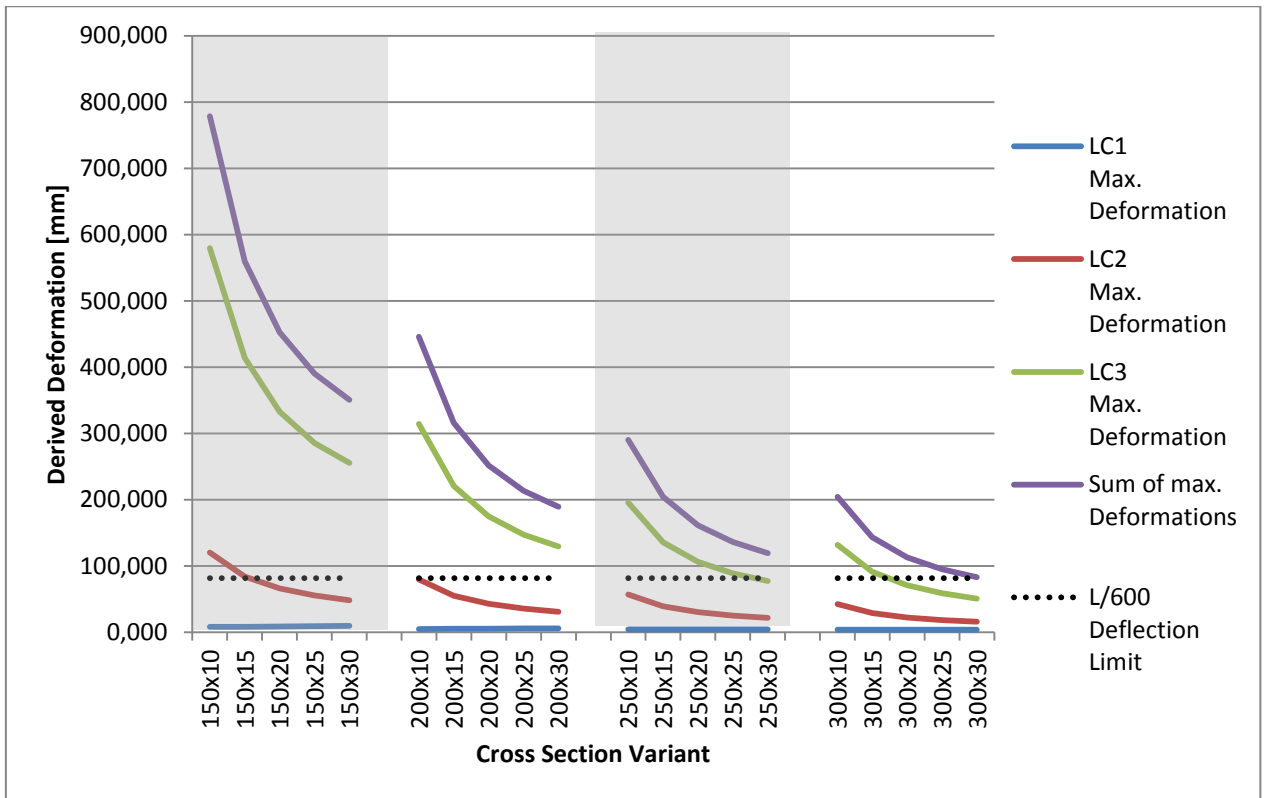


Fig. 100: Deformation results directly derived from FE-analysis for all cross section variants and load cases

The directly derived deformation results plotted in the above graph clearly show that only the cross section variant with the largest diameter and wall thickness and thus also largest stiffness meets the $L/600$ deflection criterion. All other cross section variants (drastically) exceed this limit. However this is not very surprising, since for the determination of most efficient grid size variant exactly this cross section was used. In [ch. 7.4.1.4] it was chosen to use the grid size variant that just met the deflection limit while not being overly safe, thereby becoming inefficient.

Because in the final design an inner substructure for the bridge deck will certainly be used, the added stiffness of such a substructure, as derived in [ch. 7.3], has to be taken into account. In the second graph, shown below, this factor is applied, resulting in adapted deformation values. It can be clearly seen that the overall deformation values are much lower and many cross section variants meet the deflection criterion. In particular all variants with a diameter of 300mm and 250mm (except the 250x10mm variant) meet the deflection limit. The 200x20mm, 200x25mm and 200x30mm variants also meet the deflection criterion. All other variants yield too high deflection values.

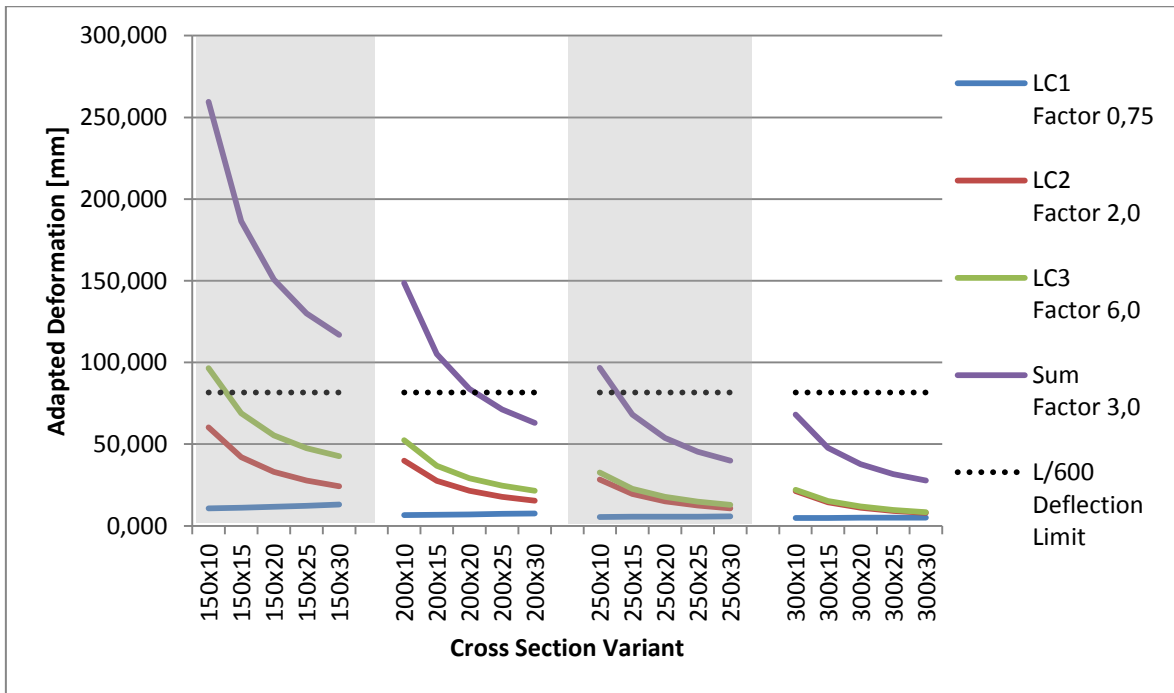


Fig. 101: Deformation results, adapted by applying the factor derived in [ch. 8.3] that takes the expected added stiffness of the bridge deck substructure into account.

To finish the analysis on the cross section variants, the table and graph below provide insight in the maximum occurring tensile- and compressive stresses in the members. The stresses have not been adapted with the bridge deck substructure influence factor derived in [ch. 7.3] because the analysis in [ch. 7.3.2] showed that the bridge deck substructure has a negligible influence on the maximum occurring stresses.

Cross Section Variant	LC1 Compression	LC1 Tension	LC2 Compression	LC2 Tension	LC3 Compression	LC3 Tension	Sum of Compression	Sum of Tension
150x10	5,854	5,084	138,800	163,700	250,000	425,000	394,654	593,784
150x15	5,909	5,029	96,630	114,200	177,800	301,900	280,339	421,129
150x20	5,963	4,975	75,760	89,760	142,200	241,500	223,923	336,235
150x25	6,016	4,955	63,420	75,290	121,300	206,200	190,736	286,445
150x30	6,067	4,955	55,360	65,850	107,800	183,400	169,227	254,205

200x10	5,366	5,549	94,370	108,300	135,800	240,700	235,536	354,549
200x15	5,405	5,515	65,110	74,890	95,590	168,500	166,105	248,905
200x20	5,443	5,481	50,560	58,310	75,710	132,700	131,713	196,491
200x25	5,481	5,447	41,900	48,440	63,960	111,600	111,341	165,487
200x30	5,518	5,412	36,180	41,930	56,270	97,710	97,968	145,052

250x10	5,016	5,816	68,950	76,720	85,100	154,000	159,066	236,536
250x15	5,045	5,797	47,290	52,780	58,840	106,800	111,175	165,377
250x20	5,074	5,777	36,510	40,860	45,780	83,360	87,364	129,997
250x25	5,103	5,757	30,070	33,740	38,010	69,420	73,183	108,917
250x30	5,132	5,736	25,800	29,040	32,880	60,230	63,812	95,006

300x10	4,743	5,956	52,930	59,510	60,690	107,200	118,363	172,666
300x15	4,767	5,947	36,150	40,370	41,720	73,700	82,637	120,017
300x20	4,790	5,937	27,790	30,810	32,270	57,040	64,850	93,787
300x25	4,814	5,926	22,790	25,090	26,630	47,160	54,234	78,176
300x30	4,837	5,915	19,470	21,290	22,900	40,660	47,207	67,865

Table 33: Maximum tensile- and compressive stresses in the cross section variants due to LC1-LC3

In the graph below it can be seen that the maximum stresses for the cross section variants that are considered to yield acceptable deformation lay within reasonable bounds. The maximum compressive and tensile strength values described in [ch. 3.3] are not reached by far. This complies very well with the earlier mentioned stiffness-driven design method for fiber reinforced polymer structures.

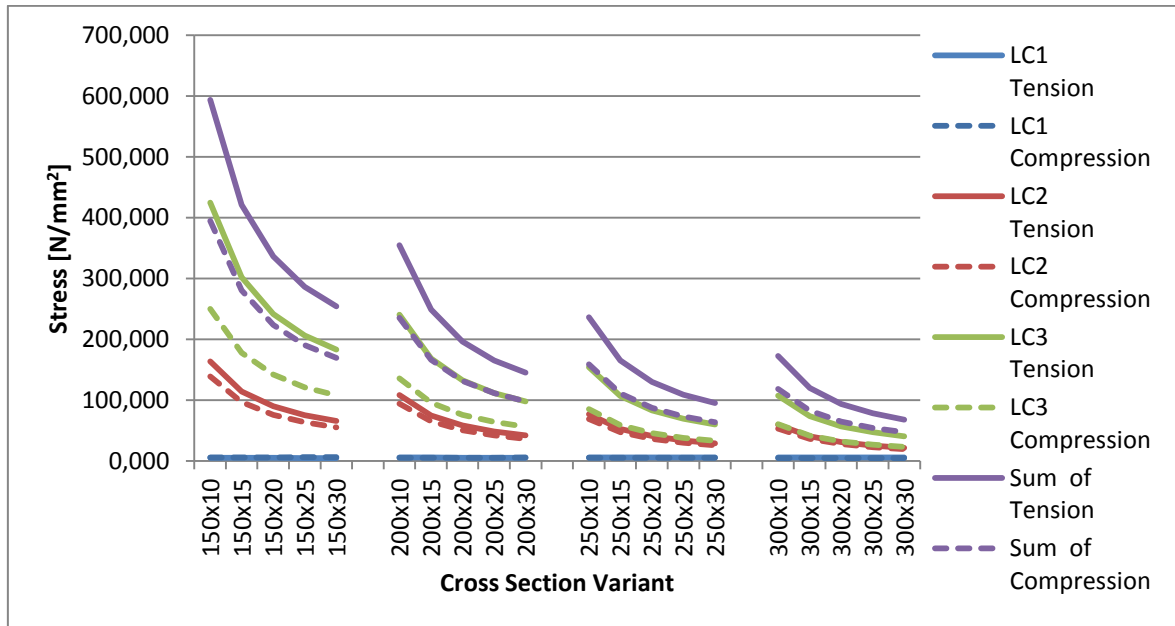


Fig. 102: Maximum tensile- and compressive stresses in the cross section variants due to LC1-LC3

7.5.1 CHOICE ON THE MOST EFFICIENT CROSS SECTION DIMENSIONS

Knowing the results of the FE-analysis on the deformations and stresses occurring in the cross section variants under LC1-LC3 a conclusion on the most efficient cross section variant can be drawn. The adapted deformation results depicted in [ch. 7.5, Fig. 101] already showed that all cross section variants with a diameter of 150mm and 300mm are definitely not the most efficient cross section variants. The 150mm cross sections do not meet the deflection limit by far and the 300mm cross section over-exceeds the deflection limit, thereby leading to an inefficient choice.

Comparing the normalized moment of inertia for each cross section variant with the normalized deformation leads to the graph shown below. From this graph a very clear conclusion can be drawn: The two lines intersect at two cross section variants: the 200x30mm variant and the 250x15mm variant. It can therefore be expected that the most efficient cross section variant, lies around these cross section, since their stiffness (or moment of inertia in this case, because the modulus of elasticity is constant for both variants) lies at about the value that is needed to cope with the deformation.

For safety reasons it is chosen to not use the smallest and thinnest possible cross section, but to use a cross section on the safer side that is the side of the graph below, where the normalized moment of inertia exceeds the normalized deformation (red line above the blue line). It is therefore chosen to use the 250x25mm cross section for the final design. It is expected that a cross section of this type can be easily produced through the pultrusion process [ch. 3.5.1] [LS, ch. 2.5.4.4, p69].

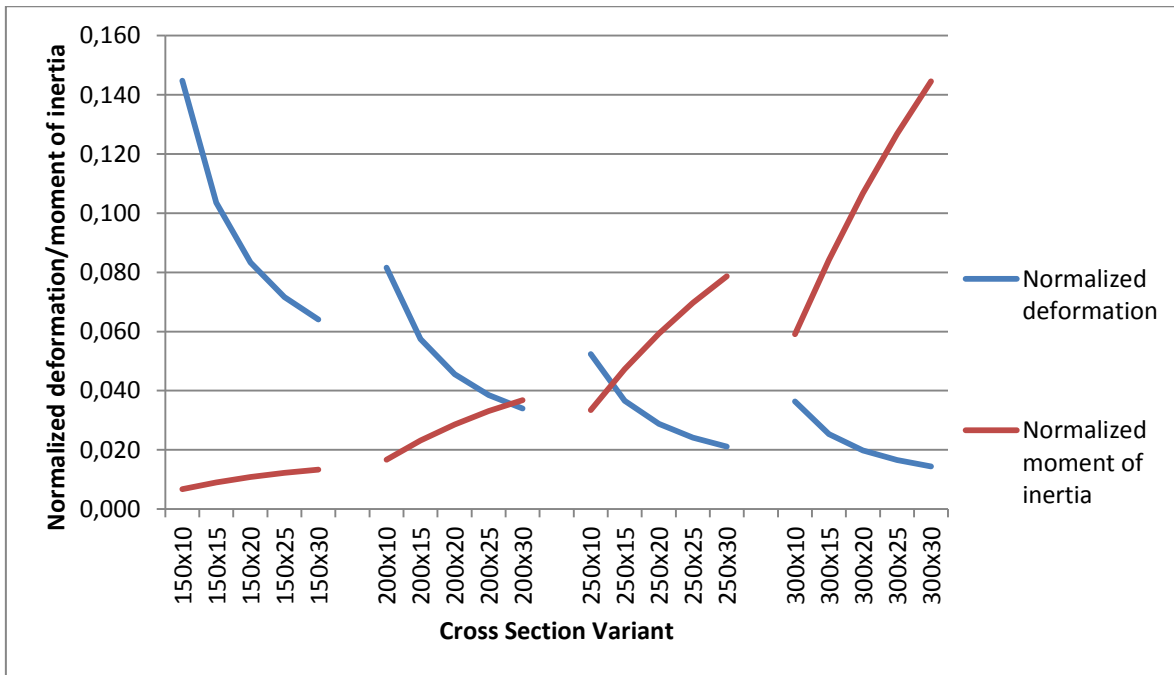


Fig. 103: Normalized deformation plotted against the normalized moment of inertia for all cross section variants.

7.6 FINAL CYLINDRICAL TRUSS GEOMETRY

In this chapter all geometry choices for the full-FRP cylindrical truss heavy traffic bridge will be recalled and clarified. This chapter is divided into the main parameters that described the bridge design: Truss topology, design span, shape and dimension of the main load bearing structure cross section, grid size of main load bearing structure truss, truss member cross section size.

7.6.1 TRUSS TOPOLOGY

First, the general truss topology will be given again. The picture below shows the chosen topology, the square truss with one diagonal layout. The choice for this topology is based on extensive FE-analyses, as described in [ch. 7.1.3]. Furthermore the type and number of nodes was also considered in this choice.

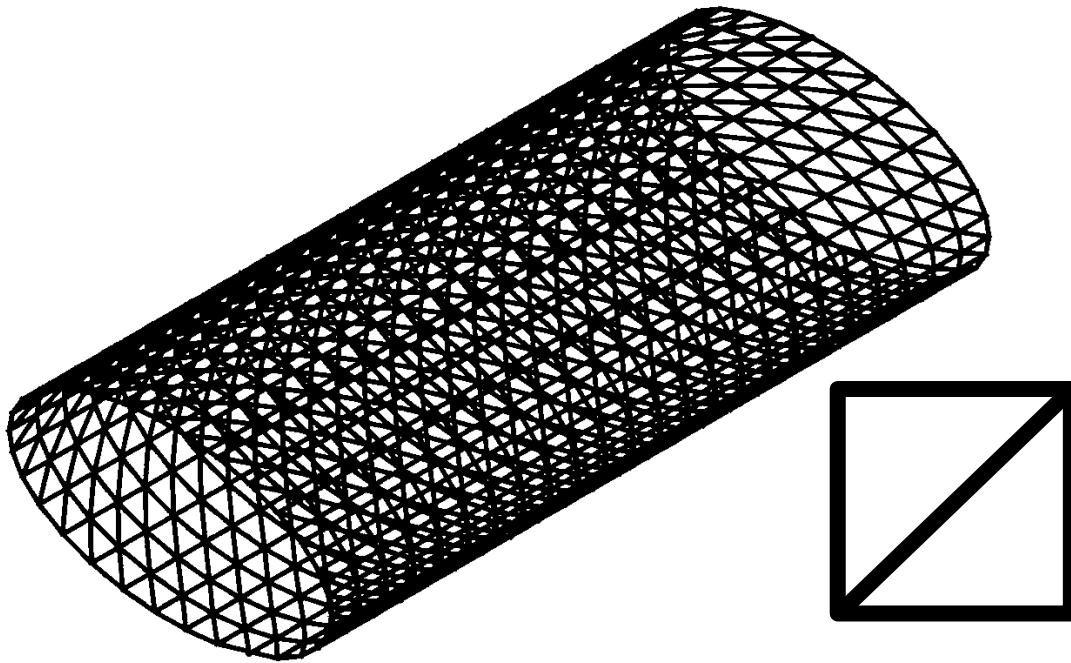


Fig. 104: Truss with one diagonal topology that is used for the main cylindrical load bearing structure of the FRP heavy traffic bridge.

7.6.2 DESIGN SPAN

The next important geometric parameter for this bridge is the design span. In [ch. 5.3] several spans were compared to each other. The bridge will be designed to span a typical Dutch highway. 3 highway configurations were considered: 2x2 lanes, 2x3 lanes and 2x4 lanes. In urban areas 2x4 lane highways are no exception anymore and therefore it was decided to use this configuration for the determination of the design span of the bridge. Rijkswaterstaat advises not to use intermediate supports for spanning busy urban highways, it is therefore chosen to use a single span of 49,00m for the FRP cylindrical truss heavy traffic bridge. In the picture below the cross-section of the highway to be spanned can be found.

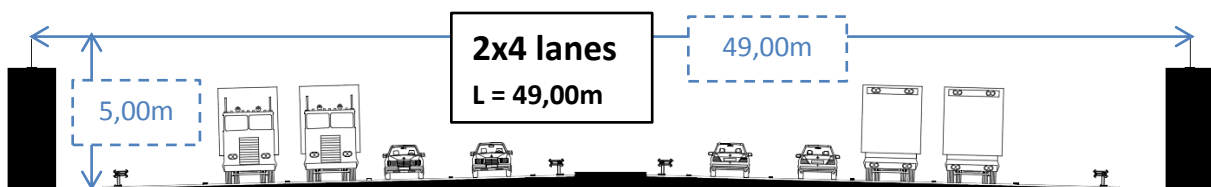


Fig. 105: Profile of the 2x4 lane highway that the bridge will span. This results in a single span of 49,00 m.

7.6.3 DIMENSIONS AND SHAPE OF THE MAIN LOAD BEARING STRUCTURE

The next important parameter for the bridge geometry is the choice for the type of main load bearing structure cross-section. In [ch. 5.2] two possibilities for this cross-section were given for each variant. These are the circular cross-section and the elliptical cross-section. The efficiency analysis that was carried out for the various variants in that chapter shows that the elliptical cross section variants yields far better ratios of used- vs. not-used-space. The exact numerical values for this parameter can be found in [ch. 5.2.7, table 15]. The improved efficiency of the elliptical cross-section compared to the circular cross-section is the reason why it is chosen to use the elliptical cross-section.

This leaves one important choice for the geometry of the main load bearing structure cross-section: the general dimensions of the cross-section as well as the configuration of the bridge deck. After analyzing the results of the bridge deck layout variants, in [ch. 5.2.8] an improved variant was derived, which yields a

relatively high space efficiency of over 50%, while having a small diameter, reducing the overall material usage. The general dimensions of this variant can be found in the picture below. Note that in this variant the slow and vulnerable traffic is logically and physically separated and protected from the fast and heavy traffic inside the cylindrical truss. The main cylindrical load bearing structure, which houses the heavy traffic has the same dimensions as the heavy traffic part of 'Variant 5B' [ch. 5.2.5], thus two main radii of 7,50m and 5,00m.

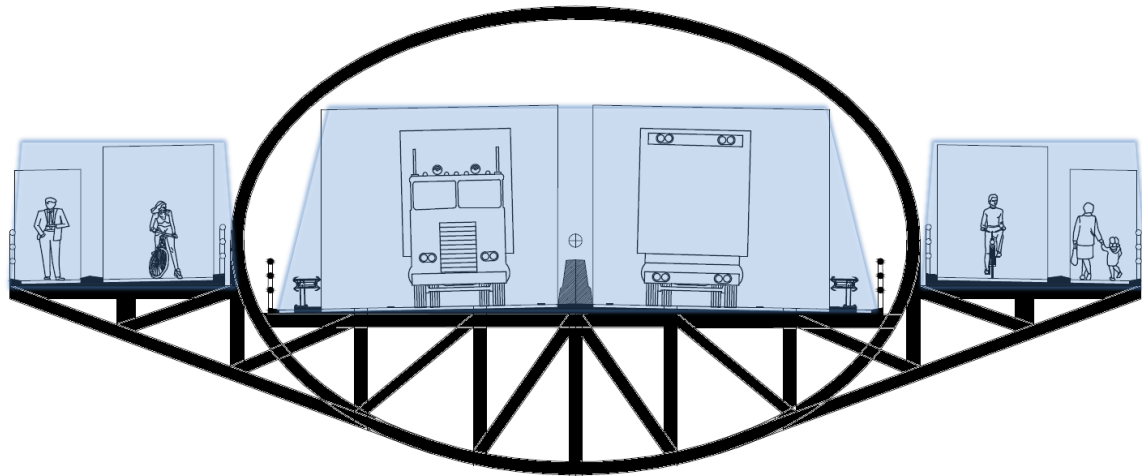


Fig. 106: Drawing of the 'Cantilever variant'. The cylindrical shape of this variant is similar to the heavy traffic part of 'Variant 5B'. A cantilevering truss structure is used to house the pedestrians and bicyclists, while keeping them physically separated from the fast, heavy traffic.

7.6.4 GRID SIZE OF THE CYLINDRICAL TRUSS

Knowing the topology of the main load bearing structure truss as well as the overall cross section shape of the bridge, the next important step in defining the structure is to specify the grid size of the elliptical truss used for the main load bearing structure. In [ch. 7.4] the most efficient grid size variant was found to be 'grid size variant 4'. The table below gives the most important specifications of this grid size variant. It is denoted as 'optimized variant (4)' in the first row. For comparison the specifications of the original variant that were derived from the truss topology optimization are given. Note the significant improvements in the field of material usage, number of nodes etc.

Grid Size Variant	# long. Divisions	# lat. Divisions	# diagonals	Cell size long. [m]	Cell size lat. [m]	long./lat. ratio	Avg. length of Diagonals	Total material usage [m]	Long. Element [m]	Short. Element [m]	# elements	# nodes
Optimized Variant (4)	16	14	224	3,063	2,833	0,925	4,172	2294,805	4,447	2,215	686	238
Original variant	24	30	720	2,042	1,322	0,648	2,432	4212,893	3,321	1,241	1320	456

Table 34: Specification of the optimized grid size variant (first row) compared to the specifications of the original variant (second row)

In the picture below the two variants are shown. Left the original variant, right the optimized variant that was found after thorough analysis on the most efficient grid size. Note the impressive differences in number of nodes, number of elements and grid size.

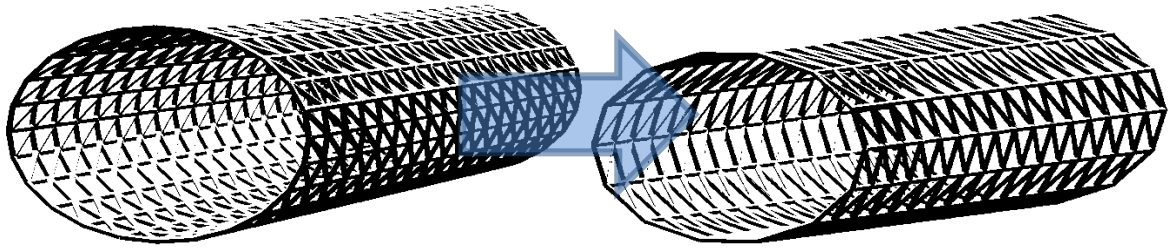


Fig. 107: Left: Original variant for the main elliptical truss. Right: Optimized variant for the main elliptical truss after finding the most efficient grid size variant.

7.6.5 CROSS SECTION DIMENSIONS OF THE TRUSS ELEMENTS

The last parameter of the bridge that was optimized is the truss member cross section size. This parameter was thoroughly investigated in [ch. 7.5]. In this chapter, the initial circular hollow cross section of CHS-300x30, that was used for the truss topology optimization, described in [ch. 7.1.2.1] was reduced to a CHS250x25 section while still complying with the deflection limit described in [ch. 6.9]. Using this cross section the weight per meter of section drastically reduced (The values below are based on the 70/30 Carbon-Epoxy-UD-composite described in [ch. 3.3])

$$\text{Weight of CHS}_{300 \times 30} = 41,453 \text{ kg/m} \quad (7.7a)$$

$$\text{Weight of CHS}_{250 \times 25} = 28,787 \text{ kg/m} \quad (7.7b)$$

Combining this light weight with the reduced material usage, due to the grid size optimization (see [ch. 7.4, ch. 7.4.1.4]) this leads to a total weight of the main load bearing structure of :

$$\text{Original weight} = 41,453 \frac{\text{kg}}{\text{m}} * 4212,893\text{m} = 174637,054 \text{ kg} \cong 175\text{t} \quad (7.8a)$$

$$\text{Optimized weight} = 28,787 \frac{\text{kg}}{\text{m}} * 2294,805\text{m} = 66060,552 \text{ kg} \cong 66\text{t} \quad (7.8b)$$

Note that this weight does not include the inner- and outer bridge deck supporting structures, the bridge deck as well as all additional structures such as railings etc. It is given here solely to illustrate the improvements that were made during the optimization of the main load bearing structure.

Part C

Final Design & Finite Element Analysis

8. FINAL DESIGN

Knowing all important dimensions of the bridge such as cross-sectional shape, the main radii, the span and the truss topology, the main load bearing truss grid size and the member cross section dimensions [ch. 7.6], the next step in designing is the addition of a bridge deck and its substructure, such that the bridge can carry traffic. Taking the choices, described in the chapter before [ch. 7.6.3] into account, shows that two main components have to be added to the cylindrical load bearing structure:

- The inner bridge deck substructure, as described in [ch. 7.3].
- The cantilever bridge deck and its substructure. This bridge deck will carry the lighter traffic. Rather than inside, this bridge deck will be placed adjacent to the main load bearing structure. The whole deck will cantilever to the sides of main cylindrical structure.

In the following the different steps to model these two parts in 'GSA' will be shown. After adding both parts to the FE-model the real-world traffic loads will be added. Furthermore the material properties, support conditions etc. will be adapted, if necessary.

8.1 ADDITION OF INNER BRIDGE DECK SUBSTRUCTURE

In [ch. 7.3] it was already described how an inner bridge deck substructure was added to the non-optimized bridge structure. The addition of the bridge deck substructure in the optimized structure happens in a very similar way. Therefore, the method will only be described very briefly in this chapter. In the picture below the topology of the lateral truss that was added to the structure is shown. The members of the truss were placed in such a way that they directly connect to the nodes of the elliptical main load bearing structure (blue in the picture below). In total 17 of the trusses shown below were placed, this number is equal to the number of longitudinal divisions plus one [ch. 7.6.4, table 34]. The c.t.c. distance of these trusses is equal to the longitudinal cell size of 3,0625m [ch. 7.6.4, table 34]. The 'i' and 'o' mark the position of the longitudinal trusses



Fig. 108: Topology of the lateral trusses that act as substructure for the inner bridge deck.

In the [ch. 7.3] a total of 9 longitudinal trusses were placed in longitudinal direction. Due to the optimization processes described before, in the final design only 4 longitudinal trusses are needed. Because of the symmetry along the length-axis of the bridge, there are only two types of longitudinal trusses, the outer trusses ('o') and the inner trusses ('i'). The inner trusses have a height of 2,878m and the outer trusses have a height of 1,825m. The inner trusses have a lateral distance of 3,128m and the outer trusses are placed at distance of 3,05m from the inner trusses. The four longitudinal trusses are displayed in the following drawing.

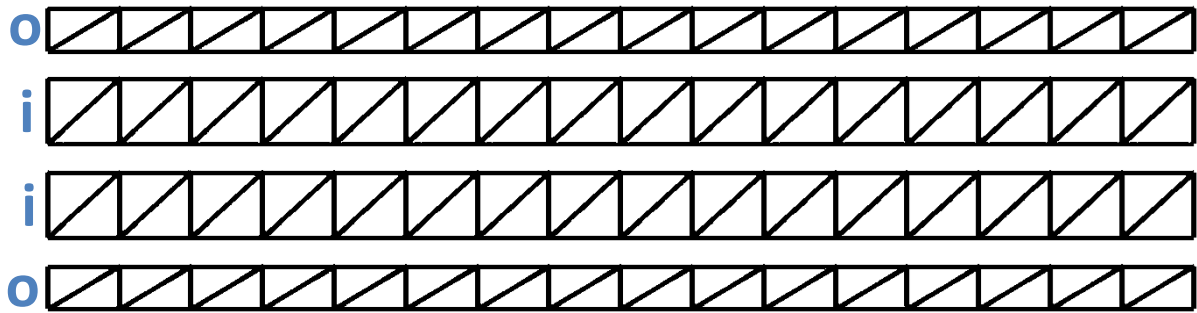


Fig. 109: Topology of the longitudinal truss that act as substructure for the inner bridge deck.

Combining the lateral- and longitudinal trusses with the main cylindrical load bearing structure yields the following FE-model of the bridge with the inner bridge deck and its substructure. Along with the large picture of the elliptical load bearing structure combined with the longitudinal and lateral inner trusses, the smaller pictures show the elliptical load bearing structure only (left) and the bridge deck supporting longitudinal and lateral inner trusses only (right).

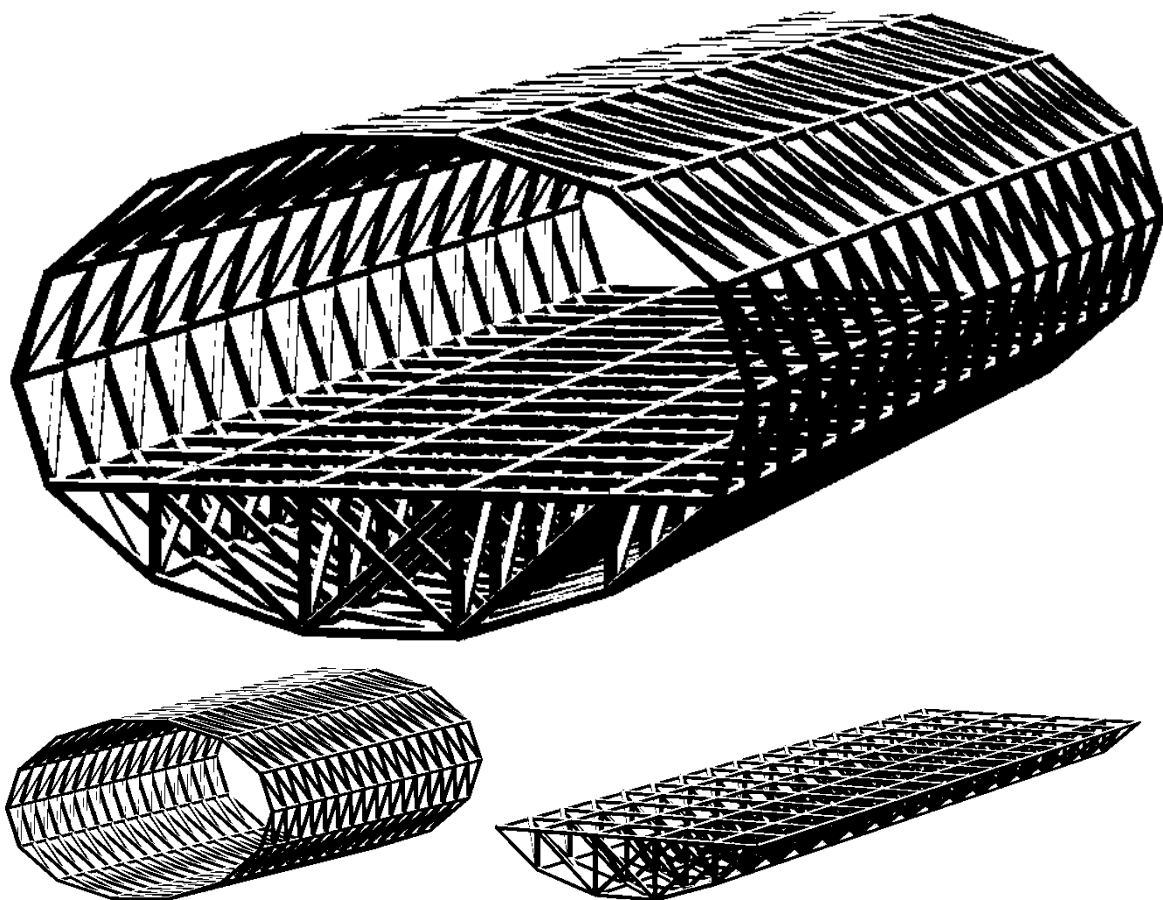


Fig. 110: Top: Main load bearing structure with inner bridge deck supporting structure. Bottom left: Elliptical main load bearing structure. Bottom right: Inner Bridge deck substructure.

In a preliminary FE-analysis the behavior of these three non-optimized structures was analyzed for the load cases used before and described in [ch. 7.2]. The graph shown below depicts the deformation that these three optimized structures undergo under the loads of LC1-LC3. It is clearly visible that the elliptical main load bearing structure only as well as the bridge deck supporting trusses only by far do not meet the $L/600$ deformation limit. The elliptical truss needs the bridge deck supporting trusses and vice versa. The combination of the two yields a maximum deformation of 64,6mm, which is comfortably below the described deformation limit of 81,667mm.

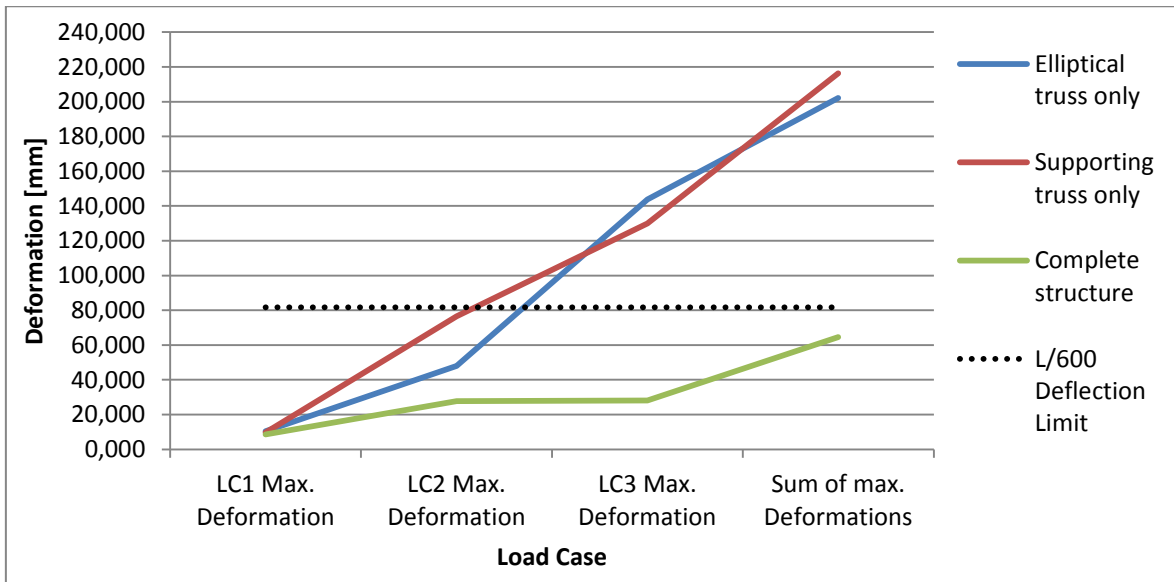


Fig. 111: Comparison of the deformation results for the three optimized parts of the bridge without cantilever substructure

8.2 ADDITION OF CANTILEVER BRIDGE DECK SUBSTRUCTURE

After the inner bridge deck substructure has been added [ch. 8.1], the next step is the addition of the cantilever bridge deck as described in the introduction of this chapter. The topology of the main load bearing structure as well as that of the inner bridge deck substructure was again also used for the cantilever bridge deck substructure. The members of the cantilever substructure directly connect at nodes of the main load bearing structure, as shown in the picture below, where these nodes are depicted by blue dots.

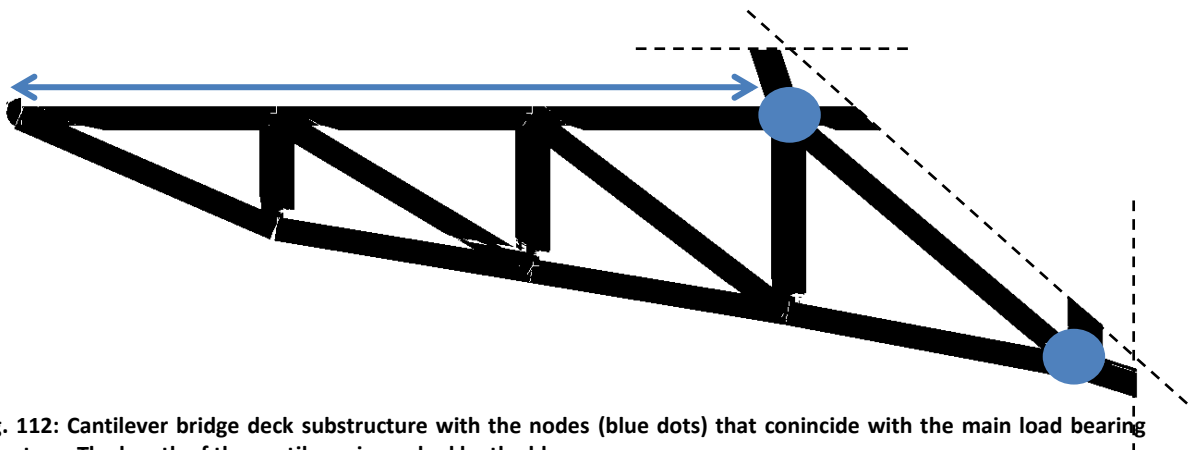


Fig. 112: Cantilever bridge deck substructure with the nodes (blue dots) that coincide with the main load bearing structure. The length of the cantilever is marked by the blue arrow.

The length in of the cantilever in lateral direction (blue arrow in the above picture) is directly determined by the required width for the users of the cantilever bridge deck: pedestrians and bicyclists. Both cantilevers are required to provide the necessary space for one one single direction bicycle lane as well as one single direction pedestrian path. The exact specifications for these lanes and paths are given in [ch. 5.1.3] [ch. 5.1.4]. The chosen lateral length of the cantilever is 5,436m. This length is equally divided in three parts of 1,867m, which together with the added diagonals form a truss in lateral direction, which directly connects to the inner bridge deck supporting lateral trusses. As with these trusses, a total of 17 cantilever trusses is placed; this number is again equal to the number of longitudinal divisions plus one [ch. 7.6.4, table 34]. The c.t.c. distance of these trusses is equal to the longitudinal cell size of 3,0625m [ch. 7.6.4, table 34]

The overview picture below shows the integration of the cantilever- and inner- bridge deck supporting trusses. Also, both trusses are very well integrated with the main elliptical load bearing structure. The part of the bridge deck supporting truss that coincides with the main load bearing truss is again marked in blue.

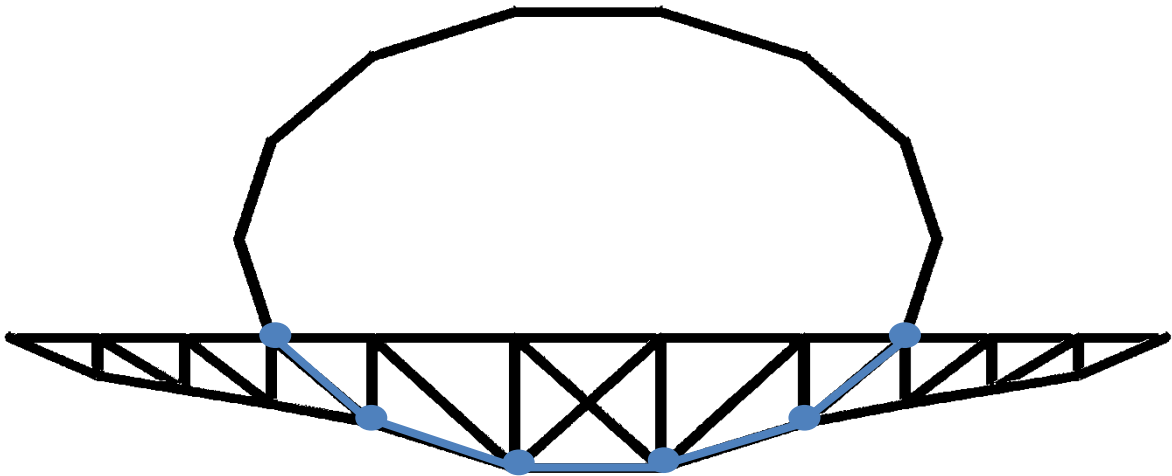


Fig. 113: Cross section of the finished structure of the bridge, complete with elliptical main load bearing truss, inner bridge deck supporting truss and cantilever bridge deck supporting truss.

To connect the lateral trusses of the cantilever in longitudinal direction simple straight members were used. These members have a length of 3,0625m and thereby span the distance between the lateral trusses. In total 6 longitudinal members are used to connect all nodes of the cantilever in longitudinal direction. The picture below gives a top view of the complete structure. The cantilever trusses are shaded blue.

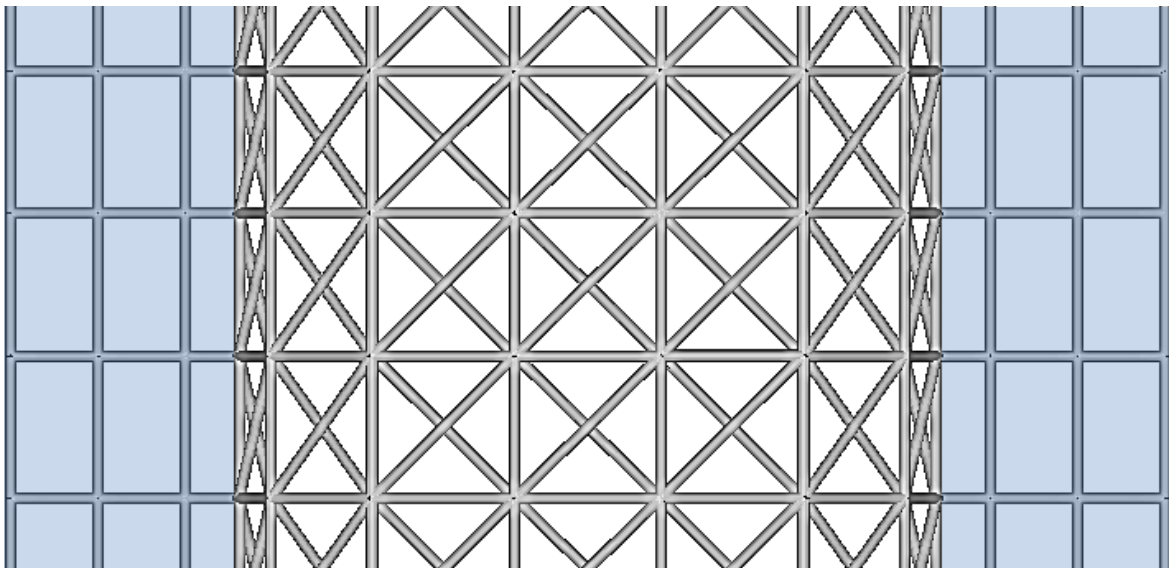


Fig. 114: Top view of the bridge structure, the cantilever part is shaded blue. The straight longitudinal members of the cantilever part that connects the lateral trusses lie vertically.

Finally the picture of the lateral cantilever truss is recalled below, this time fitted with blue dots that mark the position of the 6 straight longitudinal members that connect the lateral cantilever trusses.

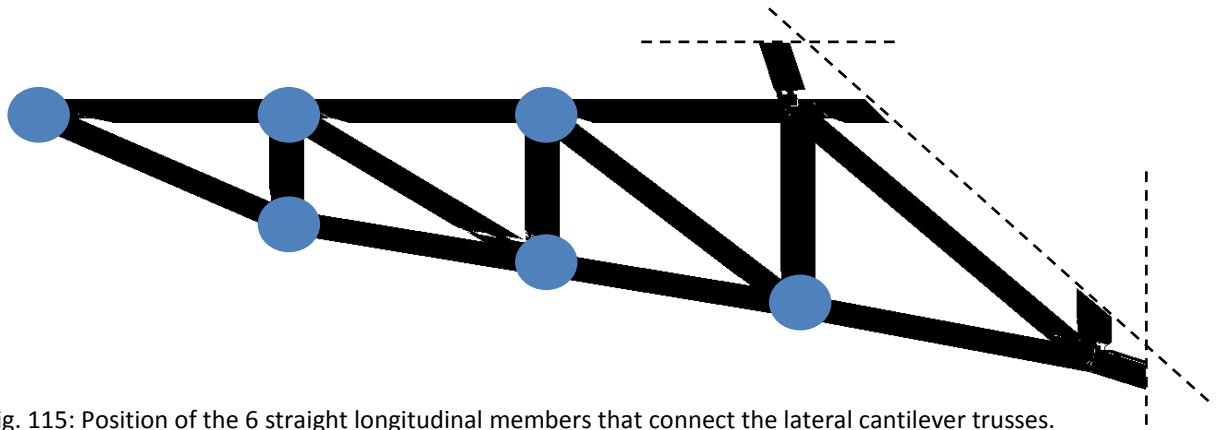


Fig. 115: Position of the 6 straight longitudinal members that connect the lateral cantilever trusses.

8.3 DRAWINGS OF THE FINAL DESIGN

In this chapter a number of technical drawings are presented that accurately describe the structural design of the full-FRP elliptical truss heavy traffic bridge.

- Cross section
- Top view
- Side view
- Bridge deck configuration

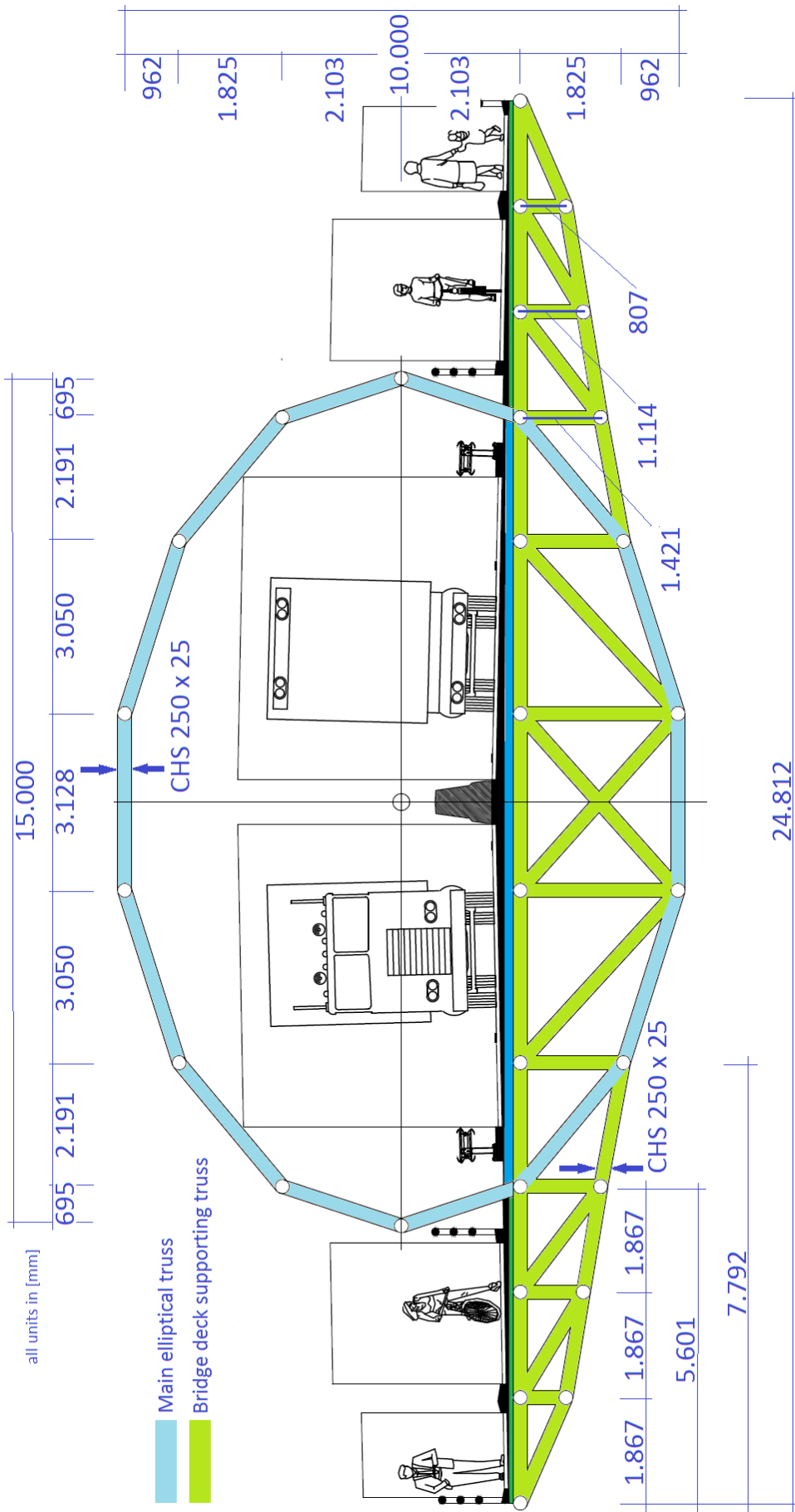


Fig. 116: Cross section of the full-FRP bridge final design

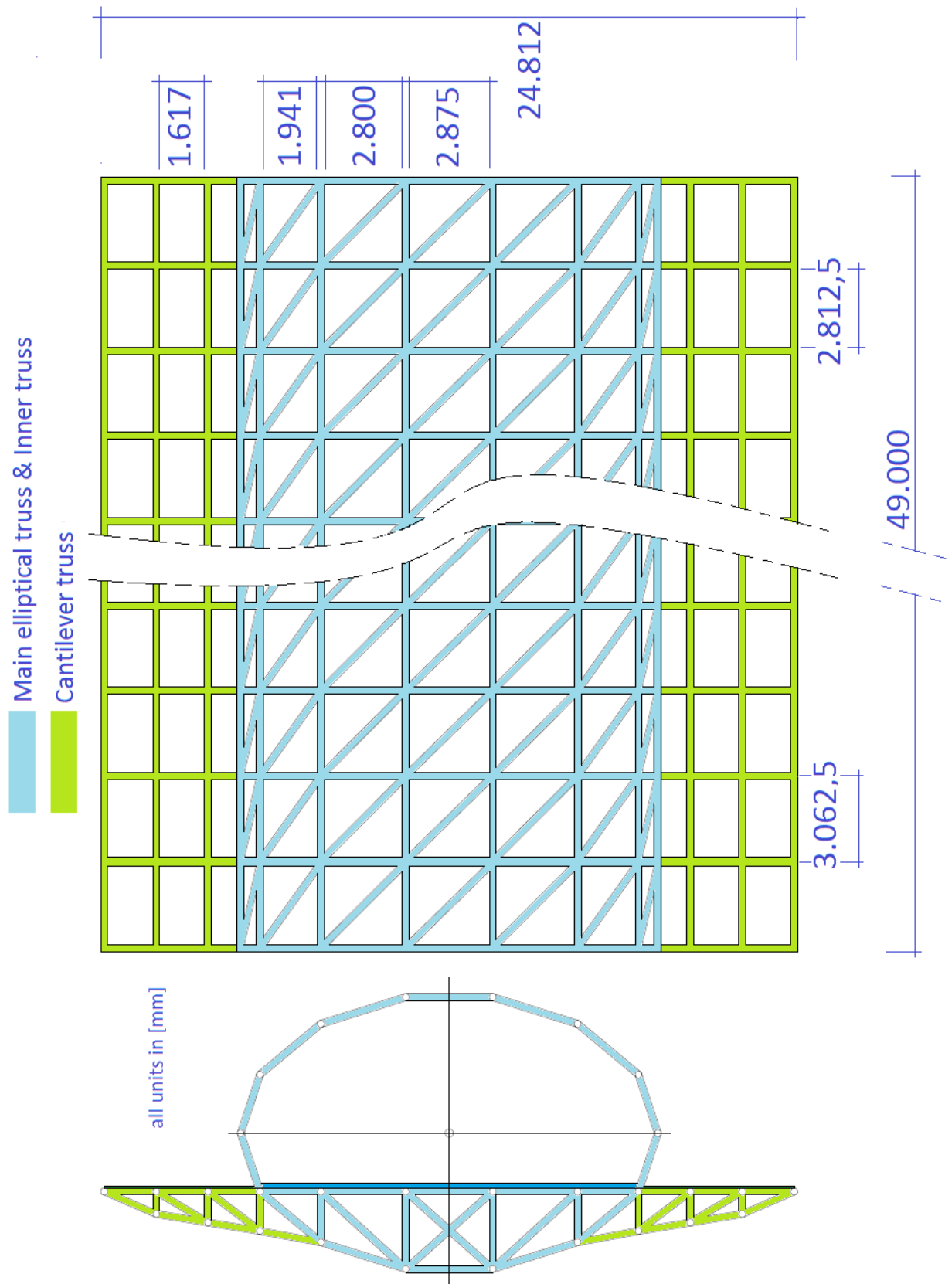


Fig. 117: Top view of the full-FRP bridge final design.

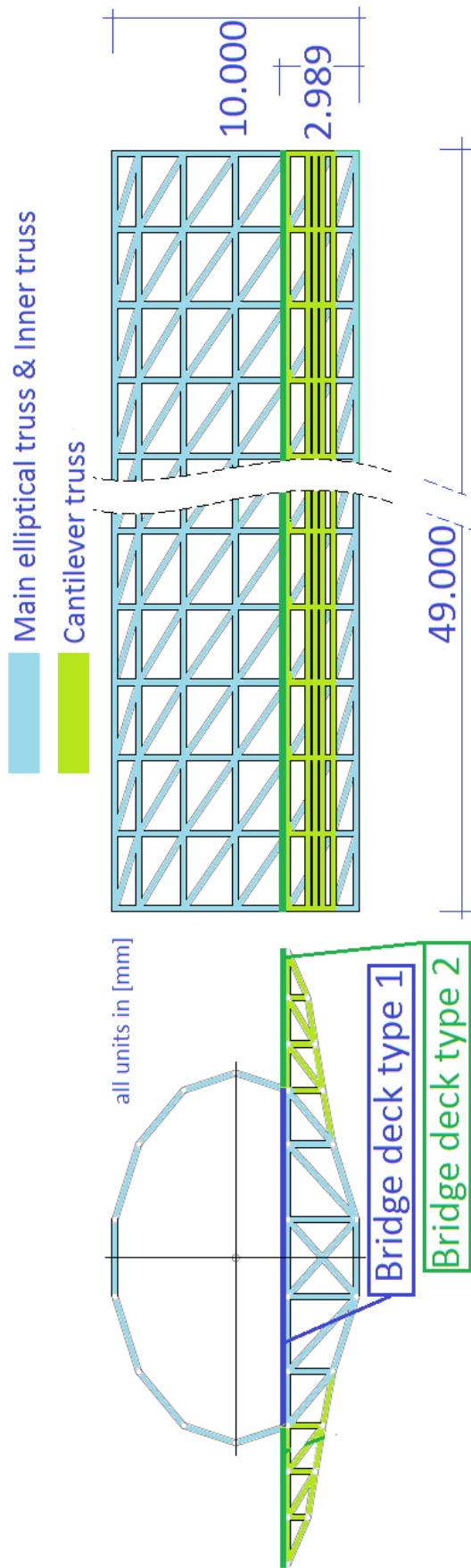
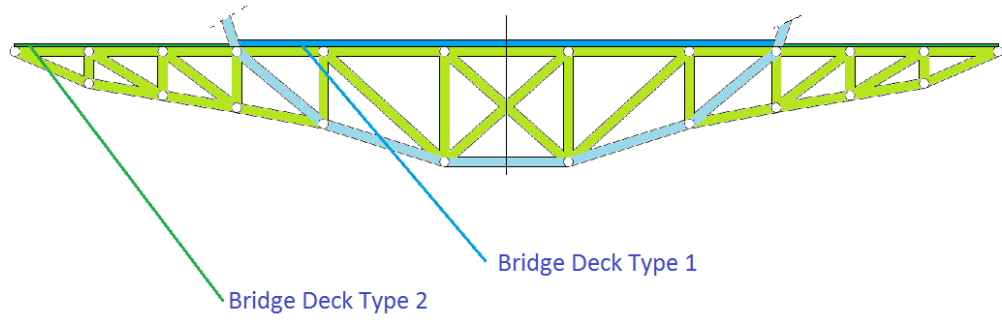


Fig. 118: Side view of the full-FRP bridge final design



24.812										
5.436			13.610					5.436		
1867	1867	1867	2.191	3.050	3.128	3.050	2.191	1867	1867	1867

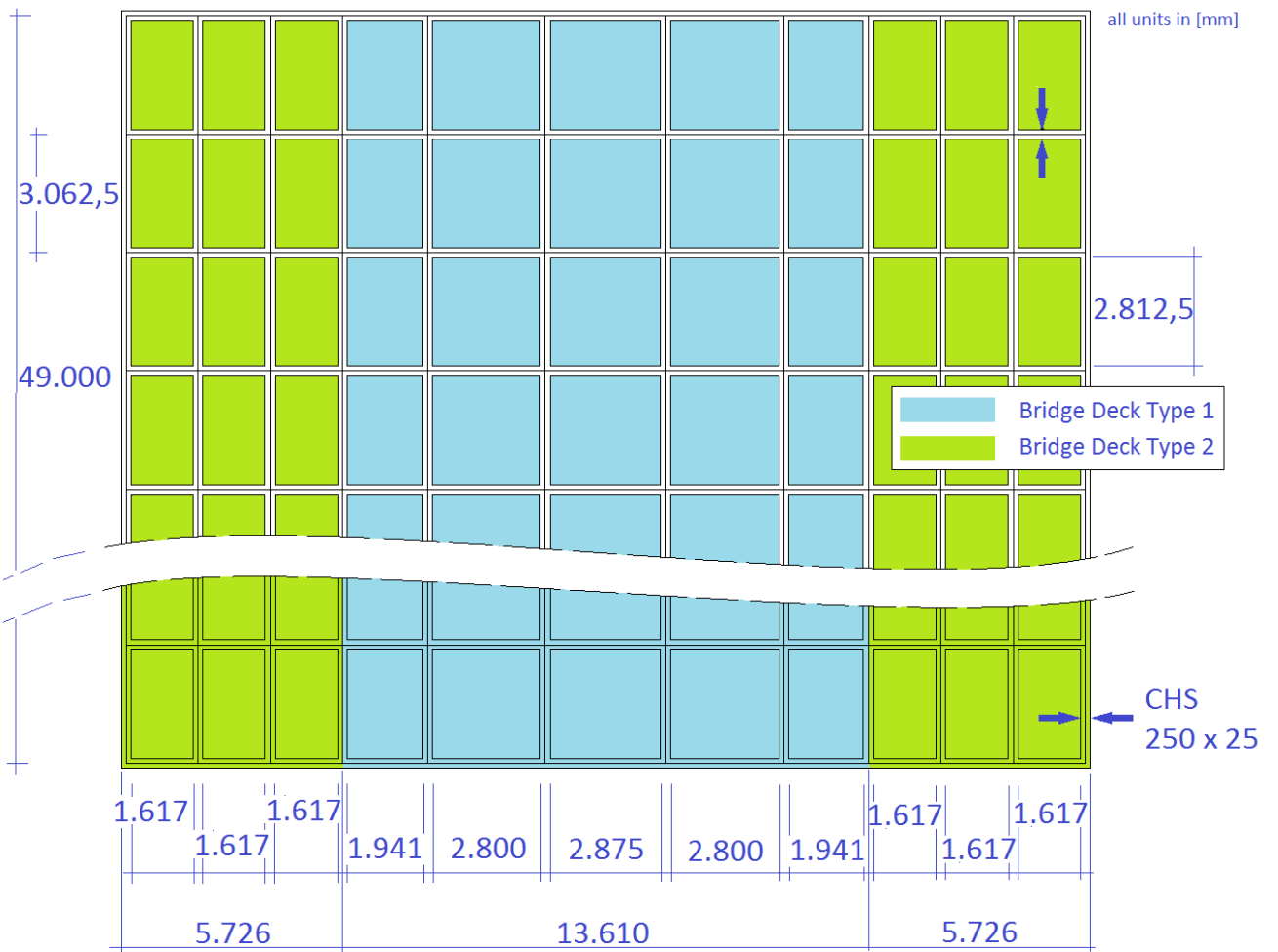


Fig. 119: Configuration of the bridge deck of the full-FRP bridge final design

8.4 LOADS & LOAD CASES

In this chapter the design loads that were described in [ch. 6] are added to the FE-model of the structure, described in [ch. 8.1] [ch. 8.2] [ch. 8.3]. Also the traffic load combination cases [ch. 6.5] and general load combination cases [ch. 6.6] were added to the model. In the table below these two types of load combinations are again given and combined in a single table; see [ch. 6.6] for more information on these cases.

Combination case	Description (combined traffic loads)	Description (separate traffic loads)
LCC1	1 * Self-weight + 1 * Gr1a + 0,6 * Wind	1 * Self-weight + 1 * LM1 + 0,4 * (Bicycle & Pedestrian Loads) + 0,6 * Wind
LCC2	1 * Self-weight + 1 * Gr1b	1 * Self-weight + 1 * LM2
LCC3	1 * Self-weight + 1 * Gr2	1 * Self-weight + 0,8 * LM1 + 1 * (Accidental & Collision Loads)
LCC4	1 * Self-weight + 1 * Gr4	1 * Self-weight + 11 * LM4
LCC5	1 * Self-weight + 1 * Wind + 0,8 * Snow	1 * Self-weight + 1 * Wind + 0,8 * Snow
LCC6	1 * Self-weight + 1 * Gr1a + 0,6 * Thermal	1 * Self-weight + 1 * LM1 + 0,4 * (Bicycle & Pedestrian Loads) + 0,6 * Thermal
LCC7	1 * Self-weight + 1 * Gr2 + 0,6 * Thermal	1 * Self-weight + 0,8 * LM1 + 1 * (Accidental & Collision Loads) + 0,6 * Thermal
LCC8	1 * Self-weight + 1 * Gr4 + 0,6 * Thermal	1 * Gr4 + 1 * LM4 + 0,6 * Thermal
LCC9	1 * Self-weight + 1 * Vehicle Impact	1 * Self-weight + 1 * Vehicle Impact

Table 35: Combination of single traffic load components with other loads according to [NEN-EN1991-2003/NB:2009, table 4.4a, p10]

The loads that are shown in the table above were inserted into 'Oasys GSA' by using a grid-plane on which point loads, line loads and area loads could be easily placed. This grid plane is a x-y-plane that is located at the same height (z-coordinate) as the bridge deck. The first picture below shows this grid plane and its dimensions, the large grid points (crosses) are spaced at 2,50m x 2,50m and the smaller grid points (dots) are spaced at 0,5m x 0,5m.

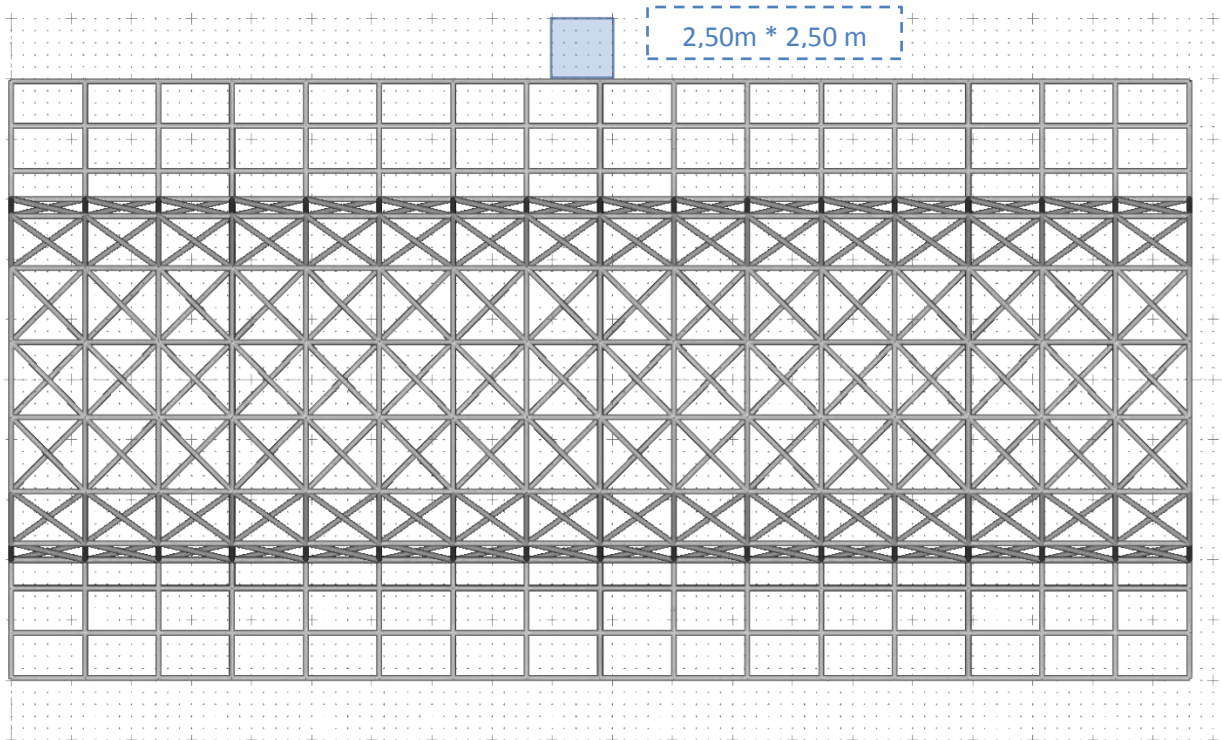


Fig. 120: Grid-plane for the insertion of grid-point- and grid-area-loads into the FE-model.

To give an example of the load definition in 'GSA', in the picture below a scheme is given, which shows the loading due to 'Load Model 1'. Note the four area loads (orange lines) and the two sets of 4 wheel loads in the center (pink arrows). The square blue lines are the bridge deck supporting grid members. Similar loading schemes were modeled in 'GSA' for all loads.

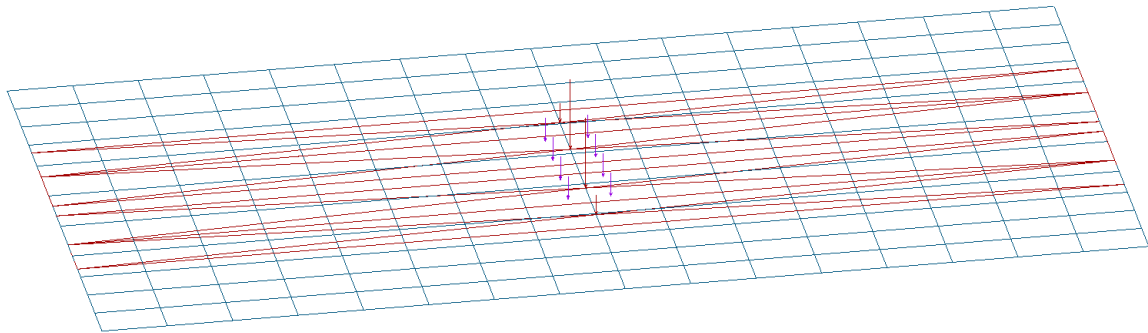


Fig. 121: LM1 loading scheme inserted in the FE-model in 'GSA'

It was chosen not to use the contact surfaces that were given in [ch. 6.2, ch. 6.3] in the FE-model. Instead, normal point loads were used. The contact surface is of major importance for the bridge deck detailed design only, and since the main objective of this research is the design of the main load bearing structure of the bridge this is considered to be a safe assumption.

8.5 SUPPORT CONDITIONS

As stated before in [ch. 5.3] the bridge will have a single span of 49m. However, the final design support conditions differ somewhat from the support conditions that were initially used for truss topology determination, the grid size determination and the cross section size determination as described in [ch. 7.1.2.2]. For the final design it is chosen to use a more practical and constructible supporting scheme and therefore reduce the number of supported nodes to 4 nodes per bridge end.

At one end of the bridge structure (for $x=0$), the 4 supported nodes are pinned in x-, y-, z-direction. At the other end of the bridge structure the 4 support nodes are only pinned in the y-, z-direction, thereby allowing the structure to freely expand or contract in x-direction under for example temperature loads. The picture below shows the support conditions.

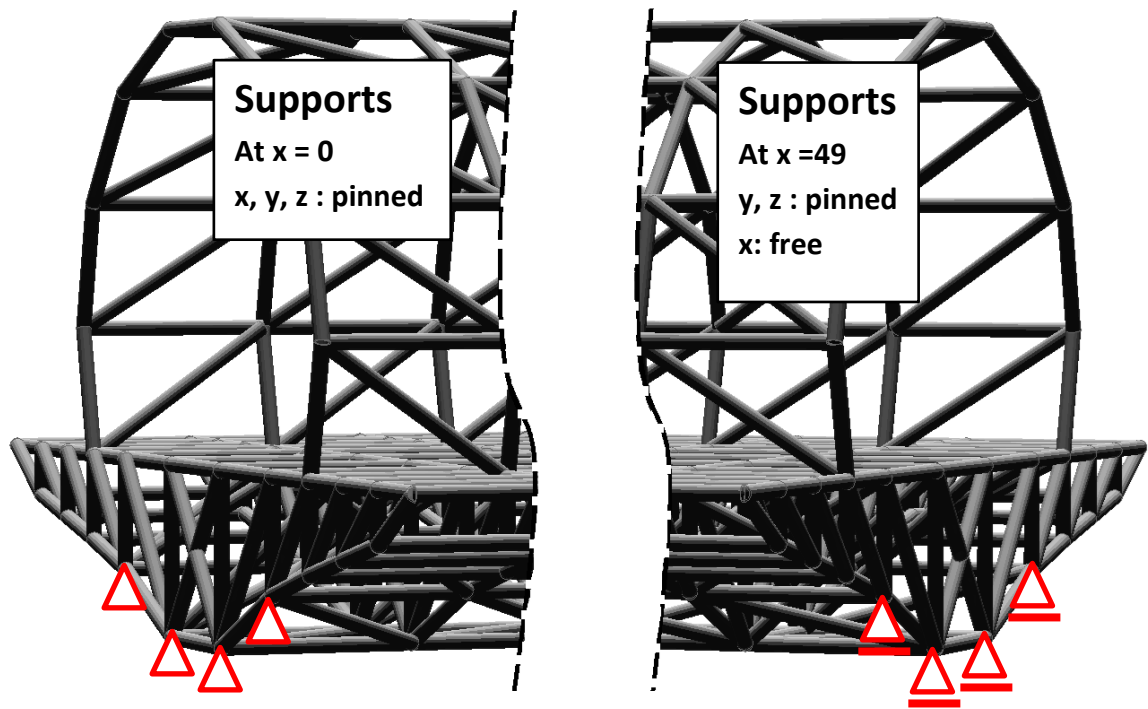


Fig. 122: Support conditions of the full-FRP bridge design

8.6 MATERIAL & CROSS SECTION

Following the material design properties section [ch. 3.4] as well as cross section optimization chapter [ch. 7.5] the bridge will completely fabricated using unidirectional reinforced 70/30 carbon epoxy composite that was already described in [ch. 7.1.2.1]. The circular hollow section truss elements will have a constant diameter of 250mm and wall thickness of 25mm (Carbon Epoxy FRP CHS250x25). It is chosen to use a single cross section only. The carbon fiber will be of the type 'Toray M35J'. The epoxy resin will also be supplied by 'Toray'.

For this research the FRP composite material is assumed to behave quasi-isotropic. This is a simplification, which is only acceptable since exclusively truss members are used in the design and these are primarily axially loaded, as already described in [ch. 3.5.1]. In the table below the design mechanical properties of the unidirectional composite are given once more.

		70% Carbon M35J
		30% Epoxy 0
ρ	kg/m ³	1.629
$E_{L-d} = E_{T-d}$	N/mm ²	148.239
$\nu_{LT} = \nu_{TL}$	-	0,245
$G_L = G_T$	N/mm ²	8.669

Table 36: Final quasi-isotropic material properties of the 70/30 carbon epoxy composite used, based on the design values derived in [ch. 3.4]

9. FINITE ELEMENT ANALYSIS ON THE FINAL DESIGN OF THE BRIDGE

In this chapter the results of the FE-analysis of the final design will be discussed. Due to the large number of separate design loads, only a limited number of selected design loads will be covered separately. Afterwards, the load combination cases will be analyzed and the normative combination case will be found. Next to that, the fatigue loads will be separately analyzed to obtain the fatigue life of the bridge. Finally a short modal analysis will be made in which the natural frequencies of the bridge structure will be determined.

9.1 DEFORMATION RESULTS FOR SEVERAL DESIGN LOADS

9.1.1 HEAVY TRAFFIC LOAD LM1

Below three pictures are shown of the deformations of the bridge structure in the z-direction. The first picture gives a side view of the structure, followed by a top view and a 3D view. The maximum z-deformation occurring due to LM1 is 49,93mm.

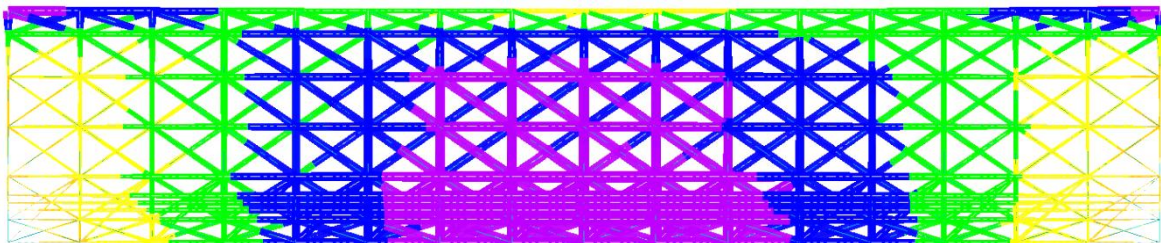


Fig. 123: Side view of the deformation of the bridge structure due to LM1 only.

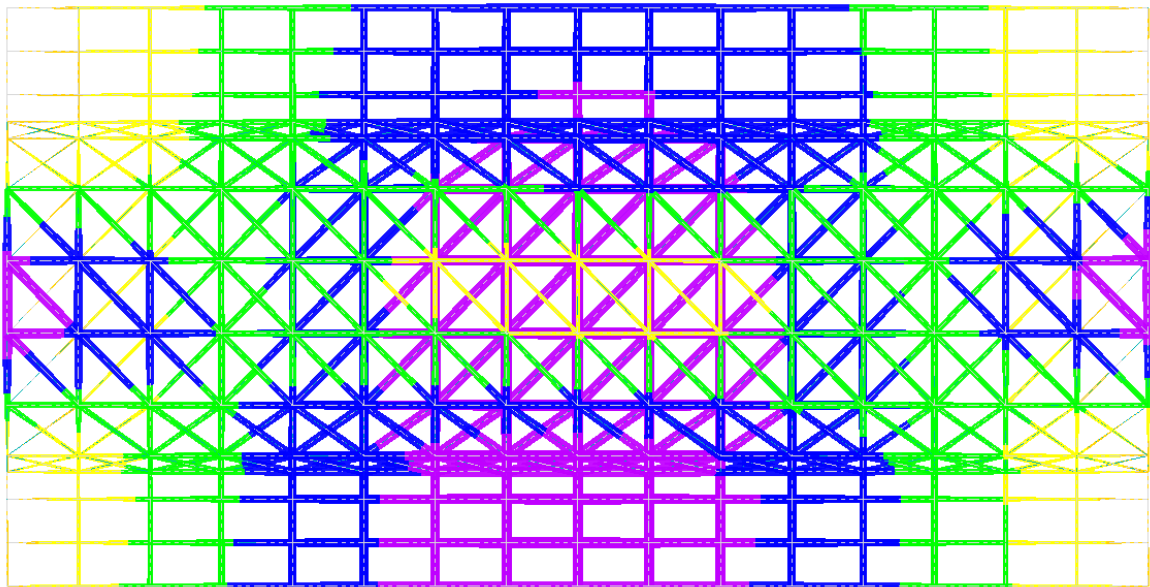


Fig. 124: Top view of the deformation of the bridge structure due to LM1 only.

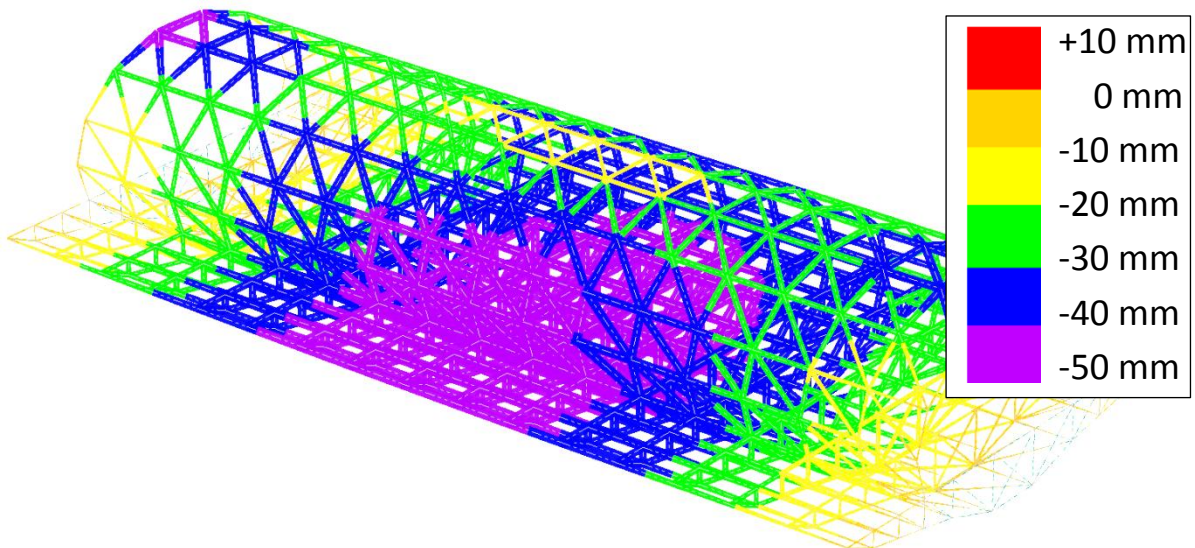


Fig. 125:3D view of the deformation of the bridge structure due to LM1 only.

9.1.2 BICYCLE & PEDESTRIAN LOAD

Below three pictures are shown of the deformations of the bridge structure in the z-direction. The first picture gives a side view of the structure, followed by a top view and a 3D view. The maximum z-deformation occurring due to bicycle and pedestrian loading is 18,67mm.

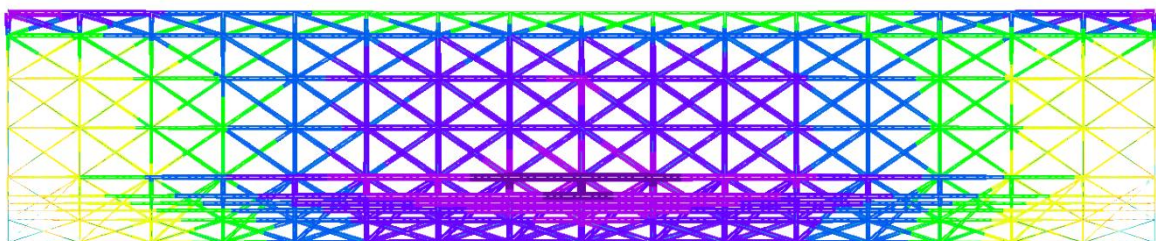


Fig. 126: Side view of the deformation of the bridge structure due to bicycle and pedestrian loads only.

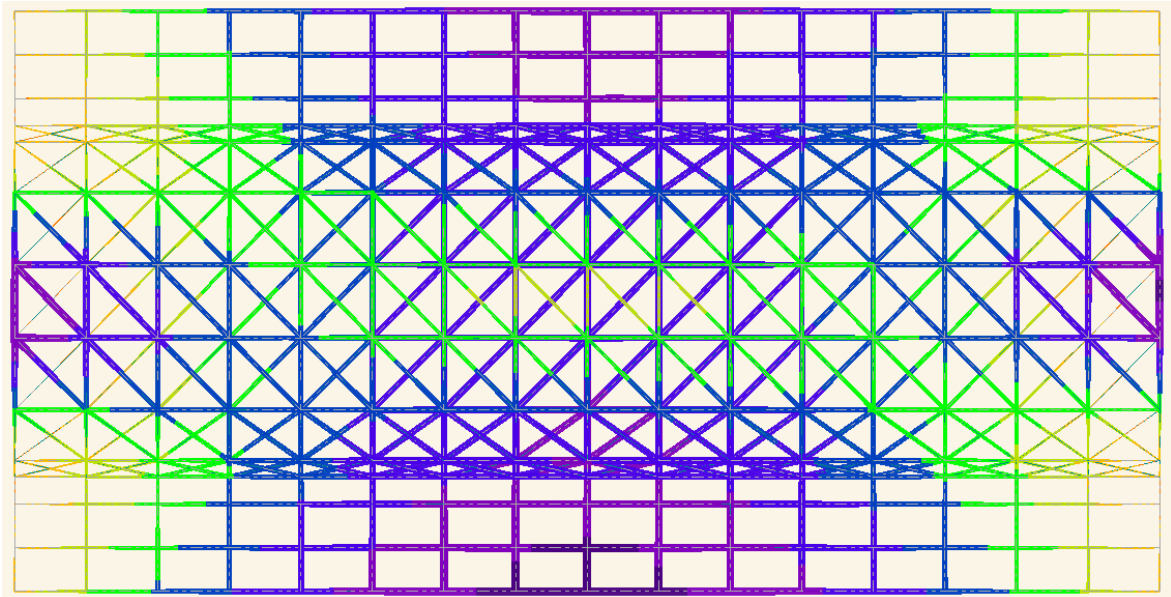


Fig. 127: Top view of the deformation of the bridge structure due to bicycle and pedestrian loads only.

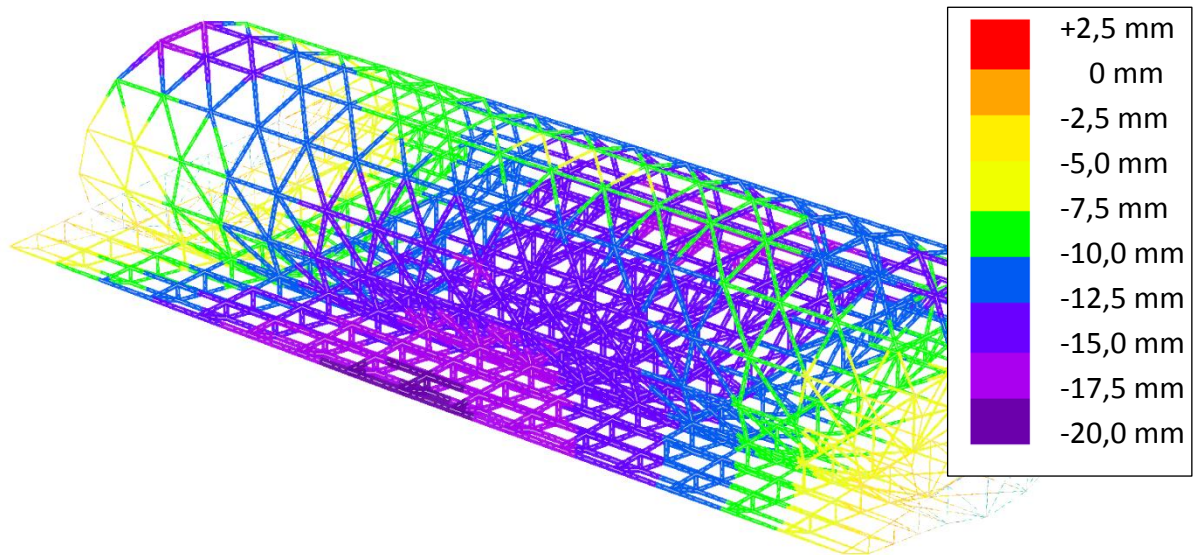


Fig. 128: 3D view of the deformation of the bridge structure due to bicycle and pedestrian loads only.

9.1.3 CROWD LOADING LM4

Below three pictures are shown of the deformations of the bridge structure in the z-direction. The first picture gives a side view of the structure, followed by a top view and a 3D view. The maximum z-deformation occurring due to crowd loading (LM4) is 33,89mm.

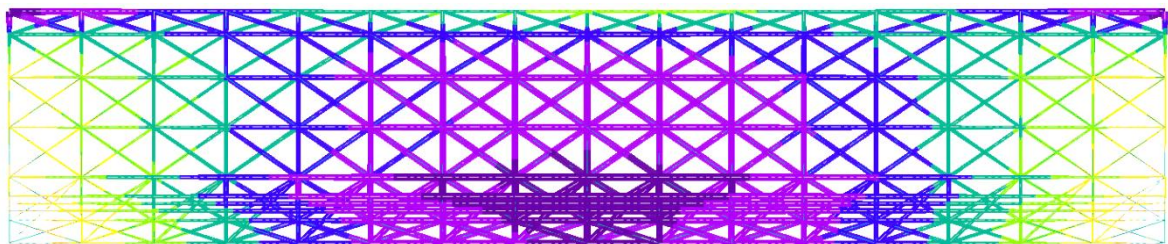


Fig. 129: Side view of the deformation of the bridge structure due to crowd loading (LM4) only.

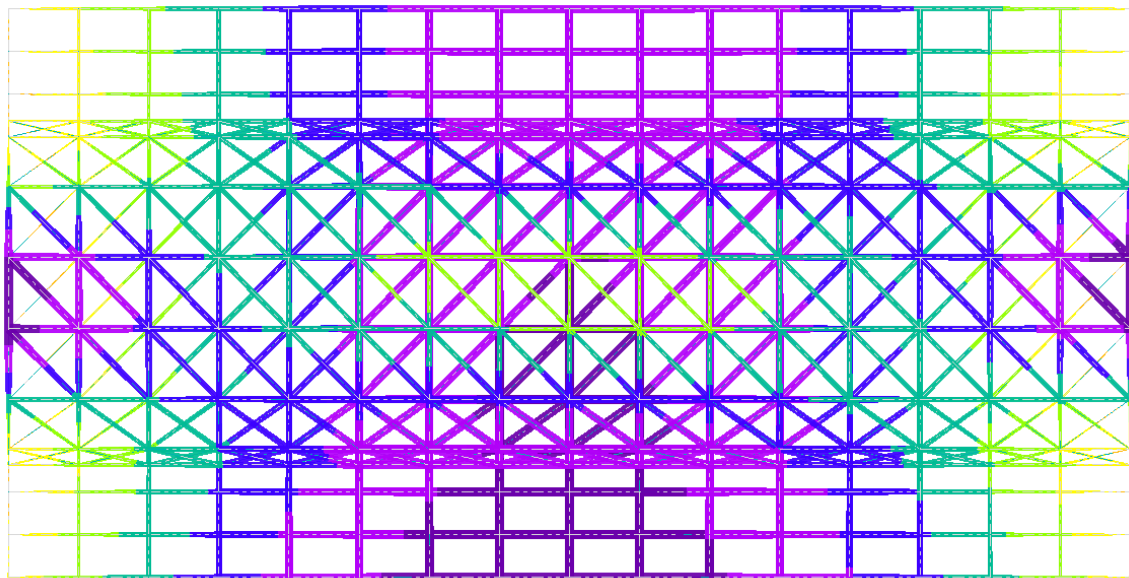


Fig. 130: Top view of the deformation of the bridge structure due to crowd loading (LM4) only

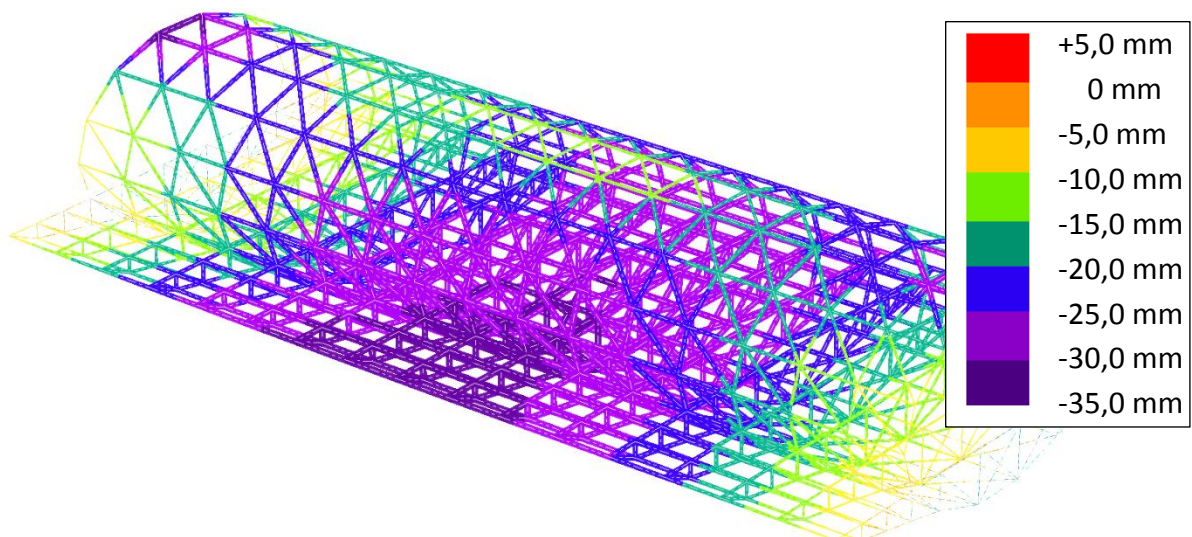


Fig. 131: 3D view of the deformation of the bridge structure due to crowd loading (LM4) only

9.1.4 WIND LOAD IN LATERAL DIRECTION

Below three pictures are shown of the deformations of the bridge structure in the z-direction. The first picture gives a side view of the structure, followed by a top view and a 3D view. The maximum z-deformation occurring due wind from one side is -31,41mm to +33,02mm.

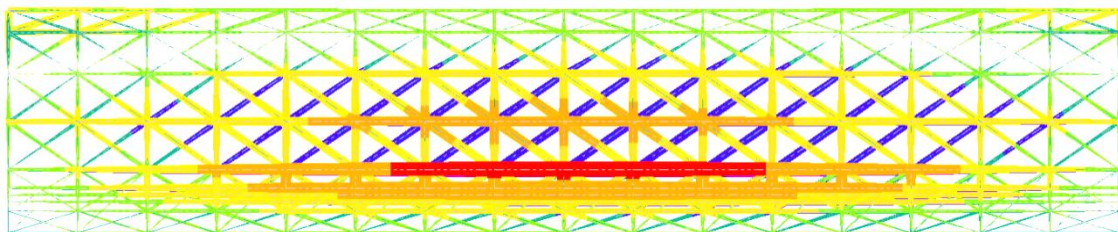


Fig. 132: Side view of the deformation of the bridge structure due to wind from one side only.

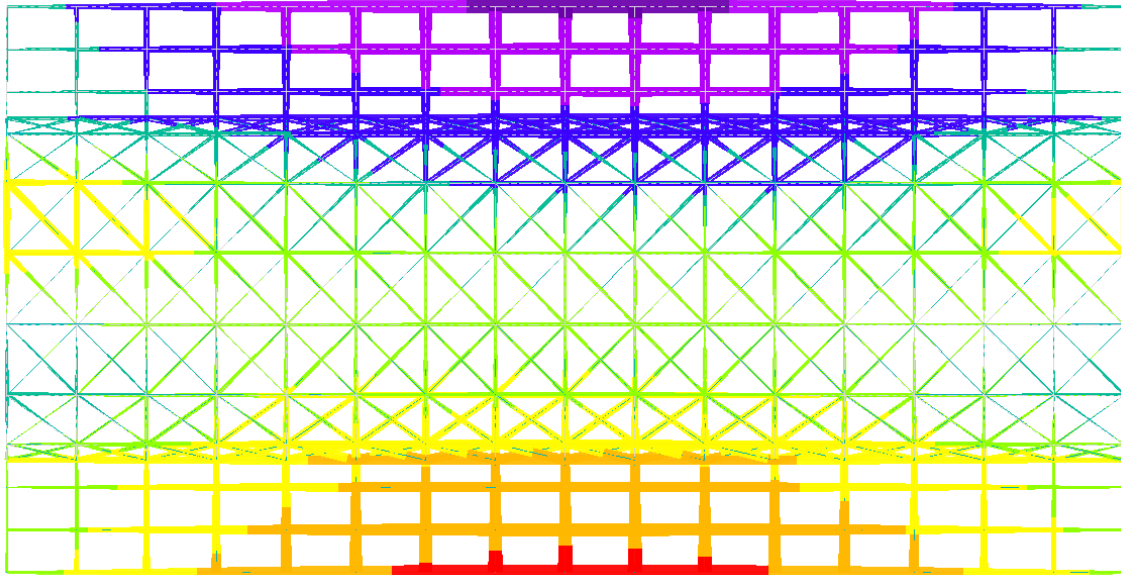


Fig. 133: Top view of the deformation of the bridge structure due to wind from one side only.

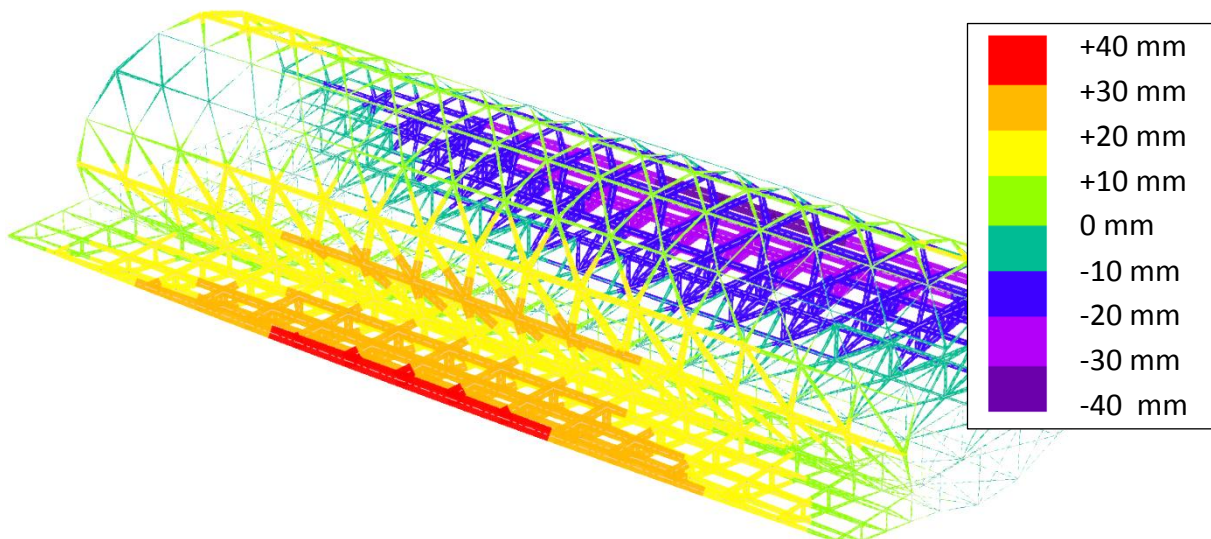


Fig. 134: 3D view of the deformation of the bridge structure due to wind from one side only.

The wind load also induces a substantial deformation in y-direction, particularly on the the top of the elliptical truss. To visualize this maximum deformation in y-direction of 62,32mm below another 3D view is given for the y-deformation.

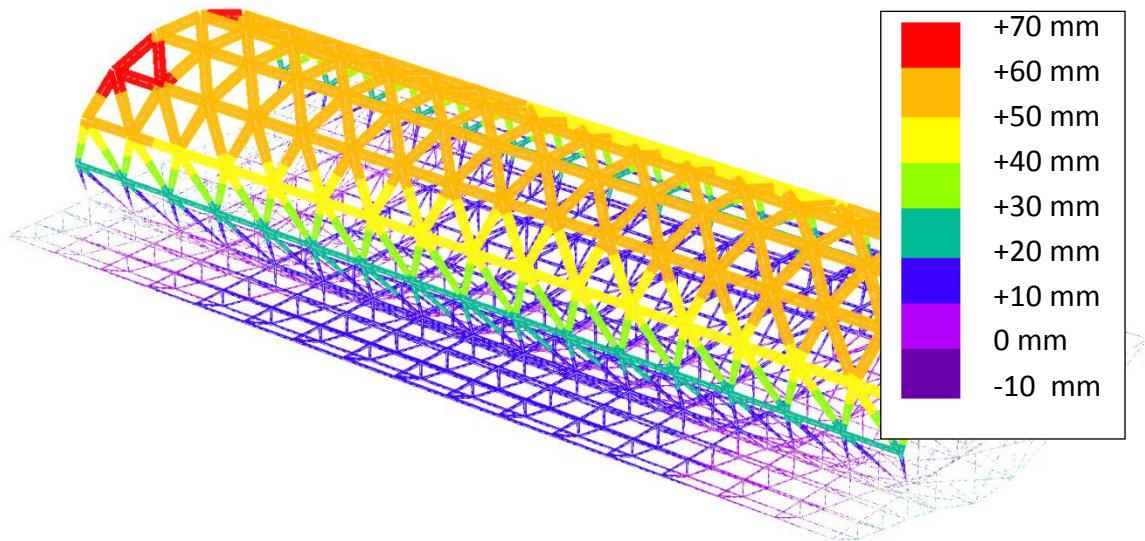


Fig. 135: 3D view of the deformation in y-direction of the bridge structure due to wind from one side only.

9.1.5 THERMAL LOAD

Below one picture is shown of the deformations of the bridge structure in the x-direction. The maximum x-deformation occurring due to thermal loading is 9,321mm. The picture shows that the deformation gradually grows larger for increasing x-coordinates. Since the structure is not restrained in x-direction at the x=49m end of the bridge, see also [ch. 8.5], this could be expected.

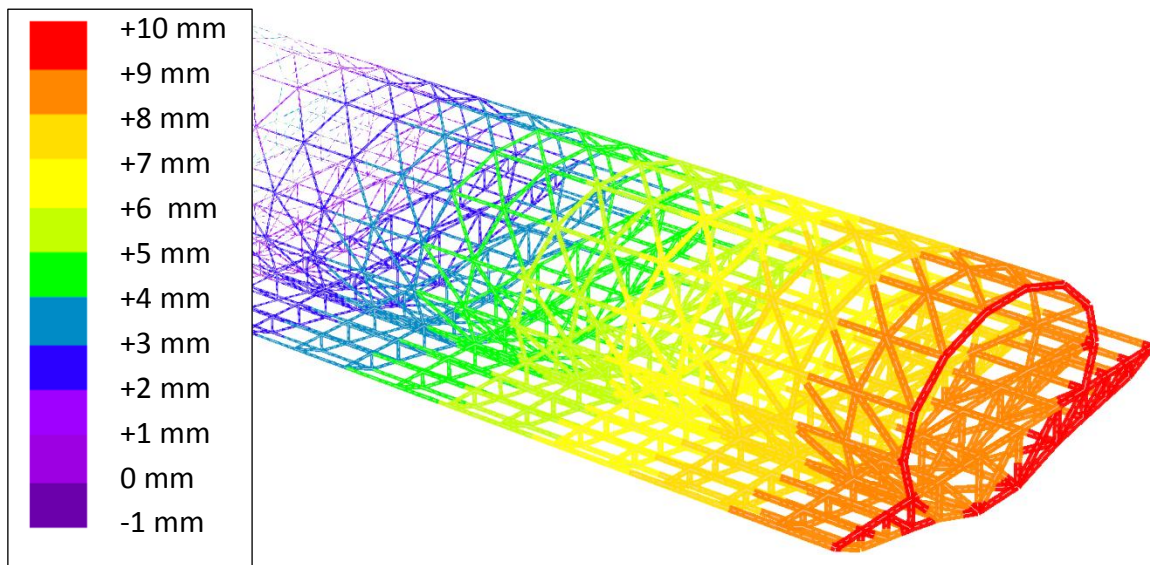


Fig. 136: 3D view of the deformation in x-direction of the bridge structure due to thermal loading only.

9.1.6 VEHICULAR IMPACT LOAD ON THE SUPERSTRUCTURE

Below one picture is shown of the deformations of the bridge structure in the combined direction. The main direction of the deformations is the y-direction due to the impact force of 2000kN that acts on the lowest node at mid-span, as described in [ch. 6.4.4]. The maximum deformation occurring due to vehicular impact is 18,25mm. This value is acceptable and is expected to certainly not cause failure of the main load bearing structure.

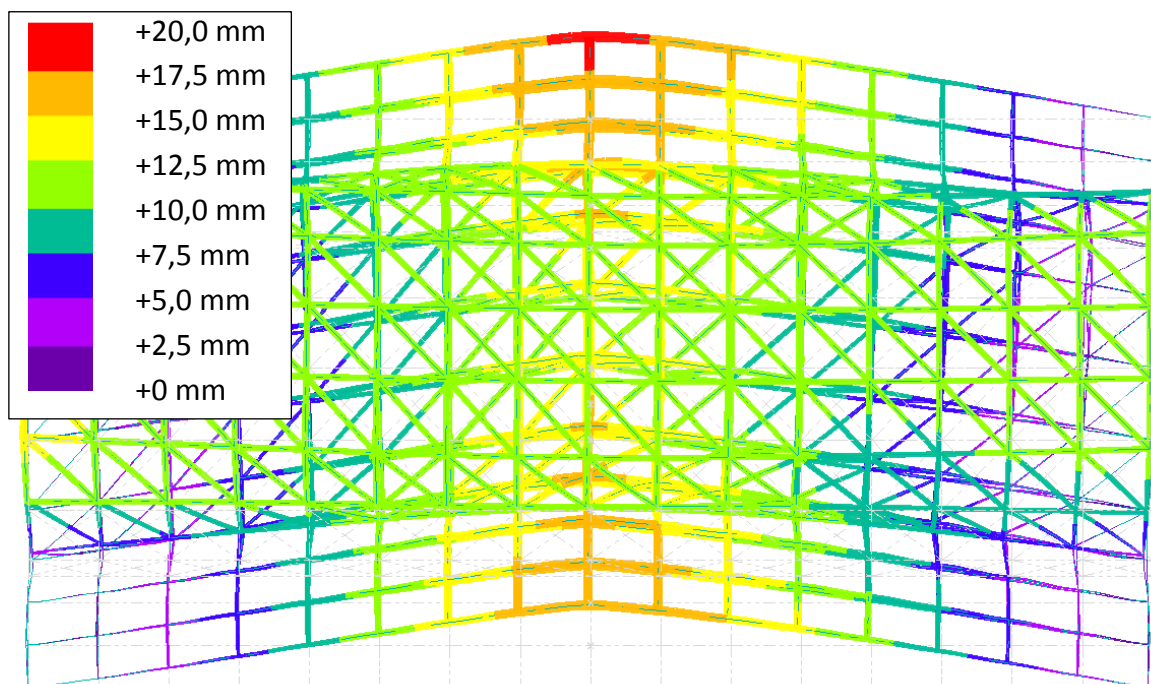


Fig. 137: 3D view of the deformation in x-direction of the bridge structure due to thermal loading only.

9.2 FINITE ELEMENT ANALYSIS RESULTS FOR THE NORMATIVE LOAD COMBINATION CASE

After having shown the effect of several single loads, in this chapter the loads are combined according to the scheme given in [ch. 6.6] and recalled in [ch. 8.4]. That way the normative load combination case is found and the maximum deformations and stresses of the bridge during its lifespan are derived.

In the table below results on all combination cases LCC1- LCC9 are given. The bridge structure is analyzed through FE-analysis. Hereby the maximum deformation in x-direction, y-direction, z-direction and in combined direction are shown in the 3rd to 6th column. The two last columns give the maximum axial stresses in tension and compression.

Per column the three largest values are marked as follows, the worst value is marked red, the second worst value is marked orange and the third worst value is marked yellow. The load combination case which has the most red, orange or yellow fields is the case that yields the highest deformations and/or stresses and is thus the normative case. Note that all deformation values just lie under the $L/600$ deflection limit of 81,667mm. Furthermore the maximum stresses are very low and far below the maximum design compressive and tensile strength values of the carbon/epoxy FRP material derived in [ch. 3.4].

It is clearly visible that for the maximum deformation in z-direction, the maximum combined deformation as well as for the maximum axial compressive and tensile stress load combination case LCC1 yields the most unfavorable values. For the maximum deformation in y-direction LCC1 yields the second worst value. It can therefore be safely concluded that load combination cases LCC1, which is a combination of self-weight, LM1 traffic load and wind load, is overall the normative load combination case for this bridge design.

However, for the maximum deformation in x- and y-direction, other load cases yield the most unfavorable values. For the maximum deformation in x-direction LCC6, the thermal load combined with LM1 traffic load and self-weight yields the highest value. For the maximum deformation in y-direction LCC5, the full wind load combined with self-weight and snow load yields the most unfavorable value.

Combination case	Description	Max. X-deformation [mm]	Max. Y-deformation [mm]	Max. Z-deformation [mm]	Max. Combined Deformation [mm]	Max. axial compr. Stress [N/mm ²]	Max. axial tensile stress [N/mm ²]
LCC1	1 * Selfweight + 1 * Gr1a + 0,6 * Wind	18,380	56,300	74,300	78,340	107,400	111,500
LCC2	1 * Selfweight + 1 * Gr1b	8,878	18,630	36,570	36,910	46,590	48,280
LCC3	1 * Selfweight + 1 * Gr2	17,850	37,390	67,190	68,130	85,340	85,760
LCC4	1 * Selfweight + 1 * Gr4	14,920	30,240	58,990	59,600	82,540	73,790
LCC5	1 * Selfweight + 1 * Wind + 0,8 * Snow	8,947	66,710	60,780	71,020	68,200	76,520
LCC6	1 * Selfweight + 1 * Gr1a + 0,6 * Thermal	24,440	37,970	72,590	74,000	96,270	92,760
LCC7	1 * Selfweight + 1 * Gr2 + 0,6 * Thermal	23,270	38,610	67,470	68,980	83,580	85,760
LCC8	1 * Selfweight + 1 * Gr4 + 0,6 * Thermal	20,350	37,970	58,660	59,980	80,790	69,350
LCC9	1 * Selfweight + 1 * Vehicle impact	6,487	19,77	29,17	32,25	34,36	58,39

Table 37: Comparison of all load combination cases for the derivation of the normative load cases.

9.2.1 FINITE ELEMENT ANALYSIS RESULTS FOR THE OVERALL NORMATIVE LOAD COMBINATION CASE LCC1

To conclude this chapter on the normative load combination case a number of schemes is given, that all provide a good overview on the deformations and stresses that this load case, load combination case LCC1, induces in the bridge structure and its elements.

First three pictures are shown of the deformations of the bridge structure in the z-direction. The first picture gives a side view of the structure, followed by a top view and a 3D view. The maximum z-deformation occurring due to the normative load combination case LCC1 is 74,30mm.

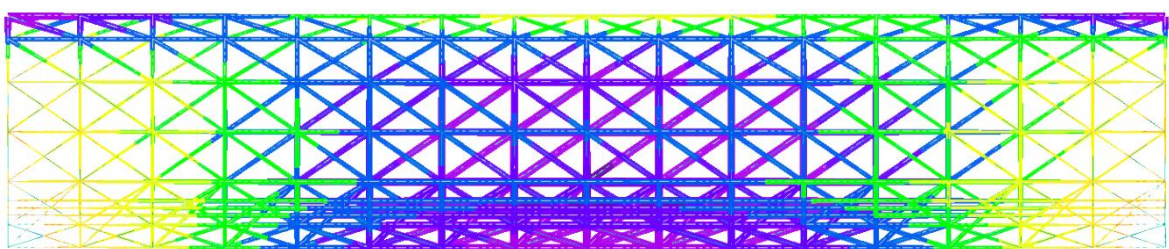


Fig. 138: Side view of the deformation in z-direction of the bridge structure due to the normative load combination case LCC1.

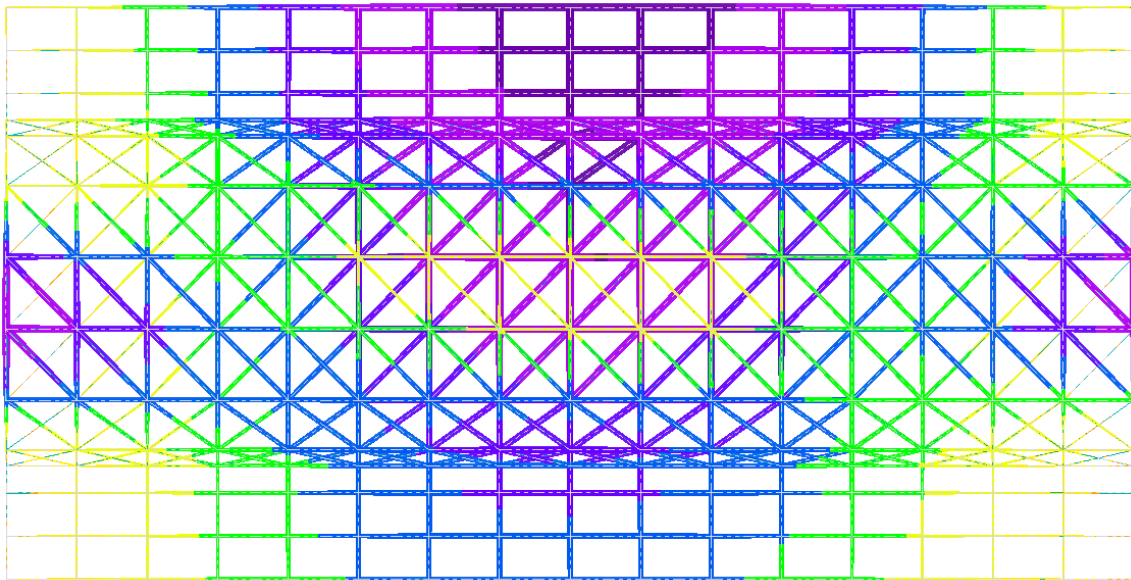


Fig. 139: Top view of the deformation in z-direction of the bridge structure due to the normative load combination case LCC1.

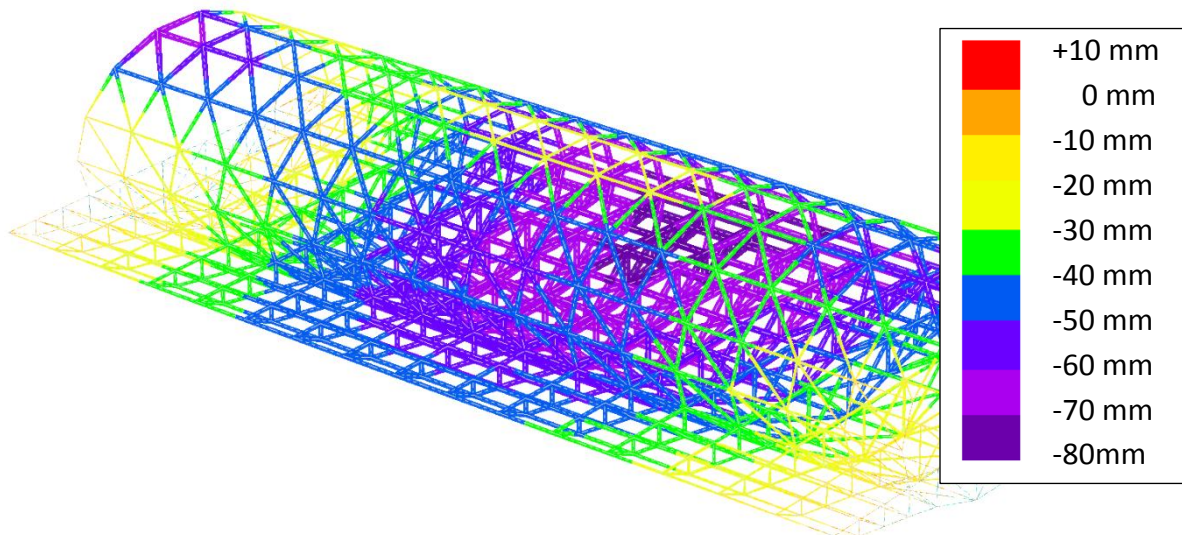


Fig. 140: 3D view of the deformation in z-direction of the bridge structure due to the normative load combination case LCC1.

In the following two schemes are given which accurately describe the results on the stress distribution in the structural members of the bridge. The first scheme shows the occurring axial stresses with a maximum compressive stress of $107,40\text{N/mm}^2$ and maximum tensile stress of $111,5\text{ N/mm}^2$. However, in most elements of the structure the axial stresses do not exceed the range of $-50,0\text{N/mm}^2$ to $+50,0\text{N/mm}^2$ structure (green and yellow elements in the picture below).

The second scheme gives the Von Mises stress, which for most parts of the structure lie under about $100,0\text{N/mm}^2$ (purple elements in the scheme). However, at the connection points of the elliptical truss with the bridge deck supporting trusses, locally the Von Mises stress can reach values up to $368,8\text{N/mm}^2$. This seems like a high value, but considering the high design tensile- and compressive strength of $1173,50\text{ N/mm}^2$ and $995,90\text{ N/mm}^2$ respectively of the carbon/epoxy FRP material, as described in [ch. 3.4] the value becomes very reasonable.

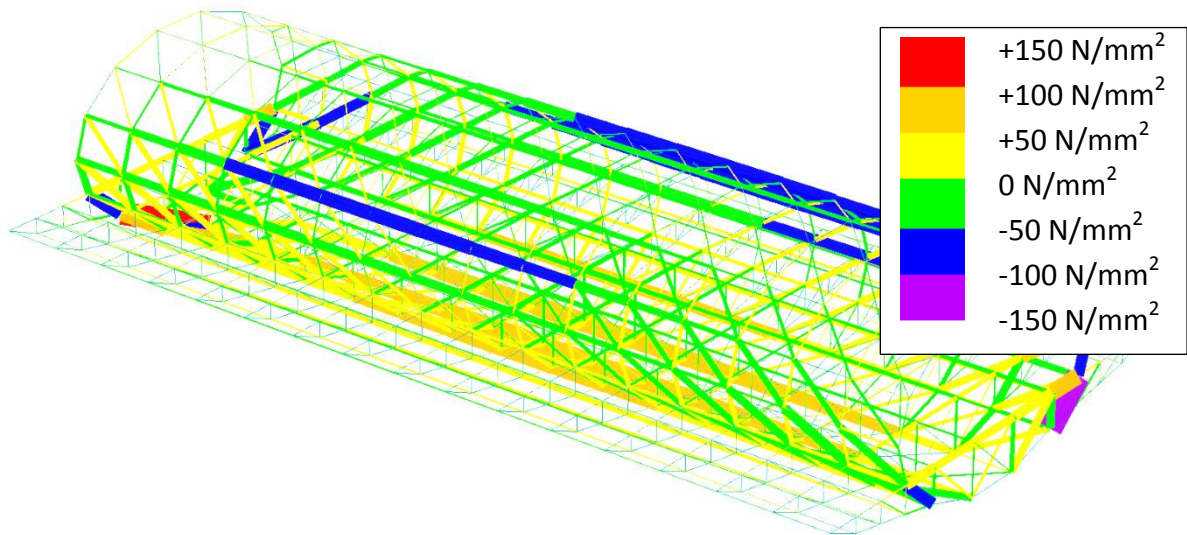


Fig. 141: 3D view of the axial stress distribution in the bridge structure due to the normative load combination case LCC1.

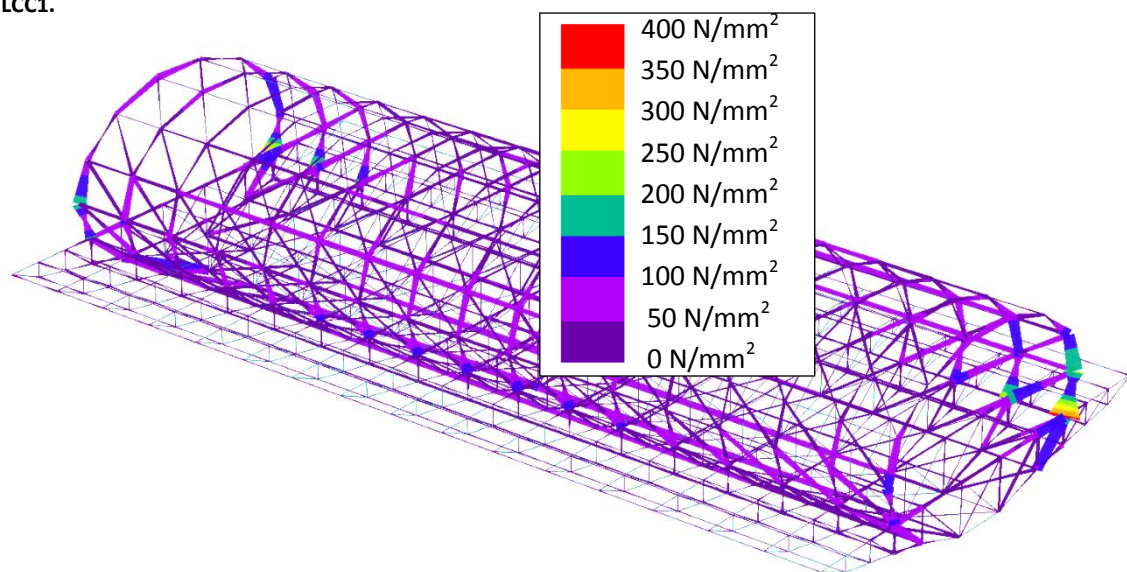


Fig. 142: 3D view of the Von Mises stress distribution in the bridge structure due to the normative load combination case LCC1.

9.2.2 FINITE ELEMENT ANALYSIS RESULTS FOR THE X- AND Y-DEFORMATION NORMATIVE LOAD COMBINATION CASES LCC5 AND LCC6

In the following chapter the maximum tensile- and compressive stresses and deformations in z-direction that occur in the bridge structure under design load were depicted and described. In this chapter the maximum deformations in x- and y-direction are covered. The first picture shows the x-deformation due to load combination case LCC6, which is the self-weight of the bridge combined with LM1 and bicycle and pedestrian loads and thermal load. The maximum deformation occurs near the x=49m support of the bridge, where a deformation of 24,44mm can be observed.

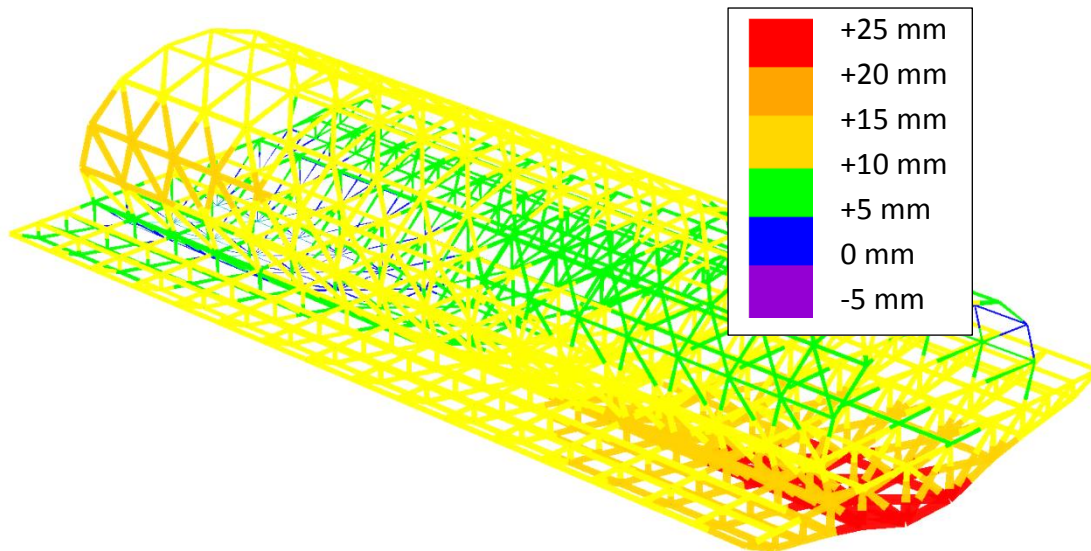


Fig. 143: 3D view of the deformation in x-direction of the bridge structure due to the load combination case LCC6

The second picture shows the deformation in y-direction due to load combination case LCC5, the combination of self-weight, wind load and snow load. The maximum deformation occurs at the top of the elliptical truss at the x=0m end of the bridge, here a deformation of 66,71mm can be observed.

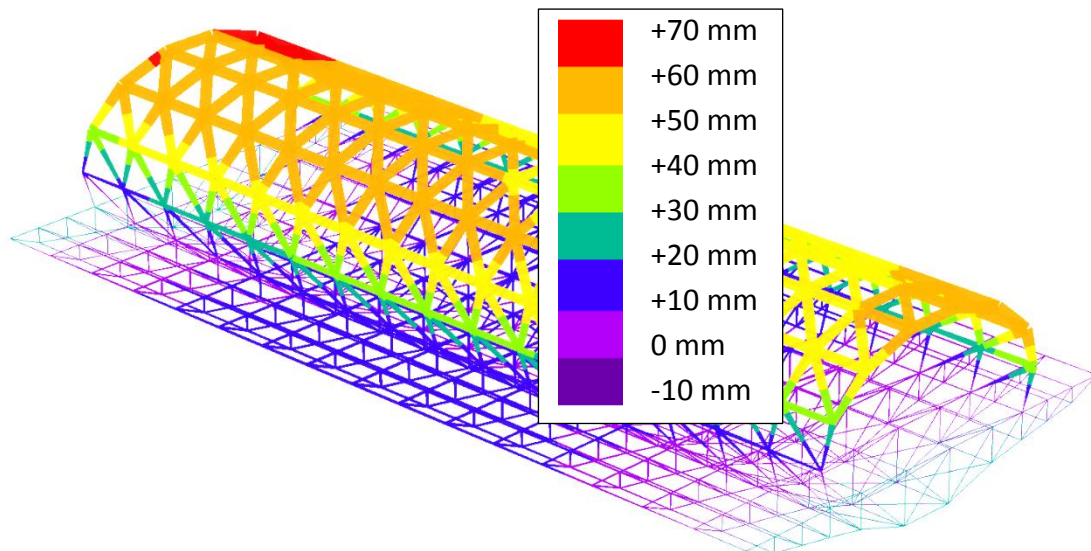


Fig. 144: 3D view of the deformation in y-direction of the bridge structure due to the load combination case LCC5

9.3 FATIGUE ANALYSIS

For the fatigue analysis of the full-FRP bridge structure is subjected to a special fatigue load model as prescribed by the Eurocode. The fatigue load model used here is 'FLM1', which was already described in [ch. 6.7]. The stress distribution that occurs due to FLM1 and self-weight of the structure is displayed in the picture below for the case that the axle loads are place at mid-span. In total the axle loads were placed at three locations: near to the support, at a quarter of the span and at mid-span.

The picture below shows three areas where the highest stresses occur. At the bottom of the elliptical truss, at mid-span the highest axial stresses occur. At the sides of the bridges, where the elliptical truss meets the bridge deck, the highest combined stresses occur (also see [ch. 10.2 for a description of the combined stresses). The stresses for all positions of the FLM1 axle loads were derived for every element as shown in the picture below:

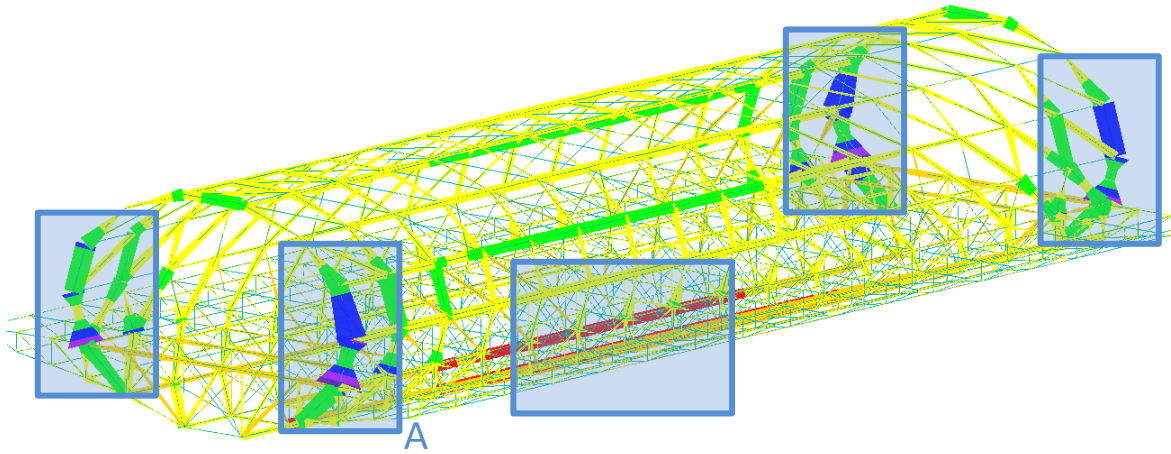


Fig. 145: Combined stresses in the full-FRP bridge due to fatigue load model FLM1. The regions with the highest stresses are highlighted. The area marked with the letter 'A' yields the highest stress amplitude

After analyzing all occurring stresses thoroughly it turned out that the area marked with the letter 'A' in the picture yields the highest stress amplitude. The highest stress amplitude occurs in the (near) vertical member of the elliptical truss that connects with the bridge deck substructure from the top. The minimum and maximum stresses occurring in this area are given below:

$$\begin{aligned}\sigma_{max-FLM1} &= -21,85\text{N/mm}^2 \\ \sigma_{min-FLM1} &= -162,2\text{N/mm}^2\end{aligned}\tag{9.1}$$

Knowing this stress range the stress amplitude σ_{amp} can be calculated. This is the difference between the minimum and the maximum stresses. This procedure is shown below [ch. 6.7]:

$$\begin{aligned}\sigma_{amp} &= \sigma_{max-FLM1} - \sigma_{min-FLM1} \\ \sigma_{amp} &= -21,85\text{N/mm}^2 + 162,2\text{N/mm}^2 \\ \sigma_{amp} &= 140,35\text{N/mm}^2\end{aligned}\tag{9.2}$$

The mean stress σ_{mean} is calculated in a similar way [ch. 6.7]:

$$\begin{aligned}\sigma_{mean} &= \sigma_{min-FLM1} + \sigma_{amp}/2 \\ \sigma_{mean} &= -162,2 + \frac{140,35}{2} \\ \sigma_{mean} &= -92,025\text{N/mm}^2\end{aligned}\tag{9.3}$$

Because the mean stress of the element with the highest stress amplitude is negative, according to [ch. 6.7] the following equation has to be used for the calculation of the number of cycles to failure [eq. 6.24c]:

$$N_f = \left(\frac{\sigma_{amp}}{\sigma_{c,RD} \left[1 - \frac{\sigma_{mean}}{\sigma_{c,RD}} \right]} \right)^k \text{ for } \sigma_{mean} < 0\tag{9.4a}$$

Substituting $\sigma_{c,RD}$ by the design compressive strength S_{L-c-d} of the carbon/epoxy composite derived in [ch. 3.4] the only unknown parameter in this equation is k . This exponent is given in the Dutch CUR96 for glass fiber reinforced epoxy only, and not for carbon epoxy [CUR96, ch. 9.4.3, p35]. Since the fatigue life of carbon fibers is significantly larger than that of glass fiber, it is a safe assumption to use the k – value of glass fibers for the carbon fiber in this fatigue life estimation. For glass fibers, the value of k is $k = -10$ is used, as prescribed by [CUR96, ch. 9.4.3, p35] for UD-glass/epoxy composite. Filling all values in, [eq. 9.4a] becomes:

$$N_f = \left(\frac{140,35\text{N/mm}^2}{995,90\text{N/mm}^2 \left[1 - \frac{-92,025\text{N/mm}^2}{995,90\text{N/mm}^2} \right]} \right)^{-10} \quad (9.4b)$$

$$N_f = (0,15548576)^{-10}$$

$$N_f = 121,085949 * 10^6 \text{ cycles to failure}$$

This obtained number of cycles should be compared to the number of expected cycles per year. For this bridge an expected number $N_{obs} = 0,5 * 10^6$ of loading cycles are expected per year, see [ch. 6.7] for the road classification for this bridge. For two driving directions the number of FLM3 vehicles per year then becomes, $1,2 * N_{obs}$, for a justification, again see [ch. 6.7].

The life expectancy in years for the heavy traffic bridge then becomes:

$$N_{FLM3-years} = \frac{N_f}{1,2 * N_{obs}} \quad (9.5)$$

$$N_{FLM3-years} = \frac{121,085949 * 10^6}{1,2 * 0,5 * 10^6}$$

$$N_{FLM3-years} = 201,81 a$$

It can therefore be concluded that the full-FRP elliptical truss heavy traffic bridge has a guaranteed fatigue life of at least 201 years.

Finally some remarks are made on the fatigue analysis. In this research the fatigue analysis was not a main goal of the investigation. However, for the sake of completeness an estimation of the fatigue life was made. In this estimation a very conservative approach was used since a lot of data, such as the k – value for carbon fibers and the exact design traffic composition, is not known. Next to that it is also known that carbon fibers behave far better under fatigue loading than glass fibers, making the choice for the glass fiber k – value conservative. Furthermore FLM1 is also considered to be the most conservative fatigue load model of the Eurocode. These are all reasons why the life expectancy given here can only be seen as a minimum value for the fatigue life of the carbon/epoxy elliptical truss bridge. The real-world fatigue life will most probably be higher than anticipated here.

The FE-analysis showed that the region where the elliptical truss meets the bridge supporting truss at the bridge edges yields the highest combined stresses under FLM1 load. Therefore it can be expected that the bridge will fail at these points, when approaching its end-of-life due to fatigue failure.

Note that the fatigue life given here considers the main load bearing structure of the bridge only. Fatigue effects in the bridge deck itself are explicitly not taken into account since the exact composite/sandwich layout of the bridge deck and the stress distribution in it is not known. For more information on the used

bridge deck type reference is made here to [ch. 11.1.5]. Note that the absence of the bridge deck in the fatigue analysis further increases the stresses on the main load bearing structure, since the spread of loads is not modeled. The addition of a bridge deck would therefore further increase the fatigue life of the full-FRP bridge.

9.4 VIBRATION BEHAVIOR AND MODAL ANALYSIS

To get an insight on the vibration behavior of the bridge structure, a modal analysis was also carried out in 'Oasys GSA' to obtain the first natural frequencies of the structure. In the following the first 5 dynamic modes along with their occurrence frequency are shown. Then these natural frequencies are compared to the limits for human and wind induces vibrations that were given in [ch. 6.7.1]. According to [NEN-EN 1990+A1+A1/C2:2011, ch. A2.4.2, remark 1, p75] a specific check on vehicle induced vibrations is not necessary. The modes are ordered by natural frequency, the first mode has the lowest natural frequency, and the 5th mode has the highest natural frequency of the five modes.

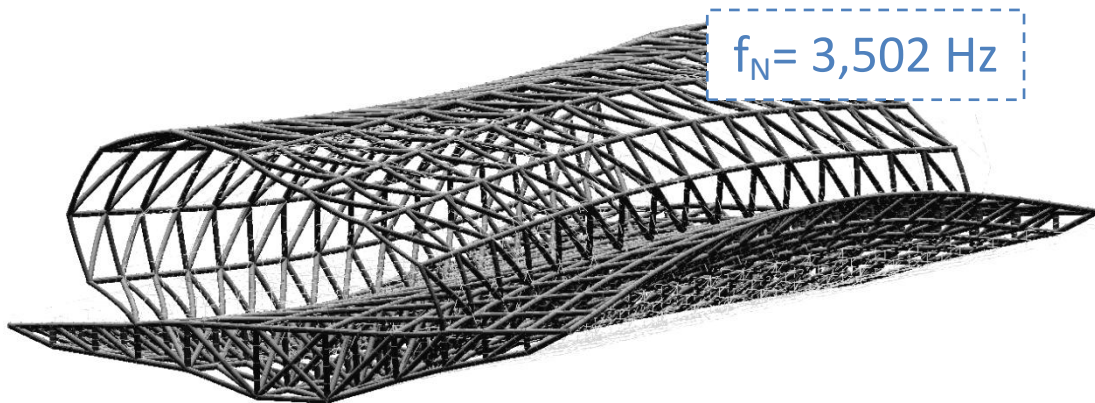


Fig. 146: Mode 1: The first horizontal mode. The complete structure tilts in y-direction at a natural frequency of $f_N=3,502 \text{ Hz}$.

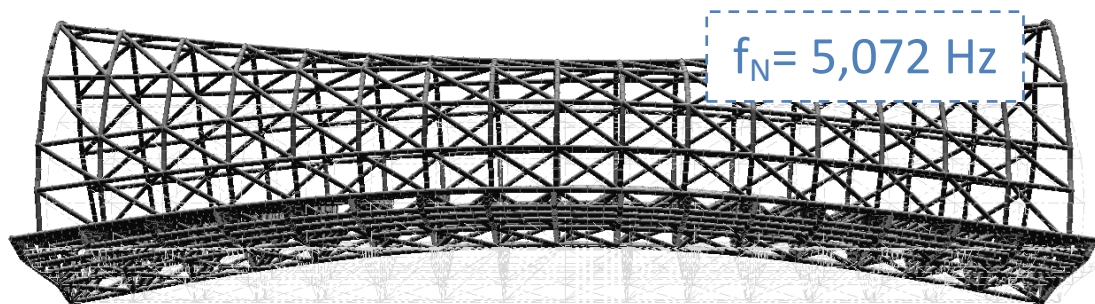


Fig. 147: Mode 2: The first vertical mode. The complete structure deforms in z-direction at a natural frequency of $f_N=5,072 \text{ Hz}$.

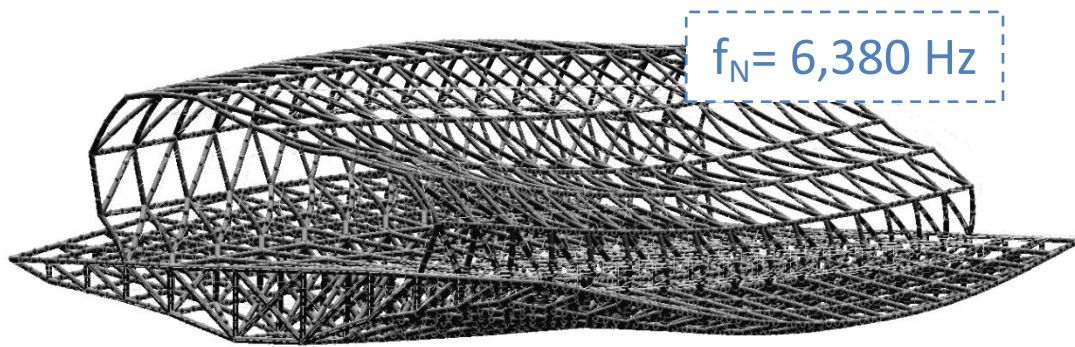


Fig. 148: Mode 3: The first torsional mode. The complete structure twists along the x-axis at a natural frequency of $f_N=6,380$ Hz.



Fig. 149: Mode 4: The second vertical mode. Only the elliptical truss deforms in z-direction at a natural frequency of $f_N=8,917$ Hz.

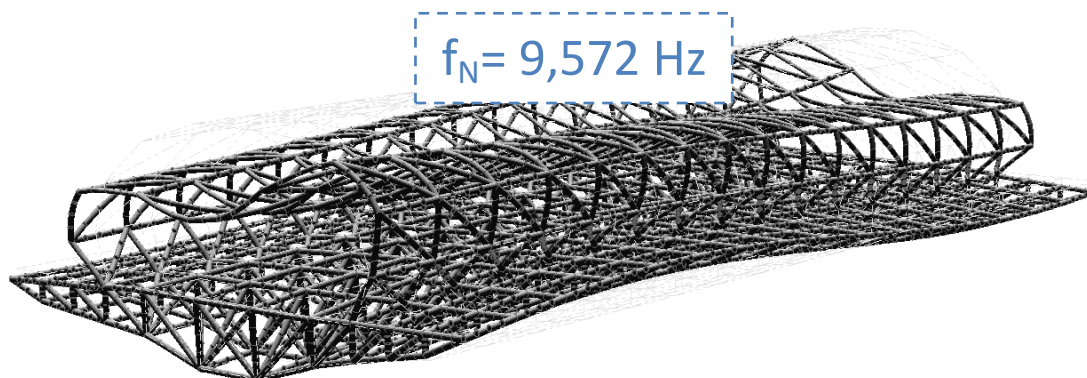


Fig. 150: Mode 5: The third vertical mode. The elliptical truss deforms in the same manner in z-direction along the whole length of the bridge at a natural frequency of $f_N=9,572$ Hz.

Knowing the first natural frequencies for vertical, horizontal and torsional vibration these values can now be compared to the frequency limits as described in [ch 6.7.1]. The table below summarizes the natural frequencies of the first 5 modes of the full-FRP bridge. Next to that the frequency limits for human induced- and wind induced vibrations are given in the last two columns and marked green.

The smallest vertical and horizontal natural frequencies of the structure are normative. In the table they are marked blue; 5,072 Hz for the first vertical natural frequency, 3,502 Hz for the first horizontal natural frequency and 6,380 Hz for the first torsional natural frequency. All three values lie above the posed limits for human induced- and wind induced vibrations. Therefore it can be concluded that the structure is not susceptible to human induced- and wind-induced vibrations. Note that the value of the first vertical natural frequency lies relatively close to the frequency limit for vertical human induced vibration. However, the bridge still complies with the Eurocode limit as described in [ch. 6.7.1] and in the literature study [LS, ch. 3.3.5.2, p129] . Here a maximum frequency of 3,20Hz for fast running is given, which still yields a relatively safe margin.

	Natural frequency Mode 1 [Hz]	Natural frequency Mode 2 [Hz]	Natural frequency Mode 3 [Hz]	Natural frequency Mode 4 [Hz]	Natural frequency Mode 5 [Hz]	Human induced frequency limit [Hz]	Wind induced frequency limit [Hz]
Vertical		5,072		8,917	9,572	>5,00	
Horizontal	3,502					>2,50	>1,00
Torsional			6,380			>2,50	>1,00

Table 38: The table shows the natural frequencies of the full-FRP bridge for the first 5 modes.

It was chosen not to perform a specific analysis for vehicle induced vibrations, since the dynamic effects of traffic loads are covered by the so-called 'dynamic factor', which is already included in the characteristic traffic load values that were used for the static analysis, described in [ch. 6.2] [ch. 9.1.1] [ch. 9.2]. For more information: [LS, ch. 3.3.5.3, p130]

10. CONNECTIONS

In this chapter some information on the configuration and properties of the connections is given. First the total number of connections and their order will be given. Afterwards the stress distribution in two characteristic connections will be given. Finally some more information on the fabrication of the connection elements will be given.

10.1 CONNECTION PROPERTIES

In total, this bridge features 529 nodes or connections and 1671 elements. In this chapter it is investigated what the order of the majority of the nodes is and how many different types of connections do exist. In the GSA model a total of 18 different connection types were identified.

The design features numerous connections, some with a low order of 3, other with a very high order of 10. In the graph below the connections are grouped by their order. Furthermore a difference is made between 2D connections and 3D connections, meaning that for the 2D connections all elements lie in a single plane (or in the ellipse without normal elements) whereas for 3D connections the elements lie in different planes.

The graph clearly shows that by far the most connections in the design have the order 6, and thus connect 6 elements. This is a good result for this design since a prerequisite to use this particular truss topology was the limited order of the nodes [ch. 7.1.3.5]. The addition of the inner bridge deck and the cantilever bridge deck thus yielded only a limited number of higher order nodes. About 100 nodes have an order around 9. The remaining about 400 nodes have an order of 6 or lower.

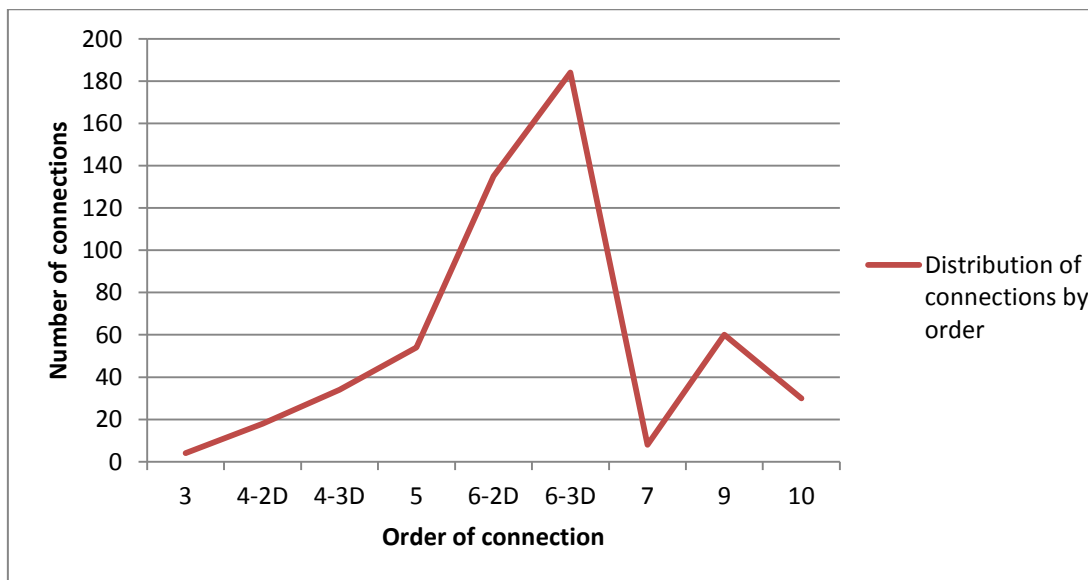


Fig. 151: Distribution of connections by order

10.2 STRESS DISTRIBUTION IN A PLANAR CONNECTION

In this chapter the stress distribution in a node of the main elliptical load bearing structure is given, to provide some insight in the maximum stresses that occur in the connections of the members. In this chapter the stresses occurring in the planar connection due to the overall normative load combination case LCC1 are considered. Below the position of the node is marked by the red arrow. Next to that, the node (number 92) is shown along with all six elements that connect at this node and their corresponding number.

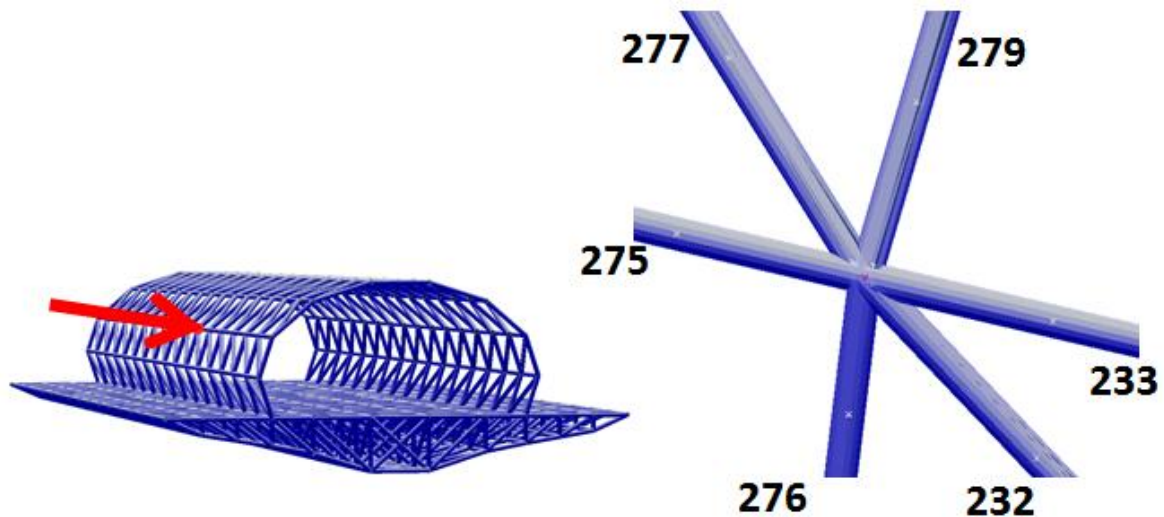


Fig. 152: Position of node 92 and configuration of the 6 elements connecting at node 92.

The picture below shows the stress distribution in the members that connect to the connection that is considered. The stresses that are given are measured directly at the connection. Per element two values are given, in the blue square the axial stresses are given. In the red square the combined stresses are shown, they also included the bending moments at the nodes and are derived by the following formulae:

$$\sigma_{ax} = \frac{F_x}{area} \quad (10.1)$$

$$\sigma_{bend-y} = \frac{M_{yy}}{I_{yy}} D_z; \quad \sigma_{bend-z} = -\frac{M_{zz}}{I_{zz}} D_y$$

$$\sigma_{comb} = \sigma_{ax} + \sigma_{bend-y} \text{ or } \sigma_{bend-z}$$

The picture below shows that the stress values at node 92 are very reasonable with minimal and maximal axial stress values of $-50,53\text{N/mm}^2$ to $13,69\text{N/mm}^2$ and combined stress values of $-51,43\text{N/mm}^2$ to $80,47\text{N/mm}^2$. Considering the stresses only, it should therefore not pose a problem to use a 2D-connection like this in the structure.

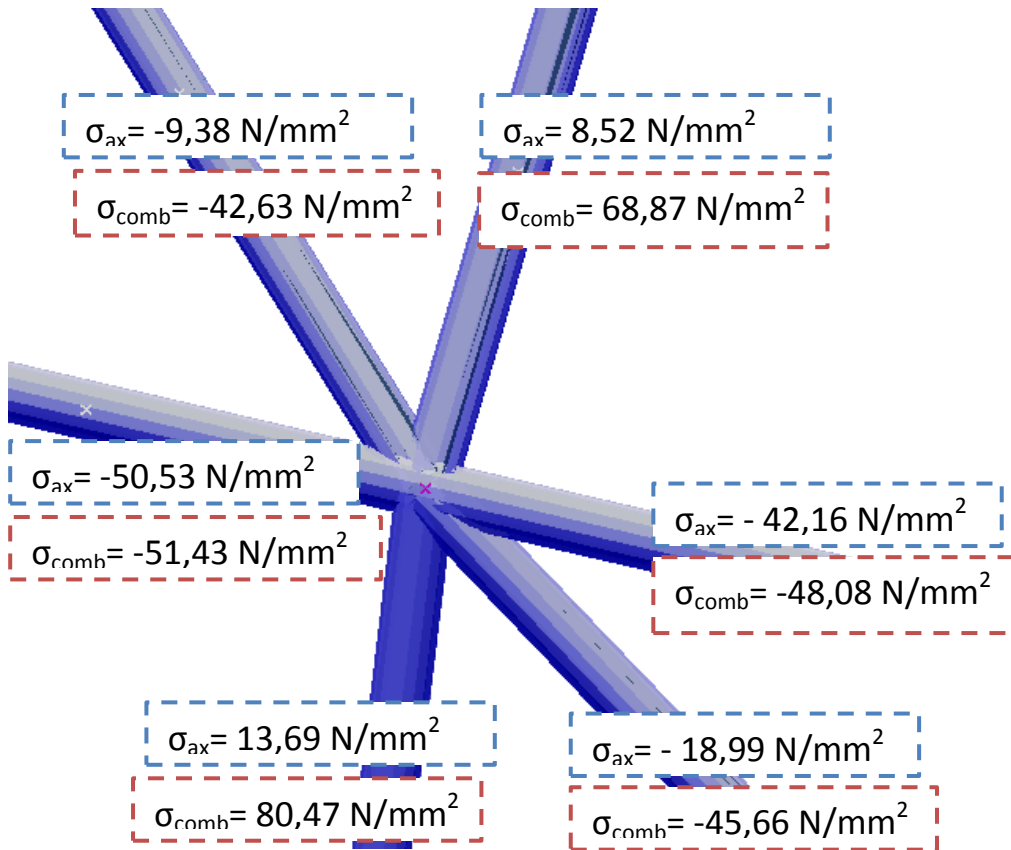


Fig. 153: Stress distribution in the 6 members that connect at node 92. The blue stresses are the axial stresses. The red stresses are the combined stresses that also incorporate the bending moments in the members.

10.3 STRESS DISTRIBUTION IN A MULTIPLANAR CONNECTION

In this chapter the stress distribution in a node of the main elliptical load bearing structure is given, in contrast to [ch. 10.2] this node is located at the bottom of the main elliptical truss and also connects elements of the inner bridge deck supporting truss. This node is a node with 9 connecting members. Below the position of the node is marked by the red arrow. Next to that, the node (number 99) is shown along with all nine elements that connect at this node and their corresponding number.

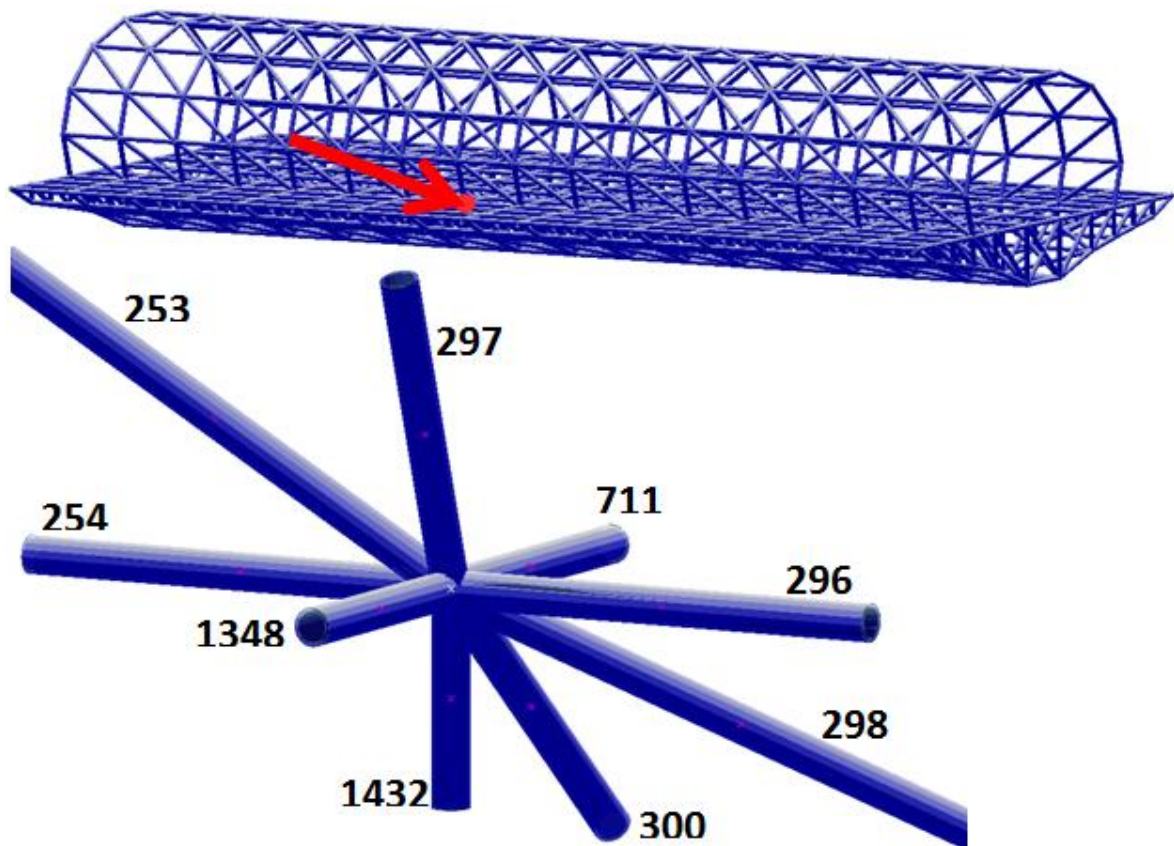


Fig. 154: Position of node 99 and configuration of the 9 elements connecting at node 99.

Similar to the planar connection chapter, in this chapter the stresses occurring in the multi planar connection due to the overall normative load combination case LCC1 are considered. The picture below shows the stress distribution in the members that connect to the connection that is considered. The stresses that are given are measured directly at the connection. Per element two values are given, in the blue square the axial stresses are given. In the red square the combined stresses are shown, they also included the bending moments at the nodes. The picture below shows that the stress values at node 99 are similar to the stress levels in node 92 that was covered before. The members connecting in at node 99 induce minimal and maximal axial stress values of $-16,51\text{N/mm}^2$ to $14,93\text{N/mm}^2$ and combined stress values of $-35,97\text{N/mm}^2$ to $85,51\text{N/mm}^2$.

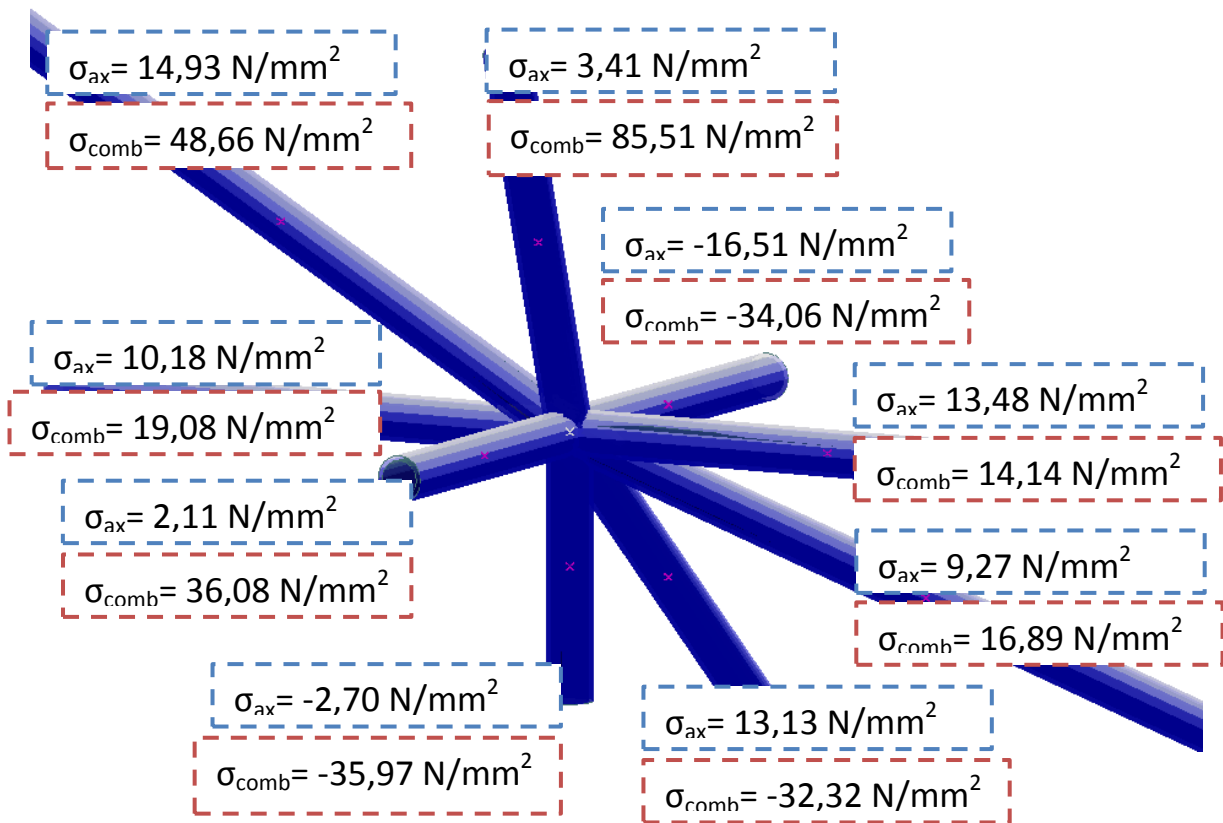


Fig. 155: Stress distribution in the 9 members that connect at node 99. The blue stresses are the axial stresses. The red stresses are the combined stresses that also incorporate the bending moments in the members.

10.4 MAKEABILITY OF FRP CHS CONNECTIONS

In [ch. 3.5.2] the possible production processes of high-order FRP-CHS connections were already discussed. There the conclusion was drawn to produce the connection elements by automated filament winding. The reason for this choice was the high rate of automation due to the use of CNC-controlled filament winding machines, which results in a lower production cost, and the possibility to quickly produce many elements, differing in shape and size by only adapting some parameters in the software. The examples that were given in [ch. 3.5.2] already date from 1989 and 1994 and at that time tee joints could already be produced on normal filament winding machine with only minor software changes.

The tee-joint shown below on the left was produced 1989 by 'Cadfil' [WEB, www.cadfil.com using a conventional filament winding machine, only adapting the software. 'J. Scholliers and H. Van Brussel' (1994) carried out another research at the KU Leuven [P105] where a GFRP tee joint was produced using computer-integrated robotic tape-winding. See the picture below on the right for the winding patterns used.

Since then automated robots, similar to those used in the automotive industry have found their way into the FRP manufacturing market. Before robots entered the market, complex elements such as tee-joints would typically have to be produced using labor-intensive hand-layup combined with very expensive vacuum- or pressure-bag techniques. This made the design and fabrication of structures, such as trusses, with a large number of (complex) connections very costly and infeasible

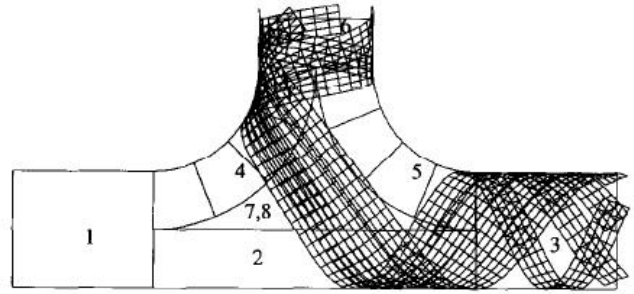
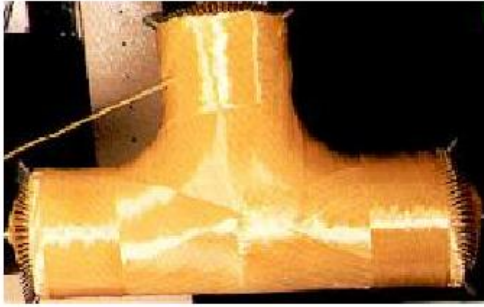


Fig. 156: Left: GFRP tee-joint used for the connection of tubular FRP members. [WEB, www.cadfil.com] Right: Robotic tape-winding patterns for the production of a tee joint [P105, p8]

However, considering the newly available state-of-the-art computer numerical controlled (CNC) and robotic techniques large (and complex) have become more and more cost-effective and feasible. Therefore the production of higher order FRP CHS connections should not be a hurdle that cannot be taken. The application of the discussed CNC-assisted filament winding techniques should not only drastically reduce the costs per connection but also simplify the production of the higher order connections.

11. DESIGN OF OTHER BRIDGE ELEMENTS

Next to the main load bearing system, which is the main subject of the design and the finite element analysis, other important bridge elements also have to be given attention. The elements that are to be considered in this chapter are the bridge deck and the bridge substructure, which includes the supports, bearing and the pillars of the bridge. Since the main focus of the research is the primary load bearing cylindrical truss, these elements will only be covered briefly.

11.1 BRIDGE DECK

It seems rather obvious that an full-FRP bridge structure should also have a bridge deck made of this modern material. This point is even strengthened by the fact that in bridge design bridge decks are the part that is most often made of fiber reinforced polymers. [LS, ch. 3.2, p111] This chapter will briefly recall the advantages of FRP bridge decks over traditional steel or concrete bridge decks. Furthermore a choice for a particular system will be made.

11.1.1 CHOICE OF BRIDGE DECK SYSTEM

Generally two different construction types of FRP bridge decks exist: firstly the multi-cellular deck panels made of adhesively bonded, mostly pultruded shapes. Most bridge decks that have been installed to this date use this system. The panels consist of differently shaped cross-sections: hexagonal, triangular, rectangular or trapezoidal cross-section are mostly used. The second construction type of FRP bridge decks is the sandwich panel with various core structure possibilities. Stiffened foams or thin walled cellular materials are most commonly used for the cores. These cores are often considered to be of a honeycomb type.

FRP bridge decks are generally very resistant to fatigue, though sandwich panels tend to be more sensitive than pultruded sections. Damages due to debonding failures between face sheets and core materials have been reported. Since this connection is somewhat more difficult to fabricate than the pultruded web connections it is expected that improvements in fabrication technology will increase the fatigue resistance of sandwich panel bridge decks. [LS, ch. 3.2.4, p113]

Below the advantages and disadvantages of FRP bridge decks are briefly recalled. These were derived in the literature study [LS, ch. 3.2.1-ch. 3.2.3, p111-113]

Advantages of FRP Bridge Decks	Disadvantages of FRP Bridge Decks
Low weight	High initial cost
Resistance to de-icing salts and other chemicals	Deflection driven design due to FRP low stiffness
Fast installation	No standard manufacturing process
Good durability	Little knowledge on thermal behavior
Lower user costs (lower maintenance costs)	Some failure of the wearing surface (i.e. cracking, debonding)
Long service life	The resultant tendency to creep over time
Fatigue resistance	Lack of long term performance data
Good quality due to fabrication in a controlled environment	Limited FRP experience within the engineering- and construction industry
Ease of installation	Lack of design standards

Table 39: Advantages and disadvantages of fiber reinforced polymer bridge decks [LS, ch. 3.2.3, p113]

Given all advantages and disadvantages, such as a smaller height and better fatigue resistance, multicellular panels are generally preferable in this design. The limited span that these systems have compared to sandwich systems is not a disadvantage, since the truss beneath the deck yields enough possibilities to connect the bridge deck. Furthermore, the fact that supporting beams for these panels would be needed can also be seen as an advantage: The supporting beam can increase the overall stiffness of the main cylindrical truss when properly connected.

Because the main objective of this design study is the structural design of the overall load-bearing system, thus the cylindrical truss, it is chosen not to completely design a new FRP bridge deck system, but rather to use an existing system. Of all systems investigated in the literature study [LS, ch. 3.2.4, p113] the only European system, the 'Fiberline' system was chosen for the following reasons. First of all, it has been applied in a number of projects already, such as for example the 'West Mill Bridge' in Oxford, England and the 'Friedberg Bridge' in Hessen, Germany [P35]. Because no codes exist for the application of FRP in bridge engineering [LS, ch. 8, p223] the authorities generally ask for mechanical load testing of the applied FRP elements in a lab environment. The 'Fiberline' bridge deck products have been tested for the application in the 'West Mill Bridge' in 2002 by 'IETcc' in Madrid, Spain. Before application of the same bridge deck in the 'Friedberg Bridge' further tests were carried out by the 'University of Stuttgart', Germany and 'EPF Lausanne', Switzerland [P35]. It is thus certain that the 'Fiberline' bridge deck products are sufficiently tested and that the mechanical data of these products that is provided by the manufacturer is readily available can be used for the design of the bridge deck and its substructure.

In bridge deck design often the principle of composite action is used. This is the mechanical interaction of the underlying girders and the bridge deck, wherein the bridge deck acts as the top flange of the girder below. In steel-concrete designs this can drastically increase the efficiency of the total load bearing system. However, for composite action, a sturdy and rigid connection between the girder and the deck is necessary.

This bridge design will not feature composite action between the girders and the bridge deck. Not only because the connections between FRP bridge decks and FRP-girders are not very well investigated yet, but also because without composite action much easier and cost-effective replacement of the deck is possible. Deck replacement is often needed due to heavy fatigue load that bridge decks typically have to endure. Since the design life of the load-bearing structure of the bridge is about 100 years and that of the bridge deck typically only 15-20 years, deck replacement is a phenomenon that has to be taken care of in the initial design. Making the girder-deck connections easy, is one important step to enable fast, easy and cost-effective deck replacement. The deck-supporting girders in the cylindrical truss will be designed in such a way, that composite action is not needed to withstand design loads.

11.1.2 DEMANDS FOR THE BRIDGE DECK OF THE FULL-FRP BRIDGE DESIGN

Here the requirements for the bridge deck that were already described in the final design drawing chapter [ch. 8.3] are briefly recalled. The drawing below shows the bridge deck supporting grid that is dictated by the layout of the main load bearing truss as well as the cantilever and inner bridge deck truss, as introduced and designed in [ch. 8.1] [ch. 8.2] . In total two different bridge deck types are needed, one for the heavy traffic, hereafter called ‘Type 1 bridge deck’ and one for the lighter bicycle and pedestrian traffic, hereafter called ‘Type 2 bridge deck’.

Since the ‘Type 1 bridge deck’ is more heavily loaded and covers a greater portion of the bridge deck surface it is of primary design importance. In the following a suitable system for the ‘Type 1 bridge deck’ will be derived. The ‘Type 2 bridge deck’ will be very briefly considered afterwards.

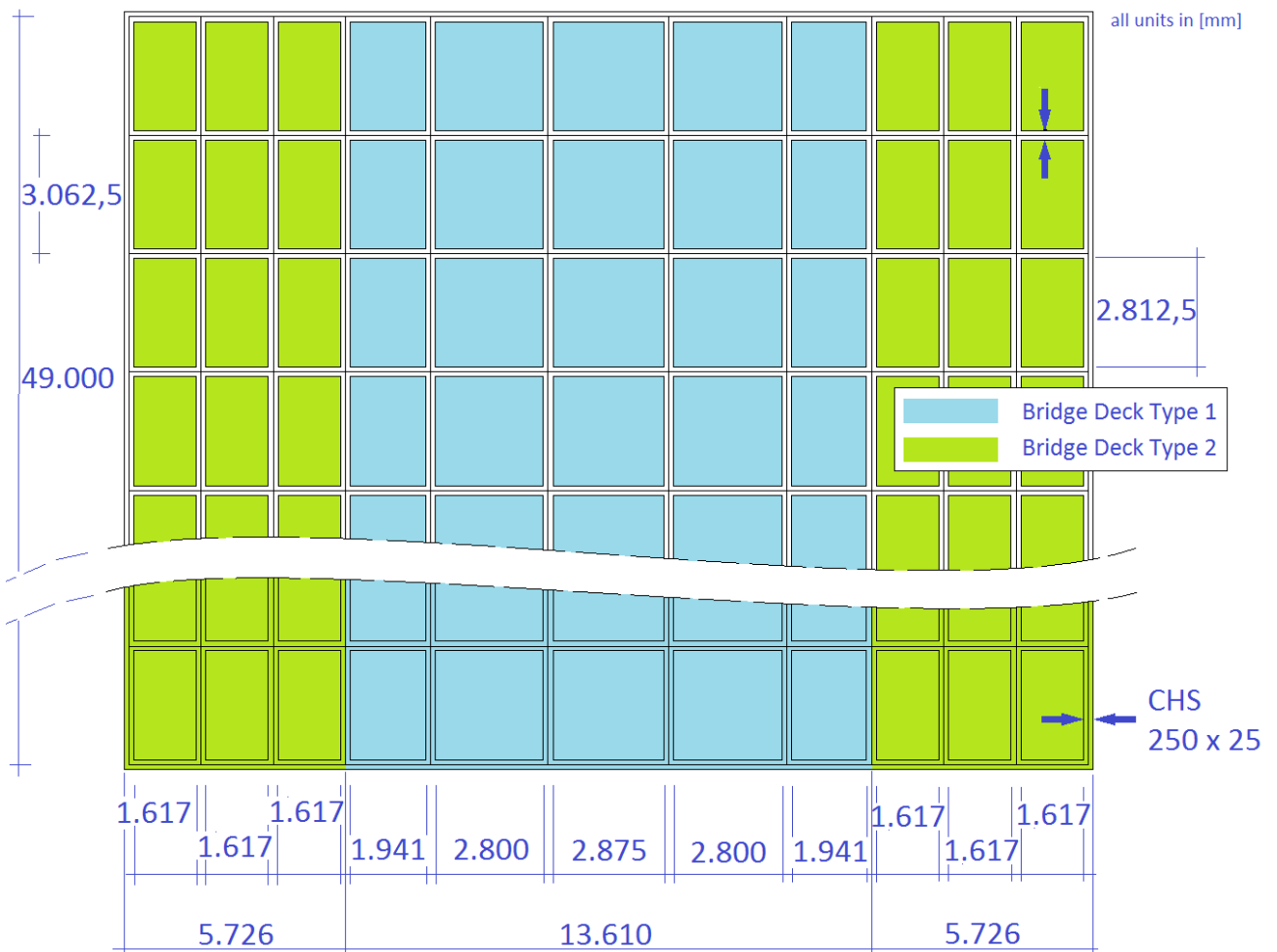


Fig. 157: Configuration of the bridge deck

11.1.3 FIBERLINE FBD600 ASSET BRIDGE DECK

Of the ‘Fiberline’ bridge deck products that were discussed in the chapter before as well as in the literature study [LS, ch. 3.2.4, p114; table 30, p115] the ‘Fiberline’ FBD600 Asset bridge deck is the heaviest bridge deck available. According to the manufacturer it complies with the loads described in ‘Eurocode 1: Actions on structures’ [NEN-EN 1991-2:2003], these are also the load cases described in [LS, ch. 3.3.3, p124] and in [ch. 6.2]. Therefore this bridge deck type is expected to be the suitable as structural system for the ‘Type 1 bridge deck’.

The FB600 Asset bridge deck is a FRP bridge deck reinforced with unidirectional E-glass reinforcement. Next to that it also reinforced with E-glass surface veils. The bridge deck profiles are produced via pultrusion. To average fiber content of the FBD600 lies at about 50%. The matrix used is the 'P3510 Vinyl ester' matrix. [B25, p0.0.10-0.0.11]

Below, the FBD600 layout is shown in the drawings. The single profiles have a width of 521,0 mm, they are adhesively bonded to each other to produce a continuous bridge deck. The height of this bridge deck is 225,0mm, which makes the bridge deck very slender, but also decreases the spacing of the supporting girders. The deck can be connected to these girders by adhesive bonding or by bolted connections. The minimum spacing of the deck substructure will be derived in the next chapter.

The table below shows all important characteristics of the FBD600 Asset bridge deck profile, the left table shows the data for a single bridge deck element, the right table shows the properties of an adhesively bonded assembly with a fixed width of 1000,0mm. Note the low E-modulus stiffness values of 20.000,0 N/mm² for the bridge deck (in fiber direction), compared to the values derived in [ch. 3.3]. These relatively low values are caused by the reinforcement type (E-glass has a much lower modulus than for example carbon) and the lower fiber content of 50% (in [ch. 3.3] the fiber contents are between 60% and 70%).

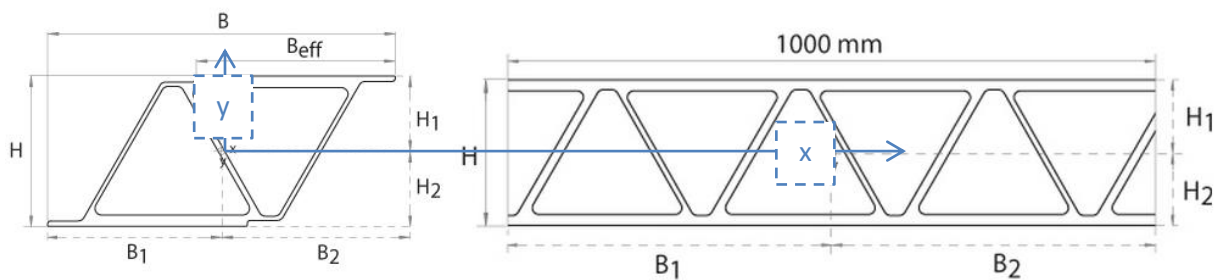


Fig. 158: 'Fiberline' FBD600 Asset bridge deck profile. Left: single profile, right: glued assembly of profiles to a width of 1000mm [WEB, www.fiberline.com]

per profile

Property	Unit	FBD600 ASSET
Height	mm	225,0
Width (single unit)	mm	521,0
Width B _{eff}	mm	299,0
B ₁	mm	260,5
B ₂	mm	260,5
H ₁	mm	112,5
H ₂	mm	112,5
A	mm ²	15.644,0
I _x	mm ⁴	125.400.000,0
I _y	mm ⁴	228.800.000,0
W _x	mm ³	1.114.000,0
W _y	mm ³	87.000,0
E Stiffness	N/mm ²	20.000,0
Weight	kg/m	29,9
t (flange)	mm	16,0
t web (thick)	mm	10,5
t web (thin)	mm	7,5

per m

Property	Unit	FBD600 ASSET
Height	mm	225,0
B ₁	mm	500,0
B ₂	mm	500,0
H ₁	mm	114,0
H ₂	mm	111,0
A	mm ²	54.252,0
I _x	mm ⁴	425.600.000,0
W _x	mm ³	3.733.300,0
E Stiffness	N/mm ²	20.000,0
Weight per m ²	kg/m ²	103,7
t (flange)	mm	16,0
t web (thick)	mm	10,5
t web (thin)	mm	7,5

Table 40: 'Fiberline' FBD600 Asset bridge deck profile properties. Left: single profile, right: glued assembly of profiles with a width of 1000mm [WEB, www.fiberline.com]

Knowing the stiffness of the bridge deck material and the moment of inertia of the bridge deck elements it is possible to calculate the spacing of the girders that will carry the bridge deck. Using a stiffness driven design method for this purpose, the deflection limits for the bridge deck are also needed. The main deflection limits were derived in [ch. 6.9]. However, since for bridge decks often other values are used, a

number of different deflection criteria are also considered in the following. The calculation of the needed spacing of the girders carrying the bridge decks will be the subject of the next chapter.

11.1.4 CALCULATION OF MINIMUM SUPPORTING GIRDER GRID SIZE FOR THE FIBERLINE FBD600 ASSET BRIDGE DECK

Following the initial choice on the type of bridge deck, described in the chapter before, it now has to be investigated what spacing and dimensions the bridge deck supporting girders need to have. Therefore a stiffness driven design method is used in which the deflection of the bridge deck will be limited to a certain value. The maximum allowable deflection is always dependent on the free span of the member that is to be designed. Using this method a maximum span of the bridge deck can be found.

The deflection w of a member with span l and stiffness EI can be calculated by the following formulae. These formulae are for simply supported beams on two supports. With the first formula the deflection w_q due to a uniformly distributed line load q can be calculated. The second formula is used to calculate the deflection w_F due to a point-load F at mid-span.

$$w_q = \frac{5}{384} \frac{ql^4}{EI} \quad (11.1a)$$

$$w_F = \frac{1}{48} \frac{Fl^3}{EI} \quad (11.1b)$$

The live loads q and F should be determined using the Eurocode, [NEN-EN 1991-2:2003]. The normal traffic loads are described in 'Load Model 1' and 'Load Model 2'. These load models are quantified in more detail in [ch. 6.2]. It is advised to use 'Load Model 2' for orthotropic (steel) bridge decks [LS, ch. 3.3.3.2, p125-126]. This load model prescribes a single point load of the following magnitude:

$$\beta_Q Q_{ak} = 400 \text{ kN} \quad (11.2)$$

In this formula β_Q is a specific adjustment factor, defined by the national annex of the code, which may be set to unity if unknown. For this calculation it is set to unity. This point load represents a single axle of a truck, consisting of two wheels of 200kN. When relevant, the Eurocode allows that only one wheel load has to be taken into account. Since the lateral spacing of the bridge deck supporting girders is larger than the design distance of the two point loads of 'Load Model 2' the design point load that is to be calculated with is:

$$F = \beta_Q Q_{ak} = 400 \text{ kN} \quad (11.3)$$

Inserting this value into formula [x.1b] for a number of different spans it yields the maximum span, as shown in the table below. The modulus of elasticity $E_0 = 20.000 \text{ N/mm}^2$ and moment of inertia $I_x = 4,256 * 10^6 \text{ mm}^4$ were taken from [ch. 11.1.3, table 39, right]

L [mm]	L/800 [mm]	L/600 [mm]	L/400 [mm]	L/200 [mm]	Deflection w_F [mm]	Max L/x
500	0,63	0,83	1,25	2,50	0,122	
600	0,75	1,00	1,50	3,00	0,211	
700	0,88	1,17	1,75	3,50	0,336	
800	1,00	1,33	2,00	4,00	0,501	
900	1,13	1,50	2,25	4,50	0,714	
1000	1,25	1,67	2,50	5,00	0,979	
1100	1,38	1,83	2,75	5,50	1,303	L/800
1200	1,50	2,00	3,00	6,00	1,692	
1300	1,63	2,17	3,25	6,50	2,151	L/600
1400	1,75	2,33	3,50	7,00	2,686	
1500	1,88	2,50	3,75	7,50	3,304	L/400
1600	2,00	2,67	4,00	8,00	4,010	
1700	2,13	2,83	4,25	8,50	4,810	
1800	2,25	3,00	4,50	9,00	5,710	
1900	2,38	3,17	4,75	9,50	6,715	
2000	2,50	3,33	5,00	10,00	7,832	
2100	2,63	3,50	5,25	10,50	9,067	
2200	2,75	3,67	5,50	11,00	10,424	L/200
2300	2,88	3,83	5,75	11,50	11,912	
2400	3,00	4,00	6,00	12,00	13,534	
2500	3,13	4,17	6,25	12,50	15,297	

Table 41: Deflection of the bridge deck for spans from L=500-2500mm due to a point load F=200kN with a safety factor $\gamma=1,5$ as prescribed by Load Model 2 of Eurocode 1 [NEN-EN 1991-2:2003]

The above table gives the maximum grid size for each of the four deflection limits from $L/800$ to $L/200$. The maximum grid size for a deflection limit of $L/200$, that can be achieved with the Fiberline FBD600 Asset bridge deck is 2,20m (row with red limit in righter column). With the self-determined deflection limit of $L/600$, as described in [ch. 6.9] the maximum grid size that can be achieved with the FBD600 bridge deck is only 1,3m.

Considering the layout of the bridge deck supporting girders dictated by the final design of the main load bearing structure in [ch. 8] and [ch. 8.3] it becomes evident that the Fiberline FBD600 Asset bridge deck is not suitable as bridge deck type 1 for this full-FRP design and the given supporting grid dimensions. Therefore other bridge systems have to be considered. This will be the subject of the next chapter.

11.1.5 FIBERCORE INFRACORE BRIDGE DECK SYSTEM

Because in the preceding chapter the Fiberline FBD600 Asset bridge deck system turned out not to be a suitable system for the application as ‘Type 1 bridge deck’ it was decided to contact another renown Dutch bridge deck manufacturer. The Dutch company ‘Fibercore’ helpfully provided very useful information on their state-of-the-art ‘Infracore Inside’ bridge deck systems. This bridge deck system was recently developed in the Netherlands and was already applied on a number of projects, such as the ‘Oosterwolde heavy traffic bridge, as already described in the literature study [LS, ch. 6.2.3, p192] and a number of other projects [WEB: www.infracore.nl].

An even more recent project is the steel/FRP composite heavy traffic bridge over the A27 near Utrecht Lunetten. Here, panels of 6,20m x 24,50m were used as bridge deck between two main steel trusses that have a total length of 140m and a lateral distance of 6,20m. Similar to the ‘Oosterwolde heavy traffic bridge’ this bridge is able to withstand heavy traffic of the 60 ton class. [WEB: www.infracore.nl]

Due to its numerous applications in heavy traffic bridges it was decided to use the Fibercore Infracore Inside systems for the ‘Type 1 bridge deck’ as well as for the lighter ‘Type 2 bridge deck’ instead of the Fiberline

FBD600 Asset system which failed to meet the deflection criteria as shown before in [ch. 11.1.4]. In contrast to the Fiberline system that is a pultruded section, as described earlier, the Fibercore system uses a sandwich system with a fiber-rich skin and a light-weight core. The following table gives all important dimensions and properties of the used Fibercore bridge deck systems.

Property	Type 1 bridge deck: 'Fibercore Infracore Inside' Heavy traffic	Type 2 bridge deck: 'Fibercore Infracore Inside' Bicycle and pedestrian traffic
Material	glass fiber reinforced polymer	glass fiber reinforced polymer
Production technique	Vacuum bag/ pressure bag/ hand layup	Vacuum bag/ pressure bag/ hand layup
Maximum load	60 ton traffic	bicycle and pedestrian load
Panel length [mm]	24.500	24.500
Panel width [mm]	6.810	5.600
Number of panels needed	4	4
Panel height [mm]	160,00	77,00
Skin thickness [mm]	20,00	10,00
Weight per area [kN/m ²]	0,95	0,45
Maximum allowable span [mm]	3.000,00	3.000,00
Maximum occurring span [mm]	2.875,00	1.617,00
Maximum allowable deflection	L/300	L/250
Maximum occurring deflection [mm]	9,58	6,47

Table 42: Design properties of the 'Fibercore Infracore Inside' systems for the use as 'Type 1 bridge deck' and 'Type 2 bridge deck' in the full-FRP bridge design

Note that these bridge deck systems were not included in the FE-analyses as described before. This is mainly due to the reason that the bridge decks are not part of main load bearing structure and are designed to be fully demountable as described before in [ch. 11.1.1]. However, the weight of the bridge decks was incorporated in the FE-analyses as a part of the self-weight of the structure [ch. 8.4]

11.1.6 WEARING SURFACE

For a traffic bridge an important part of the bridge deck is a suitable wearing surface. The two most important functions of the wearing surface are the weather-proof and water-tight coating of the bridge deck and the providence of a smooth surface that yields a comfortable ride. Next to that, a high level of smoothness of the bridge deck surface also increases fatigue life and reduces vehicle induced vibration.

Normally in bridge design epoxy asphalt layers are used. An example of a well-tested and applied European bridge deck wearing surface is 'Possehl' Thermoflex-RWB. This material can be applied on FRP composite surfaces [WEB, www.possehl.nl/nl/verkeer/brugdekbekleding/].

Epoxy asphalt wearing surfaces are very tough and have a guaranteed maintenance free time span in excess of 15 years. 'Thermoflex-RWB' can be applied directly onto the assembled FRP bridge deck elements. Typical thicknesses of epoxy asphalt bridge deck wearing surfaces are between 20mm and 50mm [WEB, chemcosystems.com/epoxy_info]. This is a substantially smaller thickness than for normal asphalt (minimum 70mm) thereby drastically reducing the weight of the wearing surface and thus the dead load on the bridge structure. Next to that it is also possible to use lightweight substrates as filler material in the epoxy asphalt, thus further reducing the weight without compromising durability and fatigue resistance.

Epoxy asphalt surfaces are furthermore compatible with the 'Fibercore Infracore Inside' bridge deck systems that are used for this bridge design. The 'Oosterwolde heavy traffic bridge, as already described in the literature study [LS, ch. 6.2.3, p192] features an 'Infracore' bridge deck for heavy traffic and also successfully uses a grit-epoxy-asphalt wearing surface.

11.2 BRIDGE SUBSTRUCTURE

In this chapter the bridge substructure above ground will be briefly covered. First the total weight of the structure will be calculated, using the specifications of the final design [ch. 8]. Next to that the reaction forces occurring at the supports due the load combination cases, as described in [ch. 6.6] will be presented. Finally some possibly structural solutions for the bridge substructure will be given.

11.2.1 WEIGHT OF THE BRIDGE

The following table gives the total usage of cross section in meters, the total volume of FRP material used weight of the parts of the structure in kg, the complete weight of the main load bearing system as well as the percentage of the weight per part of the load bearing system. Furthermore also the weight per element per meter span is given.

The second part of the table give the same information for the bridge deck system as described in the chapter before [ch. 11.1.5]

Element	Cross section type [mm x mm]	Cross section area [m ²]	Total usage cross section [m]	Total volume material used [m ³]	Total weight	Weight percentage [%]	Weight per meter [kg/m]
Main elliptical truss	CHS 250x25	0,018	2.294,805	40,553	66.060,107	50,0%	1.348,165
Inner truss	CHS 250x25	0,018	973,198	17,198	28.015,262	21,2%	571,740
Cantilever trusses	CHS 250x25	0,018	1.318,388	23,298	37.952,180	28,7%	774,534
Total structure	CHS 250x25	0,018	4.586,391	81,048	132.027,549	100,0%	2.694,440

Element	Cross section type	Thickness [mm]	Total usage deck [m ²]	Weight per [m ²]	Total weight	Weight percentage [%]	Weight per meter [kg/m]
Type 1 bridge deck	Infracore	160,000	166,845	95,000	63.401,100	71,4%	1.293,900
Type 2 bridge deck	Infracore	77,000	141,120	45,000	25.401,600	28,6%	518,400
Total bridge deck	Infracore	-	307,965	-	88.802,700	100,0%	1.812,300

Table 43: Total weight of the bridge structure, the main load bearing system elements and the bridge decks.

11.2.2 REACTION FORCES IN THE SUPPORTS DUE TO ALL LOAD COMBINATION CASES

The following table shows the minimum and maximum reaction forces that occur in the 8 supporting nodes at the two ends of the bridge due to the envelope of all combination load cases as described in [ch.6.6]. To clarify the position of the individual support nodes, the picture of the support conditions is again added here [ch. 8.5] alongside with the node numbers that are used in the table.

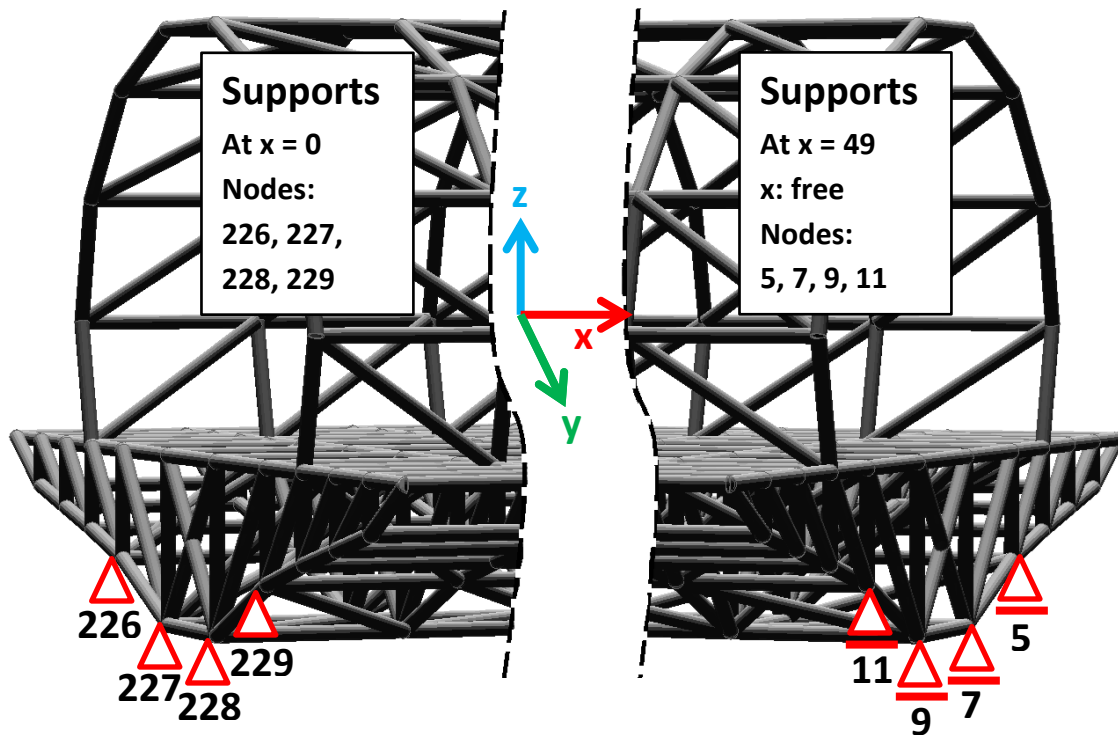


Fig. 159: Support conditions of the full-FRP bridge design with FEM node numbers

Node	Min. F_x [kN]	Max. F_x [kN]	Min. F_y [kN]	Max. F_y [kN]	Min. F_z [kN]	Max. F_z [kN]	Min. $ F $ [kN]	Max. $ F $ [kN]
226	-183,8	1.067,0	677,8	1.626,0	688,8	1.793,0	968,2	2.543,0
227	634,2	1.499,0	-403,7	597,9	63,5	304,7	684,3	1.527,0
228	22,4	891,1	-700,9	506,9	-219,8	118,2	446,8	990,5
229	-2.922,0	-1.110,0	-2.583,0	-1.206,0	488,5	1.667,0	1.841,0	4.170,0
5	0,0	0,0	970,0	2.073,0	861,0	2.089,0	1.297,0	2.943,0
7	0,0	0,0	-800,7	-92,1	-134,4	88,8	130,9	805,6
9	0,0	0,0	-619,5	150,8	-83,9	100,5	35,5	625,2
11	0,0	0,0	-1.440,0	-483,6	344,1	1.557,0	593,5	2.121,0

Table 44: Minimum and maximum reaction forces in the supports due to the envelope of all load combination cases CC1-CC8.

In this research no further detailed design of the bridge supporting structure is carried out. It is evident however that the supporting structure needs to be able to transfer the reaction forces to the foundation. From the above table it can be read that the forces can reach substantial values, such that abundant measures have to be taken. The supporting structure needs to be able to take up tensile forces as well as compressive forces in every x-, y-, z-direction.

Below two possible substructure layouts are given. Note that these have not been worked out at all, and act as in impression only. The first substructure could be made of concrete and is a monolithic structure. The second substructure could be made of structural steel or even FRP composite. This structure has a truss layout, which could possibly suit the layout of the main load bearing structure better.

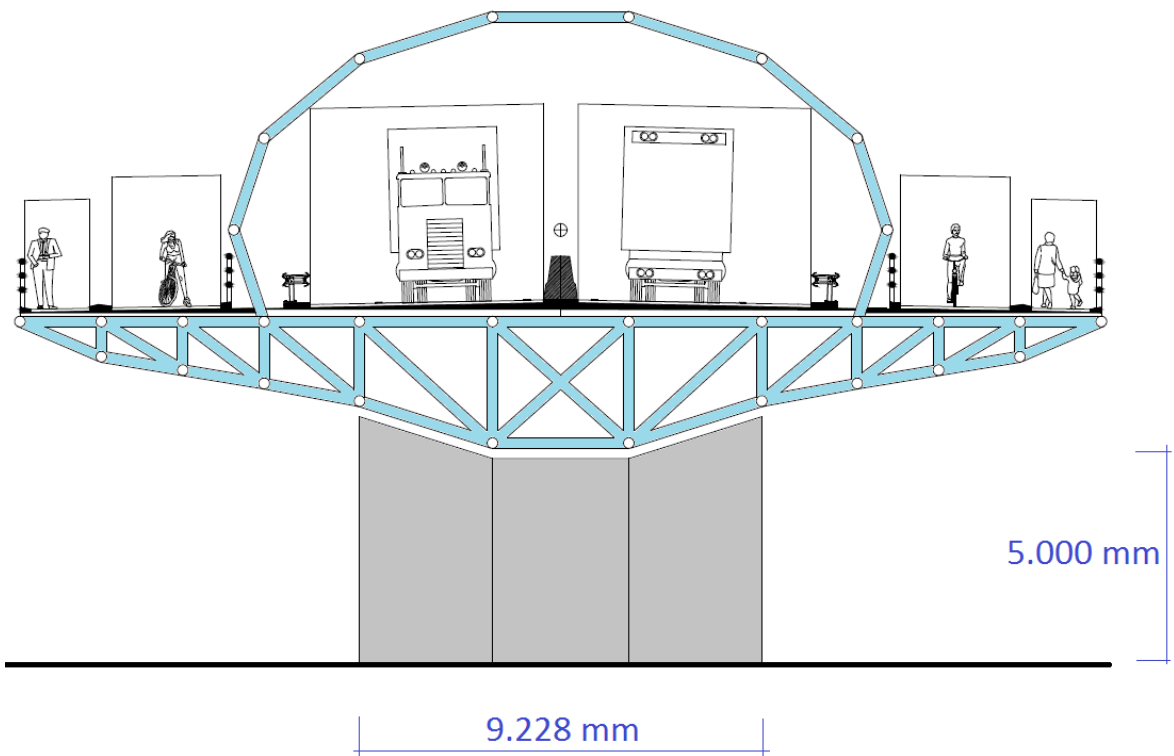


Fig. 160: The first possible bridge substructures, single pillar made of concrete.

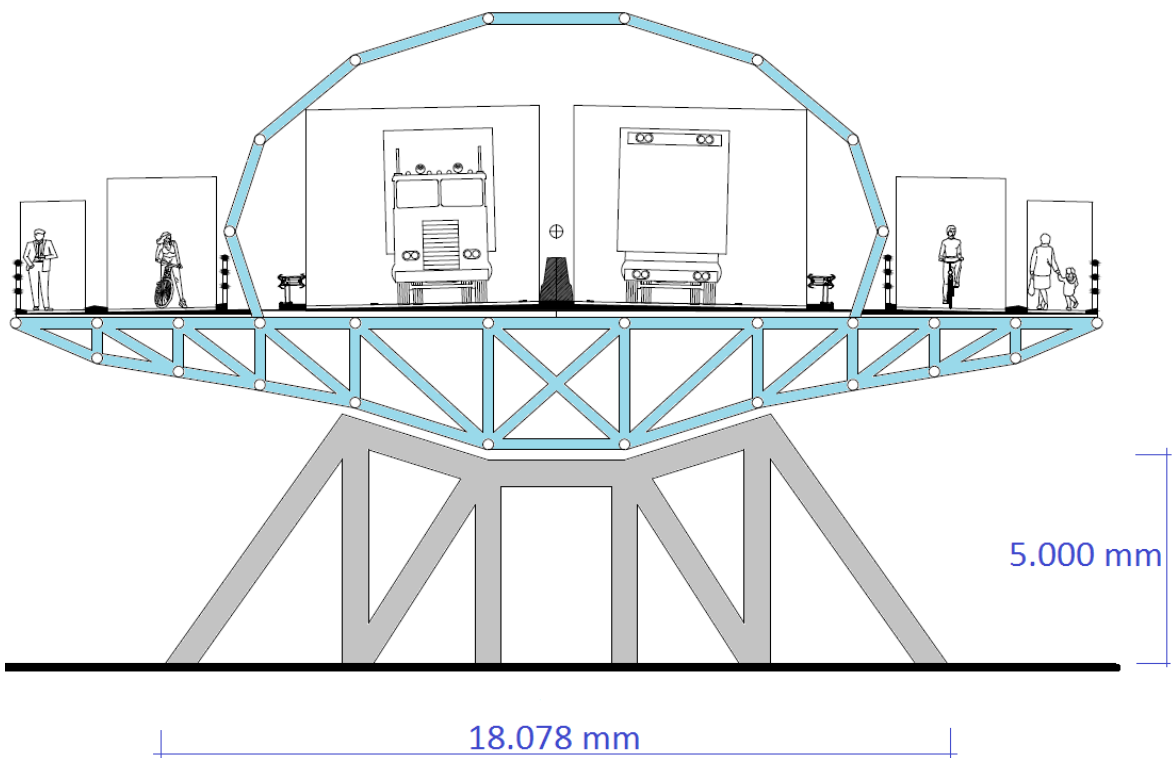


Fig. 161: The second possible bridge substructures, truss structure made of steel or FRP material.

11.3 DURABILITY & SUSTAINABILITY

During the literature research it became evident that a lot of different information on the sustainability and durability of fiber reinforced polymers is available. However to make sound estimates on the environmental impact of FRP materials exact and reliable data is needed. Since particularly the sustainability research is a constantly moving and changing field of science it is very hard to obtain reliable and recent data on the sustainability of fiber reinforced plastics. It was therefore chosen not to make any calculations on the material depletion, CO₂ emission and other greenhouse gas emissions.

The information that was derived in the literature study [LS, ch. 7.5, p218] should give a good first glimpse of the sustainability of fiber reinforced polymers in general. Furthermore papers like that of R. Daniel of Rijkswaterstaat 'R. Daniel': (2003); Environmental Considerations to structural material selection for a bridge; Paper European Bridge Engineering Conference, March 2003' [P104] yield good methods to investigate the natural resources depletion and pollution of the environment. However, these papers have to be used with care since the parameters used are bound to change in a matter of months or single years.

Here some small final remarks on the durability will be made. When currently constructing bridges in the Netherlands one is always asked to deliver structures with a design life of at least 100 years. For traditional materials such as concrete and particularly steel this often calls for costly and inefficient maintenance plans for the whole design life. The big durability advantage of FRP that was already described in the literature study [LS, ch. 7, p215] is of a very high value in this aspect. When the following measures are taken the durability of quality engineering plastics such as the used high fiber ratio carbon/epoxy can definitely enable a design life of 100 years:

- The use of mass-produced pultruded elements increases the quality of the composite and thereby also increases the durability of the bridge
- Use of suitable gel coat for durability
- Make sure that the used gel coat is of sufficient thickness
- Make sure that the used gel coat is compatible with the filler and intumescent coating used for the fire resistance
- Use of UV-resistant matrices such as the used epoxy matrix material.

11.4 COST ESTIMATION FOR THE FULL-FRP BRIDGE DESIGN

In the literature study [LS, ch. 9, p227] some information on the costs of fiber reinforced polymers as structural material for civil engineering applications was already given. Since this research was not aimed at producing a highly economical solution to span an arbitrary highway but was intended in investigating whether a full-FRP heavy traffic bridge structure in a particular shape was structurally possible the cost of the structure is only of secondary importance.

That is also the reason why in this research only a very rough assumption of the costs will be made. This estimation will be made on a price per kg of carbon/epoxy material that was derived from the 'Design Study Of FRP alternative to the Millennium Bridge in London' as described in the literature study [LS, ch. 9.1.2, p228] [A33]. This design study was carried out by David Kendall of 'White Young Green Consultants Ltd.' and published by the UK-'National Composites Network' in 2006.

In this feasibility study a carbon fiber alternative for the 'Millennium Bridge' was derived, having only one span of 330m, compared to the original 3 spans of 81m, 144m and 108m. The new carbon fiber bridge would have a total superstructure weight of 210 tons and therefore could be lifted into place from temporary barges in one single piece. The CFRP Bridge would consist of a very flat arch made of a single,

stiffened box girder with varying depth from 7m at the supports to 3m at the mid-span. The width of this half-circular cross section varies from 12,5m to 5,9m at mid-span. The table below shows the cost estimation as already described in the literature study. The most important value in this table is in the row that is highlighted in blue. This price per kg carbon fiber reinforced polymer will be used for the derivation of a very rough estimate of the price of the full-FRP final design.

Note that this price is based on a single study only which was conducted in 2006. The price given here reflects the price-level of 2006 only.

Costs in EUR	CFRP alternative
Superstructure	13.625.500
Abutments	3.206.000
Installation and transportation	1.603.000
Design and engineering	2.404.500
Dampers	1.603.000
Total Cost [€]	22.442.000
Weight [kg]	220.000
Price per kg [€/kg]	102,00

Table 45: Price per kg CFRP determination on the basis of a CFRP alternative to the London Millennium pedestrian bridge (price level 2006) [LS, ch. 9.1.2, p228] [A33, p5]

In the table below the values for the full-FRP final design bridge structure total weight, load bearing structure weight and bridge deck weight that were derived in [ch. 11.2.1] are recalled. Combining these weight values with the rough price per kg CFRP that was used for the project described before, yields an estimate of the total cost of the full-FRP elliptical truss heavy traffic bridge. This estimate is again very rough, based on the price per kg derived from a single study from 2006 and was added for informative purposes only. Note that the price level of particularly the bridge deck will most probably be lower than the 2006 estimate due to the commercial developments in this field, see also [ch. 11.1.5].

Element	Weight [kg]	Price per kg [€/kg]	Price [€]
Load bearing structure	132.027,55	102,00	13.466.809,98
Bridge deck	88.802,70	102,00	9.057.875,40
Total	220.830,25	102,00	22.524.685,38

Table 46: Rough cost estimation for the full-FRP heavy traffic elliptical truss bridge (price level 2006)

12. COMPARISON OF THE FULL-FRP BRIDGE TO AN EXISTING STEEL STRUCTURE

Initially an important reason for the choice of fiber reinforced polymers as structural material was the expected added value of this material compared to traditional structural materials such as concrete and foremost steel. In this chapter the full-FRP design is compared to an existing elliptical truss bridge that was constructed in steel. By comparing the two structures in terms of structural behavior, material usage and constructability an accurate estimate of the real added value of the FRP design can be made.

The steel structure that was chosen for the comparison is the 'Light rail Viaduct Beatrixkwartier' in The Hague, The Netherland. This structure was already covered as case study in the literature study [LS, ch. 6.1.3, p192] and used for the choice on bridge deck layout variant [ch. 5.2] [ch. 5.2.6]. Following the descriptions given there, here more detailed drawings on the geometry and layout of this bridge are presented. The two drawings below give all important dimensions that are needed to model this structure in the FEM/FEA package 'Oasys GSA'. The material for all section is S235 structural steel. The drawings were obtained from the project architect: 'Zwarts & Jansma'.

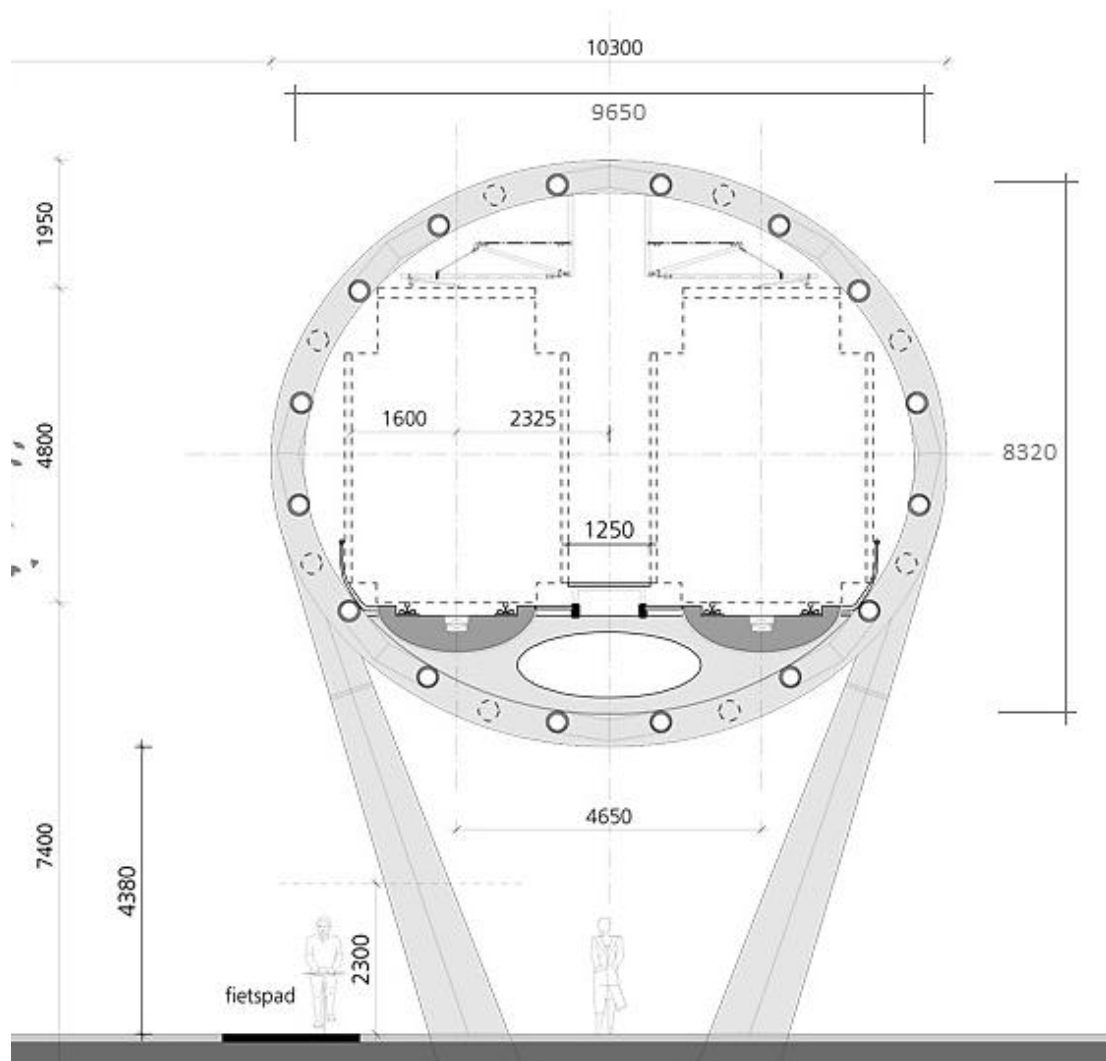


Fig. 162: Cross Section of the 'Light rail Viaduct Beatrixkwartier' [Zwarts & Jansma Architects]

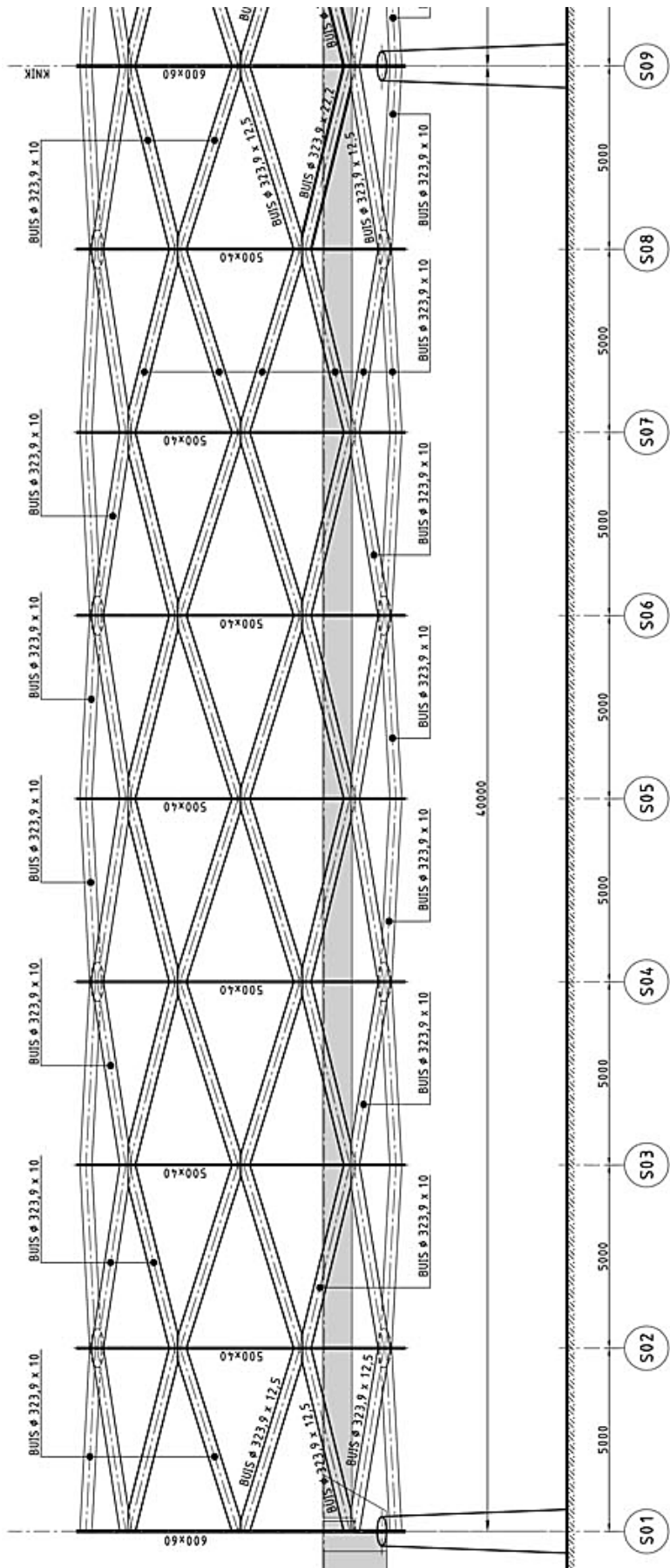


Fig. 163: Side view of the 'Light rail Viaduct Beatrixkwartier' [Zwarts & Jansma Architect]

Knowing all dimensions of the 'Light rail Viaduct Beatrixkwartier' in The Hague, The Netherlands the complete structure was modeled in 'Oasys GSA'. An important remark to be made here is that the 'The Hague viaduct' features two different types of spans, one of 40,0m and one of 50,0m. Both span types were modeled. Next to that, the original design features two large concrete girders on which the light rail tracks run. Because no information on the reinforcement and/or pre-stress of these girders is available, they were modeled as CHS 324x22mm steel elements, the heaviest cross section used in the 'Zwarts & Jansma' design. To give an impression of the finished FE-model of the 'Light rail Viaduct Beatrixkwartier' in comparison to the full-FRP elliptical design, digital drawings of both structures are shown below. Note that the full-FRP elliptical design was modeled without the cantilever truss. That way the behavior of the bridges can be better compared, as all loads are placed within the elliptical perimeter.

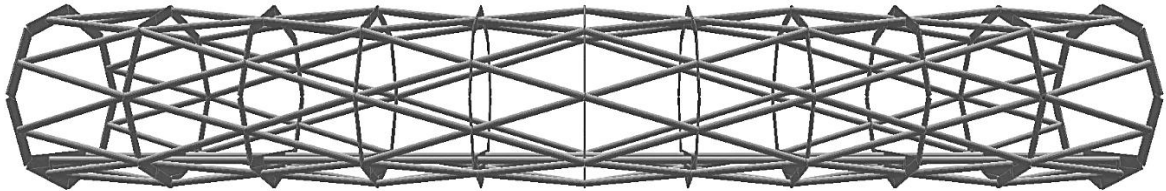


Fig. 164: FE-model of the 'Light rail Viaduct Beatrixkwartier'

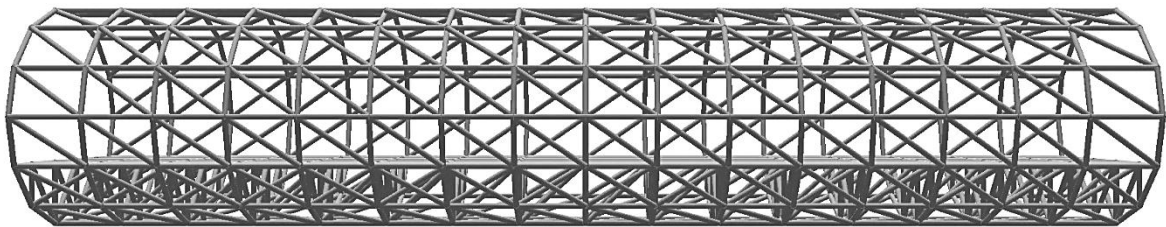


Fig. 165: FE-model of the final FRP design with inner bridge deck only

For the comparison of the structural behavior of the two structures, again three different load cases were used. The load cases are described below. Since both structures were originally designed for different load conditions (light rail traffic vs. heavy road traffic) arbitrary loads had to be found, for which a detailed and fair comparison of the two structures would be possible. Next to that a load case is added (LC4) in which all structures undergo the light rail design loads, as described in [ch. 6.8].

- **LC1:** Self-weight only
- **LC2:** Two line loads of 20kN/m each
- In the case of the 'Light rail Viaduct Beatrixkwartier' these line loads are placed longitudinally at the place of the light rail tracks. For the final FRP design they were placed on the two most central longitudinal bridge deck supporting beams.
- **LC3:** 2 point loads of 500kN each
- These loads were placed mid-span on the same beams as for LC2.
- **LC4:** Light rail loads as described in [ch. 6.8]
- The 16 point loads of 57,5kN per driving direction loads were placed mid-span.

12.1 COMPARISON OF STRUCTURAL BEHAVIOR

In this chapter the structural behavior of both structures will be compared, following the FE-analysis that was performed on the all FRP final design and the two spans of the ‘Light rail Viaduct Beatrixkwartier’. In the following table and graph the results on the deformations are presented. Both spans of the ‘The Hague Viaduct’ are separately covered.

Note that the deformations of all structures lie comparably close to each other. The deformation of the all FRP design lies between that of the 40m and 50m span of the ‘The Hague Viaduct’ for all load cases as well as for the summation of all load cases. Note that particularly the deformation results for LC3 (two point loads) are very much in favor of the full-FRP variant. The reason for this lies in the fact that this design features a very good spread of loads due to higher number of members and nodes. In general it can be said that the full-FRP elliptical design yields deformation values that are about 20%-25% lower than that of the ‘Light rail Viaduct Beatrixkwartier’ for equal span and loads.

Variant	LC1 Max. Deformation [mm]	LC2 Max. Deformation [mm]	LC3 Max. Deformation [mm]	LC4 Max. Deformation [mm]	Sum of max. Deformations [mm]
All FRP Design	13,140	20,180	17,560	25,270	76,150
The Hague Viaduct (40m span)	9,055	14,370	19,370	20,080	62,875
The Hague Viaduct (50m span)	16,680	25,250	24,700	31,920	98,550

Table 47: Comparison of maximum deformation for all load cases of the all FRP design and the ‘Light rail Viaduct Beatrixkwartier’

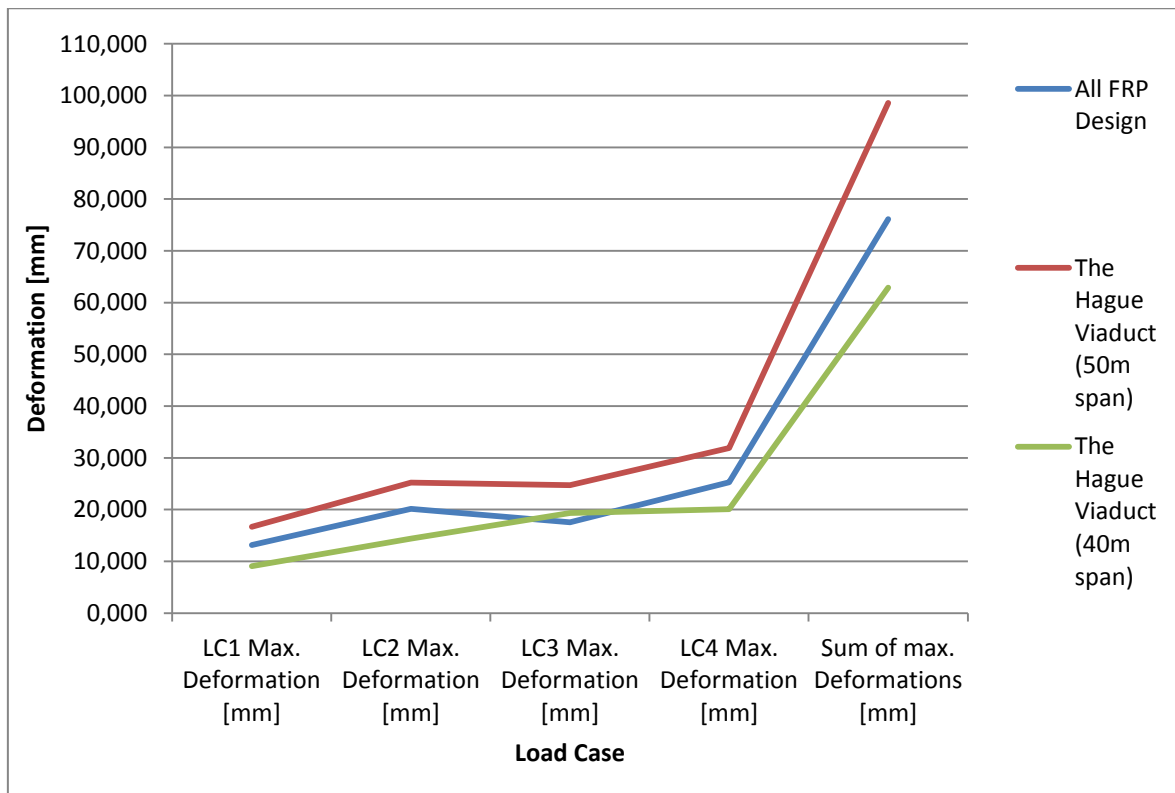


Fig. 166: Comparison of maximum deformation for all load cases of the all FRP design and the ‘Light rail Viaduct Beatrixkwartier’

In the next table and two graphs the results on the occurring stresses in all three structures are presented. All structures share the outcome that the maximum stresses are well within the bounds given by the material tensile- and compressive strength. However, the axial strength values of the carbon-epoxy-FRP material used are much higher than that of steel (tensile strength of UD-reinforced carbon/epoxy:

1173,50N/mm² [ch. 3.4] compared to tensile strength of S235 steel: 235 N/mm²). It can therefore be concluded that loading ratio is much smaller for the FRP Bridge.

Furthermore the full-FRP final design features lower stress values than the ‘The Hague Viaduct’ for all load cases as well as the sum of the load cases. The only exception is LC2, where the ‘The Hague Viaduct’ 40m span yields a slightly lower tensile stress. The full-FRP design yields lower stresses than the 50m span of the ‘The Hague Viaduct’ for all load cases as well as the sum of the load cases.

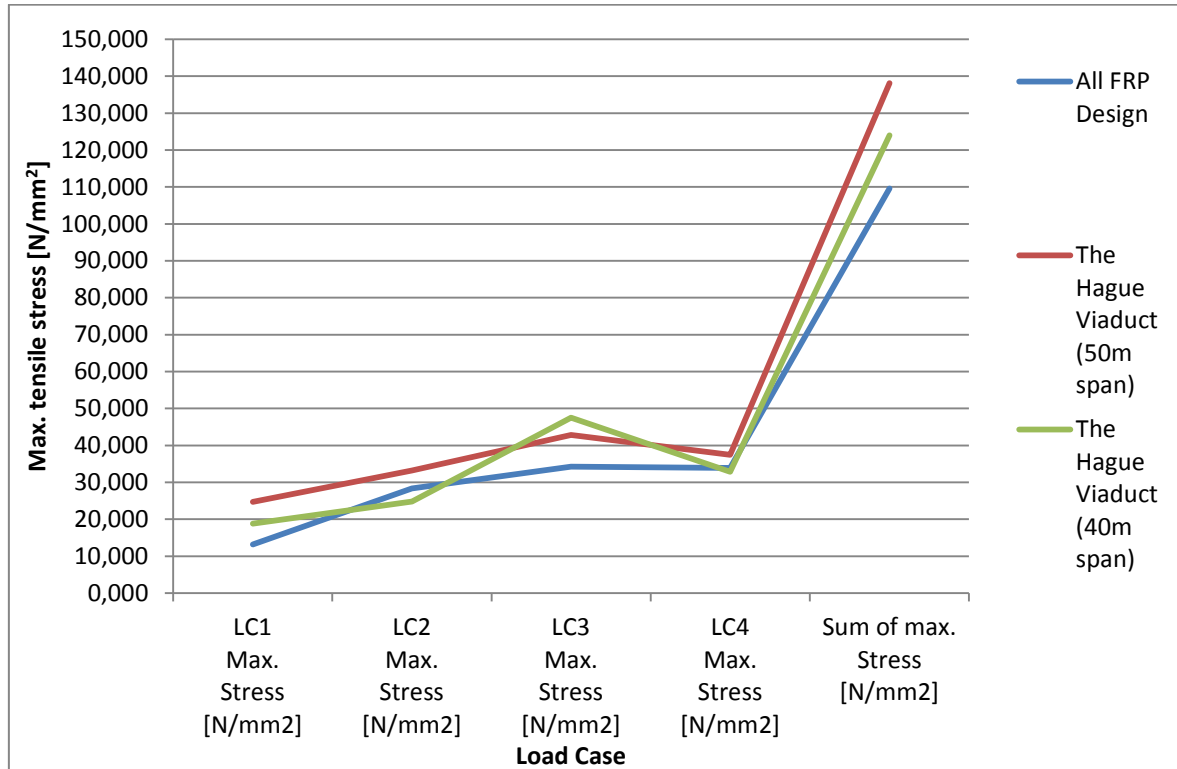


Fig. 167: Comparison of max. tensile stresses for all load cases of the all FRP design and the ‘Light rail Viaduct Beatrixkwartier’

Tensile stress	Variant	LC1 Max. Stress [N/mm ²]	LC2 Max. Stress [N/mm ²]	LC3 Max. Stress [N/mm ²]	LC4 Max. Stress [N/mm ²]	Sum of max. Stress [N/mm ²]
	All FRP Design		13,180	28,330	34,260	33,870
The Hague Viaduct (40m span)		18,830	24,780	47,480	32,890	123,980
The Hague Viaduct (50m span)		24,680	33,190	42,840	37,460	138,170
Compressive stress	Variant	LC1 Max. Stress [N/mm ²]	LC2 Max. Stress [N/mm ²]	LC3 Max. Stress [N/mm ²]	LC4 Max. Stress [N/mm ²]	Sum of max. Stress [N/mm ²]
	All FRP Design		15,360	29,380	19,160	33,560
The Hague Viaduct (40m span)		23,430	34,590	32,270	46,810	137,100
The Hague Viaduct (50m span)		32,980	48,240	35,290	54,480	170,990

Table 48: Comparison of maximum tensile- and compressive stresses for all load cases of the all FRP design and the ‘Light rail Viaduct Beatrixkwartier’

Also, the second graph shows that the maximum compressive stress arising in the full-FRP design is substantially lower than that of the two other structures. Compared to the ‘The Hague Viaduct’ 40m span the maximum compressive stress is about 15% lower and compared to the 50m span of the same bridge the compressive stress is about 30% lower. For an unidirectional reinforced full-FRP structure low compressive stresses are very advantageous since the material behaves more efficient under tension than under compression, see also [ch. 2.1.7] [ch. 2.1.8].

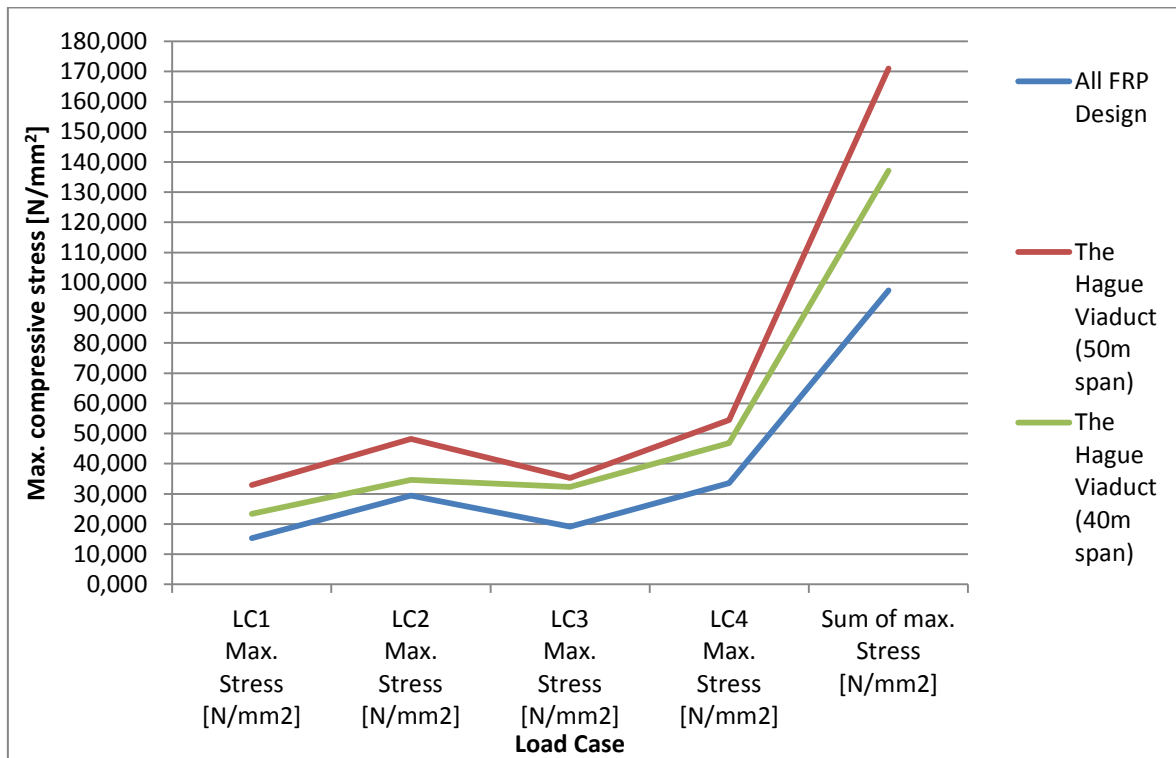


Fig. 168: Comparison of maximum compressive stresses for all load cases of the all FRP design and the ‘Light rail Viaduct Beatrixkwartier’

12.2 COMPARISON OF GEOMETRIC PROPERTIES AND MATERIAL USAGE

In this chapter the non-structural properties of the three structures are considered. In the following table the geometric properties, such as number of elements and nodes, length of the elements and the order of the nodes are given.

Variant	# nodes	# elements	Shortest element [m]	Longest element [m]	Max order of nodes
All FRP Design	323	1.069	1,825	4,447	10
The Hague Viaduct (40m span)	162	342	0,609	5,318	6
The Hague Viaduct (50m span)	198	422	0,609	5,318	6

Table 49: Geometric properties of the full-FRP design and the ‘Light rail Viaduct Beatrixkwartier’ with 40m and 50m span

The next table shows several important parameters on the total material usage: The number of different cross section types used, the total length of all structural members combined, the total volume of structural material, the total weight of the structural material used and the weight of the structures per meter span. The most important difference between the steel- and FRP- structure is the much lower weight that the FRP structure has. Compared to the FRP structures, which weighs about 91 tons, the total weight of the steel structures is about 1,5x times higher for the 40m span (133 tons) and about 1,8x times higher for 50m span (158 tons). Because the full-FRP structure has a span of 49m, the larger steel span can best be compared.

When the weight of the bridges per meter span is considered, it becomes even more evident how light the full-FRP structure really is. The full-FRP design has a weight of only about 1.850 kg/m, compared to the steel structure weight of 3.300kg/m (40m span) and 3.150kg/m (50m span). Expressed in a percentage, the FRP Bridge is about 40% lighter than the steel bridge.

Variant	Types of cross section	Tot. length cr. section [m]	Total vol. material [m ³]	Tot. weight material [kg]	Weight per m span [kg/m]
All FRP Design	1	3.268,003	57,750	91.361,101	1.864,512
The Hague Viaduct (40m span)	5	1.111,374	16,892	132.603,719	3.315,093
The Hague Viaduct (50m span)	5	1.354,826	20,055	157.433,658	3.148,673

Table 50: Material usage of the full-FRP design and the 'Light rail Viaduct Beatrixkwartier' with 40m and 50m span

12.3 MODAL ANALYSIS

In this chapter a quick comparison of the different natural frequencies of the structure is made. Here only the 50m span of the 'Light rail Viaduct Beatrixkwartier' is compared to the full-FRP design with inner truss only. Next to the comparison of the steel variant to the full-FRP variant, it is also interesting to see how the natural frequencies of the full-FRP change when the cantilever truss is not present.

First, the three first modes of the 'Light rail Viaduct Beatrixkwartier' are given; the first mode is a vertical mode at 4,30Hz, the second mode is a horizontal mode at 5,018Hz and the third mode is a torsional mode at 7,419Hz.

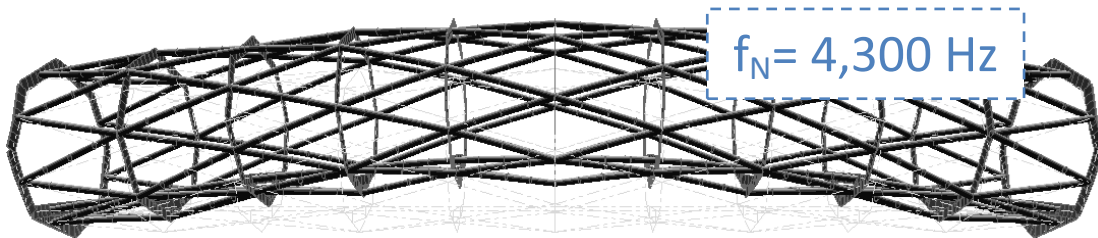


Fig. 169: Mode 1 of the 50m span of the 'Light rail Viaduct Beatrixkwartier' : The first vertical mode. The complete structure deforms in z-direction at a natural frequency of $f_N = 4,300$ Hz.

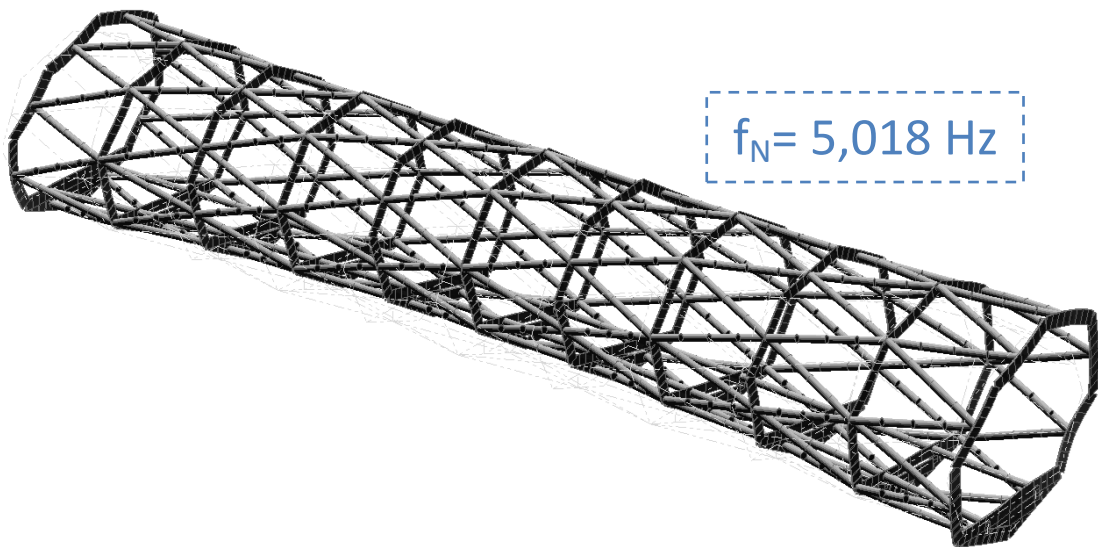


Fig. 170: Mode 2 of the 50m span of the 'Lightrail Viaduct Beatrixkwartier': The first horizontal mode. The complete structure tilts in y-direction at a natural frequency of $f_N = 5,018$ Hz.

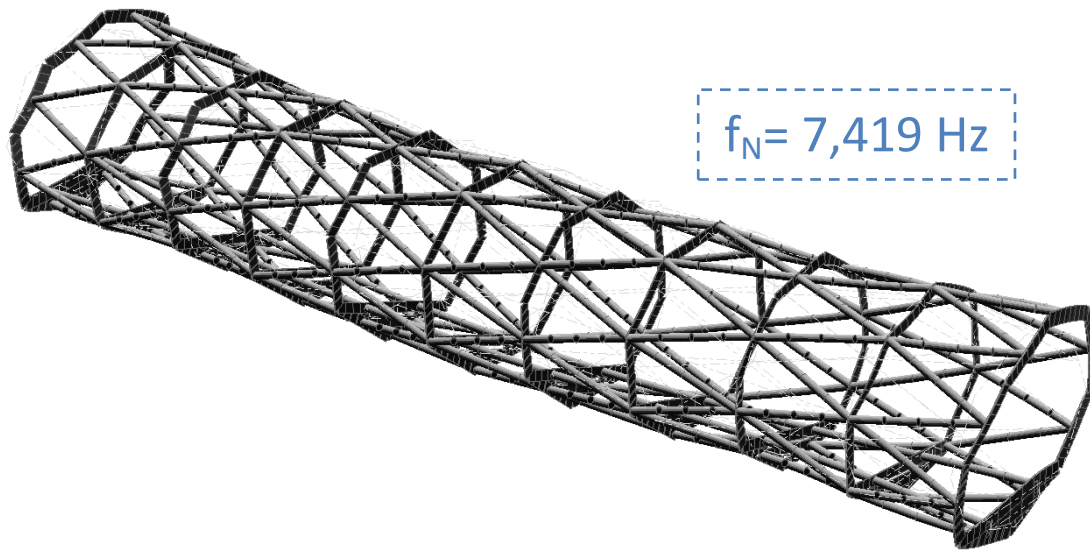


Fig. 171: Mode 3 of the 50m span of the ‘Lightrail Viaduct Beatrixkwartier’: The first torsional mode. The complete structure twists along the x-axis at a natural frequency of $f_N = 7,419$ Hz.

In the following the first three modes of the full-FRP structure with inner truss only are given. Here the first mode is a horizontal mode at 3,522 Hz, the second mode is a vertical mode at 5,596 Hz and the third mode is a torsional mode at 7,475Hz.

Particularly the third mode is very similar for both the steel and the full-FRP structure. The first vertical mode lies at higher natural frequency for the full-FRP bridge design, wherein the first horizontal mode lies at lower natural frequency for full-FRP bridge design.

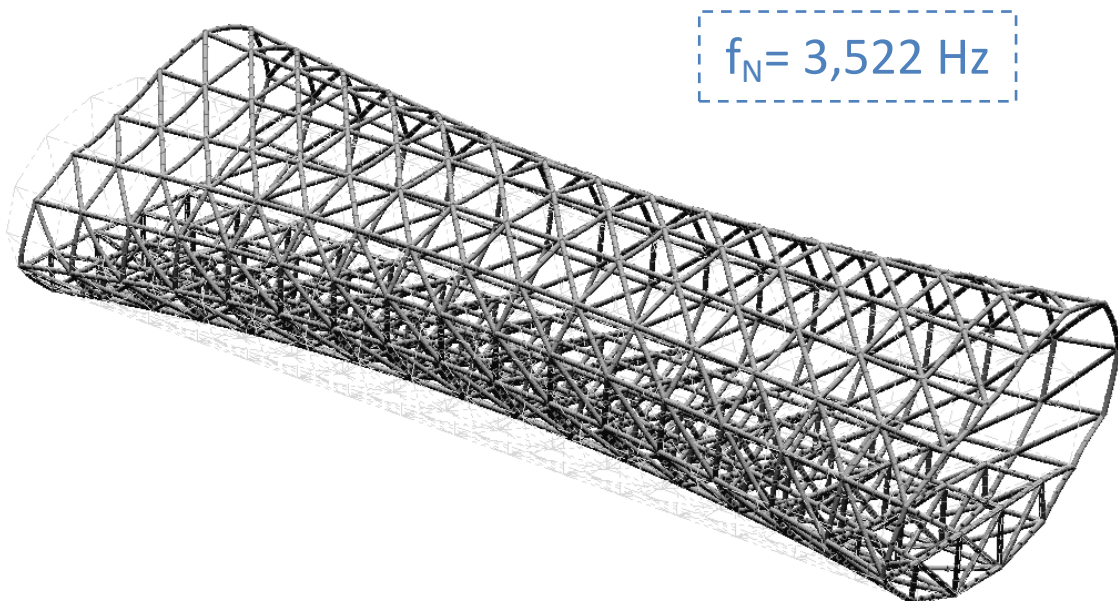


Fig. 172: Mode 1 of the full-FRP bridge design with inner truss only: The first horizontal mode. The complete structure tilts in y-direction at a natural frequency of $f_N = 3,522$ Hz.

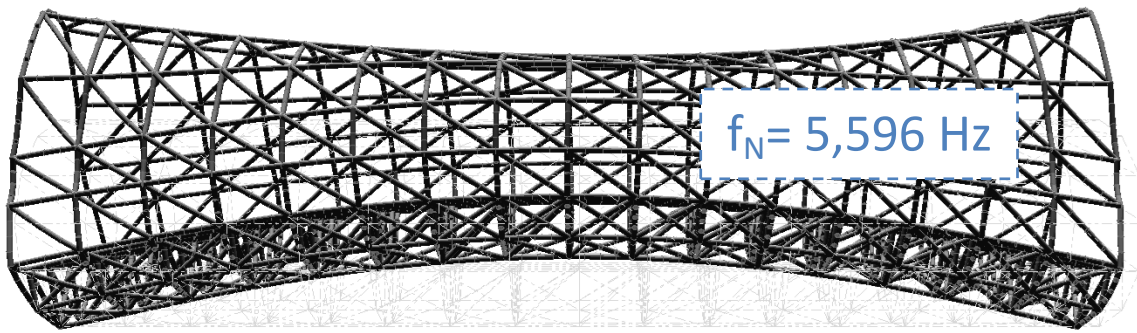


Fig. 173: Mode 2 of the full-FRP bridge design with inner truss only: The first vertical mode. The complete structure tilts deforms in z-direction at a natural frequency of $f_N = 5,596$ Hz.

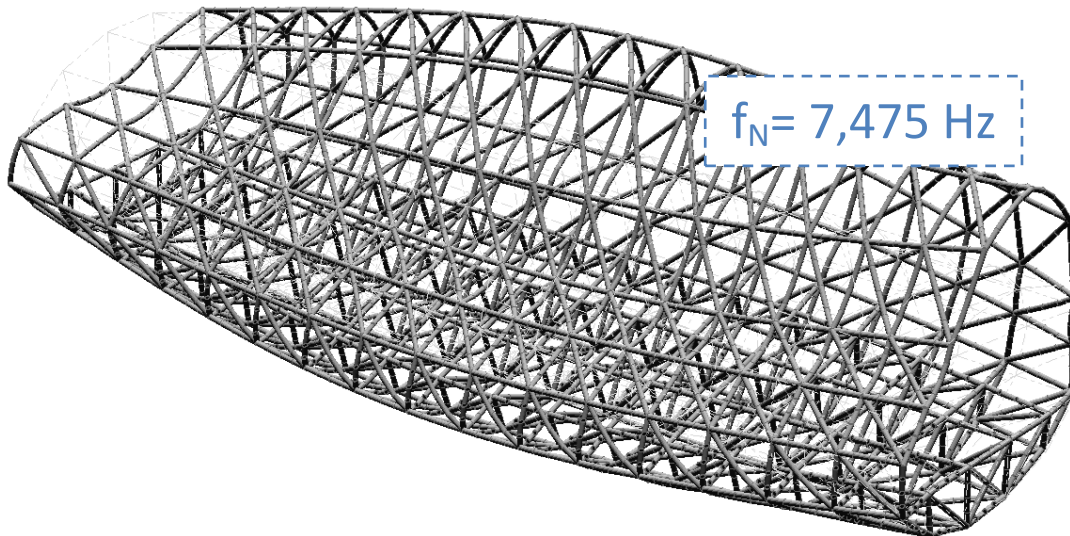


Fig. 174: Mode 3 of the full-FRP bridge design with inner truss only: The first torsional mode. The complete structure twists along the x-axis at a natural frequency of $f_N = 7,475$ Hz.

Comparing the natural frequencies of the full-FRP bridge design with [ch. 9.4] and without the cantilever truss as well as the 50m span of the ‘The Hague Viaduct’, it becomes clear that the cantilever truss has a slightly detrimental influence on the natural frequencies of the full-FRP bridge. The first vertical natural frequency decreases about 10% by the addition of the cantilever truss, the first torsional natural frequency even decreases about 15% by the addition of the extra truss. The first horizontal natural frequency only decreases about 5% due to the cantilever truss. However, as already stated in [ch. 9.4], the final design with cantilever truss also fulfilled the frequency limit requirements. The ‘Light rail Viaduct Beatrixkwartier’ does meet the horizontal and torsional frequency limit; however it does not meet the human induced frequency limit for vertical vibration. Most probably this is because this bridge was not designed for the use by pedestrians.

	Full-FRP bridge with cantilever truss	Full-FRP bridge without cantilever truss	The Hague Viaduct 50m	Human induced frequency limit [Hz]	Wind induced frequency limit [Hz]
Vertical	5,072	5,596	4,300	>5,00	
Horizontal	3,502	3,522	5,018	>2,50	>1,00
Torsional	6,380	7,475	7,419	>2,50	>1,00

Table 51: Comparison of the natural frequencies of the full-FRP structure with and without cantilever truss as well as the 50m span of the ‘Light rail Viaduct Beatrixkwartier’.

12.4 CONCLUSION ON THE COMPARISON OF FULL-FRP AND STEEL CYLINDRICAL TRUSS BRIDGES

After having compared the full-FRP bridge with the existing steel bridge is clearly evident that both structures show a very similar behavior. The overall deformations for all used load cases are within a 15% margin. However, the deformations of the full-FRP bridge are lower for almost all load cases, therefore giving this bridge design a slight advantage. To be fair one must also consider the different loading types both bridges were designed for. The 'Light rail Viaduct Beatrixkwartier' was designed for a light rail load [ch. 6.8] and the full-FRP bridge was designed for a much heavier traffic load, 'Load Model 1' as described in [ch. 6.2.1]. That is also part of the reason why the deformation behavior of the full-FRP bridge is better than that of the steel bridge.

The same holds for the maximum axial stress that occur in the structures, particularly the compressive stresses in the full-FRP bridge design are clearly lower than that of the steel structure. As described earlier, this is a real advantage for fiber reinforced structure because the tensile loading is much more favorable for this kind of material.

The modal behavior of both structures is also very similar. Since normally heavy structures show a better vibration behavior this might surprise a little bit; especially because the vibration behavior of the lighter full-FRP bridge is even noticeably better than that of the steel bridge.

This also shows another big advantage of the full-FRP structure: the total weight. The weight per meter span of the steel bridge is 3.150kg/m (for the 50m span), whereas the full-FRP bridge only weighs 1870kg/m, which is only 60% of the steel bridge. For a bridge that behaves stiffer than the steel bridge and can handle much larger loads, this is a very impressive property, which in itself should be reason enough to consider FRP as a really competitive structural material for medium span heavy traffic bridges.

However the comparison of the two bridge types also showed some drawbacks of the full-FRP design. Perhaps the biggest fact to be pointed out is the high number and order of nodes of the full-FRP bridge. With 323 nodes it features about 60% more nodes than the steel competitor which only has 198 nodes. The maximum order of nodes of the full-FRP design is with 10 also substantially higher than that of the steel design with maximum 6. This makes the fabrication of the FRP connections certainly more complex, costly and time consuming than that of the steel connections. Certainly also because there is a lot more experience with the fabrication of high order CHS-connections in steel than in FRP material. However the low weight of the FRP sections and connections could also be advantageous for the FRP fabrication.

The general shape of the bridge that both design share is a far more complex shape than a typical girder bridge. Therefore the construction of both bridges is far more complicated for these types of bridges. For the 'Light rail Viaduct Beatrixkwartier' an on-site prefabrication tactic was chosen for the construction of the bridge, wherein a large prefabricated parts were brought by truck to special assembly tents right next to the final position of the structure. In the tents the prefabricated parts were assembled to form the complete elliptical truss load bearing structure. These elements were then hoisted into place onto the concrete pillars that were already erected.

There is no reason why an full-FRP structure such as designed in this research could not be fabricated in a similar way as the 'The Hague Viaduct'. Therefore it can be concluded that overall, the full-FRP design is as constructible as the steel design, perhaps only with some slight disadvantages in the (pre-) fabrication of the connections.

13. CONCLUSION & RECOMMENDATIONS

In this chapter the results of the feasibility study on the design of a fiber reinforced polymer cylindrical truss bridge for heavy traffic will be discussed. This chapter is split into two parts: the conclusion will provide feedback and answers to the initial research objective and -questions as described in [ch.1.2] [ch.1.3]. Secondly, this chapter will offer a number of recommendations for future research in fields where this feasibility study can be extended and further improved.

13.1 CONCLUSION

Having concluded this feasibility study and recalling the initial research objective, displayed again below, leaves the question whether this objective could be met or not?

“Analysis on the structural feasibility of a cylindrical truss bridge design with a superstructure made up completely of fiber reinforced polymers. This bridge has to withstand heavy traffic loads and remain structurally safe under fire and heat loads. The structural design of the cylindrical truss and its members will be the primary research objective.”

First of all, this research showed that fiber reinforced polymers can be used as stand-alone structural material for medium span heavy traffic bridges. Next to that, this research clarified that there is no legitimate structural reason for the fact that fiber reinforced polymers are used so scarcely in the civil- and bridge-engineering industry compared to traditional building materials such as steel and concrete. Furthermore, the research also showed that the ‘new’ cylindrical truss bridge type, which actually is a revived, modern form of traditional square truss bridges is not only an aesthetically very appealing structure but also performs structurally very well when combined with fiber reinforced polymer as structural material. Concerning the used material, this research also showed that it is possible to construct a heavy traffic bridge with FRP as structural material while complying with the known fire safety standards. This part of the research showed that virgin FRP material can be adapted by several fire-protection measures that drastically increase the fire resistance and thereby make the bridge sufficiently resistant against fire- and heat-induced damage. In the following the conclusion of the three parts of this research are given in more detail.

13.1.1 PART A – MATERIAL PROPERTIES & FIRE SAFETY

Going into more detail on the used material, this research has shown that of all investigated FRP composites medium modulus carbon epoxy is most suitable for the application in high strength/high stiffness applications such as bridge engineering. Following a comparison on the best calculation procedures for unidirectional reinforced composites the Hashin-Shtrikman approach combined with the law of mixtures was chosen as preferred method to calculate the mechanical properties of composite materials. A number of different matrix- and reinforcement-combinations were compared for high fiber contents in excess of 60%. This yielded carbon/epoxy as most suitable FRP composite. The reason for this lies in the high longitudinal modulus of elasticity and strength of carbon fiber reinforcements and the overall high strength and durability of epoxy resins. The design values of strength and stiffness of the unidirectional reinforced composite were calculated using the Dutch CUR96+ approach.

Because the bridge type was already defined in the research objective, it is known the bridge consists of truss elements only, which are joined by connection elements. The most convenient cross section type for the truss elements was found to be the circular hollow cross section. For these truss elements, the most suitable production method considering fiber content, cost and precision amongst others was found to be the pultrusion process. For the connection elements, which were not of the main interest in this study, CNC-assisted filament winding was chosen as production method.

In the next step, a literature study and -research on the fire safety properties of plastic composites in general was used to investigate their behavior under fire and heat. This study showed the weaknesses of various different virgin FRP composites under fire- and heat-load. A number of different strategies, both passive and active, for the improvement of the fire resistance of FRP composites were derived from this study and the most suitable strategies were applied in the bridge design. This yielded a combination of an intumescent gel coating and a low volume phosphorous filler system for the carbon epoxy composite. Using this combination, the full-FRP bridge could guarantee a fire resistance class of R30 for the most severe design fire scenario: the hydrocarbon fire curve.

13.1.2 PART B – DESIGN STUDY & PARAMETER STUDY

Since the general shape of the bridge had already been defined in the research objective the next logical step was to investigate the spatial demands of all bridge users. Keeping the Dutch requirements of trucks, cars, bicyclists and pedestrians in mind, several bridge deck layout variants were generated and compared considering the space efficiency and material usage. It turned out that a relatively small elliptical cross-section, which only housed one heavy traffic lane per driving direction, combined with two lateral cantilevers which house the lighter traffic is the most economical choice. One great advantage of this layout is the logical separation of light, slow and vulnerable traffic from the heavy and fast traffic by the main load bearing truss itself. Furthermore it was also chosen that the bridge had to span a typical 2x4 Dutch highway in a single span.

Next to the dimensions of the bridge, the design loads that have to be applied on the bridge were another important result of the design study. All environmental- and traffic-loads prescribed by the Eurocode were summarized and combined to yield load cases and load combination cases for the final design of the bridge. Furthermore a suitable deflection limit for full-FRP bridges was derived from a multitude of relevant scientific papers on this subject.

After having defined the general dimension of the bridge, several truss topology variants were generated for the main load bearing elliptical cross section. These variants shared an equivalent material usage, but differed in in truss layout and grid-height over grid-length ratio. They were generated using a dynamic parametric geometric model in the modeling tools 'Rhinoceros' and 'Grasshopper' by 'Robert McNeel & Associates'. To obtain the most economical truss topology all variants were analyzed by comparing the deflections and stresses due to unity loads, number of elements and nodes as well as the complexity of these nodes. For the analyses the FEM-suite 'Oasys GSA' was used. This initial analysis showed that the deflection of FRP structures is normative, thereby calling for the need of a stiffness driven design. The truss with one diagonal and a square grid turned out to yield the best overall results, just outperforming the triangular grid. It was chosen to continue the parameter study with the square truss with one diagonal topology only.

Knowing the most economical and structurally efficient truss topology, the most efficient grid size for the main load bearing elliptical truss was derived. For this cause several grid size variants with different material usage were analyzed and compared by occurring deflections and stresses in finite element analysis software for a number of load cases which were simplified versions of the actual Eurocode load cases for heavy traffic bridges. An optimum was found between a minimum material usage and simultaneously a minimum deflection, while still meeting the deflection limit.

Following the analysis on the most efficient grid size a similar analysis was performed for the cross section dimensions of the truss members. A number of variants with differing diameters and wall thicknesses were compared by deflections and stresses in finite element analysis and again the most efficient variant was found, meaning the variant with a minimized material usage and simultaneously minimized deflections.

Comparing the initial truss topology that was derived in the design study with the, in terms of grid-size and member cross-section optimized, elliptical truss layout after the parameter study, this research showed that the two optimization steps decreased the overall weight of the main elliptical load bearing truss by about 40%.

13.1.3 PART C – FINAL DESIGN & FINITE ELEMENT ANALYSIS

During the final design stage the optimized main elliptical load bearing truss was fitted with an inner heavy bridge deck supporting structure as well as two cantilever trusses to carry the light traffic bridge deck. These supporting structures were set up as trusses as well and follow the grid layout of the main elliptical truss. In the final design a comparative FE-analysis on the deformation behavior of the main elements of the structure showed that only the combination of main load bearing truss with inner bridge deck supporting truss is able to meet the deflection requirements. Thereby the necessity of both elements is further underlined. Next to that, this analysis also showed that the elliptical truss shape with its large construction height is very suitable as design shape for FRP materials with its -compared to steel- relatively low stiffness values.

The final finite element analysis in 'Oasys GSA' for the complete structure with main load bearing truss, inner bridge deck supporting truss and cantilever trusses was performed for all load cases and load combination cases prescribed by the Eurocode. It turned out that the structure meets the deflection limit for all cases, and that the combination of self-weight with heavy traffic loading and lateral wind load is the normative load case. Furthermore the FE-analysis also showed that the stress levels in the structure are considerably low, even for the normative load case, which further justifies the stiffness driven design method chosen for this research.

Next to that the structure was further analyzed on fatigue behavior, showing that the main load bearing structure of the bridge is able to comply with the design life demands dictated by the Eurocode. For this cause the Dutch CUR96 approach was chosen. Furthermore a modal analysis of the complete bridge structure was carried out in the FEM-software. This analysis showed that the natural frequencies of the main load bearing structure lied within the bounds defined by the Eurocode.

Furthermore an existing full-FRP bridge deck system was used for both decks (light- and heavy bridge decks) of this bridge. The Dutch manufacturer 'Fibercore' provided a suitable sandwich bridge deck solution which was able to comply with the geometric requirements of the supporting truss structure as well as the structural requirements. The proposed 'Infracore' bridge deck system has already been used for a number of projects in the Netherlands and has thereby proven its suitability for heavy traffic bridges with similar or bigger spans.

The stress distribution in two types of connections of the truss elements was analyzed and it turned out that the normative load cases yielded small stress values, which are definitely acceptable when comparing them with the design strength values of the composite. Furthermore the design showed that the vast majority of the connections has an order of six or smaller, meaning that six or less truss members meet at the connection. Although the detailed design of these connections was not the primary objective of this research, several papers were found in which filament wound tee-joints made of glass fiber reinforced polymer were fabricated using computer controlled machines. Considering the recent developments in computer controlled CNC filament winding it is expected that connections with a higher order than three can also be produced using this technique.

The substructure of the bridge was briefly considered, the main load bearing structure was designed in such a way that it is simply supported at four points per side. Such supporting conditions have been used for various bridge structures in the past and this research presents two general possibilities on the layout of these supporting structures.

The designed full-FRP elliptical truss bridge was furthermore compared to an existing steel bridge with a similar design: the 'Light rail viaduct Beatrixkwartier' in The Hague, The Netherlands. The two structures were compared using FE-analysis in 'Oasys GSA' for a number of load cases, including the light rail load, for

which the 'The Hague viaduct' was designed. This comparison showed that the full-FRP structure yielded smaller deformations and stresses for all load cases while weighing only 60% of the steel bridge and providing a considerably larger amount of usable space. Furthermore, the vibration behavior of both structures is very similar; the natural frequencies of both structures were very close to each other.

Finally the costs of the full-FRP bridge were addressed. A price per kg values for carbon fiber reinforced epoxy was derived from a 2006 feasibility study for a CFRP alternative to the 'Millennium Bridge' in London, United Kingdom. The total construction costs of the full-FRP bridge turned out to be substantially higher than that of a conventional structure. However, it has to be said that the durability and sustainability advantages of FRP compared to concrete and steel have not been explicitly considered in this cost estimation. It is expected that the initial cost disadvantage of FRP materials is drastically reduced when the long term costs are considered through life-cycle analysis and the environmental impact is added to this analysis as monetary value.

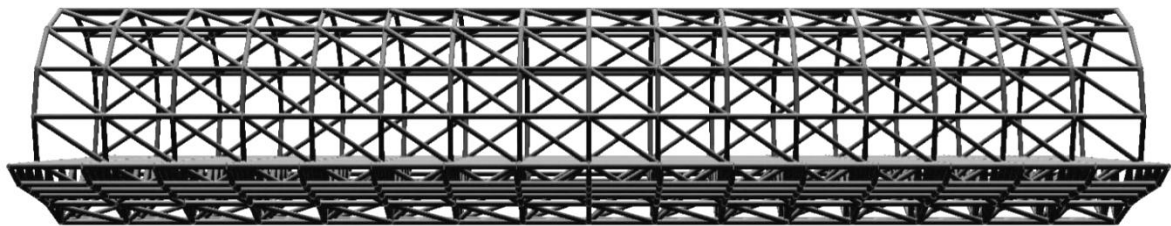


Fig. 175: Side view of the full-FRP bridge structure with main load bearing elliptical truss, inner bridge deck supporting truss and cantilever trusses.

13.2 RECOMMENDATIONS

As described in the chapter before, the main conclusion of this research on the design of a cylindrical truss bridge for heavy traffic is that a structure of this kind is definitely feasible with the use of fiber reinforced polymers only. However during the research a number of points of interest emerged that could or should be further investigated. Most of these points arose from the fact that a master's thesis cannot contain an unlimited amount of information and that choices on the contents have to be made.

In the following a number of topics are given which should receive more attention in future research to provide an even more solid basis for the design of large span full-FRP bridges suitable for heavy traffic.

13.2.1 SHAPE

This research showed that a spatial truss, such as the elliptical truss used here, is a very interesting shape that can also be used for other material than FRP. Recently several, mostly pedestrian, bridges of this kind have been constructed. Since such structural layouts have a great potential in the field of heavy traffic bridges, certainly more research is needed on this particular bridge shape. Traditionally trusses were often used for medium- to long-span bridges in the past. It is imaginable that the modern cylindrical variant of the traditional square truss could grow as popular as trusses at that time. One great advantage of the elliptical shape combined with the cantilever trusses is the logical separation of light, slow and vulnerable traffic from the heavy and fast traffic by the main load bearing truss itself. Little other bridge design shapes exist that automatically provide this advantageous feature.

Furthermore a detailed design of a bridge also features other bridge elements such as the bridge deck, the bearings, the substructure and the foundation, next to the main load bearing structure. In future research these elements should also be designed in more detail to yield a more integrated full-FRP- or even hybrid-FRP-structure.

13.2.2 MATERIAL

One of the main topics of this study is the FRP material itself. This research clearly shows that FRP material deserves much more attention in the civil engineering industry than it currently receives. Although more and more partly FRP bridges are now being constructed, the potential of the material calls for a higher number of applications. In this research only unidirectional reinforced elements were used. Fiber reinforced polymers have the advantage that they can be tailor-made to meet different stress and strain conditions. Usually this is done by applying the reinforcement in several differently orientated layers, or lamellas, thereby obtaining multidirectional reinforced composites. Further research is needed in the field of application of multidirectional reinforced composites in the bridge engineering industry. It is expected that the mechanical properties of multidirectional reinforced composites can fit the stress profile of for example the connection elements much better than unidirectional reinforced composites.

In this research a single cross section type was used for the main load bearing structure. Further research is necessary to show what structural improvements can be achieved when more than one kind of cross section is applied. In comparable steel structures, such as the 'Light rail viaduct Beatrixkwartier' The Hague, The Netherlands, it is often chosen to use different types of cross sections, such as CHS and rectangular cross sections, different wall thicknesses and different diameter or dimensions of similar cross sections. It is expected that the application of different cross sections can further decrease deformations and stresses and/or the material usage in the bridge structure.

Another point of interest is the use of different materials next to fiber reinforced polymers for the construction of similar bridges. Recently more and more hybrid bridges have been developed and installed in the Netherlands; the most recent example being the heavy traffic bridge over the A27, near Lunetten, Utrecht, The Netherlands which uses a sandwich-FRP bridge deck in combination with a steel truss as main load bearing structure. Combining several materials in the construction of heavy traffic could possibly further increase the structural efficiency of the bridge by using the characteristic strengths of each material.

13.2.3 CONNECTIONS

This research showed that when using an elliptical truss structural system a large number of connections is needed. Since connections are usually the most expensive and complex part of trusses, further research is needed into how the number and complexity of the connections can be reduced. One possibility to reduce the complexity of the connections is the fabrication of the inner lateral trusses and the cantilever trusses as a single plate girder element instead of a truss girder. This would reduce the order of the nodes by omitting the lateral and vertical truss elements in the bridge deck.

Another method of decreasing the number and complexity of the connections is further investigation on increasing the cross section dimensions for some elements only, as described in the materials section of this chapter. Thereby the grid size could possibly be increased and the complexity of the nodes could be reduced, because for example in steel, it is easier to fabricate connections of differently sized circular hollow sections.

This shows another point of interest which could be further investigated: the detailed design of the connections. In this research the connections design was only performed briefly. Future research could be focused on the detailed finite element design and -analysis of several types of FRP CHS connections, including the detailed design of laminate lay-up etc. Following this topic, further investigations could also be made on the make-ability of such higher order connections. Previous studies have only shown that filament winding of FRP tee-joints is possible. Since these studies are about 15-20 years old, it is expected that following the introduction of more and more computer controlled filament winding machines, more complex nodes can be produced using this fabrication method. However, this assumption would have to be validated in future research.

13.2.4 FIRE SAFETY

Although the literature study on the fire safety of FRP yielded the desired results, it also showed that a lot more research is needed on the fire safety of FRP structures, especially in the civil engineering industry. A lot of the information found is originally intended for other fields of application, such as the automotive- or aviation-industry. This research showed that FRP materials have a great potential in terms of fire resistance but that more research on FRP specific fire safety improvement methods is needed.

Next to that, the research also showed that very little information is available on the fire safety of bridges in general and even less on bridges with load bearing structures above the bridge deck in specific. Since large fires on the bridge deck have a great influence on the structure above the deck, more research is needed on the possibilities of protecting this structure from fire-induced damage. In fact, a spatial truss bridge lies somewhere in between a tunnel and a bridge. Since for tunnels extensive fire safety researches have been carried out that have even led to the introduction of specific design codes, similar researches should also be carried out for spatial truss bridges such as the elliptical truss bridges that was designed in this study.

13.2.5 CODIFICATION

To propagate the use of fiber reinforced polymers in the civil engineering industry, design codes equivalent to the Eurocode are needed for FRP materials. Currently (2012) the preliminary Dutch design code CUR96 from 2003 is updated and extended for reinforcement materials other than glass fiber. This code should definitely be further extended across Europe to further amplify the use of fiber reinforced polymers in the civil engineering industry. The Eurocode for traditional materials such as steel, concrete and timber was introduced by pan-European groups of renowned scientists;, similar developments should also be propagated for fiber reinforced polymers.

BIBLIOGRAPHY

Note that this list only contains a selected number of source documents (books, papers, theses, articles and codes) that were needed for this research next to the literature study. Throughout the research, most references to literature were made by referencing to the literature study by using the reference [LS, ch. x.y, pz]. For a complete bibliography list please refer to the literature list of the literature study.

Books

- B1** A.H.J. Nijhof (2004); *Vezelversterkte Kunststoffen – Mechanica en Ontwerp*; Delft University Press
- B7** A.P. Mouritz, A.G. Gibson (2006); *Fire Properties of Polymer Composite Materials*; Springer
- B16** D.V. Rosato (2004); *Reinforced Plastics Handbook*; Elsevier
- B21** G.Parke, N.Hewson (2008); *ICE Manual of Bridge Engineering*; Thomas Telford
- B23** D.V. Rosato, (2003); *Plastics Engineered Product Design*, Elsevier
- B25** H.Thorning (et al.) (2003); *Fiberline Design Manual*; Fiberline A/S
- B28** P.K. Sinha (1995); *Composite Materials and Structures*; Composite Centre of Excellence, Department of Aerospace Engineering, I.I.T Kharagpur

Papers

- P23** Dr. ir. R.A. Daniel (2009); *Composieten in Infrastructuur*; Presentatie Paton '09
- P35** J. Knippers, M. Gabler (2006); *New Design Concepts for Advanced Composite Bridges - Friedberg Bridge*, Paper University of Stuttgart, Knippers Helbig Consultants
- P90** P.P. Greigger (et al.) (2002); *Fire protection of steel bridges*; Presentation PPG & Hughes Associates Fire Science
- P102** J.R. Demitz (et al.) (2003); *Deflection Requirements for Bridges Constructed, with Advanced Composite Materials*; Paper Journal of Bridge Engineering March/April 2003
- P103** Z.G. Liu (et al.) (2007); *Challenges for Use of Fixed Fire Suppression Systems in Road Tunnel Fire Protection*; Paper Fire Research Program, National Research Council of Canada
- P104** R. Daniel (2003); *Environmental Considerations to structural material selection for a bridge*; Paper European Bridge Engineering Conference, March 2003
- P105** J. Scholliers, H. Van Brussel (1994); *Computer-integrated filament winding: computer-integrated design, robotic filament winding and robotic quality control*; Paper KU Leuven

Theses

- T9** T. van den Driessche (2006); *Een tubulair vakwerk als voetgangersbrug*; MSc thesis Universiteit van Gent
- T16** C.D. Tracy (2005); *Fire Endurance of Multicellular Panels in an FRP Building System*; PhD thesis Ecole Polytechnique Federale de Lausanne (EPFL)

Articles

- A33** D. Kendall (2006); *Fiber reinforced polymer composite bridges*; Article White Young Green Consulting Ltd., National Composites Network
- A53** Alstom (2011); *Alstom Citadis Dualis*; Product Brochure
- A54** Alstom (2006); *Alstom Regio Citadis*; Product Datasheet

CODES

Fiber reinforced polymers

CUR96	CUR Aanbeveling 96: VVK in Civiele Draagconstructies, 2003
CUR 2003-6	CUR Achtergrondrapport 2003-6; Achtergrondrapport bij CUR Aanbeveling 96
CUR 96+ Draft 2012	Revised CUR Recommendation 96: Update 2012, Draft

Fire safety

NEN-EN 13501-2:2007+A1:2009	Fire Classification of construction products and building elements – Part 2: Classification using data from fire resistance tests, excluding ventilation services
NEN-EN 1991-1-2:2003	Eurocode 1: Actions on structures – Part 1-2: General actions – Actions on structures exposed to fire
NEN-EN 1991-1-2:2003/NB:2007	Dutch Natial Annex to Eurocode 1: Actions on structures – Part 1-2: General actions – Actions on structures exposed to fire
NEN 4001+C1:2008	Fire protection - Planning of portable and mobile fire extinguishers
NEN-Praktijkgids Brandveiligheid	NEN-Praktijkgids Brandveiligheid; Bouwbesluit,2006 (in English: Practice Guide Fire Safety in buildings issued by the Dutch normative authority NEN)
NFPA502	US-American National Fire Safety Protection Association; Standard for Road Tunnels, Bridges and Other Limited- Access Highways, 2008

Bridge deck layout & road/highway layout

RWS-RONA1986	Richtlijn voor het ontwerpen van niet-autosnelwegen, 1986 (in English: Regulations for the design of non-highways)
RWS-ROA1989	Richtlijn voor het ontwerpen van autosnelwegen, 1989 (in English: Regulations for the design of highways)
RWS-SATO2005	Rijkswaterstaat, Specifieke Aspecten Tunnel Ontwerp,2005 (in English: specific aspects of tunnel design)
RWS-NOA2007	Nieuwe Ontwerprichtlijn Autosnelwegen, 2007 (in English: New Design Guide for Highways)

Loads & deformations/deflections

NEN-EN 1990: 2002	Eurocode 0: Basis of structural design
NEN-EN 1990:2002/A2	Eurocode 0 - Basis of Structural Design – Annex 2 Application for bridges
NEN-EN 1990+A1+A1/C2:2011	Eurocode 0 - Basis of Structural Design – Correction C1:2004, Annex A1:2005, Correction C2: 2010
NEN-EN 1991-1-3:2003	Eurocode 1: Actions on structures – Part1-3: General actions – Snow loads
NEN-EN 1991-1-3:2003/ NB:2007	Dutch National Annex to Eurocode 1: Actions on structures – Part1-3: General actions – Snow loads
NEN-EN 1991-1-4:2005	Eurocode 1: Actions on structures – Part1-4: General actions – Wind actions
NEN-EN 1991-1-4:2005/NB:2007	Dutch National Annex to Eurocode 1: Actions on structures– Part1-4: General actions – Wind actions
NEN-EN 1991-1-5:2011	Eurocode 1: Actions on structures – Part 1-5: General actions – Thermal actions
NEN-EN 1991-1-5:2011/NB:2011	Dutch National Annex to Eurocode 1: Actions on structures – Part 1-5: General actions – Thermal actions
NEN-EN 1991-1-7:2006	Eurocode 1 – Actions on structures – Part 1-7: General actions – Accidental actions

NEN-EN 1991-1-7:2006/NB:	Dutch National Annex to Eurocode 1 – Actions on structures – Part 1-7: General actions – Accidental actions
NEN-EN 1991-2:2003	Eurocode 1: Actions on structures – Part 2: Traffic loads on bridges
NEN-EN 1991-2:2003/NB:2009	Dutch National Annex to Eurocode 1: Actions on structures – Part 2: Traffic loads on bridges
NEN-EN 1991-2:2003	Eurocode 1: Actions on structures – Part 2: Traffic loads on bridges
NEN-EN 1991-2:2003/NB:2009	Dutch National Annex to Eurocode 1: Actions on structures – Part 2: Traffic loads on bridges
AASHTO-LFRD 1998	US-American Association of State Highway and Transportation Officials, AASHTO, LFRD Bridge Design Specifications, 1998
HIVOSS 2008	Human induced vibrations of steel bridges, design of footbridges, guideline, 2008

TABLE OF FIGURES

FIG. 1: SELECTION OF MODERN TRUSS BRIDGES: (CLOCKWISE FROM TOP LEFT): WEBB BRIDGE, MELBOURNE, AUSTRALIA; PEACE BRIDGE, CALGARY, CANADA; GREENSIDE PLACE LINK BRIDGE, EDINBURGH, SCOTLAND; LIGHT RAIL VIADUCT, THE HAGUE, THE NETHERLANDS	2
FIG. 2: LEFT: GFRP TEE-JOINT USED FOR THE CONNECTION OF TUBULAR FRP MEMBERS. [WEB, WWW.CADFIL.COM] RIGHT: ROBOTIC TAPE-WINDING PATTERNS FOR THE PRODUCTION OF A TEE JOINT [P105, P8].....	18
FIG. 3: SCHEME DEPICTING THE COMPOSITE DECOMPOSITION DURING FIRE [B07, P21]	22
FIG. 4: LEFT: TYPICAL HEAT RELEASE PROCESS FOR GLASS VINYL ESTER COMPOSITES UNDER CONSTANT HEAT FLUX OF 50kW/M ² . RIGHT: COMPARISON OF HRR'S OF NORMAL AND HIGH FIRE PERFORMANCE COMPOSITES. [B07, P72-73]	25
FIG. 5: TIME-TO-IGNITION OF DIFFERENT THERMOSET (LEFT) AND THERMOPLASTIC (RIGHT) RESIN BASED COMPOSITES. [B07, P61,62]	25
FIG. 6: CORRELATION BETWEEN HEAT FLUX AND AVERAGE SMOKE DENSITY FOR DIFFERENT THERMOSET POLYMER COMPOSITES [B07, P88]	26
FIG. 7: LEFT: BACK-FACE TEMPERATURE BUILD-UP IN CELLULOSIC FIRE CONDITIONS. RIGHT: COMPARISON OF TIME TO REACH A BACK-FACE TEMPERATURE OF 160°C CORRELATED TO THE MEMBER THICKNESS FOR DIFFERENT COMPOSITES. [B07, P96,97].....	27
FIG. 8: LEFT: YOUNG'S MODULUS OF UD- 60% REINFORCED GLASS POLYESTER PULTRUDED SECTION (INCLUDING ITS COMPONENTS) AND RANDOM SWIRL MAT CORRELATED TO THE TEMPERATURE. RIGHT: YOUNG'S MODULUS OF WOVEN GLASS VINYL ESTER LAMINATE AND ITS PARTS CORRELATED TO THE TEMPERATURE [B07, P183, 185]	28
FIG. 9: FAILURE TIMES UNDER NORMALIZED TENSILE (LEFT) OR COMPRESSIVE (RIGHT) STRESSES OF DIFFERENT RESINS [B07, P195, 196]	29
FIG. 10: RETAINED POST-FIRE FLEXURAL STRENGTH OF DIFFERENT THERMOSET (LEFT) AND THERMOPLASTIC (RIGHT) COMPOSITES [B07, P217, 226]	29
FIG. 11: EFFECT OF 30% ATH FILL ON THE FIRE REACTION PROPERTIES OF A GLASS PHENOLIC COMPOSITE SUBJECTED TO A HEAT FLUX OF 50kW/M ² [B07, P248]	31
FIG. 12: INTUMESCENT COATING BEFORE (LEFT, THICKNESS = 0,8 MM) AND AFTER (RIGHT, THICKNESS = 52 MM) FIRE LOADING [B07, P282].....	33
FIG. 13: LEFT: BACK-FACE-TEMPERATURE OF AN INTUMESCENT PROTECTED COMPOSITE PANEL. RIGHT: IGNITION TIME OF A GLASS POLYESTER COMPOSITE PROTECTED WITH THIN AND THICK INTUMESCENT COATINGS AT DIFFERENT HEAT FLUXES [B07, P283]	33
FIG. 14: POST-FIRE FLEXURAL STRENGTH OF GLASS POLYESTER COMPOSITES WITH DIFFERENT COATINGS. RIGHT: CORRELATION BETWEEN HEATING TIME AND POST-FIRE FLEXURAL STRENGTH OF PROTECTED AND UN-PROTECTED GLASS POLYESTER COMPOSITE. [B07, P234].....	34
FIG. 15: STANDARD FIRE CURVES, INCLUDING THE HYDROCARBON FIRE CURVE [NEN-1991-1-2-2002, P23]	35
FIG. 16: ROAD CATEGORIES ACCORDING TO RIJWSWATERSTAAT [RWS-SATO2005, TABLE 2.4.1, P70]	45
FIG. 17: SPACE DEMANDS FOR HEAVY TRAFFIC ON BRIDGES. [RWS, SATO2005]	46
FIG. 18: DIMENSIONS OF THE FREE-STANDING GUIDANCE BARRIER 'STEPBARRIER' AS DEFINED BY RIJWSWATERSTAAT [RWS-SATO, CH. 5.4.2.1, P606]	46
FIG. 19: DIMENSIONS OF THE GUIDANCE RAIL 'VLP 1LV 133-60' AS DEFINED BY RIJWSWATERSTAAT [RWS-ROA1989, CH. 6.4.2.4, P49].....	47
FIG. 20: SPACE DEMANDS FOR FOOTPATHS ON BRIDGES [RONA1986, CH. 1.2, P1, CH. 2.1, P2]	47
FIG. 21: SPACE DEMANDS FOR BICYCLE PATHS ON BRIDGES [RONA1986, CH. 1.2, P1, CH. 2.1, P2]	48
FIG. 22: VARIANT 1A (CIRCULAR) FOR THE BRIDGE CROSS SECTION SIZE DETERMINATION.	49
FIG. 23: VARIANT 1B (ELLIPTICAL) FOR THE BRIDGE CROSS SECTION SIZE DETERMINATION.	50
FIG. 24: VARIANT 2A (CIRCULAR) FOR THE BRIDGE CROSS SECTION SIZE DETERMINATION.	51
FIG. 25: VARIANT 2B (ELLIPTICAL) FOR THE BRIDGE CROSS SECTION SIZE DETERMINATION.	52
FIG. 26: VARIANT 3A (CIRCULAR) FOR THE BRIDGE CROSS SECTION SIZE DETERMINATION.	53
FIG. 27: VARIANT 3B (ELLIPTICAL) FOR THE BRIDGE CROSS SECTION SIZE DETERMINATION.	53
FIG. 28: VARIANT 4A (CIRCULAR) FOR THE BRIDGE CROSS SECTION SIZE DETERMINATION.	54
FIG. 29: VARIANT 4B (ELLIPTICAL) FOR THE BRIDGE CROSS SECTION SIZE DETERMINATION.	54
FIG. 30: VARIANT 5A (CIRCULAR) FOR THE BRIDGE CROSS SECTION SIZE DETERMINATION.	55
FIG. 31: VARIANT 5B (ELLIPTICAL) FOR THE BRIDGE CROSS SECTION SIZE DETERMINATION.	55
FIG. 32: VARIANT 6A (CIRCULAR) FOR THE BRIDGE CROSS SECTION SIZE DETERMINATION. THIS VARIANT IS A CIRCULAR VERSION OF THE EXISTING 'LIGHT-RAIL VIADUCT BEATRIXKWARTIER' IN THE HAGUE, THE NETHERLANDS [LS, CH. 6.1.3, P192]	57
FIG. 33: VARIANT 6B (ELLIPTICAL) FOR THE BRIDGE CROSS SECTION SIZE DETERMINATION. THIS VARIANT IS A REPLICA OF THE EXISTING 'LIGHT-RAIL VIADUCT BEATRIXKWARTIER' IN THE HAGUE, THE NETHERLANDS [LS, CH. 6.1.3, P192]	57
FIG. 34: DRAWING OF THE 'CANTILEVER VARIANT'. THE CYLINDRICAL SHAPE OF THIS VARIANT IS SIMILAR TO THE HEAVY TRAFFIC PART OF 'VARIANT 5B'. A CANTILEVERING TRUSS STRUCTURE IS USED TO HOUSE THE PEDESTRIANS AND BICYCLISTS, WHILE KEEPING THEM PHYSICALLY SEPARATED FROM THE FAST, HEAVY TRAFFIC.	59
FIG. 35: SAFETY BARRIER OF THE 'RIMOB' TYPE TO PROTECT BRIDGE PILLARS. [RWS-ROA1989, CH. 6.5.4, P92]	60
FIG. 36: PROFILE OF THE 2x2 LANE HIGHWAY THAT THE BRIDGE COULD SPAN. THE SINGLE SPAN WOULD BE 35,20 M, IF AN INTERMEDIATE SUPPORT IS USED, THE SPAN WOULD BE 2x17,60 M.	61
FIG. 37: PROFILE OF THE 2x3 LANE HIGHWAY THAT THE BRIDGE COULD SPAN. THE SINGLE SPAN WOULD BE 42,10 M, IF AN INTERMEDIATE SUPPORT IS USED, THE SPAN WOULD BE 2x21,05 M.	61
FIG. 38: PROFILE OF THE 2x4 LANE HIGHWAY THAT THE BRIDGE COULD SPAN. THE SINGLE SPAN WOULD BE 49,00 M, IF AN INTERMEDIATE SUPPORT IS USED, THE SPAN WOULD BE 2x24,50 M.	61
FIG. 39: PARAMETRIC MODEL OF THE BASIC CYLINDRICAL LOAD BEARING SHAPE IN 'GRASSHOPPER'	63
FIG. 40: MODEL OF THE BASIC SHAPE OF THE CYLINDRICAL LOAD BEARING SHAPE IN 'RHINO'	63
FIG. 41: DETAILS OF THE POINT GENERATION IN GRASSHOPPER.....	64
FIG. 42: GENERATION OF LINEAR HORIZONTAL MEMBERS IN 'GRASSHOPPER'	64
FIG. 43: HORIZONTAL MEMBERS PARAMETRICALLY GENERATED IN 'GRASSHOPPER' BY CONNECTING 'POINT 0' AND POINT 1' OF EVERY SUB-SURFACE.....	65
FIG. 44: VERTICAL MEMBERS OR ELLIPTICAL RINGS PARAMETRICALLY GENERATED IN 'GRASSHOPPER' BY CONNECTING 'POINT 0 AND 'POINT 3' OF EVERY SUB-SURFACE.	65

FIG. 45: HORIZONTAL AND VERTICAL MEMBERS PARAMETRICALLY GENERATED IN 'GRASSHOPPER' BY CONNECTING 'POINT 0 AND 'POINT 1' AS WELL AS 'POINT 0 AND 'POINT 3' OF EVERY SUB-SURFACE.	66
FIG. 46: PARAMETRICALLY GENERATED 'GRASSHOPPER' MODEL WITH HORIZONTAL-, VERTICAL- AND DIAGONAL MEMBERS. THIS RESULT IS ACHIEVED BY CONNECTING 'POINT 0 AND 'POINT 1', 'POINT 0 AND 'POINT 3' AS WELL AS 'POINT 0 AND 'POINT 2' OF EVERY SUB-SURFACE.	66
FIG. 47: PARAMETRICALLY GENERATED 'GRASSHOPPER' MODEL WITH HORIZONTAL-, VERTICAL- AND DIAGONAL MEMBERS IN TWO DIRECTIONS. THIS RESULT IS ACHIEVED BY CONNECTING 'POINT 0 AND 'POINT 1', 'POINT 0 AND 'POINT 3', 'POINT 0 AND 'POINT 2' AS WELL AS 'POINT 1 AND 'POINT 3' OF EVERY SUB-SURFACE.	67
FIG. 48: PARAMETRICALLY GENERATED 'GRASSHOPPER' MODEL WITH DIAGONAL MEMBERS IN TWO DIRECTIONS. THIS RESULT IS ACHIEVED BY CONNECTING 'POINT 0 AND 'POINT 2' AS WELL AS 'POINT 1 AND 'POINT 3' OF EVERY SUB-SURFACE.	67
FIG. 49: THE THREE REGULAR TESSELLATIONS DIVIDING A PLANE INTO EQUAL HEXAGONS, SQUARES OR TRIANGLES [WEB, MATHWORLD.WOLFRAM.COM/TESSellation].....	68
FIG. 50: PARAMETRICALLY GENERATED 'GRASSHOPPER' MODEL OF THE HEXAGONAL GRID TYPE CYLINDRICAL TRUSS BRIDGE.	68
FIG. 51: A TRIANGULAR GRID-SHELL MADE OF STEEL PROVIDES THE ROOF STRUCTURE FOR THE COURTYARD OF THE BRITISH MUSEUM IN LONDON	69
FIG. 52 : PARAMETRICALLY GENERATED 'GRASSHOPPER' MODEL OF THE TRIANGULAR GRID TYPE CYLINDRICAL TRUSS BRIDGE.	69
FIG. 53: 'GRASSHOPPER' CODE TO GENERATE A NON-UNIFORM GRID	70
FIG. 54: PARAMETRICALLY GENERATED 'GRASSHOPPER' MODEL OF THE NON-UNIFORM GRID TYPE CYLINDRICAL TRUSS BRIDGE. THIS MODEL IS BASED ON THE TWO-DIAGONAL TRUSS, DESCRIBED IN [CH. 5.7.2.3] ADAPTED BY A 'BEZIER-CURVE'	71
FIG. 55: PARAMETRICALLY GENERATED 'GRASSHOPPER' MODEL OF THE DOUBLE-LAYERED SPACE FRAME GRID TYPE CYLINDRICAL TRUSS BRIDGE.	72
FIG. 56: SCHEME OF A SECTION OF THE FINAL DESIGN OF THE BRIDGE FOR THE CALCULATION OF THE REFERENCE SURFACE AREA.	76
FIG. 57: FORCE COEFFICIENT FOR TRUSSES WITHOUT END EFFECTS AS A FUNCTION OF THE SOLIDITY FACTOR [NEN-EN 1991-1-4:2005, P71]	77
FIG. 58: DEFINITION OF LM1 FOR THE BRIDGE TO BE DESIGNED, AS PRESCRIBED BY EUROCODE 1 [NEN-EN 1991-2:2003, CH. 4.3.2, P35-38]	80
FIG. 59: DEFINITION OF LM2 FOR THE BRIDGE TO BE DESIGNED, AS PRESCRIBED BY EUROCODE 1 [NEN-EN 1991-2:2003, CH. 4.3.3, P38-39]	81
FIG. 60: DEFINITION OF LM4 FOR THE BRIDGE TO BE DESIGNED, AS PRESCRIBED BY EUROCODE 1 [NEN-EN 1991-2:2003, CH. 4.3.5, P39-40]	81
FIG. 61: VEHICULAR IMPACT FORCES ON THE SUBSTRUCTURE PRESCRIBED BY THE EUROCODE DUTCH NATIONAL ANNEX [NEN-EN-1991-1-7:2006/NB: 2011, TABLE NB.1-4.1, P5]	84
FIG. 62: VEHICULAR IMPACT FORCES ON THE SUPERSTRUCTURE PRESCRIBED BY THE EUROCODE DUTCH NATIONAL ANNEX [NEN-EN-1991-1-7:2006/NB: 2011, TABLE NB.2-4.2, P6]	84
FIG. 63: DEFINITION OF FLM1 FOR THE BRIDGE TO BE DESIGNED, AS PRESCRIBED BY EUROCODE 1 [NEN-EN 1991-2:2003, CH. 4.6.2, P48]	87
FIG. 64: EXPECTED NUMBER OF 'SINGLE VEHICLES' PER NOTIONAL DRIVING LANE PER YEAR ACCORDING TO THE EUROCODE [EN1991-2:2003, TABLE 4.5(n), P46]	88
FIG. 65: DIMENSIONS OF THE LIGHT RAIL TRAM 'ALSTOM, REGIO CITADIS 3-CAR' [A54, P2]	89
FIG. 66: LOADING SCHEME FOR THE ALSTOM LIGHT RAIL TRAM 'ALSTOM, REGIO CITADIS 3-CAR' [A53] [A54].....	89
FIG. 67: DERIVING THE TOTAL MATERIAL USAGE OF ALL TOPOLOGY VARIANTS USING 'GRASSHOPPER' CODE	92
FIG. 68: DEFINITION OF ELLIPTICAL RINGS AND HORIZONTAL LINEAR MEMBERS AND THEIR MUTUAL DISTANCE FOR THE 'SQUARE VIERENDEEL' VARIANT.	93
FIG. 69: ADDITIONAL TRUSS LAYOUT VARIANTS USED FOR THE ADAPTATION OF THE ORIGINAL TOPOLOGY; LEFT: ORIGINAL SQUARE LAYOUT; MIDDLE: LONGITUDINAL RECTANGULAR LAYOUT; RIGHT: LATERAL SQUARE LAYOUT.	93
FIG. 70: FLOW CHART FOR THE TRANSFORMATION OF THE INITIAL GEOMETRY TO A FULLY FUNCTIONAL FE-MODEL.....	95
FIG. 71: FIRST SUPPORT CONDITION: FULLY FIXED EDGE NODES. THIS SUPPORT CONDITION MODELS THE OFTEN USED EDGE BEAM, AS IS THE CASE WITH THE CALATRAVA PEACE BRIDGE, CALGARY, CANADA, MARCH 2012 THAT IS SHOWN IN THE PICTURE [WEB: WWW.BROCCOLICITY.COM]	96
FIG. 72: SECOND SUPPORT CONDITION: BOTTOM HALF OF THE EDGE NODES PINNED ON CONCRETE/SAND EMBANKMENT.	96
FIG. 73: GENERAL SUPPORT CONDITIONS OF THE INITIAL FE-MODELS. LEFT: FULLY FIXED EDGE NODES. RIGHT: BOTTOM HALF OF THE EDGE NODES PINNED. ...	97
FIG. 74: TRUSS TOPOLOGY VARIANT 0A, 0B, 0C: VIERENDEEL SQUARE, -RECTANGULAR LATERAL AND -RECTANGULAR LONGITUDINAL.....	98
FIG. 75: TRUSS TOPOLOGY VARIANT 1A, 1B, 1C: TRUSS ONE DIAGONAL SQUARE, -RECTANGULAR LATERAL AND -RECTANGULAR LONGITUDINAL	98
FIG. 76: TRUSS TOPOLOGY VARIANT 2A, 2B, 2C: TRUSS TWO DIAGONALS SQUARE, -RECTANGULAR LATERAL AND -RECTANGULAR LONGITUDINAL	98
FIG. 77: TRUSS TOPOLOGY VARIANT 3A, 3B, 3C: DIAGRID SQUARE, -RECTANGULAR LATERAL AND -RECTANGULAR LONGITUDINAL	98
FIG. 78: TRUSS TOPOLOGY VARIANT 4A, 4B, 4C: TRIANGULAR GRID SQUARE, -RECTANGULAR LATERAL AND -RECTANGULAR LONGITUDINAL	99
FIG. 79: TRUSS TOPOLOGY VARIANT 5A, 5B, 5C: HEXAGONAL GRID SQUARE, -RECTANGULAR LATERAL AND -RECTANGULAR LONGITUDINAL.....	99
FIG. 80: DEFORMATION OF VARIANT 1A, A TRUSS WITH ONE DIAGONAL, DUE TO LOADING BY SELF-WEIGHT.	99
FIG. 81: DEFORMATION OF VARIANT 1A, A TRUSS WITH ONE DIAGONAL, DUE TO LOADING BY SELF-WEIGHT. THE BOTTOM HALF OF THE EDGE NODES IS PINNED.	100
FIG. 82: DEFORMATION OF VARIANT 1A, A TRUSS WITH ONE DIAGONAL, DUE TO LOADING.....	100
FIG. 83: DEFORMATION OF VARIANT 1A, A TRUSS WITH ONE DIAGONAL, DUE TO LOADING BY A POINT LOAD OF 100kN, PLACED CENTRALLY AT MID=SPAN. THE BOTTOM HALF OF THE EDGE NODS IS PINNED.	100
FIG. 84: GRAPH OF GENERAL DEFLECTION RESULTS DUE TO LOAD CASES LC1-LC4 FOR ALL 18 SUB VARIANTS.....	102
FIG. 85: GRAPH FOR THE COMPARISON OF THE SUMMATION OF ALL SUB-VARIANT DEFLECTIONS FOR ALL LOAD CASES.....	103
FIG. 86: GRAPH OF THE DEFLECTION OF ALL SQUARE SUB VARIANTS FOR THE DETERMINATION OF THE STIFFEST MAIN VARIANT	104
FIG. 87: GRAPH OF THE DEFLECTION OF THE SUMMATION OF THE SUB VARIANTS FOR EACH MAIN VARIANT FOR THE DETERMINATION OF THE STIFFEST MAIN VARIANT	104
FIG. 88: TOPOLOGY OF THE LATERAL TRUSSES THAT ACT AS SUBSTRUCTURE FOR THE INNER BRIDGE DECK.	107
FIG. 89: TOPOLOGY OF THE LONGITUDINAL TRUSS THAT ACT AS SUBSTRUCTURE FOR THE INNER BRIDGE DECK.....	107
FIG. 90: MAIN LOAD BEARING STRUCTURE WITH (LEFT) AND WITHOUT (RIGHT) INNER SUBSTRUCTURE FOR BRIDGE DECK.	108
FIG. 91: DEFORMATION CAUSED BY LC1-LC3 FOR THE MAIN LOAD BEARING STRUCTURE WITH AND WITHOUT INNER SUPPORTING TRUSSES.	109
FIG. 92: 'GRID SIZE VARIANT 1' (LEFT) AND 'GRID SIZE VARIANT 2' (RIGHT).....	110
FIG. 93: 'GRID SIZE VARIANT 3' (LEFT) AND 'GRID SIZE VARIANT 4' (RIGHT)	110

FIG. 94: 'GRID SIZE VARIANT 5' (LEFT) AND 'GRID SIZE VARIANT 6' (RIGHT)	111
FIG. 95: GRAPH SHOWING THE MATERIAL USAGE AS WELL AS THE NUMBER OF CONNECTIONS AND TRUSS ELEMENTS FOR EACH GRID SIZE VARIANT.....	112
FIG. 96: GRAPH SHOWING THE RESULTS FOR THE DEFLECTIONS OF THE FE-ANALYSIS FOR ALL GRID SIZE VARIANTS AND ALL THREE LOAD CASES.	113
FIG. 97: RESULTS FOR THE MAXIMUM COMPRESSIVE- AND TENSILE STRESSES, FOLLOWING THE FE-ANALYSIS FOR ALL GRID SIZE VARIANTS AND ALL THREE LOAD CASES.	114
FIG. 98: NORMALIZED MAXIMUM DEFORMATIONS AND NORMALIZED MATERIAL USAGE FOR ALL GRID SIZE VARIANTS, LEADING TO A CHOICE THE MOST EFFICIENT VARIANT.	116
FIG. 99: NORMALIZED MAXIMUM DEFORMATIONS AND NORMALIZED NUMBER OF NODES FOR ALL GRID SIZE VARIANTS, LEADING TO A CHOICE THE MOST EFFICIENT VARIANT.	116
FIG. 100: DEFORMATION RESULTS DIRECTLY DERIVED FROM FE-ANALYSIS FOR ALL CROSS SECTION VARIANTS AND LOAD CASES	119
FIG. 101: DEFORMATION RESULTS, ADAPTED BY APPLYING THE FACTOR DERIVED IN [CH. 8.3] THAT TAKES THE EXPECTED ADDED STIFFNESS OF THE BRIDGE DECK SUBSTRUCTURE INTO ACCOUNT.	120
FIG. 102: MAXIMUM TENSILE- AND COMPRESSIVE STRESSES IN THE CROSS SECTION VARIANTS DUE TO LC1-LC3	122
FIG. 103: NORMALIZED DEFORMATION PLOTTED AGAINST THE NORMALIZED MOMENT OF INERTIA FOR ALL CROSS SECTION VARIANTS.	123
FIG. 104: TRUSS WITH ONE DIAGONAL TOPOLOGY THAT IS USED FOR THE MAIN CYLINDRICAL LOAD BEARING STRUCTURE OF THE FRP HEAVY TRAFFIC BRIDGE.	124
FIG. 105: PROFILE OF THE 2x4 LANE HIGHWAY THAT THE BRIDGE WILL SPAN. THIS RESULTS IN A SINGLE SPAN OF 49,00 M.	124
FIG. 106: DRAWING OF THE 'CANTILEVER VARIANT'. THE CYLINDRICAL SHAPE OF THIS VARIANT IS SIMILAR TO THE HEAVY TRAFFIC PART OF 'VARIANT 5B'. A CANTILEVERING TRUSS STRUCTURE IS USED TO HOUSE THE PEDESTRIANS AND BICYCLISTS, WHILE KEEPING THEM PHYSICALLY SEPARATED FROM THE FAST, HEAVY TRAFFIC.	125
FIG. 107: LEFT: ORIGINAL VARIANT FOR THE MAIN ELLIPTICAL TRUSS. RIGHT: OPTIMIZED VARIANT FOR THE MAIN ELLIPTICAL TRUSS AFTER FINDING THE MOST EFFICIENT GRID SIZE VARIANT.	126
FIG. 108: TOPOLOGY OF THE LATERAL TRUSSES THAT ACT AS SUBSTRUCTURE FOR THE INNER BRIDGE DECK.	129
FIG. 109: TOPOLOGY OF THE LONGITUDINAL TRUSS THAT ACT AS SUBSTRUCTURE FOR THE INNER BRIDGE DECK.....	130
FIG. 110: TOP: MAIN LOAD BEARING STRUCTURE WITH INNER BRIDGE DECK SUPPORTING STRUCTURE. BOTTOM LEFT: ELLIPTICAL MAIN LOAD BEARING STRUCTURE. BOTTOM RIGHT: INNER BRIDGE DECK SUBSTRUCTURE.	130
FIG. 111: COMPARISON OF THE DEFORMATION RESULTS FOR THE THREE OPTIMIZED PARTS OF THE BRIDGE WITHOUT CANTILEVER SUBSTRUCTURE	131
FIG. 112: CANTILEVER BRIDGE DECK SUBSTRUCTURE WITH THE NODES (BLUE DOTS) THAT CONINCIDE WITH THE MAIN LOAD BEARING STRUCTURE. THE LENGTH OF THE CANTILEVER IS MARKED BY THE BLUE ARROW.	131
FIG. 113: CROSS SECTION OF THE FINISHED STRUCTURE OF THE BRIDGE, COMPLETE WITH ELLIPTICAL MAIN LOAD BEARING TRUSS, INNER BRIDGE DECK SUPPORTING TRUSS AND CANTILEVER BRIDGE DECK SUPPORTING TRUSS.	132
FIG. 114: TOP VIEW OF THE BRIDGE STRUCTURE, THE CANTILEVER PART IS SHADED BLUE. THE STRAIGHT LONGITUDINAL MEMBERS OF THE CANTILEVER PART THAT CONNECTS THE LATERAL TRUSSES LIE VERTICALLY.	132
FIG. 115: POSITION OF THE 6 STRAIGHT LONGITUDINAL MEMBERS THAT CONNECT THE LATERAL CANTILEVER TRUSSES.	133
FIG. 116: CROSS SECTION OF THE FULL-FRP BRIDGE FINAL DESIGN	134
FIG. 117: TOP VIEW OF THE FULL-FRP BRIDGE FINAL DESIGN	135
FIG. 118: SIDE VIEW OF THE FULL-FRP BRIDGE FINAL DESIGN	136
FIG. 119: CONFIGURATION OF THE BRIDGE DECK OF THE FULL-FRP BRIDGE FINAL DESIGN	137
FIG. 120: GRID-PLANE FOR THE INSERTION OF GRID-POINT- AND GRID-AREA-LOADS INTO THE FE-MODEL.	138
FIG. 121: LM1 LOADING SCHEME INSERTED IN THE FE-MODEL IN 'GSA'	139
FIG. 122: SUPPORT CONDITIONS OF THE FULL-FRP BRIDGE DESIGN.....	140
FIG. 123: SIDE VIEW OF THE DEFORMATION OF THE BRIDGE STRUCTURE DUE TO LM1 ONLY.	141
FIG. 124: TOP VIEW OF THE DEFORMATION OF THE BRIDGE STRUCTURE DUE TO LM1 ONLY.	142
FIG. 125: 3D VIEW OF THE DEFORMATION OF THE BRIDGE STRUCTURE DUE TO LM1 ONLY.....	142
FIG. 126: SIDE VIEW OF THE DEFORMATION OF THE BRIDGE STRUCTURE DUE TO BICYCLE AND PEDESTRIAN LOADS ONLY.	142
FIG. 127: TOP VIEW OF THE DEFORMATION OF THE BRIDGE STRUCTURE DUE TO BICYCLE AND PEDESTRIAN LOADS ONLY.....	143
FIG. 128: 3D VIEW OF THE DEFORMATION OF THE BRIDGE STRUCTURE DUE TO BICYCLE AND PEDESTRIAN LOADS ONLY.....	143
FIG. 129: SIDE VIEW OF THE DEFORMATION OF THE BRIDGE STRUCTURE DUE TO CROWD LOADING (LM4) ONLY.	143
FIG. 130: TOP VIEW OF THE DEFORMATION OF THE BRIDGE STRUCTURE DUE TO CROWD LOADING (LM4) ONLY.....	144
FIG. 131: 3D VIEW OF THE DEFORMATION OF THE BRIDGE STRUCTURE DUE TO CROWD LOADING (LM4) ONLY.....	144
FIG. 132: SIDE VIEW OF THE DEFORMATION OF THE BRIDGE STRUCTURE DUE TO WIND FROM ONE SIDE ONLY.	144
FIG. 133: TOP VIEW OF THE DEFORMATION OF THE BRIDGE STRUCTURE DUE TO WIND FROM ONE SIDE ONLY.	145
FIG. 134: 3D VIEW OF THE DEFORMATION OF THE BRIDGE STRUCTURE DUE TO WIND FROM ONE SIDE ONLY.	145
FIG. 135: 3D VIEW OF THE DEFORMATION IN Y-DIRECTION OF THE BRIDGE STRUCTURE DUE TO WIND FROM ONE SIDE ONLY.	146
FIG. 136: 3D VIEW OF THE DEFORMATION IN X-DIRECTION OF THE BRIDGE STRUCTURE DUE TO THERMAL LOADING ONLY.	146
FIG. 137: 3D VIEW OF THE DEFORMATION IN X-DIRECTION OF THE BRIDGE STRUCTURE DUE TO THERMAL LOADING ONLY.	147
FIG. 138: SIDE VIEW OF THE DEFORMATION IN Z-DIRECTION OF THE BRIDGE STRUCTURE DUE TO THE NORMATIVE LOAD COMBINATION CASE LCC1.....	148
FIG. 139: TOP VIEW OF THE DEFORMATION IN Z-DIRECTION OF THE BRIDGE STRUCTURE DUE TO THE NORMATIVE LOAD COMBINATION CASE LCC1.	149
FIG. 140: 3D VIEW OF THE DEFORMATION IN Z-DIRECTION OF THE BRIDGE STRUCTURE DUE TO THE NORMATIVE LOAD COMBINATION CASE LCC1.....	149
FIG. 141: 3D VIEW OF THE AXIAL STRESS DISTRIBUTION IN THE BRIDGE STRUCTURE DUE TO THE NORMATIVE LOAD COMBINATION CASE LCC1.....	150
FIG. 142: 3D VIEW OF THE VON MISES STRESS DISTRIBUTION IN THE BRIDGE STRUCTURE DUE TO THE NORMATIVE LOAD COMBINATION CASE LCC1.	150
FIG. 143: 3D VIEW OF THE DEFORMATION IN X-DIRECTION OF THE BRIDGE STRUCTURE DUE TO THE LOAD COMBINATION CASE LCC6	151
FIG. 144: 3D VIEW OF THE DEFORMATION IN Y-DIRECTION OF THE BRIDGE STRUCTURE DUE TO THE LOAD COMBINATION CASE LCC5	151

FIG. 145: COMBINED STRESSES IN THE FULL-FRP BRIDGE DUE TO FATIGUE LOAD MODEL FLM1. THE REGIONS WITH THE HIGHEST STRESSES ARE HIGHLIGHTED. THE AREA MARKED WITH THE LETTER 'A' YIELDS THE HIGHEST STRESS AMPLITUDE.....	152
FIG. 146: MODE 1: THE FIRST HORIZONTAL MODE. THE COMPLETE STRUCTURE TILTS IN Y-DIRECTION AT A NATURAL FREQUENCY OF $F_N=3,502$ Hz.....	154
FIG. 147: MODE 2: THE FIRST VERTICAL MODE. THE COMPLETE STRUCTURE DEFORMS IN Z-DIRECTION AT A NATURAL FREQUENCY OF $F_N=5,072$ Hz.	154
FIG. 148: MODE 3: THE FIRST TORSIONAL MODE. THE COMPLETE STRUCTURE TWISTS ALONG THE X-AXIS AT A NATURAL FREQUENCY OF $F_N=6,380$ Hz.	155
FIG. 149: MODE 4: THE SECOND VERTICAL MODE. ONLY THE ELLIPTICAL TRUSS DEFORMS IN Z-DIRECTION AT A NATURAL FREQUENCY OF $F_N=8,917$ Hz.....	155
FIG. 150: MODE 5: THE THIRD VERTICAL MODE. THE ELLIPTICAL TRUSS DEFORMS IN THE SAME MANNER IN Z-DIRECTION ALONG THE WHOLE LENGTH OF THE BRIDGE AT A NATURAL FREQUENCY OF $F_N=9,572$ Hz.	155
FIG. 151: DISTRIBUTION OF CONNECTIONS BY ORDER.....	157
FIG. 152: POSITION OF NODE 92 AND CONFIGURATION OF THE 6 ELEMENTS CONNECTING AT NODE 92.	158
FIG. 153: STRESS DISTRIBUTION IN THE 6 MEMBERS THAT CONNECT AT NODE 92. THE BLUE STRESSES ARE THE AXIAL STRESSES. THE RED STRESSES ARE THE COMBINED STRESSES THAT ALSO INCORPORATE THE BENDING MOMENTS IN THE MEMBERS.....	159
FIG. 154: POSITION OF NODE 99 AND CONFIGURATION OF THE 9 ELEMENTS CONNECTING AT NODE 99.	160
FIG. 155: STRESS DISTRIBUTION IN THE 9 MEMBERS THAT CONNECT AT NODE 99. THE BLUE STRESSES ARE THE AXIAL STRESSES. THE RED STRESSES ARE THE COMBINED STRESSES THAT ALSO INCORPORATE THE BENDING MOMENTS IN THE MEMBERS.....	161
FIG. 156: LEFT: GFRP TEE-JOINT USED FOR THE CONNECTION OF TUBULAR FRP MEMBERS. [WEB, WWW.CADFIL.COM] RIGHT: ROBOTIC TAPE-WINDING PATTERNS FOR THE PRODUCTION OF A TEE JOINT [P105, p8].....	162
FIG. 157: CONFIGURATION OF THE BRIDGE DECK.....	165
FIG. 158: 'FIBERLINE' FBD600 ASSET BRIDGE DECK PROFILE. LEFT: SINGLE PROFILE, RIGHT: GLUED ASSEMBLY OF PROFILES TO A WIDTH OF 1000MM [WEB, WWW.FIBERLINE.COM].....	166
FIG. 159: SUPPORT CONDITIONS OF THE FULL-FRP BRIDGE DESIGN WITH FEM NODE NUMBERS.....	171
FIG. 160: THE FIRST POSSIBLE BRIDGE SUBSTRUCTURES, SINGLE PILLAR MADE OF CONCRETE.	172
FIG. 161: THE SECOND POSSIBLE BRIDGE SUBSTRUCTURES, TRUSS STRUCTURE MADE OF STEEL OR FRP MATERIAL.	172
FIG. 162: CROSS SECTION OF THE 'LIGHT RAIL VIADUCT BEATRIXKWARTIER' [ZWARTS & JANSMA ARCHITECTS]	176
FIG. 163: SIDE VIEW OF THE 'LIGHT RAIL VIADUCT BEATRIXKWARTIER' [ZWARTS & JANSMA ARCHITECT]	177
FIG. 164: FE-MODEL OF THE 'LIGHT RAIL VIADUCT BEATRIXKWARTIER'	178
FIG. 165: FE-MODEL OF THE FINAL FRP DESIGN WITH INNER BRIDGE DECK ONLY	178
FIG. 166: COMPARISON OF MAXIMUM DEFORMATION FOR ALL LOAD CASES OF THE ALL FRP DESIGN AND THE 'LIGHT RAIL VIADUCT BEATRIXKWARTIER'	179
FIG. 167: COMPARISON OF MAX. TENSILE STRESSES FOR ALL LOAD CASES OF THE ALL FRP DESIGN AND THE 'LIGHT RAIL VIADUCT BEATRIXKWARTIER'	180
FIG. 168: COMPARISON OF MAXIMUM COMPRESSIVE STRESSES FOR ALL LOAD CASES OF THE ALL FRP DESIGN AND THE 'LIGHT RAIL VIADUCT BEATRIXKWARTIER'	181
FIG. 169: MODE 1 OF THE 50M SPAN OF THE 'LIGHT RAIL VIADUCT BEATRIXKWARTIER': THE FIRST VERTICAL MODE. THE COMPLETE STRUCTURE DEFORMS IN Z-DIRECTION AT A NATURAL FREQUENCY OF $F_N= 4,300$ Hz.	182
FIG. 170: MODE 2 OF THE 50M SPAN OF THE 'LIGHTRAIL VIADUCT BEATRIXKWARTIER': THE FIRST HORIZONTAL MODE. THE COMPLETE STRUCTURE TILTS IN Y-DIRECTION AT A NATURAL FREQUENCY OF $F_N= 5,018$ Hz.	182
FIG. 171: MODE 3 OF THE 50M SPAN OF THE 'LIGHTRAIL VIADUCT BEATRIXKWARTIER': THE FIRST TORSIONAL MODE. THE COMPLETE STRUCTURE TWISTS ALONG THE X-AXIS AT A NATURAL FREQUENCY OF $F_N= 7,419$ Hz.	183
FIG. 172: MODE 1 OF THE FULL-FRP BRIDGE DESIGN WITH INNER TRUSS ONLY: THE FIRST HORIZONTAL MODE. THE COMPLETE STRUCTURE TILTS IN Y-DIRECTION AT A NATURAL FREQUENCY OF $F_N= 3,522$ Hz.	183
FIG. 173: MODE 2 OF THE FULL-FRP BRIDGE DESIGN WITH INNER TRUSS ONLY: THE FIRST VERTICAL MODE. THE COMPLETE STRUCTURE TILTS DEFORMS IN Z-DIRECTION AT A NATURAL FREQUENCY OF $F_N= 5,596$ Hz.	184
FIG. 174: MODE 3 OF THE FULL-FRP BRIDGE DESIGN WITH INNER TRUSS ONLY: THE FIRST TORSIONAL MODE. THE COMPLETE STRUCTURE TWISTS ALONG THE X-AXIS AT A NATURAL FREQUENCY OF $F_N= 7,475$ Hz.	184
FIG. 175: SIDE VIEW OF THE FULL-FRP BRIDGE STRUCTURE WITH MAIN LOAD BEARING ELLIPTICAL TRUSS, INNER BRIDGE DECK SUPPORTING TRUSS AND CANTILEVER TRUSSES.	190

TABLE OF TABLES

TABLE 1: EXTENDED MECHANICAL PROPERTIES OF SELECTED FIBER MATERIALS.....	10
TABLE 2: EXTENDED MECHANICAL PROPERTIES OF SELECTED MATRIX MATERIALS.....	10
TABLE 3: EXTENDED MECHANICAL PROPERTIES OF SEVERAL UNIDIRECTIONAL REINFORCED COMPOSITES, CALCULATED USING THE CALCULATION METHODS DESCRIBED BEFORE.....	11
TABLE 4: DESIGN VALUES OF THE MECHANICAL PROPERTIES OF THE HIGH PERFORMANCE CARBON/EPOXY COMPOSITE WITH FIBER RATIOS OF 60% AND 70%.....	14
TABLE 5: FRP PRODUCTION METHODS SUITABLE FOR FABRICATION OF HIGH FIBER CONTENT FRP ELEMENTS.....	17
TABLE 6: EMISSION OF TOXIC GASES OF DIFFERENT FIBER REINFORCED COMPOSITES [B07, p90].....	26
TABLE 7: TOXIC GAS EXPOSURE LIMIT [B07, p367].....	27
TABLE 8: FIRE LOADS DUE TO DIFFERENT ROAD VEHICLES FIRES [NFPA502, p19].....	36
TABLE 9: MOST IMPORTANT CHARACTERISTICS OF SUB-VARIANTS 1A AND 1B.....	50
TABLE 10: MOST IMPORTANT CHARACTERISTICS OF SUB-VARIANTS 2A AND 2B.....	51
TABLE 11: MOST IMPORTANT CHARACTERISTICS OF SUB-VARIANTS 3A AND 3B.....	52
TABLE 12: MOST IMPORTANT CHARACTERISTICS OF SUB-VARIANTS 4A AND 4B.....	54
TABLE 13: MOST IMPORTANT CHARACTERISTICS OF SUB-VARIANTS 5A AND 5B.....	56
TABLE 14: : MOST IMPORTANT CHARACTERISTICS OF SUB-VARIANTS 5A AND 5B.....	56
TABLE 15: COMPARISON OF THE MOST IMPORTANT CHARACTERISTICS OF THE DIFFERENT SUB-VARIANTS.....	58
TABLE 16: COMPARISON OF DIFFERENT SPAN OPTIONS.....	61
TABLE 17: COMBINATION OF SINGLE TRAFFIC LOAD COMPONENTS ACCORDING TO [NEN-EN1991-2003/NB: 2009, TABLE 4.4A, p10].....	85
TABLE 18: RECOMMENDED VALUES OF Ψ FACTORS FOR ROAD BRIDGES [NEN-EN1990:2003/A2, CH. A2.2.2, TABLE A2.1, p13].....	86
TABLE 19: COMBINATION OF TRAFFIC LOADS WITH OTHER LOADS ACCORDING TO [NEN-EN1990:2003/A2, CH. A2.2.2, TABLE A2.1, p13].....	86
TABLE 20: MATERIAL USAGE FOR ALL ADAPTED 18 SUB VARIANTS. THESE ADAPTED MODELS WERE USED FOR FURTHER ANALYSIS.....	94
TABLE 21: SIMPLIFIED ISOTROPIC MATERIAL PROPERTIES FOR THE INITIAL COMPARATIVE FE-ANALYSIS, BASED ON [CH. 3.3, TABLE 4].....	95
TABLE 22: GENERAL DEFLECTION RESULTS DUE TO LOAD CASES LC1-LC4 FOR ALL 18 SUB VARIANTS.....	101
TABLE 23: NUMBER- AND ORDER OF NODES AS DESIGN PARAMETER OF THE CYLINDRICAL TRUSS TOPOLOGIES.....	105
TABLE 24: DEFORMATIONS OF THE MAIN LOAD BEARING STRUCTURE WITH AND WITHOUT INNER TRUSS STRUCTURE FOR ALL LOAD CASES.....	108
TABLE 25: MAXIMUM TENSILE AND COMPRESSIVE AXIAL STRESSES CAUSED BY LC1-LC3 FOR THE MAIN LOAD BEARING STRUCTURE WITH AND WITHOUT INNER SUPPORTING TRUSSES.....	109
TABLE 26: MAIN GEOMETRIC PARAMETERS FOR ALL 6 GRID SIZE VARIANTS.....	110
TABLE 27: EXTENDED GEOMETRIC PROPERTIES OF THE GRID SIZE VARIANTS.....	111
TABLE 28: RESULTS OF THE DEFLECTIONS FE-ANALYSIS FOR ALL GRID SIZE VARIANTS AND LOAD CASES.....	112
TABLE 29: MAXIMUM COMPRESSIVE- AND TENSILE STRESSES FOUND IN THE FE-ANALYSIS FOR ALL GRID SIZE VARIANTS AND LOAD CASES.....	113
TABLE 30: NORMALIZED MAXIMUM DEFORMATIONS AND NORMALIZED MATERIAL USAGE AND NUMBER OF NODES FOR ALL GRID SIZE VARIANT.....	115
TABLE 31: MAIN PARAMETERS OF ALL 20 CROSS SECTION VARIANTS.....	117
TABLE 32: RESULTS ON THE DEFLECTION OF ALL CROSS SECTION VARIANTS DIRECTLY DERIVED FROM FE-ANALYSIS AND ADAPTED FOR INFLUENCE OF THE BRIDGE DECK SUBSTRUCTURE (LIGHT BLUE SHADED).....	118
TABLE 33: MAXIMUM TENSILE- AND COMPRESSIVE STRESSES IN THE CROSS SECTION VARIANTS DUE TO LC1-LC3.....	121
TABLE 34: SPECIFICATION OF THE OPTIMIZED GRID SIZE VARIANT (FIRST ROW) COMPARED TO THE SPECIFICATIONS OF THE ORIGINAL VARIANT (SECOND ROW).....	125
TABLE 35: COMBINATION OF SINGLE TRAFFIC LOAD COMPONENTS WITH OTHER LOADS ACCORDING TO [NEN-EN1991-2003/NB:2009, TABLE 4.4A, p10].....	138
TABLE 36: FINAL QUASI-ISOTROPIC MATERIAL PROPERTIES OF THE 70/30 CARBON EPOXY COMPOSITE USED, BASED ON THE DESIGN VALUES DERIVED IN [CH. 3.4].....	140
TABLE 37: COMPARISON OF ALL LOAD COMBINATION CASES FOR THE DERIVATION OF THE NORMATIVE LOAD CASES.....	148
TABLE 38: THE TABLE SHOWS THE NATURAL FREQUENCIES OF THE FULL-FRP BRIDGE FOR THE FIRST 5 MODES.....	156
TABLE 39: ADVANTAGES AND DISADVANTAGES OF FIBER REINFORCED POLYMER BRIDGE DECKS [LS, CH. 3.2.3, p113].....	164
TABLE 40: 'FIBERLINE' FBD600 ASSET BRIDGE DECK PROFILE PROPERTIES. LEFT: SINGLE PROFILE, RIGHT: GLUED ASSEMBLY OF PROFILES WITH A WIDTH OF 1000MM [WEB, WWW.FIBERLINE.COM].....	166
TABLE 41: DEFLECTION OF THE BRIDGE DECK FOR SPANS FROM L=500-2500MM DUE TO A POINT LOAD F=200kN WITH A SAFETY FACTOR $\gamma=1,5$ AS PRESCRIBED BY LOAD MODEL 2 OF EUROCODE 1 [NEN-EN 1991-2:2003].....	168
TABLE 42: DESIGN PROPERTIES OF THE 'FIBERCORE INFRACORE INSIDE' SYSTEMS FOR THE USE AS 'TYPE 1 BRIDGE DECK' AND 'TYPE 2 BRIDGE DECK' IN THE FULL-FRP BRIDGE DESIGN.....	169
TABLE 43: TOTAL WEIGHT OF THE BRIDGE STRUCTURE, THE MAIN LOAD BEARING SYSTEM ELEMENTS AND THE BRIDGE DECKS.....	170
TABLE 44: MINIMUM AND MAXIMUM REACTION FORCES IN THE SUPPORTS DUE TO THE ENVELOPE OF ALL LOAD COMBINATION CASES CC1-CC8.....	171
TABLE 45: PRICE PER KG CFRP DETERMINATION ON THE BASIS OF A CFRP ALTERNATIVE TO THE LONDON MILLENNIUM PEDESTRIAN BRIDGE (PRICE LEVEL 2006) [LS, CH. 9.1.2, p228] [A33, p5].....	174
TABLE 46: ROUGH COST ESTIMATION FOR THE FULL-FRP HEAVY TRAFFIC ELLIPTICAL TRUSS BRIDGE (PRICE LEVEL 2006).....	174
TABLE 47: COMPARISON OF MAXIMUM DEFORMATION FOR ALL LOAD CASES OF THE ALL FRP DESIGN AND THE 'LIGHT RAIL VIADUCT BEATRIXKWARTIER'.....	179
TABLE 48: COMPARISON OF MAXIMUM TENSILE- AND COMPRESSIVE STRESSES FOR ALL LOAD CASES OF THE ALL FRP DESIGN AND THE 'LIGHT RAIL VIADUCT BEATRIXKWARTIER'.....	180
TABLE 49: GEOMETRIC PROPERTIES OF THE FULL-FRP DESIGN AND THE 'LIGHT RAIL VIADUCT BEATRIXKWARTIER' WITH 40M AND 50M SPAN.....	181
TABLE 50: MATERIAL USAGE OF THE FULL-FRP DESIGN AND THE 'LIGHT RAIL VIADUCT BEATRIXKWARTIER' WITH 40M AND 50M SPAN.....	182
TABLE 51: COMPARISON OF THE NATURAL FREQUENCIES OF THE FULL-FRP STRUCTURE WITH AND WITHOUT CANTILEVER TRUSS AS WELL AS THE 50M SPAN OF THE 'LIGHT RAIL VIADUCT BEATRIXKWARTIER'.....	184